SOLID STATE NMR OF SULFA-DRUGS

by

Alessia Portieri

Graduate Society
University of Durham

A thesis submitted for the degree of Doctor of Philosophy

Department of Chemistry
University of Durham
2001

SOLID-STATE NMR STUDY OF SULFA DRUGS

Alessia Portieri

Submitted for the degree of Doctor of Phylosophy, 2001

Abstract

This work has been a study of systems, mostly of sulfa-drugs, showing polymorphic behaviour. Using different means as solid state NMR, X-ray analysis, and theoretical calculations, we have seen how it is possible to understand results obtained from the different techniques, proving how the study of polymorphic systems needs cooperative advice from the different techniques that are able to detect polymorphic differences.

Within the sulfa-drugs I have been mostly concentrating on sulfanilamide, studying ^{13}C and ^{15}N solid state NMR spectra of the different polymorphs. The NMR parameters that have been most interesting to study, have been the relaxation times that have revealed complicated motion of the molecule despite it being a small molecule. In order to obtain detailed information from ^{15}N spectra it has been necessary to enrich the samples and this has enabled a study of the shielding tensors of the nitrogens in the molecule. ^{13}C spectra were also recorded of systems studied sulfathiazole solvates, that proved to show some of the same solid state effects in the NMR spectra as sulfanilamide.

Shielding calculations have proved to be still limited in order to obtain reliable information on the shielding of both ^{13}C and ^{15}N nuclei but considering hydrogen-bonded molecules, as opposed to isolated molecules, seemed to have improved the calculations quite a lot, so that some idea of intermolecular effects could be deducted. Exact positions of the hydrogen has proved to be essential as well in order to improve the calculations.

Finally a case study for the REDOR pulse sequence has been carried out. Different attempts to understand the effects influencing this particular experiment have been carried out on 20% and 99% doubly enriched glycine, as well as on a particular sample, doubly enriched BRL55834, but the internuclear distances measured with this technique still displayed some uncertainties that made results not thoroughly reliable.

Memorandum

The research presented in this thesis has been carried out in the University of Durham, in partial collaboration with the University of York. The work has been carried out between October 1998 and September 2001. The work within this thesis, unless otherwise stated is the original work of the author.

Acknowledgements

First of all I would like to thank my supervisor, Prof. R. K. Harris, who has been of fundamental support and great encouragement in the most difficult moments of my PhD. Dr. Terry Threlfall, from the University of York, for providing me with the samples needed for the work carried out in this laboratory. Dr. R. Fletton and R. Lancaster for their useful advice and discussions. I would like to thank Dr. A. Howes from the University of Warwick, for his help and advice on the use of the 600 MHz spectrometer. From the University of Durham: acknowledgments to Dr. P. Hodgkinson, for his patience, to Dr. D. Apperley and P. Worwald, for their help with the 300 MHz spectrometer and to Dr. H. Puschmann for the X-ray work done in Durham. Last, but not least thank you to all the people of CG22 with whom I shared so much while I have been here in Durham: Paolo, Lindsey, Helen, Lucy, Shinji, Bruno, Philip, Pierre, Ulrich, Naser, Debbie, Giancarlo, Diane, Thomas, Paul, Ohm and Ian.

SYMBOLS AND ABBREVIATIONS

FDA	Food and Drug Administration
TGA	thermogravimetric analysis
DSC	differential scanning calorimetry
DTA	differential thermal analysis
IR	Infrared
XRD	X-ray diffraction
NMR	Nuclear Magnetic Resonance
CSA	Chemical Shift Anisotropy
SA	Shielding Anisotropy
CP	Cross Polarisation
MAS	Magic Angle Spinning
H-H	Hartmann Hahn
AMT	American Microwave technology
CE	Creative electronics
CMX	Chemagnetix
PDMSO	polydimethyldisiloxane
T_1^x	Spin-Lattice relaxation time of nucleus x
$T_{1\rho}^x$	Spin-Locked relaxation time of nucleus x
T_{IS}	Cross Polarisation time from the I spin to the S spin
B_0	The static magnetic field
VT	Variable Temperature
CW	Continuous wave
rf	Radiofrequency
FID	Fourier Induction Deacay
γ	Magnetogyric ratio
$\hbar$	Planck constant

k	Boltzmann constant
T_L	Lattice temperature
C_H	Curie Constant
N	total number of nuclei of a given kind in a sample
T_S	spin temperature
NQS	non- quaternary suppression
TPPM	two pulse phase modulation
τ_p	pulse duration
r_{ij}	internuclear distance
$J(\omega_0)$	spectral density function at angular frequency ω_0
$J(\omega_1)$	spectral density function at angular frequency ω_1
τ_c	correlation time
E_a	activation energy
T_1^{DDU}	nuclear dipole-dipole relaxation time from unlike nuclei
$T_{1\rho}^{DDU}$	spin-locked relaxation time of nucleus x
τ	time between rf pulses
ρ	density matrix
$\hat{H}$	Hamiltonian operator
U(t)	spin evolution operator

Chapter 1

INTRODUCTION

1.1. Investigation of polymorphic behaviour in organic compounds

Many organic compounds as well as many drugs exist in the solid state as a crystalline form due to ease in handling and for reasons of stability. However they can exist in more than one crystalline form, and knowledge about the crystal structure and the properties of the form under investigation is of great importance for pharmaceutical industries[1].

In this work the main issue is the to use, investigation, and development of the technique of Solid State NMR for the study of compounds that can crystallise in different forms (polymorphic forms). The limits as well as the potentialities of Solid State NMR in the study of polymorphism will be discussed and analysed. Polymorphic forms can also be quite useful to the practice of solid state NMR in order to increase the understanding about how conformational differences and intermolecular effects can influence chemical shift isotropy and anisotropy.

The main compound under investigation will be sulfanilamide, the most simple of the sulfa-drugs, exhibiting polymorphic behaviour. I will also analyse different pseudo-polymorphs (solvates), which are crystalline adducts containing solvent molecules within the crystal structures of sulfathiazole.

1.2. Polymorphism [2, 3]

Polymorphism is defined as the ability of a given substance to crystallise in different structural arrangements. Since different polymorphs possess different properties, such as solubility, density, melting point, enthalpy of fusion, electrical conductivity, and chemical reactivity, it is quite important to be able to choose the most suitable polymorph of a given compound that will possess the right properties for the particular application that is needed; hence the importance of finding better and faster ways to distinguish different polymorphs[4]. Polymorphism for pharmaceutical compounds has also another, most important aspect: different polymorphic forms may have different bioavailability and therapeutic efficacy so that the identification of a particular polymorph is a major task for pharmaceutical industries. This arises because different polymorphic forms of the same drug may have solubilities which differ by a large amount. The production of a wrong polymorph at the crystallisation stage or at any other stage can result in pharmaceutical dosage forms which can be ineffective if not toxic[5]. These factors concerning polymorphism have led to an increased regulatory procedure. For the approval of a new drug, the drug substance guideline of the US Food and Drug Administration (FDA) states that "appropriate" analytical procedures need to be used to detect polymorphs, hydrates and amorphous forms of the drug substance and also underlines the importance of controlling the crystal form of the drug substance during the various stages of product development[1]. It is also important to discover a new polymorph since it will enable the industry to prolong the patent protection (as has been the case for Glaxo-Wellcome`s *Zantac*[6]). From these considerations we can see how the issue of polymorphism is related to all phases of pharmaceutical industry, from discovery to successful marketing.

The great problem encountered with polymorphs is that it is possible to have metastable forms that will crystallise first and then disappear[6, 7]. This can be a great problem when considering storage of drugs and tabletting problems. The burden over the whole issue of polymorphism is that the control over the nucleation and

growth in polymorphic systems is poor. Even attempts to revert to the wanted form after transformation are not always successful.

The importance of defining the stability hierarchy among different polymorphs is underlined by the fact that metastable forms often have the highest dissolution rate so that, consequently, they might have the highest bioavailability[8]. This is also noted in Ostwald's rule, which is the only rule that has been fully accepted for the problem of control over crystallisation. Ostwald's rule of stages states that, upon crystallisation, a system will initially adopt the crystal structure which leads to the minimum loss in free energy (the most soluble and thermodynamically least stable) and the crystals of this form will transform subsequently to the most stable crystal form.

Further complications in handling solid drugs arise since undesirable changes can be led by manufacturing processes including crystallisation scale-up, drying, heating, and compression, so that careful quality controls are always needed and checks for polymorphic transformations are routine practice in pharmaceutical industries.

1.2.1. Polymorphic transformations

When talking about phase transformations, it is important to have clearly in mind the concepts of enantiotropy and monotropy, since relations between two polymorphs are divided into these categories[9].

A criterion to define monotropy is that no transition point between the forms exists at any temperature below the melting points of both forms. So that when we are considering a monotropic relationship we are considering one form to be metastable in respect to others. In this case there is no observable transition point although a thermodynamic analysis would imply a theoretical transition point above the melting point which is, obviously, unobservable[2].

An enantiotropic relationship implies that each form has a range of temperature over which it is stable with respect to the other and a transition point at a given temperature at which the forms are equi-stable. Above that temperature the thermodynamic tendency is to formation exclusively of the form stable at higher temperature. Forms outside their range of stability are considered as metastable.

Although we often find in the literature discussions of whether a form is monotropic or not in respect to another it might well be that this definition is the product of unnecessary discussions, without any particular and actual meaning.

1.3. Characterization of polymorphic forms

Having outlined the problems related to polymorphism as well as the fundamental importance of the issue, we shall proceed to analysis of the methods most commonly used for detection of polymorphic forms, bearing in mind that no technique should be used alone[10, 11]. Among the oldest methods with which we can examine the presence of different polymorphic forms are the thermal methods of analysis, for example thermogravimetric analysis (TGA), differential scanning calorimetry (DSC) and differential thermal analysis (DTA). These techniques will, though, only show a transformation, if present, but if no thermal transformation appears for one particular form we cannot be sure of the non-existence of a different polymorph. The other limit of this technique is that it is possible to obtain different temperatures for the same transition when crystallisation from different solvents was used. It is the case detected for sulfanilamide[12], for which transition from the β form to the γ form has a range of about 20 degrees depending on whether the sample was crystallised from water, ethanol, n-propanol or acetone. When this is the case, characterisation of the polymorph might prove to be very difficult.

Infrared spectroscopy (IR) is very valuable also since it is able to give information on the motion of functional groups which might be structurally different for the distinct polymorphs. However, great attention must be paid to the fact that different

IR spectra may be caused by sample impurities, and that during preparation of the sample (usually by trituration of the sample and suspension in Nujol or by pressing a co-ground mixture with KBr into a disk) polymorphic transformation may be affected. This may even occur by gentle manual grinding, so that it is important in this case to confirm the polymorphic form under consideration before infrared analysis is carried out. Infrared spectroscopy is a good technique but it is limited in the scope and the rationalisation of the effects is anyway easier if the crystal structures are already known.

Powder XRD is a very valuable tool, although impurities below 5% can be missed when using this particular technique, and also powder patterns are susceptible to differences in particle sizes and preferred orientation which can result in the incorrect identification of polymorphs. The final and most secure method for distinguishing different polymorphic types is single-crystal X-ray, which will detect the presence of non-equivalent crystal structures, although, as we will see in detail, solid-state NMR is also a fine method to distinguish and characterise polymorphic differences. Since it will not always be possible to grow crystals of sufficient size[13] the use of solid-state NMR becomes more important, and comparison between X-ray powder diffraction and solid-state NMR is necessary[14].

1.3.1. Solid-state NMR, the technique

NMR studies concerning organic polymorphism will employ mostly ^{13}C and ^{15}N nuclei since ^{1}H spectra typically produce broad bands because of strong dipolar interactions. In order to be able to achieve high-resolution NMR we need to mediate anisotropic interactions, including homo- and hetero-nuclear dipolar coupling. Magic Angle Spinning (MAS), for which a cylindrical sample is spun at high frequency (normally, when considering ^{13}C and ^{15}N rates of about 6000 Hz are sufficient) when positioned at an angle of 54.7° to the applied magnetic field, will remove interactions of the order of the spinning speed so that a considerable narrowing of the lines due to averaging of the chemical shift anisotropies is seen.

Heteronuclear decoupling is needed in order to eliminate interactions due to dipolar ^{13}C, ^{1}H coupling, which are of the magnitude of about 50 kHz, so that MAS is not able to efficiently average the effects due to it. Decoupling fields equivalent to about 50 KHz are needed.

The other question to be solved when considering solid-state NMR of organic compounds is the fact that we are generally looking at non-abundant ("dilute") spins for which we will see a poor signal-to-noise ratio as well as problems with relaxation times being long for these nuclei. This problem is solved with Cross-Polarisation (CP), which was first implemented by Pines et al.[15] in 1972, with which enhancement of the rare-spin system is achieved by transfer of magnetisation from the abundant-spin system.

1.3.2 Solid-state NMR for the study of polymorphs

Powder and single-crystal X-ray diffraction are fundamental techniques to distinguish polymorphs, but solid-state NMR is able to give other kinds of information, such as local electronic environment, which can be of great value in order to understand better the effects that are at the origin of polymorphism. Solid-state NMR is able to characterise conformational differences, crystal packing diversities and the effects of hydrogen bonding. In recent years it has become widely used as a technique, in different applications being able to show readily crystallographic effects, since more lines may be seen than in the solution spectrum, and these can be attributed to structural inequivalence, differences of molecules in the unit cell or deformations due to the crystal packing[16, 17].

The initial information available from solid-state NMR comes from the analysis of changes in the isotropic chemical shifts (which is a fast and immediate way to confirm the existence of different polymorphs). Changes in chemical shift anisotropy also have been quite helpful in order to discriminate between polymorphs, and in some cases these changes are more sensitive than the isotropic ones[18].

Other important pieces of information can be retrieved by varying the sample temperature, which allows dynamic studies of solid-solid phase transformations as well as giving knowledge about molecular motion. This aspect is very important since it can give complementary and valuable information to that retrieved from X-ray diffraction. We must in fact remember how the time scales are different for these two techniques: NMR may detect motions over a very wide range of time scales (10^{1}-10^{-10} s) whereas the diffraction process occurs on a time scale of 10^{-18}s in which period atoms can only move very short distances. Processes as phenyl ring flips, or other motional events that do not lead to positional disorder, may remain undetected by diffraction techniques, where, in contrast, NMR is able to detect them[19]. In other cases, where dynamic properties lead to disorder in the position of atoms, they will be detected from diffraction techniques by the location of partially occupied atomic positions but then we will not be able to distinguish if the partially occupied atomic positions derive from two molecules or from a single molecule that is moving. Solid-state NMR can distinguish static or dynamic disorder since it will see only one peak if the molecule is exchanging rapidly between the two sites, but two peaks if there are two distinct molecules.

There are also other cases for which NMR data are actually able to reveal structural information beyond the limits of diffraction methods. In many of these cases it has proved to be useful to combine the information that could be achieved from experimental NMR with results from *ab initio* calculations. For situations in which the symmetry of a molecule is lowered from the gas phase to the crystal structure, single-crystal NMR has been useful in order to clarify if the different symmetry is due only to intermolecular effects or to actually different symmetry in the molecule which cannot be detected by X-ray diffraction[20]. Moreover, NMR is quite important to detect in a fast and reliable way if there is more than one molecule in the asymmetric unit, since in this case the signals will exhibit splittings.

Another advantage of NMR over powder X-ray diffraction is that the latter is not sensitive to amorphous or poorly crystallised forms, whereas NMR can still detect

differences[21]. Solid-state NMR is for these reasons becoming a very important technique for studying polymorphism[22-28].

1.4. REFERENCES

1) S. R. Viggapunta, H. G. Brittain and D. J. W. Grant, *Adv. drug delivery Rev.* **2001**, *48*, 3.

2) T. L. Threlfall, *Analyst* **1995**, *120.*

3) R. K. Harris,*'Polymorphism and related phenomena' Encyclopedia of NMR*, 1996; Vol. 6.

4) H. G. Brittain, *J. Pharm. Sci* **1997**, *86*, 405.

5) M. R. Caira, *Topics in current chemistry* **1998**, *198*, 163.

6) N. Blagden and R. Davies, *Chem. Br.* **1999**, *3*, 44.

7) J. D. Dunitz and J. Bernstein, *Acc. Chem. Res.* **1995**, *28*, 193.

8) S. Toscani, *Therm. Acta* **1998**, *321*, 73.

9) K. Sekiguchi, Y. Tsuda and M. Kanke, *Chem. Pharm. Bull.* **1975**, *23*, 1362.

10) G. A. Stephenson, J. G. Stowell, P. H. Toma, D. E. Dorman, J. R. Greene and S. R. Byrn, *J. Am. Chem. Soc.* **1994**, *116*, 5767.

11) G. A. Stephenson, R. R. Pfeiffer and S. R. Byrn, *Int. J. Pharm.* **1997**, *146*, 93.

12) S. Toscani, S. Thoren, V. Agafonov, R. Ceolin and J. Dugue, *Pharm. Res.* **1995**, *12*, 1453.

13) R. K. Harris, P. Jonsen and K. J. Packer, *J. Chem. Soc. Perkin Trans. II* **1987**, 1383.

14) B. E. Padden, M. T. Zell, Z. Dong, S. A. Schroeder, D. W. Grant and E. J. Munson, *Anal. Chem.* **1999**, *71*, 3325.

15) A. Pines, M. G. Gibby and J. S. Waugh, *J. Chem. Phys.* **1972**, *56*, 1776.

16) K. Wozniack, T. M. Krygowsky, E. Greech, W. Kolodziejski and J. Klinowsi, *J. Phys. Chem.* **1993**, 1862.

17) W. Kolodzieski, I. Wawer, K. Wozniack and J. Klinowski, *J. Phys. Chem.* **1993**, *97*, 12147.

18) E. McManara and J. Smith, *J. Am. Chem. Soc.* **1998**, *20*, 11710.

19) J. Fattah and J. M. Twyman, *J. Am. Chem. Soc.* **1993**, *115*, 5636.

20) J. C. Facelli and D. M. Grant, *Nature* **1993**, *365*, 325.

21) S. Doyle, R. A. Pethrick, R. K. Harris, J. M. Lane, K. J. Packer and F. Heatley, *Polymer* **1986**, *27*, 19.

22) S. R. Byrn, G. Gray, R. R. Pfeiffer and J. Frey, *J. Pharm. Sci.* **1985**, *74*, 565.

23) R. K. Harris, A. M. Kenwright, B. J. Say, R. R. Yeung, R. A. Fletton, R. W. Lancaster and G. L. Hardgrove, *Spectrochimica Acta* **1990**, *46*, 927.

24) S. R. Byrn, R. R. Pfeiffer, G. Stephenson, D. J. W. Grant and W. B. Gleason, *Chem. Mater.* **1994**, *6*, 1148.

25) S. A. Carss and R. K. Harris, *Magn. Res. Chem.* **1995**, *33*, 501.

26) G. McGeorge, R. K. Harris, A. M. Chippendale and J. F. Bullock, *J. Chem. Soc. Perkin Trans. II* **1996**, 1733.

27) S. C. Campbell, R. K. Harris, M. J. Hardy, D. C. Lee and D. J. Busby, *J. Chem. Soc. Perkin Trans. II* **1997**.

28) D. C. Apperley, R. A. Fletton, R. K. Harris, R. W. Lancaster, S. Tavener and T. L. Threlfall, *J. Pharm. Sci.* **1999**, *88*, 1275.

Chapter 2

EXPERIMENTAL

2.1. Sample preparation

At first, sulfanilamide samples were prepared by Dr. T. L. Threlfall (York University) from different solvents. To obtain the α form, sulfanilamide was recrystallised from n-butanol, to obtain the β form it was recrystallised from acetonitrile, and to obtain the γ form it was recrystallised from n-pentanol. Different attempts were made to recrystallise the fourth form of sulfanilamide that in literature[1] is said to be obtained form either isoamyl alcohol or n-butanol, from the highly saturated solutions, but with no success. The syntheses for the ^{15}N-enriched samples, as explained in chapter 4, were carried out by me, together with the crystallisations.

The solvates described in chapter 6 were also prepared by Dr. Threlfall, in general by boiling the compound (sulfathiazole) in the solvent, using different temperature ranges as well as different cooling procedures. Particular crystallisation procedures will be described for the samples in the relative chapter.

2.2. X-ray analysis

The X-ray data was obtained partly (α-sulfanilamide) from Durham University (Horst Pushmann), partly (β and γ sulfanilamide and sulfathiazole solvates) from Southampton university (Michael Hursthouse). The diffractometer in Durham is a Bruker SMART-CCD diffractometer equipped with a molybdenum target providing radiation of a mean wavelength of 0.71073 Å. The detailed data collection and structure refinement for the crystal structure of the α polymoprh of sulfanilamide

obtained in Durham is listed below, the data was recorded at the temperature of 150 K :

Theta range for data collection	2.21 to 27.49°
Index ranges	-18<=h<=18, -7<=k<=4, -23<=l<=23
Reflections collected	8657
Independent reflections	1722 [R(int) = 0.0646]
Completeness to theta = 27.49°	99.9%
Refinement method	Full-matrix lest-squares on F^2
Data/restraints/parameters	1722 / 0 / 133
Goodness-of-fit on F^2	1.038
Final R indices [I>2sigma(I)]	R_1 = 0.0339, wR2 = 0.0836
R indices (all data)	R_1 = 0.0450, wR2 = 0.0908
Extinction coefficient	0.0047(14)
Largest diff. peak and hole	0.455 and –0.360 e.$Å^{-3}$

The data from Southampton was recorded on a Nonius KappaCCD area-detector diffractometer, again with molybdenum radiation, and an absorption correction of a multi-scan (SORTAV Blessing, 1995). The data was recorded at 293(2) Kelvin.

2.2. Solid-state NMR spectroscopy

Most of the experiments were performed using a Chemagnetics CMX 200 spectrometer, operating at 200.13 MHz for protons. Acquisition and processing of the data are controlled by a Sun workstation running the Chemagnetics 'Spinsight' software. The amplifiers that were accessible during the course of my PhD were three; a middle-frequency broad-band AMT (American Microwave Technology) that could be tuned to frequencies within the range from 6 to 220 MHz, a narrow-band CE (Creative Electronics) amplifier that was generally used for proton frequencies, and a Bruker amplifier, for which the range could be changed by using different final-stage amplifier boxes. This last Bruker amplifier was the one I have used for acquiring nitrogen in the REDOR experiments, using a box for frequencies

within the range of 20 to 30 MHz. This amplifier is the only one not to have blanking. Two of the amplifiers work in class A/B, but the Bruker amplifier, works in class C.

An other spectrometer used was the 300 MHz Varian Unity Plus spectrometer, which uses Doty probes, one taking 7 mm rotors, the other 5 mm rotors. This is a two-channel spectrometer.

The third system used was 600 MHz CMX Infinity, which is situated in Warwick University, and is similar to the 200 CMX. The amplifiers are CE for ^{1}H and AMT for ^{13}C. The probe that I used was a three-channel 4 mm T3 probe, where T3 characterises the kind of tuning technique which employs long tubes as capacitors (T3 stands for Tuning Tube Technology).

2.2.1. Probes

In the Durham laboratory there are a number of probes. There are fast-spinning systems, such as the HX probe, which requires rotors of 4 mm outside diameter, and there are static probes, such as the HX wideline probe, which has 5 mm and 10 mm stationary sample containers. There are also two three-channel probes, HXY and HFX, the first takes rotors of 5 mm outside diameter, and the second rotors of 7.5 mm outside diameter. Finally there is an HF probe. I have mostly used MAS probes, the wideline probe having arrived just recently. Each of the MAS probes possesses "stators" in which the rotor is placed and the design is such that rotors can spin at low or fast rates, depending on the design. Stators may be made from brass, Vespel, or other material. In all cases, a mechanism exists whereby the angle between the spinning axis and the magnetic field can be adjusted to the magic angle.

2.2.1.1. HX probe

This probe is able to operate two channels, where one needs to be tuned to 200.13 MHz for protons, whereas the other channel can be tuned to frequencies ranging from 19.2 MHz to 82.6 MHz just by changing the capacitors, of which there are two different sets (namely, top and bottom capacitors). The frequency for carbon tuning is 50.329 MHz.

The rotors for this probe are 7.5 mm in outside diameter and made of zirconia with drive tips in Kel-F, polychlorotrifluoro-ethylene, since it contains no protons (-CF_2-CFCl-) and Teflon end caps. These rotors contain about 350 mg of sample. The proton decoupling power that is used for this probe is, generally equivalent to 50 kHz ($\gamma B_1/2\pi$) corresponding to a 5 μs pulse duration. It is important to always use filters (a 100 MHz low-pass filter for the carbon channel and a 200 MHz band-pass filter for the proton).

The spinning speeds for this probe can go up to about 6 kHz, which is not very high, but this is mostly because the rotors are quite large in comparison with fast spinning probes, whose diameters are of 3.2 mm, as in the case of the HXY probe I have been using in Warwick on the 600 MHz spectrometer. My spinning speeds were usually of 4 kHz, this spin rate being enough to have a clear spectrum without spinning side bands overlapping; the speed can be controlled to ±1 Hz.

2.2.1.2. HXY probe

This is a triple-channel probe which can be tuned to three different frequencies that need to be of some difference one from the other, since the isolation between the channels is not as good as when one needs to isolate frequencies that are quite near one another. For this reason it is also called the HML probe (High, Medium, Low probe). The tuning I have used has been for ^{1}H, ^{13}C, ^{15}N. The design of this probe is quite complicated, and changing the capacitors in this probe means partially dismantling the probe, and fixing a front capacitor, which isolates the low frequency from the middle one, and a back capacitor which controls the tuning in

the low-frequency. Finally a trap needs to be set which will isolate the middle frequency from the lower one. Calculations for the capacitor combinations and traps were done according to the manual in order to tune to ^{1}H, ^{13}C and ^{15}N. Although the manual would suggest a front capacitor of 200 pF, a back one of 130 pF, and a trap of 47 pF, it was seen that this combination did not work properly for the tuning. Different checks showed that changing the trap with one of 33 pF works better, so that this has been the combination used in order to tune the probe to these three isotopes.

This probe is capable of spinning faster than the HX probe, since smaller rotors of outer diameter are to be used for it. It can spin up to 12 kHz.

2.3. The NMR experiment

2.3.1. Line-widths and magic-angle spinning

All my samples were crystalline and the ^{13}C linewidths were typically between 30 and 50 Hz. When proton decoupling and magic-angle spinning is applied, these are quite typical linewidths. Broadening of the lines can be due to a number of factors that all need to be carefully checked before starting an experiment. Among the reasons we can outline magic-angle missetting, rotor instability, insufficient decoupling power, being off-resonance for proton decoupling, and bad shimming.

Sample characteristics can obviously be part of the reasons for broader lines, such as having different crystalline modifications in the sample, or the presence of quadrupolar nuclei.

I will describe here the basics of commencing an NMR experiment for the solid state so that the setting of the decoupling, MAS, and cross-polarisation are described.

2.3.2. Setting the magic angle

The setting of the magic angle is an operation that should be carried out each time before starting a session at the spectrometer. This operation can be done by observing either the FID of KBr (potassium bromide), which shows a great number of rotational echoes that are very sensitive to changes of about 0.5° from the magic angle. When the maximum number of rotational echoes is seen, we can consider the rotor to be at the magic angle.

Sometimes it can prove to be difficult to start from observation of KBr if we are a long way off from the magic angle. In this case it is important to use hexamethylbenzene (HMB), since its aromatic carbons will be at 171 ppm, with a sharp line only when the angle is set at 54.7°. For any other value we will observe the line to broaden and shift to other frequencies.

2.3.3. Setting the proton 90° and shimming the probe

PDMSO (polymethylsiloxane) can be used to set the 90° ^{1}H pulse. This operation is carried out by aquiring continuously the proton spectrum of PDMSO, while adjusting manually the power going into the probe. When the amount of power is such that the first null signal is seen, this means that the magnetisation has precessed through 180°, so that half of the pulse duration will give the correct proton 90°. This will then need to be checked by arraying the pulse duration and monitoring the magnetisation behaviour. The software control for the 200 MHz has a small role, since by software it is only possible to diminish the power used. The new Infinity 600 console has a different way of setting up powers, since it is totally controlled by software, so that one needs to array the amplitudes of power from the software.

Before any other operation it is important to shim the probe, and this is done using the signal of PDMSO, which should have a ^{1}H linewidth of about 3 Hz. The linewidths for solids are generally broader than this limit and this is the case for

which there is no additional broadening due to bad shimming. Obtaining a narrow linewidth will mean good signal-to-noise, so that it is fundamental for the setup.

2.3.4 Proton decoupling

The amount of decoupling needed varies with the width of the region that is to be decoupled, so that it will depend on the magnetic field strength at which the experiments are performed. The amount of decoupling power also depends upon the strength of the dipolar interactions in the sample, as well as depending on the efficiency of the probe circuit. For the 200 MHz spectrometer, a decoupling of about 50 kHz was generally sufficient, but this was obtained with different powers depending on the probe: for example, about 100 W was generally needed for the HX probe where only 20 W were needed for the HXY. This is the reason why it is so important, especially in a laboratory like ours, where quite a large number of different probes are used, to check the powers used previously for the probes, and to start by using low powers that can eventually be increased. For the 600 MHz spectrometer a higher power was generally needed, 40 W being the lower limit, but sometimes decoupling powers of 130 W were used. This is the reason why, at higher fields, it is important to use different decoupling pulse sequences that will allow the same decoupling strength with less power, such as the TPPM pulse sequence.

2.3.5 Cross Polarisation

As we have seen above, the line narrowing for dilute spins in solids is guaranteed by a careful check of decoupling and the condition of magic-angle spinning. There is still a problem of sensitivity. Directly observing dilute spins will suffer from the disadvantage of long experiments due to the long relaxation times, which often characterise nuclei such as ^{13}C and ^{15}N, as well as low sensitivity.

Using the cross-polarisation technique, spin polarisation is transferred from abundant spins to dilute spins, and provides both signal enhancement and shorter recycle delays. This technique involves concepts not normally encountered in liquids, so that it will need some description. The concepts of spin diffusion and spin temperature need to be introduced, although I will give here a very brief and qualitative description.

2.3.5.1. Spin diffusion

Spin diffusion is an effect for strongly dipolar coupled spins, such as protons, which can be described as forming a thermodynamic spin reservoir in internal equilibrium. This happens when a spin-flip process provides a mechanism for bringing the system to a common spin temperature at a rate which may be fast compared to T_1. This term is a direct consequence of the nature of homonuclear dipolar coupling. When we consider such coupling, we can write the Hamiltonian in an alphabet expansion[2], and the second term is the one involving coupled spins of opposite orientation which can undergo rapid energy-conserving transitions by spin-flips, $(+1/2,-1/2)\leftrightarrow(-1/2,+1/2)$.

This is an important phenomenon to be considered when calculating T_1 values in solids. In fact, in general, different spins of a system should relax at different rates. The energy conserving flip-flops between neighbouring proton spins even out the distribution of polarisation, so that one chemical group will not relax independently from its immediate neighbour.

2.3.5.2. Spin temperature

When an ensemble of spin-1/2 nuclei is considered in an external magnetic field, the Boltzmann distribution of populations for the two states is described by the Boltzmann equation:

$$p_{-1/2} / p_{+1/2} = \exp(-\frac{\gamma\hbar B_0}{kT_L}) \qquad (2\text{-}1)$$

so that, because $\gamma\hbar B_0 << kT_L$,

$$p_{-1/2} - p_{+1/2} \approx \frac{N\gamma\hbar B_0}{2kT_L} \tag{2-2}$$

where T_L is considered the temperature of the lattice[3].

The total equilibrium magnetisation of the assembly of spins can be written to be:

$$M_0 = \frac{C_H B_0}{T_L} \tag{2-3}$$

where C_H is the Curie constant $C_H = \frac{\gamma^2\hbar^2}{4k}N$.

This equation describes magnetisation in equilibrium with the lattice, while, if we consider some different nonequilibrium state following absorption of RF energy, the populations may be described by the same equation but we will need to replace the lattice temperature with the spin temperature. So that in this case the magnetisation M will be given by:

$$M = \frac{C_H B_0}{T_S} \tag{2-4}$$

In the spin locking experiment, we apply an rf field B_1, which is much smaller than B_0. A 90° pulse in the x direction followed immediately by a $\pi/2$ phase shift so that the magnetisation will be locked in the y direction in the rotating frame. Since $B_1 \ll B_0$ the equilibrium magnetisation in the rotating frame will recover following a different relaxation time from T_1, which we will call $T_{1\rho}$.

2.3.5.3. The Hartmann-Hahn condition

The concepts of spin-diffusion and spin-temperature need now to be used to understand the conditions under which we are able to get cross polarisation. We could consider a spin-diffusion mechanism, such as the one described above for one kind of nucleus, but now used for different kinds of spins, if only we can find a way to turn on the spin-flip mechanism. We need dipolar interactions but the same frequencies for the two spins as well, since as we have seen before the spin-flip process is an energy-conserving process so that no difference in energy can exist between spin systems that undergo spin-flip processes. Realisation of the fact that abundant and rare spins can be brought to the same internal equilibrium in the rotating frame is the basis of the cross-polarisation experiment. Under the condition for which $\omega_I=\gamma_I B_{1I} = \gamma_S B_{1S} = \omega_S$ we establish thermal contact between the rare (S) and the abundant (I) spins, so that the two spin systems, initially at different spin temperatures, can be considered to have reached a common spin temperature in a characteristic time T_{IS}, the cross-polarisation time constant.

Practically, the Hartmann-Hahn condition for carbon is obtained by placing a sample of adamantane in the rotor, spinning at about 2000 Hz (faster spin rates can cause the H-H condition to break up), and observe the FID while changing the power on the carbon channel. When the maximum FID is seen we can consider it to be under H-H conditions. For ^{15}N the procedure is analogous but the sample used is $NH_4{}^{15}NO_3$.

2.4. Acquisition of spectra

The acquisition parameters varied from sample to sample, although some of the parameters were quite similar from one experiment to another: I have mostly set a spectrum width of 33.33 kHz, which means a dwell time of 30.00 μs (the time between two acquisition points is called the dwell time and is the inverse of the spectral width) and I have used 2048 points in most acquisitions, which sets the acquisition time to 61.44 ms. Although the inverse of the acquisition time sets the

real resolution, this parameter must not be much in excess of this value when the decoupler is on during acquisition because too much power might go into the probe. The resolution can be improved in the processing by zero-filling.

2.5. Basic acquisition pulse sequences

The combination of all the techniques seen above allows spectra of dilute spins to be acquired by overcoming all the problems related to observation of non-abundant spins. The pulse sequence shown in figure 1 indicates how the techniques are used together, if we consider that we are simultaneously spinning the rotor at the magic angle.

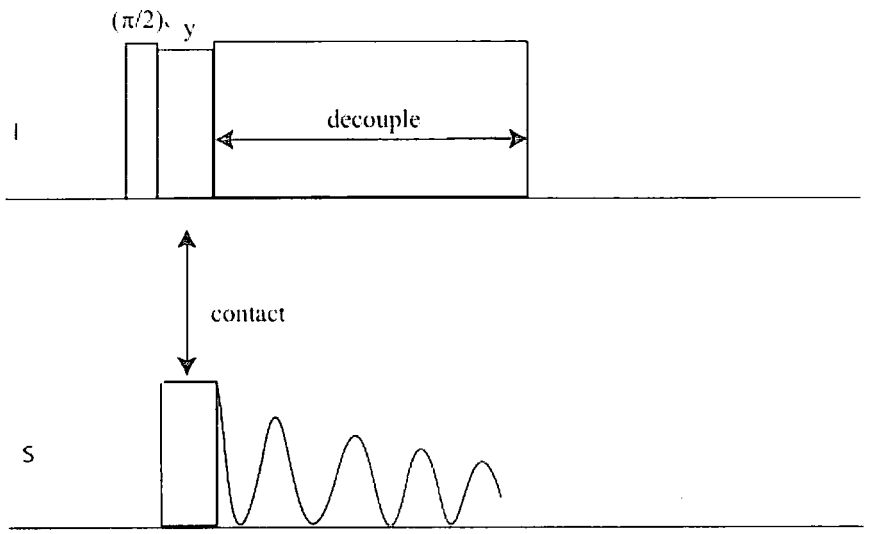

Figure 1. Pulse sequence for cross polarisation.

Sometimes the experiment can be changed by applying a 90° pulse of opposite phase from the first one (i.e. 90°-x if the first one was 90°x) after the acquisition time on the proton channel. This has the effect of flipping back the remaining ^1H magnetisation so that less time is needed before the next cycle of pulses[4]. This is useful only when $T_1\rho(I)$ is greater than the contact time and the time for observation of a single FID, since, in this case, a substantial fraction of the abundant I-spin polarisation will remain at the end of the observation period.

2.5.1. Dipolar dephasing [5, 6]

This is a technique with which it is possible to retrieve only the signals due to quaternary carbons. It is a spectral editing technique, also called non-quaternary suppression.

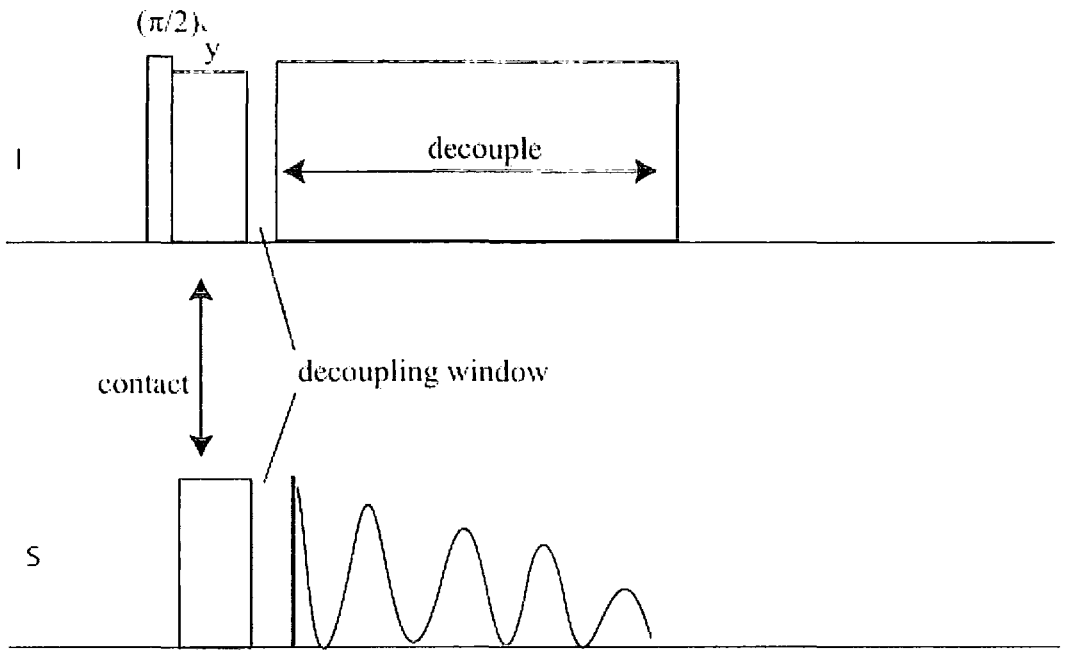

Figure 2. Pulse sequence for dipolar dephasing experiment.

The main difference with the basic experiment is that after the CT a decoupling window is open. The fact that there is no decoupling in this interval allows the protonated carbons to decay faster since they have a strong interaction with the protons to which they are attached and this has the effect of shortening the transverse relaxation time to the extent to which no more signal is seen after a short interval. The decoupling window I have used has been of 50 μs duration, and this seemed to be long enough to be able to differentiate between quaternary and protonated carbons. Methyl groups are possible to be detected as well, with this method, since frequently they undergo rapid internal motion in the solid-state so that the local dipolar field is significantly reduced.

2.6. Experiments using echoes and spinning side band suppression

In most cases, when a more quantitative comparison between quaternary and protonated spectra is needed the actual pulse sequences that can be used differ from the two basic ones that I have just described by the presence of an echo. This means that there is a 180° pulse along x after a short period of time, τ (which in principle has to be the inverse of the spinning rate). This refocuses chemical shifts and allows the subtraction of the peaks from the two spectra (total and NQS) to be straightforward, since all experiments with an echo allow the phase coherence to refocus at the same time after the initial perturbation so that there will be no loss of magnetisation during the experiment. This would cause a different intensity for the respective signals of the two spectra and the subtraction would not be exact. The exact subtraction is of fundamental importance to be able to compare in a precise way the total and the NQS spectra. These two sequences are called, in our laboratory, ancpecho and anDDecho, the first one being shown in figure 3, analogously the NQS experiment.

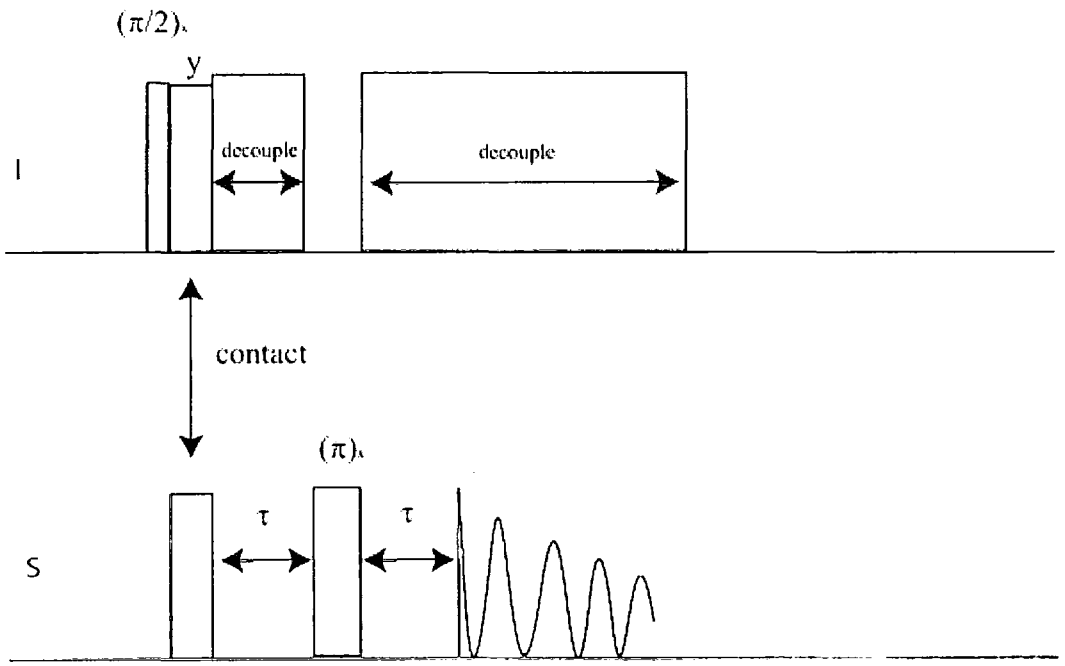

Figure 3. Cross polarisation with echo (ancpecho).

The other difference from the basic CP experiments that I have used has been sideband suppression. TOSS (TOtal Side band Suppression[7]) is a technique that allows only the isotropic peaks to be seen by means of a series of 180° pulses that dephase all but the isotropic peaks.

2.7. A heteronuclear decoupling technique: the TPPM pulse sequence

The most common way to decouple protons in the solid state is by using CW (continuous wave) decoupling, where a strong rf field, is applied to the proton channel during the acquisition, so that a fast nutation of the proton spins is responsible for averaging dipolar interactions between the observed spins and the protons.

I will describe here a different way to obtain heteronuclear decoupling. In particular, this pulse sequence is able to obtain the same effectiveness in decoupling although using less power. It is particularly important to implement these pulse sequences when working at higher field.

A widely used pulse sequence is the TPPM (two pulse phase modulation), which is able to greatly reduce broad linewidths arising from insufficient proton decoupling. This pulse sequence was first introduced by Bennett et al[8] and it is here shown in figure 4, from which we can see a region of the decoupling period expanded so to note the particularity of the pulse sequence, which is the application of rf pulses of length τ_p, alternating between two phases separated by an angle ϕ. Improvement by this decoupling technique is generally good, and it is even able to improve signals from quaternary carbons. When one is to use TPPM, particular attention should be paid to optimisation of both τ_p and ϕ, although generally it is seen that good values for τ_p are ones corresponding to the π pulse duration in the regime of a small angle ϕ (about 5 to 15 degrees). The values must be optimised for different spinning speeds. We must note that the efficiency of the TPPM decoupling technique does vary between the compounds on which it is used.

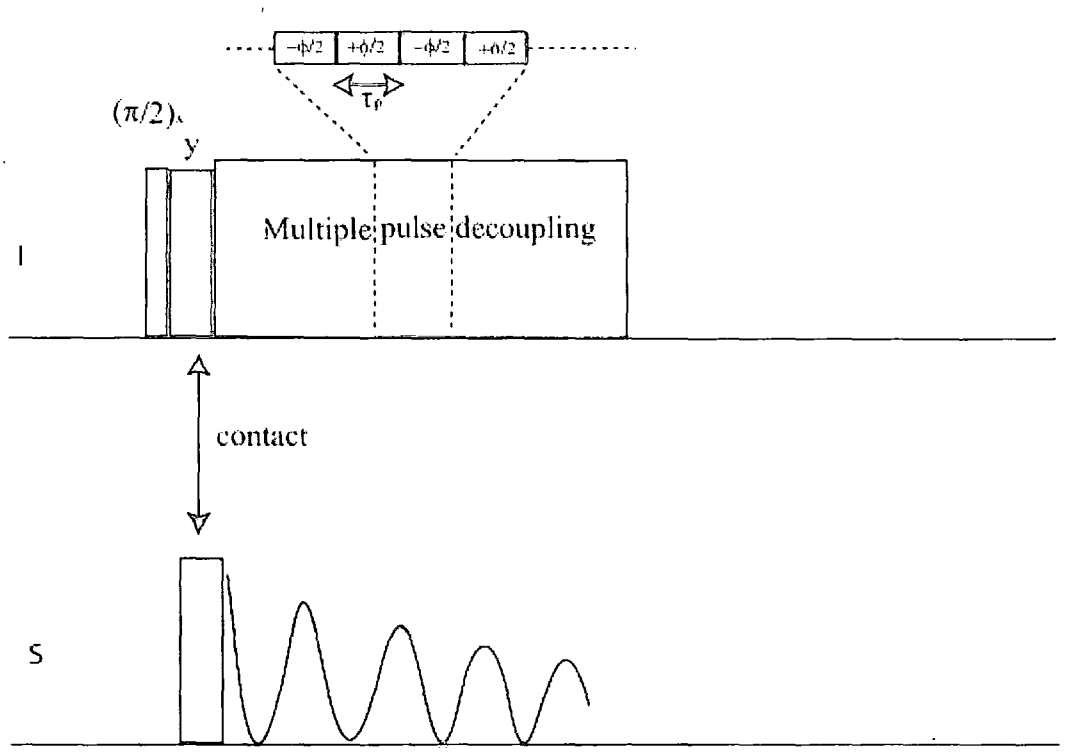

Figure 4. The TPPM pulse sequence for heteronuclear decoupling.

2.8. Relaxation times [9]

Relaxation times measure the time for which the spin system, once in the excited state, will take to go back to its basic state, exchanging energy with the surrounding medium (vibrational motions of the lattice in the case of a solid) and with the nearby nuclei. For relaxation to occur, there needs to be a fluctuating magnetic field at the Larmor frequency. The sources that provide relaxation can be of different natures and I will here briefly introduce them in order to understand the complexity of relaxation phenomena[10]. Like the additivity of rates in any set of parallel reactions, the contributions to the observed T_1 (longitudinal relaxation time) caused by different relaxation mechanisms are additive as reciprocals:

$$\frac{1}{T_1} = \frac{1}{T_1^{DD}} + \frac{1}{T_1^{Q}} + \frac{1}{T_1^{SC}} + \frac{1}{T_1^{CSA}} + \frac{1}{T_1^{P}} + \frac{1}{T_1^{SR}} \qquad (2\text{-}5)$$

where DD = nuclear dipole-dipole relaxation

Q = electric quadrupolar relaxation

SC = scalar interaction

CSA = chemical shift anisotropy

P = paramagnetic relaxation

SR = spin-rotation relaxation

As we can see, the "spin-lattice" relaxation time, T_1, is governed by various factors. As mentioned before, fluctuations from nuclear spins can govern the relaxation, but any nucleus having spin quantum number I greater than ½ is subject to electric quadrupolar relaxation, or, when a nucleus is J-coupled to one or more nuclei, relaxation can occur from fluctuation of the coupling constant (thorough–bond relaxation mechanism). Anisotropy of the chemical shift can also provide a fluctuating magnetic field as the molecule tumbles. Considering that an unpaired spin can act like a nuclear spin with a much larger magnetic moment, the cause of the paramagnetic relaxation time is clear, and, finally, the relaxation could be caused by motion of the molecule that generates a current from the motion of the electrons and a molecular magnetic moment.

Generally, it can be assumed that, for non quadrupolar nuclei, relaxation processes occur mainly as a result of dipolar interactions. The general theory of magnetic dipole-dipole nuclear spin relaxation has been treated thoroughly by Solomon[11]. The derived equation of the dipole-dipole homonuclear relaxation time as a function of the spectral density function J(ω), for two nuclei *i* and j, is:

$$\left(\frac{1}{T_1}\right)_{ij} = \frac{3}{2}\gamma^4\hbar^2 r_{ij}^{-6}\frac{1}{2}\left(\frac{1}{2}+1\right)\left[J_1(\omega_0)+J_2(2\omega_0)\right] \qquad (2\text{-}6)$$

where γ is the gyromagnetic ratio and ω_0 is the Larmor frequency. The spectral density function is a function derived from orientational mobility of the internuclear axis. By considering the form of these density functions in terms of the correlation time, we can obtain the following useful equation for like nuclei:

$$\left(\frac{1}{T_1^{DD}}\right)=\frac{2}{5}\gamma^4\hbar^2\frac{1}{2}\left(\frac{1}{2}+1\right)r_{ij}^{-6}\left(\frac{1}{1+\omega^2\tau_c^2}+\frac{4}{1+4\omega^2\tau_c^2}\right)\tau_c \qquad (2\text{-}7)$$

With this equation, considering variable temperature experiments (in which we monitor how the relaxation time varies with temperature), enable the determination of τ_0 and the activation energy needed to jump between rotational sites, E_a, by considering Arrhenius form for which:

$$\tau_c=\tau_0\exp\left(\frac{E_a}{RT}\right) \qquad (2\text{-}8)$$

When we are dealing with heteronuclear relaxation times, (and this will be the case in this thesis for variable temperature relaxation times measured for ^{15}N), the equation is slightly different, taking into consideration the frequencies of both the spins involved[10]:

$$\left(\frac{1}{T_1^{DDU}}\right)=\frac{2}{5}\gamma_X^2\gamma_S^2\hbar^2\frac{1}{2}\left(\frac{1}{2}+1\right)r_{XS}^{-6}\left(\frac{1}{1+(\omega_S-\omega_X)^2\tau_c^2}+\frac{3}{1+\omega_X{}^2\tau_c^2}+\frac{6}{1+(\omega_S+\omega_X)^2\tau_c^2}\right)\tau_c \qquad (2\text{-}9)$$

where the subscripts X and S are for the nucleus being observed and the nucleus causing relaxation, respectively.

We can apply all the considerations above to a different relaxation time, which is $T_{1\rho}$, the spin-lattice relaxation time. Analogously, the form of this relaxation time as a function of the correlation time for homonuclear pairs of nuclei, can be written as[12]:

$$\left(\frac{1}{T_{1\rho}^{DD}}\right)=\frac{3}{20}\gamma^4\hbar^2I(I+1)r_{ij}^{-6}\left(\frac{1}{1+\omega_0{}^2\tau_c^2}+\frac{4}{1+4\omega_0{}^2\tau_c^2}+\frac{4}{1+4\omega_1{}^2\tau_c^2}\right)\tau_c \qquad (2\text{-}10)$$

Where ω_1 is the frequency equivalent of the B_1 field ($\omega_1=\gamma B_1$). These equations prove useful for analysis of relaxation time curves as a function of temperature. Analogously when considering the heteronuclear case, for $T_{1\rho}$ the equation to use will be[13]:

$$\left(\frac{1}{T_{1\rho}^{DDU}}\right)=\frac{2}{20}\gamma^4\hbar^2 I(I+1)r_{ij}^{-6}\left(\frac{3}{\left(1+\omega_0^2\tau_c^2\right)}+\frac{2}{1+\omega_1^2\tau_c^2}+\frac{1}{2\left(1+(\omega_S-\omega_X)^2\tau_c^2\right)}+\frac{3}{2\left(1+\omega_X^2\tau_c^2\right)}+\frac{3}{1+(\omega_S+\omega_X)^2\tau_c^2}\right)\tau_c \quad (2\text{-}11)$$

2.8.1. Longitudinal relaxation time measurements

I have measured such relaxation times for protons, indirectly via the carbon signal, by irradiating the protons prior the cross-polarisation[14]. The basic pulse sequence to measure T_1 is **[180°-τ-90° (FID)-ad]** where **ad** is the acquisition delay (which must be at least $5T_1$) and the 90° is called the "read pulse" since it is there only to bring back the z magnetisation on to the x-y plane in which there is the detector. After the 180° pulse the magnetisation (which is now along –z) starts to decay due to spin-lattice relaxation effects and the decay can usually be described by the equation:

$$M_{z(t)} - M_0 = (M_{z(0)} - M_0)[\exp(-\tau/T_1)]. \quad (2\text{-}12)$$

The pulse sequence is shown in figure 5.

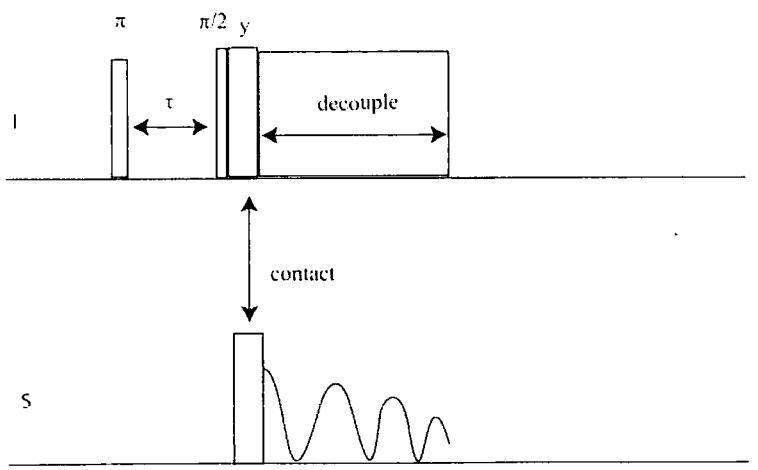

Figure 5. The relaxation time experiment for measuring proton T_1.

The actual pulse sequence that I have used is slightly different, and it can be divided into two different parts. In the first part there is a normal T_1 pulse sequence followed by CP and ^{13}C acquisition (as shown for the sequence in figure 5), whereas in the second part there is a normal cross-polarisation experiment (as seen in figure 6). The two FIDs are subtracted before processing, so that, instead of having a series of peaks ranging from $-M_0$ to M_0 as in a simple T_1 measurement, we have a series of peaks which are all positive ranging from $2M_0$ when $\tau=0$ (the signal from the second acquisition being the same in absolute value as the one from the first acquisition but opposite in sign) to a null signal when τ approaches infinity (and the two signals are exactly the same). This pulse sequence has been designed in order to minimise errors due to any spectrometer drifts. The pulse program is called T1HCP. A simple exponential decay curve can be used to fit the data.

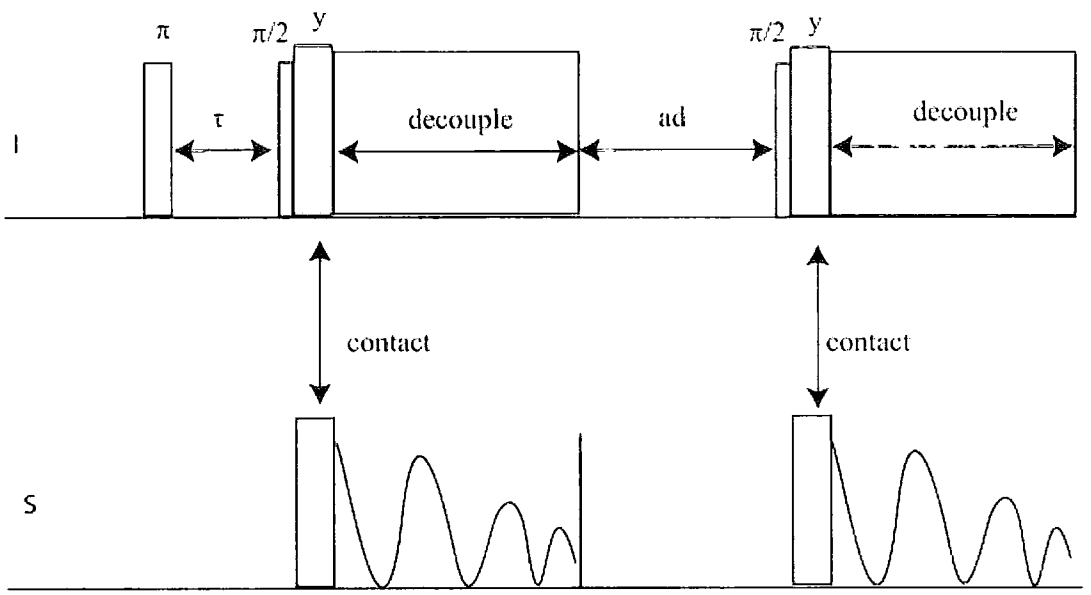

Figure 6. T_1HCP pulse sequence for measuring proton T_1

In order to observe relaxation times from nuclei other than proton (rare nuclei) the pulse sequence T_1XCP was used. The scheme is shown in figure 7.

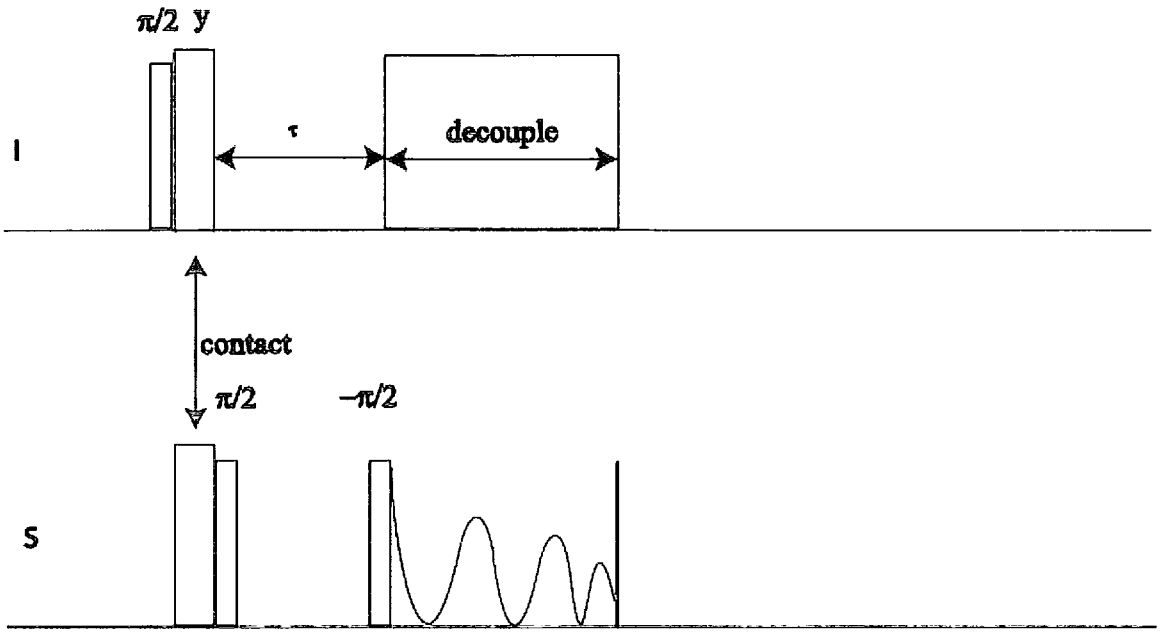

Figure 7. The T_1XCP experiment for measuring T_1 of the X nucleus.

2.8.2. Spin-lock relaxation time measurements

Another important parameter to measure is the proton relaxation time in the rotating frame, $T_{1\rho}$. This gives information about motions of the order of tens of kHz whereas T_1 depends on motions of the order of hundreds of MHz.

For $T_{1\rho}$ measurements I have used a series of normal cross polarisation experiments in which I have varied the contact time used; varying the contact time will have the effect of varying the intensity of the signal, since during this time the magnetisation flows from proton to carbon. The equation used has been:

$$M(t) = M_0[\exp(-\tau_{CP}/T_{1\rho}) - \exp(-\tau_{CP}/T_{IS})] \qquad (2\text{-}13)$$

The other way to measure $T_{1\rho}$ is to employ the pulse sequence shown in figure 8, where a variable spin-lock RF field is used, and an exponential decay curve will be seen as this RF field becomes longer in duration. I have used both methods for comparison.

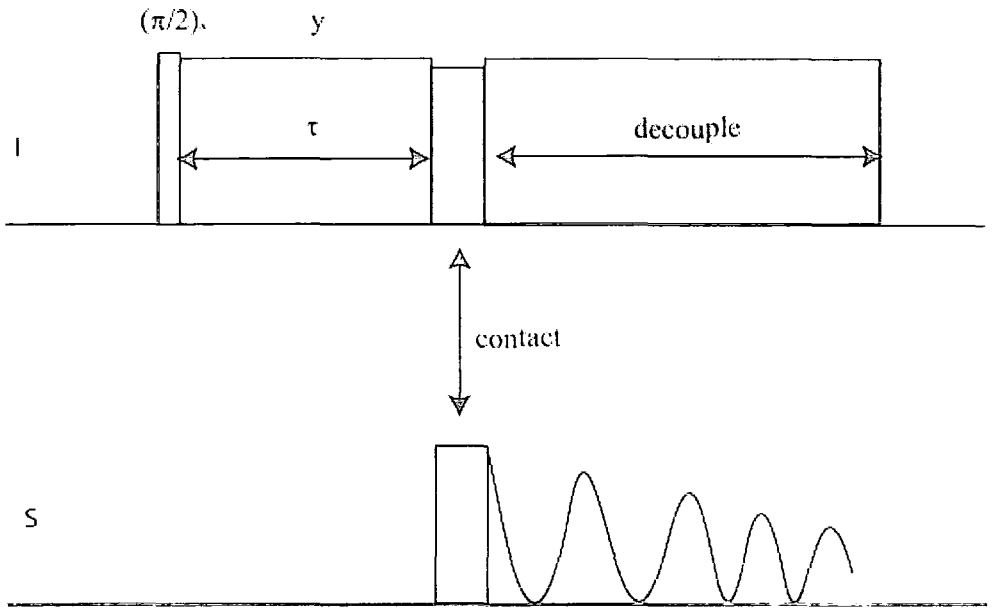

Figure 8. Variable spin-lock experiment to measure $T_{1\rho}$.

2.9. Variable temperature operation

The probes that I have been using were suitable to carry out VT experiments, and the viable temperature range is from 123 to 523 K. Most of the experiments in this PhD work involved high-temperature operation. Because of the long relaxation times of most of the samples, low temperature work would make experiments quite long. The variable temperature operation is carried out differently whether we need to use high or low temperatures. For low temperature, nitrogen gas (for temperatures below 263 K) or air (for temperatures between room temperature and 263 K) is cooled by passage through a copper coil that is immersed in a dewar of liquid nitrogen. The temperature is controlled by a thermocouple that measures the temperature of the outlet gas and eventually heats the gas if necessary. It is important to calibrate the actual sample temperature with respect to the thermocouple reading.

One of the most widely used temperature calibration methods in the MAS NMR experiment is based on the use of the measurement of the frequency difference ($\Delta\nu$)

between resonances for the methyl and the hydroxyl protons of methanol, in the 1H NMR spectrum of a sample of tetrakis (trimethylsilyl)silane (TTMSS) soaked in liquid ethanol[15].

This technique was proposed by van Geet[15], and the equation used by him is reported in the article by Aliev[15]. The equation, modified for the CMX 200 spectrometer, is

$$T_{cal}(K) = 403.0-0.1475*|\Delta\nu(Hz)|-(0.00059*|\Delta\nu(Hz)|^2 \qquad (2\text{-}14)$$

The results for the HXY probe are shown in graph 1. Since no previous calibration was done for this probe, I have carried out this operation with a great number of points. The graph shows the calibration for a spin rate of 4 kHz although changing the spinning speed between 2 kHz and 5 kHz did not change the calibration significantly.

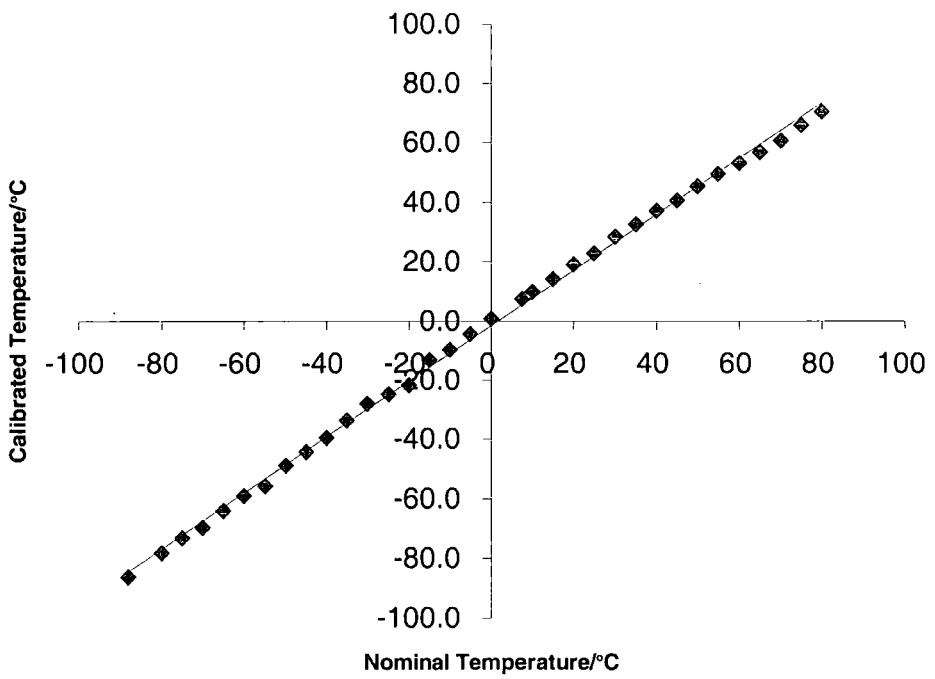

Figure 9. Calibration of the temperature for the HXY probe, where the equation found for the correction is Tcal= 0.94(Tnom) - 1.7, with an R^2 value of 0.9985.

As can be seen from figure 9, the differences are of a maximum of 8 percent between the nominal temperature (the one read from the temperature control unit) and the calibrated temperature. The coefficient in the equation found for correction (Tcal=0.94(Tnom)-1.7), denotes only a small correction is needed.

2.10. WISE [16]

An important experiment to investigate the existence of mobility in a system (although generally it is used on polymer systems[17, 18]) is the WISE (Wideline Separation) experiment (Figure 10). This heteronuclear 2D NMR technique allows investigation of structural and dynamic information. It is an important experiment that correlates faster motions of fragments of molecules or polymers with ^{13}C or ^{15}N chemical shifts. In fact, in heterogeneous systems, the dynamics of the individual components cannot be derived from 1D spectra without a priori assumptions, WISE overcomes this problem. Differences of molecular dynamics are probed by ^{1}H wideline shapes, where broad lines arise from rigid conformations and narrow lines from averaging due to mobility, and these are separated in the second dimension by the dilute spin chemical shift. The simplest version of this experiment just places an incremented delay t_1 after the initial ^{1}H 90° pulse[19]. This allows the detection of the decay of the proton magnetization through amplitude modulation for the magnetisation of the dilute spin, generated by cross polarisation. Fourier transformation over t_1 and t_2 provide ^{1}H wideline spectra separated by the corresponding ^{13}C or ^{15}N chemical shifts.

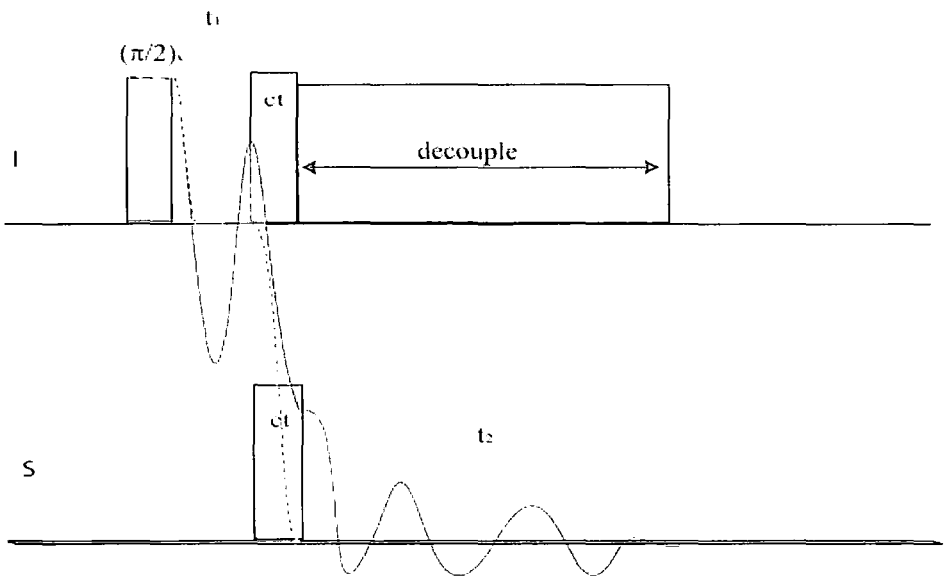

Figure 10. Pulse program for WISE. The thick line represents the magnetisation of a mobile group, the dashed line that of a rigid group.

It is very important for this experiment to avoid spin diffusion, so that it is advisable to use short contact times.

2.11. Evolution of the spin systems

In most of the descriptions here and in the course of this thesis, it has been possible to describe the magnetisation as a vector, which is a very good method to visualise spin behaviour for simple systems. But this method has a limit, especially when we think that the simple concept of spin does not have a classical mechanics analogue magnitude and it is only a quantum mechanical observable, so that quantum mechanical methods should rigorously be used for the study of spin systems.

2.11.1. The density matrix

The evolution of the spin system is determined by the spin Hamiltonian. The theory used to follow the evolution is known as density matrix formalism[20, 21]. The density matrix, ρ, describes the probability that each spin within the ensemble

considered is in a certain spin state at any given time, and it describes the evolution of the entire spin system.

The equation of motion is given by the Liouville-von Neumann equation.

$$\frac{\hbar}{i}\frac{d\rho}{dt} = -\left[\hat{H}, \rho\right] \qquad (2\text{-}15)$$

For a time-invariant Hamiltonian, integration yields the density matrix describing the state of the spin ensemble at any given time.

$$\rho(t) = U^{-1}(t)\rho(0)U(t) \qquad (2\text{-}16)$$

where U(t) is the spin evolution operator, or propagator, given by

$$U(t) = \exp(-I\hat{H}\,t) \qquad (2\text{-}17)$$

This small introduction to the density matrix should be needed especially when treating more complicated experiments such as REDOR.

2.12. REFERENCES

1) H. OuLin, N. C. Baezinger and J. K. Guillory, *J. Pharm. Sci.* 1974, *63*, 145.

2) R. K. Harris,*Multinuclear magnetic resonance in liquids and solids-chemical applications* Maratea, 1988.

3) R. K. Harris,*Nuclear Magnetic Resonance Spectroscopy- a physicochemical approach* Longmans, 1987.

4) J. Tegenfeld and U. Haeberlen, *J. Magn. Reson.* 1979, *36*, 453.

5) S. J. Opella and M. H. Frey, *J. Amer. Chem. Soc.* 1979, 5854.

6) K. W. Zilm *Encyclopedia of NMR, 'Spectral editing techniques'*; D. M. Grant and R. K. Harris, Ed.; Wiley, 1996; Vol. 7, pp 4498.

7) E. T. Olejnnicczac, S. Vega and R. G. Griffin, *J. Chem. Phys.* 1984, *81*, 4808.

8) A. E. Bennett, C. M. Rienstra, M. Auger, K. V. Lakshmi and R. G. Griffin, *J. Chem. Phys.* 1995, *103*, 6951.

9) C. P. Poole and H. A. Farach,*Relaxation in magnetic resonance*; Academic Press: New York, 1971.

10) J. L. Sudmeier, S. E. Anderson and J. S. Frye, *Concepts Magn. Reson.* 1990, *2*, 197-212.

11) I. Solomon, *Phys. Rev.* 1955, *99*, 559.

12) D. C. Look and I. J. Lowe, *J. Chem. Phys.* 1966, *44*, 2995.

13) R. A. Komoroski,*High resolution NMR Spectroscopy of Synthetic Polymers in Bulk*; VCH publishers Inc.: Denton, 1986.

14) D. Torchia, *J. Magn. Reson.* 1987, *30*, 613.

15) A. E. Aliev and K. D. M. Harris, *Magn. Reson. Chem.* 1994, *32*, 366.

16) K. Schmidt-Rohr, J. Clauss and H. W. Spiess, *Macromolecules* 1992, *25*, 5273.

17) S. Lehmann, A. D. Meltzer and H. W. Spiess, *J. Polym. Sci.* 1998, *36*, 693.

18) K. Nagapudi, J. Hunt, C. Sheperd, J. Baker and H. W. Bekham, *Macromol. Chem. Phys.* 1999, *200*, 2541.

19) K. Schmidt-Rohr and H. W. Spiess,*Multidimensional solid-state NMR and polymers* San Diego, 1994.

20) T. C. Farrar, *Concepts Magn. Reson.* 1990, *2*, 1.

21) T. C. Farrar, *Concepts Magn. Reson.* 1990, *2*, 55.

Chapter 3

X-RAY DATA OF SULFANILAMIDE

3.1. Introduction

The existence of polymorphic forms of sulfanilamide has been known since 1938 when, recrystallising from a drop of water, Zyp[1], under microscope examination, observed three different crystal forms. Watanabe[2, 3] conducted an X-ray diffraction study of sulfanilamide crystallised from various solvents, and he also determined that the compound crystallised in at least three different polymorphic modifications, which he designated as α-, β-, and γ forms. The first time four forms were mentioned was in the X-ray book of McLachlan[4] where he calls them by the names of β-, γ-, δ-, ε-. X-ray diffraction (neutron diffraction only for β sulfanilamide) has been used to clarify the crystal structures of the polymorphic forms of this compound. O'Connor and Maslen have determined the structures of α-sulfanilamide[5] and of β-sulfanilamide[6], while Alleaume and Decap have reported the structures of β[7]-and γ-sulfanilamide[8].

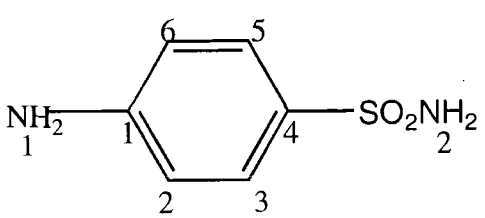

Figure 1. Sulfanilamide

Although these structures already existed in the literature, we needed, for our purposes, especially for shielding calculations (see chapter 5), better quality ones since the original results did not have the coordinates of the protons attached to the nitrogens, at least for the α and γ forms. We also have a new crystal structure, the one for the δ form. The β, γ and δ crystals structures were run in Southhampton. As for the α form, crystal data were obtained here in Durham, since I had obtained good crystals of α.

The crystal data of the four forms are shown in table 1, in which we can see that the space groups for α and δ are Pbca where β and γ have $P2/_{1c}$. The dimension of the cells are all quite different.

	alpha	beta	gamma	delta
space group	**Pbca**	**$P2_1/c$**	**$P2_1/c$**	**Pbca**
a(Å)	14.592	8.869	7.824	9.706
b(Å)	5.571	8.915	12.991	8.679
c(Å)	18.472	9.962	7.620	17.890
α(°)	90.00	90.00	90.00	90.00
β(°)	90.00	110.40	104.97	90.00
γ(°)	90.00	90.00	90.00	90.00
Z	8	4	4	8
n	1	1	1	1

Table 1. Space groups and unit cell dimensions for the four forms. Z is the number of molecules per unit cell, and n is the number of molecules per asymmetric unit.

3.2. Intramolecular data

The reason why very careful analysis of the bonds and angles is needed, is to understand whether the differences in the isotropic chemical shifts and anisotropy values measured for nitrogen, and all other solid-state NMR experimental parameters, are in any way related to the conformational differences of the three polymorphs. Obviously careful analysis of intermolecular data is needed as well. I analyse in table 2 the bonds of the benzene ring. Since none of the three forms displays a dihedral angle C(3)-C(4)-S-N(2) of 90°, as we will see further in more detail, the numbering of the phenylene ring was arbitrarily chosen, so that C(3)-C(4)-S-N(2) was the dihedral angle bigger than 90°.

Bond	α	β **(X-ray, *neutron diffraction*[7])**	γ	δ
C(1)-C(2)	1.401	1.408 *1.390 ε=0.0024*	1.391	1.390
C(2)-C(3)	1.381	1.384 *1.379 ε=0.0019*	1.380	1.374
C(3)-C(4)	1.393	1.396 *1.402 ε=0.0020*	1.392	1.382
C(4)-C(5)	1.398	1.398 *1.401 ε=0.0020*	1.387	1.392
C(5)-C(6)	1.375	1.381 *1.382 ε=0.0027*	1.383	1.379
C(6)-C(1)	1.405	1.408 *1.390 ε=0.0031*	1.389	1.393

Table 2. Benzene ring bond lengths (Å) for the four polymorphs of sulfanilamide (errors on X-ray data: 0.002 Å).

where ε is the error from the neutron diffraction data. From this table we can see that:

(i) for α sulfanilamide there are differences between chemically equivalent pairs of bonds within the ring meaning that the molecule is not symmetrical according to the long axis. This is slightly more evident in this form than in others.

(ii) very differently, for β sulfanilamide, there is a very pronounced symmetry along the long axis. The shortest bonds are C(2)-C(3) and C(5)-C(6) suggesting that there is some contribution from the resonance form shown in figure 2:

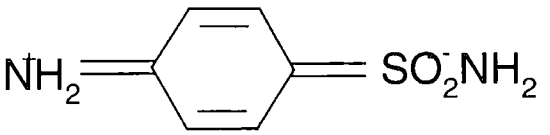

Figure 2. Resonant form of importance for the β form.

(iii) for γ sulfanilamide the ring seems to be quite distorted, and in general the bonds are quite shorter than in the previous two forms: the average value for the γ form is 1.387 Å where for the previous two the values were 1.392 Å and 1.396 Å respectively for α and β.

(iiii) for the δ form, the bonds are even shorter, the average value here is 1.385 Å, which is considerably shorter than the average value for crystalline benzene (1.392 Å calculated by Cox et al. [9]) .

These considerations are very well summarised when looking at a chart of the bonds of the four forms; see chart 1.

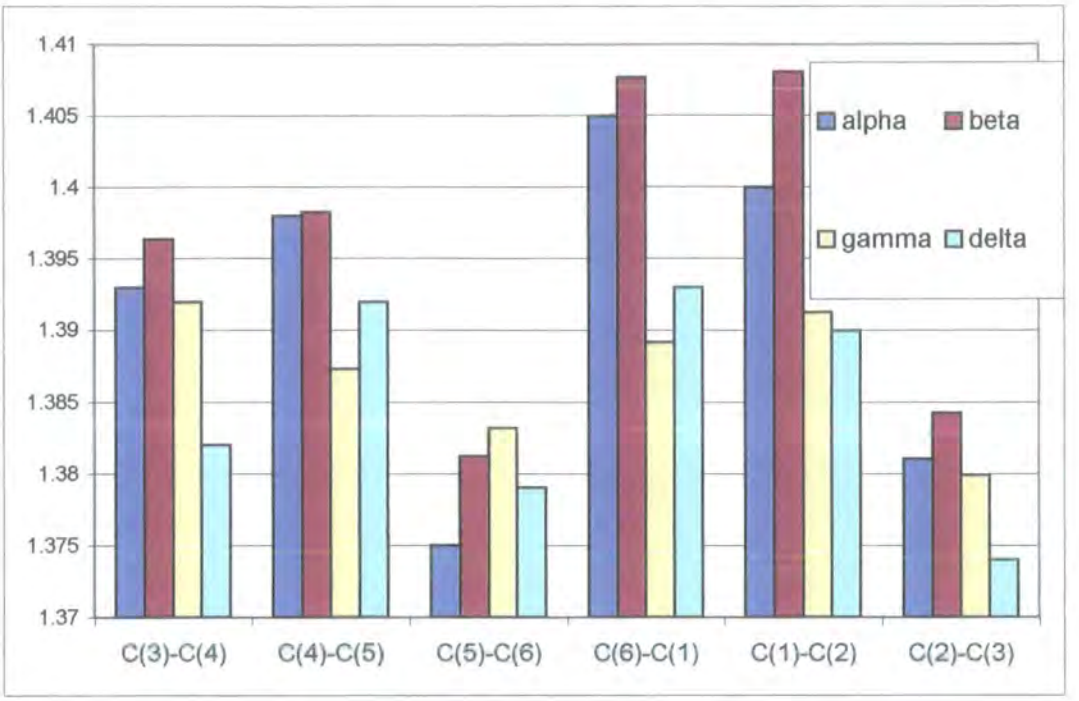

Chart 1. Bonds of the benzene ring of the sulfanilamide forms.

I have also compared the values of the benzene ring for sulfathiazole[10-12], which is presently known to have five forms (note that the numbering of the polymorphs is different from the Cambridge Crystallographic Data Base since I have followed the numbering used in the work carried out with the solid state NMR[13]). For sulphathiazole polymorphs the one that has the strongest contribution from a resonance form, like that in figure 2, is polymorph IV, although it has a mean value of 1.386(5) Å for the benzene rings that is less than that of the β form of sulfanilamide. In the other forms the values range from 1.382(5) to 1.389(6) Å, which are still shorter than the benzene ring.

Now we can take a look at how non-aromatic ring bonds differ; before doing this it is necessary, though, to define the numbering of the atoms more precisely, as in figure 3:

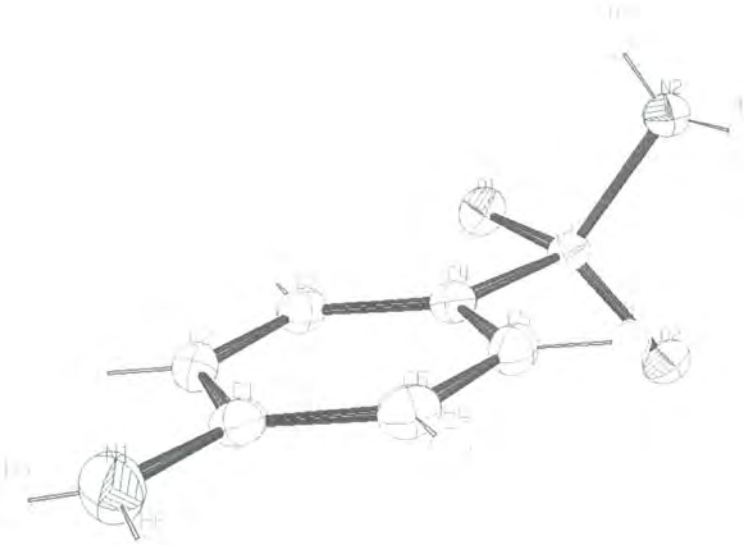

Figure 3. α-sulfanilamide. The numbering in this molecule is the one followed for comparison of the crystal data.

Bond	α	β	γ	δ
C(4)-S(1)	1.750	1.750 *1.750 ε=0.0018*	1.749	1.748
C(1)-N(1)	1.375	1.368 *1.385 ε=0.0026*	1.377	1.381
S(1)-O(1)	1.445	1.446 *1.454 ε=0.0017*	1.444	1.441
S(1)-O(2)	1.440	1.440 *1.448 ε=0.0014*	1.439	1.435
N(2)-S(1)	1.618	1.614 *1.620 ε=0.0016*	1.620	1.611

Table 3. Lengths of bonds that include hetero-atoms(Å)_(errors on X-ray data: 0.002Å).

The S-C bond length is consistently shorter than it should be in a single bond, if we compare it with the S-C single bond distance of 1.82 Å calculated by Abrahams[14], which is close to the sum of the covalent radii. Also, I have compared it with values from about 60 structures taken from the Cambridge Crystallographic Database with

the sulfamide group attached to a benzene ring, and they mostly had distances between 1.766 and 1.773. The values for sulfanilamide are at the lower limit of this search. From this it seems reasonable to think that there is some degree of double bond-character for S-C in these compounds, probably involving the vacant d-orbitals of sulfur.

In sulfathiazole this bond ranges from 1.745(5) to 1.769(6), covering quite a large range but still being on the short side. I have compared it also with the same bond present in the group of sulfathiazole solvates that is presented in chapter 6 and for these the range is quite big, since the minimum value is found to be 1.699 and the maximum 1.760.

The C-N bond lengths for the sulfanilamide polymorphs are shorter than a single C-N bond, for example in sulfanilic acid in which the C-N bond is 1.49 Å, and this also should account for a degree of double bond, especially when we consider that for the β form we find the shortest value, confirming the resonant form shown above (figure 2) of the β form.

In sulfathiazole polymorph IV the same bond is 1.401 Å, whereas polymorph III (which has two molecules in the asymmetric unit) has values of 1.399 and 1.422 Å. Polymorph I has values which are closer together, i.e. 1.368 Å for one molecule and 1.382 Å for the other molecule. For the sulfathiazole solvates it ranges from 1.302 to 1.385, with most of the values between 1.361 and 1.365, which is lower than the values shown for sulfanilamide.

The difference between the two bonds S-O(1) and S-O(2) in the sulfanilamide polymorphs might be caused from different hydrogen bonding within the crystal. For all the forms, but α, the difference between these bonds is 0.006, with O(1) longer than O(2), for α it is 0.005 (although within experimental error). This might reflect the fact that for this form the hydrogen bonds involving the oxygens have the greatest difference between each other, as will be discussed further.

Angles	α	β	γ	δ
O(1)-S-O(2)	118.5°	118.3° *118.2° ε=1°*	118.4° ε=0.9 °	118.2°
N(2)-S-O(1)	107.1°	107.1 *107.2° ε=1°*	106.3° ε=0.8 °	105.8°
N(2)-S-O(2)	105.5°	105.2° *105.5° ε=1°*	105.9° ε=0.9 °	106.8°
C(4)-S-O(1)	107.1°	107.0° *107.5° ε=1°*	108.0° ε=0.7°	107.5°
C(4)-S-O(2)	108.3°	107.2° *107.8° ε=1°*	108.2° ε=0.9 °	107.6°
C(2)-C(1)-N(1)	120.2°	120.9° *120.9° ε=2°*	119.5° ε=1.8 °	120.7°
C(6)-C(1)-N(1)	120.8°	120.4° ε=2 ° *120.4° ε=2°*	119.0° ε=1.6°	128.0°

Table 4. Values for angles (errors : 0.1°, for angles including more than one carbon 0.2°)

From this table we see that angles vary very little from one polymorph to the other. The sulfamide group is approximately tetrahedral. The angle O(1)-S-O(2) (about 118°, for all the polymorphs) is much larger than the tetrahedral value, while N(2)-S-O(1) is smaller and also N(2)-S-O(2), although by a smaller amount. This indicates that the tetrahedron is distorted in a manner consistent with minimum steric hindrance.

3.2.1. Dihedral angles

The biggest differences for the isolated molecules of sulfanilamide polymorphs are in the dihedral angle of the sulfonamide group. In table 5 I have considered the angles clockwise when looking down at the molecule from the amino group, as in

figure 3, as positive values and anticlockwise as negative values. I have written all the angles so that they were less than 180°.

dihedral angles	alpha	beta	gamma	delta
C(3)-C(4)-S(1)-N(2)	124.2	108.2	91.4	97.1
C(5)-C(4)-S(1)-O(2)	54.8	42.4	29.4	30.7
C(3)-C(4)-S(1)-O(1)	8.2	-8.8	-24.2	-18.2

Table 5. Values of the dihedral angles (errors 0.1°)

The other dihedral angles to be considered are the ones containing the amino group. We can see from table 6 is that, if we consider the same orientation as before, so we are looking at the molecule from the amino group, now the positive is counter-clockwise and the negative clockwise. So for the α and δ forms the amino group is on the opposite face of the phenylene ring than for the β and γ forms.

dihedral angles	alpha	beta	gamma	delta
C(2)-C(1)-N(1)-H(5)	10.4	-14.4	-20.9	22.8
C(6)-C(1)-N(1)-H(6)	-21.0	17.5	17.6	-20.2

Table 6. Values of the dihedral angles of the amino group (errors 0.1°).

Another way to see the planarity of groups is to add the values, as shown in table 7.

	alpha	beta	gamma	delta
H(6)-N(1)-C(1)	115.5	117.6	118.2	111.8
H(6)-N(1)-H(5)	123.2	116.7	113.0	117.7
H(5)-N(1)-C(1)	114.1	118.6	118.8	116.1
sum	**352.8**	**352.9**	**350.0**	**345.6**
H(8)-N(2)-S(1)	112.6	114.1	109.4	114.4
S(1)-N(2)-H(7)	114.1	114.7	114.1	113.0
H(7)-N(2)-H(8)	115.3	110.3	112.4	112.8
sum	**342.1**	**339.1**	**335.8**	**340.2**

Table 7. Sum of the angles for the amino group and for the nitrogen of the sulfamide group (errors 0.1°).

From this table we can see that in general the amino group involving N(1) has groups that are closer to planarity (nearer to a value of 360°), meaning less distortion of this group, that just might be in relation with the fact that this nitrogen is involved in less strong hydrogen bonds for all the polymorphs (see tables 8,9,10, 11). Among the polymorphs, considering N(1), it is α and β that have the amino group closer to planarity, and the δ form displays the greatest distortion, instead when considering N(2) it is the γ form that displays the greatest distortion.

3.3. Intermolecular data

From the X-ray data that were obtained in Southhampton, and here in Durham, I have also looked at the hydrogen bonding distances. All the hydrogen bonding is due to NH donors and S=O acceptors. For the α form the molecules pack into layers that are parallel to the to the c axis. Each molecule bonds to four others in the same layer by means of two strong (2.96 Å) and two very weak (3.20 Å) hydrogen bonds. The layers of molecules are linked by weak (3.07 Å) N-H....O bonds. The values of the hydrogen bonding distances are given in table 8, and a representations of the crystal structure and of the hydrogen bonding within it is in Figure 4.

	Contact	Distance (Å)
α		
	O(2) ....N(1)	3.20
	O(1) ....N(1)	3.07
	O(1) ....N(2)	2.99
	O(2) ...N(2)	2.96

Table 8. Contacts among oxygen and nitrogen atoms for the α polymorph

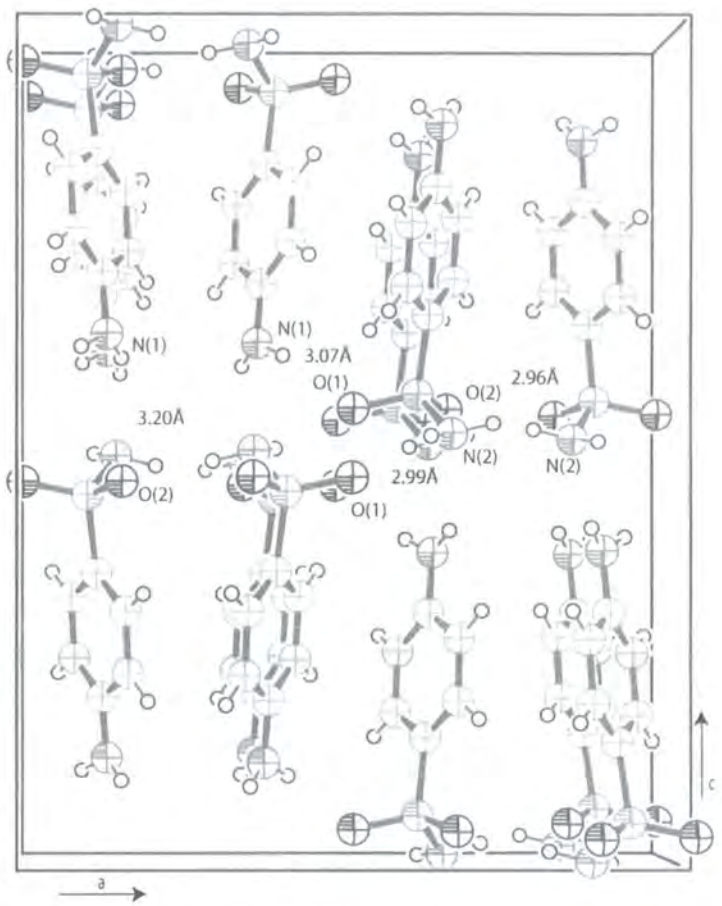

Figure 4. α sulfanilamide cell view a=1 b=1 c=1.

For the β polymorph the hydrogen bonding also is among both hydrogens and both oxygens although the shortest distance between N(1) and O(2) of is 3.22 Å which is starting to be a little too long for an hydrogen bonding. The packing of this form is not organised in layers as for the previous form.

	Contact	Distance (Å)
β		
	O(2).... N(1)	3.03
	O(2).... N(2)	3.00
	O(1).....N(2)	3.10
	O(2).... .N(1)	3.22

Table 9. Contacts among oxygen and nitrogen atoms for the β polymorph.

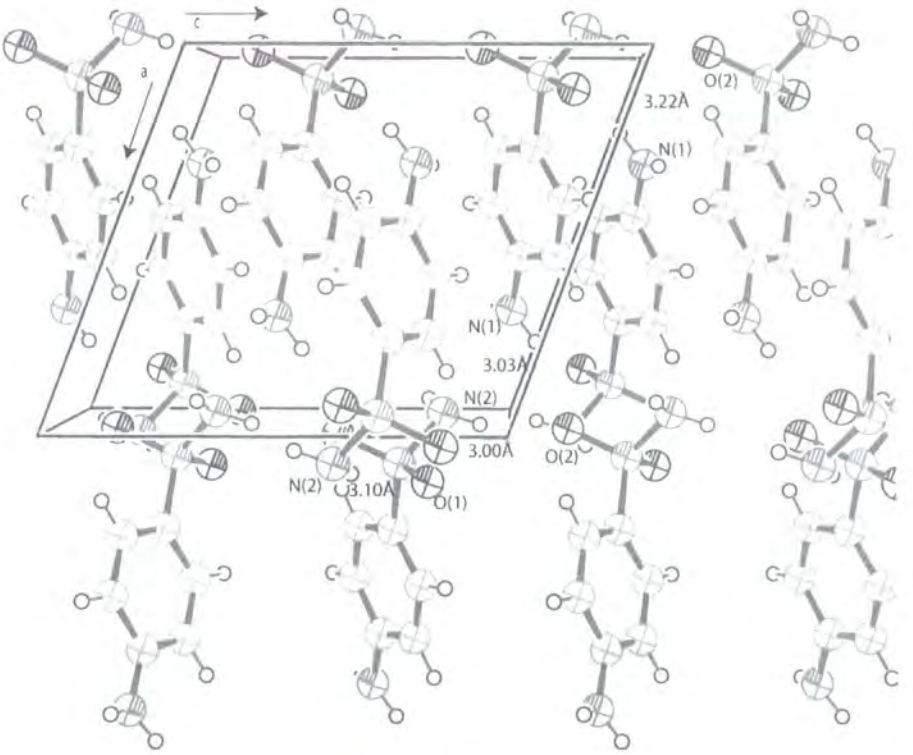

Figure 5. β polymorph packing, cell view a=1,b= ½, c=2 since it can show all the bonds.

For γ polymorphs the values are shown in table 10. Also this polymorph packs in layers, though here these are parallel to b, a representation is given in Figure 6.

	Contact	Distance (Å)
γ		
	O(1)....N(1)	3.17
	O(2)....N(1)	3.18
	O(1).....N(2)	3.01
	O(2).....N(2)	3.00

Table 10. Contacts among oxygen and nitrogen atoms for the γ polymorph.

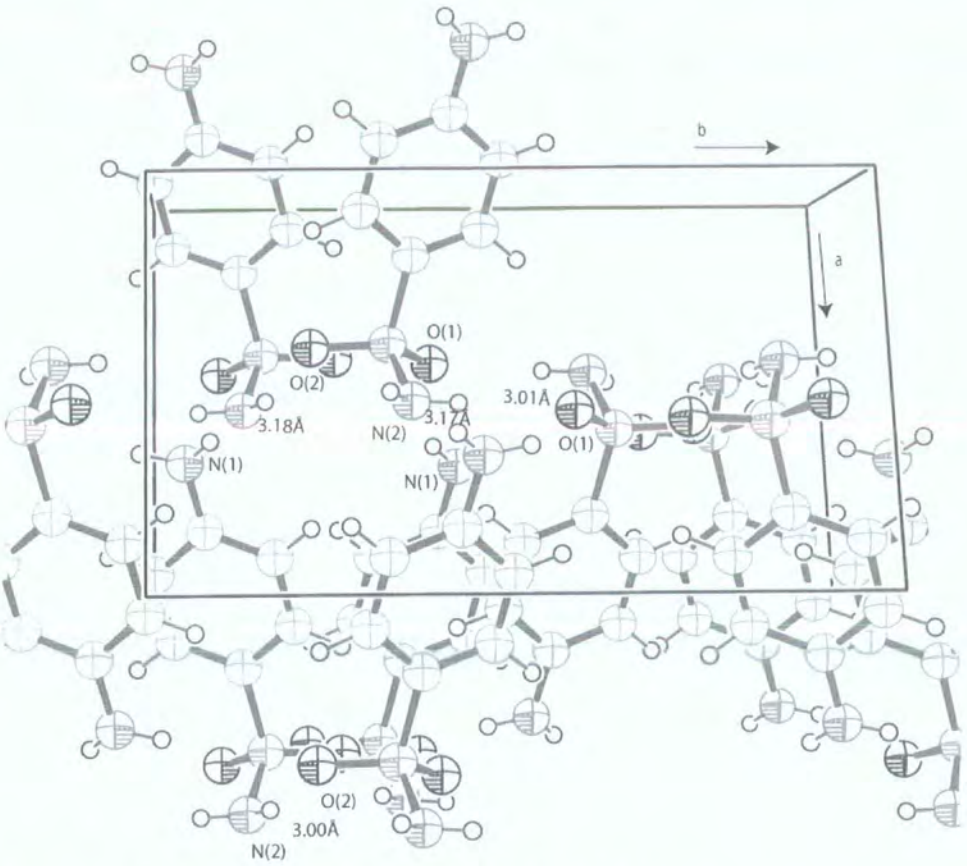

Figure 6. γ polymorph packing a=1/2, b=1,c=1 view.

For the δ polymorph three of the contacts considered involve N(2) where only one involves N(1); the contacts are shown in table 10.

	Contact	Distance (Å)
δ		
	O(2)….N(1)	3.14
	O(1)…..N(2)	3.02
	O(1)…..N(2)	2.99
	O(2).....N(2)	3.07

Table 11. Contacts among oxygen and nitrogen atoms for the δ polymorph.

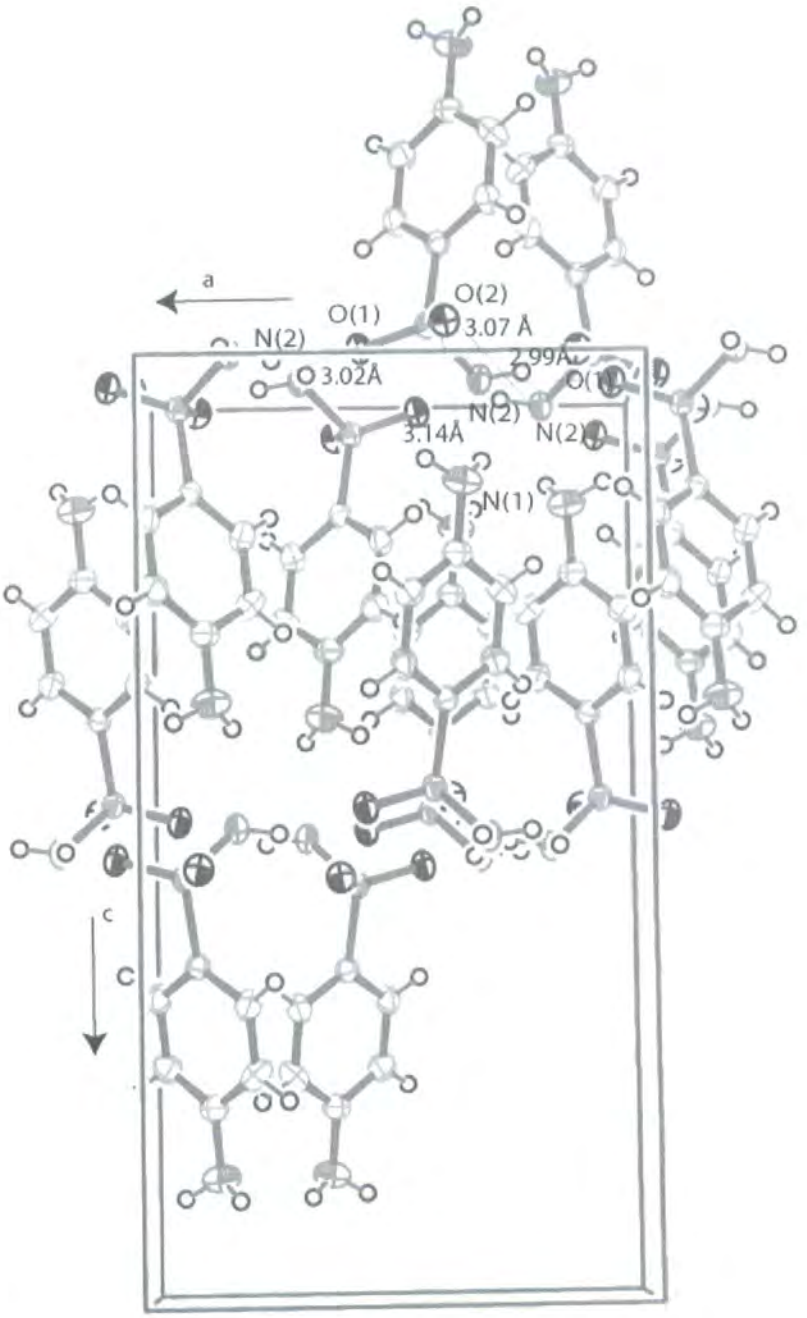

Figure 7. δ polymorph packing a=1 ,b=1, c= 1/2 view.

To understand how the hydrogen bonding is actually different from one polymorph to the other, it is very useful to use a method in which we define a hydrogen bonding network[15]. A network is a pattern in which every molecule is connected to every other molecule by at least one hydrogen bond. To describe the system by networks and motifs (motifs are networks in which we consider only one type of hydrogen bond) we can use graph sets which are specified by the symbol $G_d^a(r)$ where G describes the pattern that the hydrogen bonding makes, (G is substituted

by R if the pattern forms a ring, by C if it forms a chain) a and d the number of acceptors and donors in the pattern and r the number of atoms that take part to the motif.

Graph sets are very useful to be able to understand how hydrogen bonding influences molecular packing, especially if we consider that similarities and differences in the graph sets of polymorphs provide a way to compare chemical behaviour analogies. Similar graph sets designate similar chemical behaviours.

For sulfanilamide Toscani et al.[16] have described the networks for N(1) and N(2) separately, and we see that the network for α is : N(1)=C(8) C(4) $R_2^2(8)$, N(2)=$C_2^2(6)$ $R_6^6(20)$. For γ-form N(1)= C(4) $R_2^2(8)$, N(2)=$C_2^2(6)$ $R_6^6(20)$, and for the β- form N(1)= C(8) C(4), N(2)=$R_3^4(22)$.

These assignments show that the difference between the α– and γ-forms is mainly in the presence of a C(8) chains, whereas the β-form has a more different pattern. This analysis was done on only three of the four polymorphs not being available before the fourth structure.

This analysis of hydrogen bonding should be encountered in some properties of the three polymorphs. In the same paper as above[16] there are the calculated packing energies that for α and γ sulfanilamide are quite similar, whereas, for the β form it is quite different (the hierarchy they have found was Eα≥Eγ>>Eβ) and they think the similarities in the hydrogen-bond pattern could account for the low difference in energy between the α and the γ form.

3.4. Conclusions

From the detailed examination of the crystal structures of these polymorphs it has been possible to find very different intermolecular and intramolecular bond and angle values, that, would need to be related to the differences shown in the solid-state NMR spectra; although this is not always possible, it is of fundamental

importance to have analysed the crystal structures in a particular way, since, as we will see there will be some correlations that we will be able to do with the ^{13}C and ^{15}N solid-state spectra of these molecules.

3.5. REFERENCES

1) C. V. Zyp, *Pharm. Weekbl.* **1938**, *75*, 585.

2) A. Watanabe, *Naturwissenschaften* **1941**, *29*, 116.

3) A. Watanabe and H. Kamio, *J. Pharm. Soc. Jap.* **1942**, *62*, 501.

4) D. McLachlan,*X-ray crystal structure*; McGraw Hill: New York, 1957.

5) B. H. O'Connor and E. N. Maslen, *Acta Cryst.* **1965**, *18*, 363.

6) A. M. O'Connell and E. N. Maslen, *Acta Cryst.* **1967**, *22*, 134.

7) M. Alleaume and J. Decap, *Acta Cryst.* **1965**, *18*.

8) M. Alleaume and J. Decap, *Acta Cryst.* **1965**, *19*, 934.

9) E. G. Cox, D. W. J. Cruickshank and J. A. S. Smith, *Proc. Roy. Soc. A* **1958**, *247*, 1.

10) G. J. Kruger and G. Gafner, *Acta Cryst.* **1971**, *B27*, 326.

11) G. J. Kruger and G. Gafner, *Acta Cryst.* **1972**, *B28*, 272.

12) D. S. Hughes, M. B. Hursthouse, T. Threlfall and S. Tavener, *Acta Cryst.* **1999**, *C55*, 1831.

13) D. C. Apperley, R. A. Fletton, R. K. Harris, R. W. Lancaster, S. Tavener and T. L. Threlfall, *J. Pharm. Sci.* **1999**, *88*, 1275.

14) S. C. Abrahams, *Acta Cryst.* **1955**, *8*, 661.

15) J. Bernstein, *Acta Cryst.* **1990**, *B46*, 256.

16) A. Dzyabchenko and S.Toscani, *Pharm. Res.* **1996**, *13*.

Chapter 4

SOLID STATE NMR OF SULFANILAMIDE

4.1. Sulfanilamide and its biological activity

Sulfanilamide is an antibacterial agent, although its activities are numerous; it is used as an anti-thyroid, anti-diabetic and anti-inflammatory as well as for chemotherapy effects. The mechanism with which sulfanilamide works has been through quite a number of explanations but they were all based on one original idea[1] which was that of the interference of sulfanilamide with p-aminobenzoic acid (PABA), through competitive enzyme inhibition.

Sulfanilamide inhibits the enzymatic steps of the bacteria that are involved in the synthesis of folic acid. In fact, enzymes within these bacteria use p-amino benzoic acid to synthesise folic acid. For higher animals, folic acid is not synthesised but derived from dietary sources. So that, since bacterial enzymes do not distinguish between a molecule of p-aminobenzoic acid and sulfanilamide, the microorganism is unable to synthesis folic acid, so that it will die.

Once the action of sulfanilamide was discovered in 1935 by Domack[2] many other chemicals were synthesised as analogues of sulfanilamide, and their therapeutic effects were tested. The best therapeutic effects were found in compounds in which one hydrogen of the $-SO_2NH_2$ group was replaced by some other group, usually a heterocyclic amine. Among the most successful variations were compounds such as sulfapyridine, sulfathiazole and sulfadiazine.

Until today, it is not clear how sulfanilamide and its derivatives interact with the enzyme, what are the conditions for their activity of inhibiting bacterial growth[3] which part of the molecule is more involved, and what relationship there is between the structure of the molecule and its activity[4]. The work of Kumler et al.[5] suggests the amino group of sulfanilamide is the functional part of the molecule for activity. The property that most likely influences the effect is probably the coplanarity with the ring, due to the resonant form, that, as we have seen from the previous analysis of X-ray data, all forms have in a more or less pronounced way.

This work has been an attempt to understand, through solid-state NMR measurable parameters, more about the structural differences of the different polymorphs. Findings from this work can relate to previously analysed properties of the molecule, such as the electronic structure of the nitrogens[1, 6], properties that most likely have a role in the antibacterial activity of this molecule. It has been possible, moreover, to link solid-state effects seen in both ^{13}C and ^{15}N spectra to conformational polymorphic differences, something of fundamental importance in order to be able to develop the use of solid-state NMR in polymorphic analysis.

4.2. ^{13}C Solid-state NMR of Sulfanilamide

The carbon spectra of the three polymorphs of sulfanilamide are shown in figure 1, and the assignment were done with the use of NQS experiments. The three forms represented here are α, β and γ since, as previously mentioned, for the δ only a small quantity of small crystals was obtained, not sufficient for NMR analysis.

We can see from figure 1 that the differences between the three polymorphs are immediately visible from the solid-state NMR spectra. Values of the chemical shifts are given in table 1.

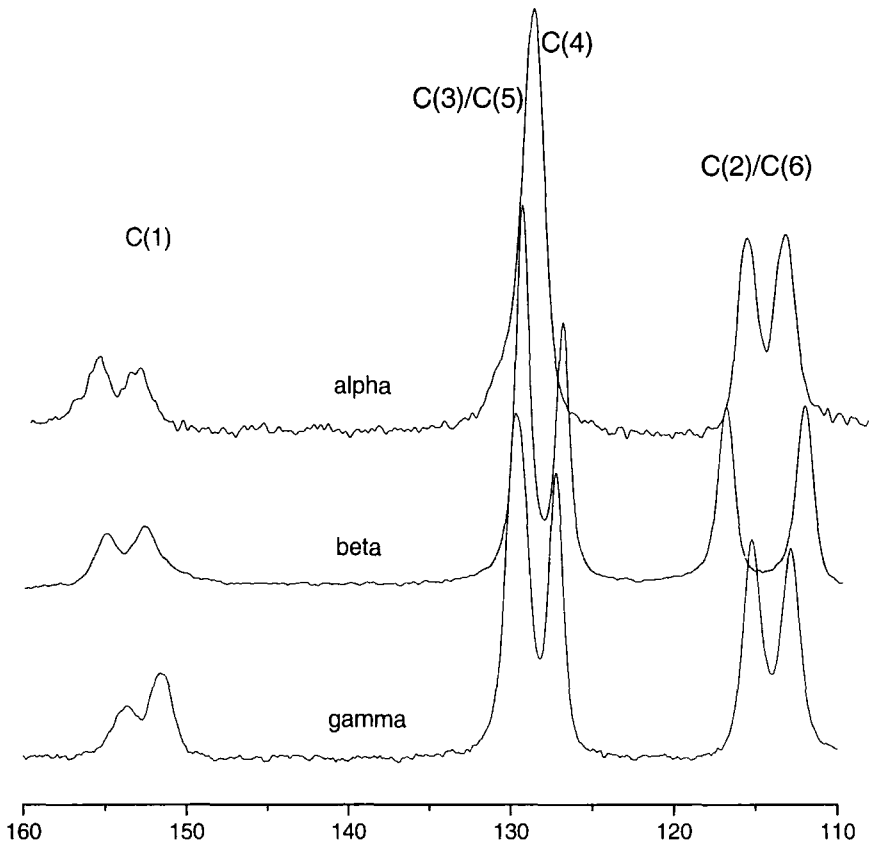

Figure 1. Comparison of the ^{13}C spectra for the three different polymorphs of sulfanilamide. The spectra were acquired under MAS conditions, with cross polarisation from proton all using ct=1 ms. The recycle delays were of 270 s, for the α form, 50s for the β form, and of 250 seconds for the γ form. The spinning speed was of 4500 kHz.

These spectra were run under different conditions, since very different recycle delays were needed. A recycle delay of 270 seconds was used in order to acquire the spectrum of the α form. For β sulfanilamide a recycle delay of 50 seconds was sufficient to obtain the maximum signal whereas for γ I had to use a longer recycle delay of at least 250 seconds. The optimum contact time for all these forms was 1 ms.

Polymorph	C(4)(ppm)	C(3)/(5) (ppm)	C(2)/(6) (ppm)	C(1) (ppm)
alpha	128.0	128.3	115.3,113.1	154.6,152.0
beta	127.1	129.5	117.1,112.3	154.9,152.6
gamma	127.1	129.6	115.1,112.7	153.7,151.7
solution[7] (DMSO)	128.3	130.8	113.5	152.7

Table 1. Chemical shifts from solid-state spectra.

All carbon–13 spectra were referenced to the higher frequency peak of adamantane at 38.4 ppm. The effects that the single substituents of the aromatic ring (NH_2 and SO_2NH_2) have on carbon chemical shifts of the benzene ring (which are considered to have a chemical shift of 128.5 ppm[8]) are seen in table 2.

On the two peaks corresponding to the quaternary carbon C(1) we can see the quadrupolar effect of the directly-coupled ^{14}N on the shape of the peak. The splitting present is due to the effect of residual dipolar coupling from the quadrupolar nucleus of the nitrogen. The signals from the protonated carbons C(2)/C(6), are separated although corresponding to chemically equivalent carbons because intramolecular molecular motion is frozen in the solid state. Further analysis of the reasons for the splitting will be discussed below.

Carbons	Effect of NH_2(ppm)	Effect of SO_2NH_2(ppm)	Absolute values (ppm) (Effects of the substituents added to 128.5 ppm)
C(4)	-9.5	+15.3	134.3
C(3)/(5)	+1.3	-2.9	126.9
C(2)/(6)	-12.4	+0.4	116.5
C(1)	+19.2	+3.3	151

Table 2. Incremental shifts of the aromatic carbon atoms due to NH_2 and SO_2NH_2[8].

4.2.1. Detecting impurities

Impurities in polymorphism can be quite difficult to detect. Powder XRD will not detect very small impurities. With solid-state NMR if one obtains narrow enough lines it is possible to distinguish more easily the peaks for each sample, so that characterization of the impurities is easier.

Quantitative analysis is not immediate, since we are considering experiments under cross polarisation conditions, so that for the same contact time the signal may be differently enhanced. Problems with detecting impurities in NMR arise especially if the sample is not very crystalline so that the linewidths can be of the order of tens of Hz, hiding particularities of the peaks. Figure 2 shows a spectrum of α sulfanilamide with an impurity of β. The impurity was not detected immediately, although the sample had been previously analysed with other techniques as powder XRD, and it seemed as if the samples were from different forms. The linewidths of the spectrum in figure 2 are about 50 Hz, and as we can see they are just at the limit in order to see the impurity of the β form, visible in the spectrum from the shoulder at 129.5 ppm.

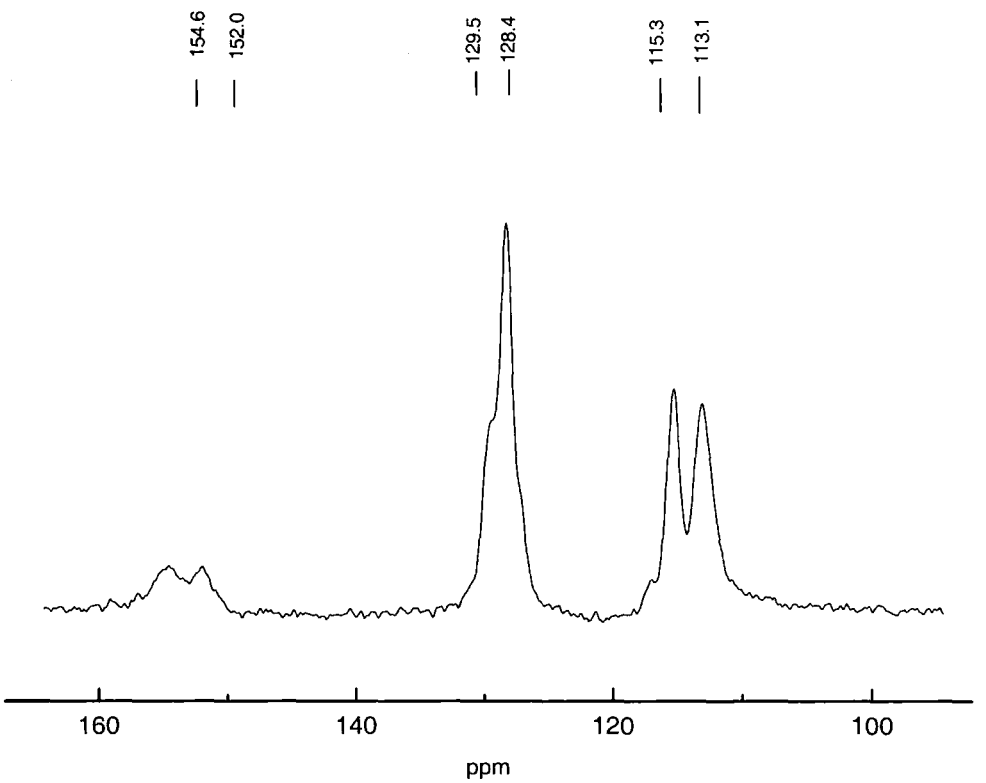

Figure 2. MAS α sulfanilamide spectrum showing a small impurity of β cpflip pulse program ct=1ms, nt=240, pd=270 s, spinning speed 4500 Hz).

In order to be sure of the impurity present it has been necessary to compare both the total spectrum and that from non-quaternary suppression, where it was confirmed that the shoulder at 127.2 ppm (well visible in figure 3) was from a quaternary carbon. Since, knowing from X-ray data that there had to be only one molecule in the asymmetric unit, only one quaternary carbon had to be present, so that it could not be other than an impurity. In figure 3 we can see the quantitative difference between the protonated and the quaternary spectrum.

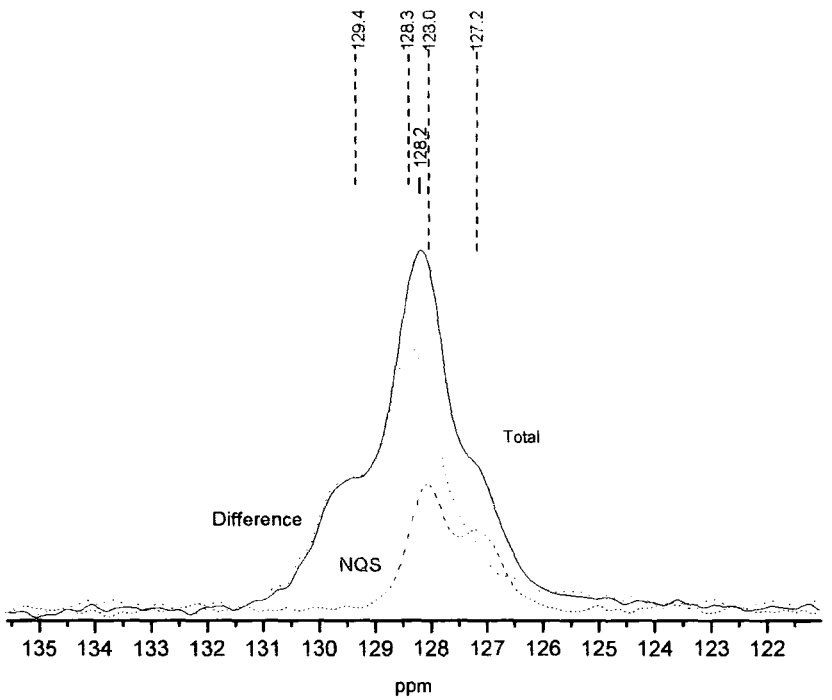

Figure 3. Quantitative difference between the total spectrum and the non-quaternary suppression experiment.

From this analysis it was clear that the shoulders were from an impurity of the β form. In order to confirm this I used another major difference that I have found between these two polymorphs; the recycle delays needed for the two forms were, in fact, quite different, the one for the β form being much smaller, as we will see below, so that running an experiment with a short recycle delay for the α sample will enhance the signal of the β impurity. The results are shown in figure 4, confirming quite clearly that there is an impurity of the β form, since the presence of the peak at 117.1 is evident, which is characteristic only for the β form.

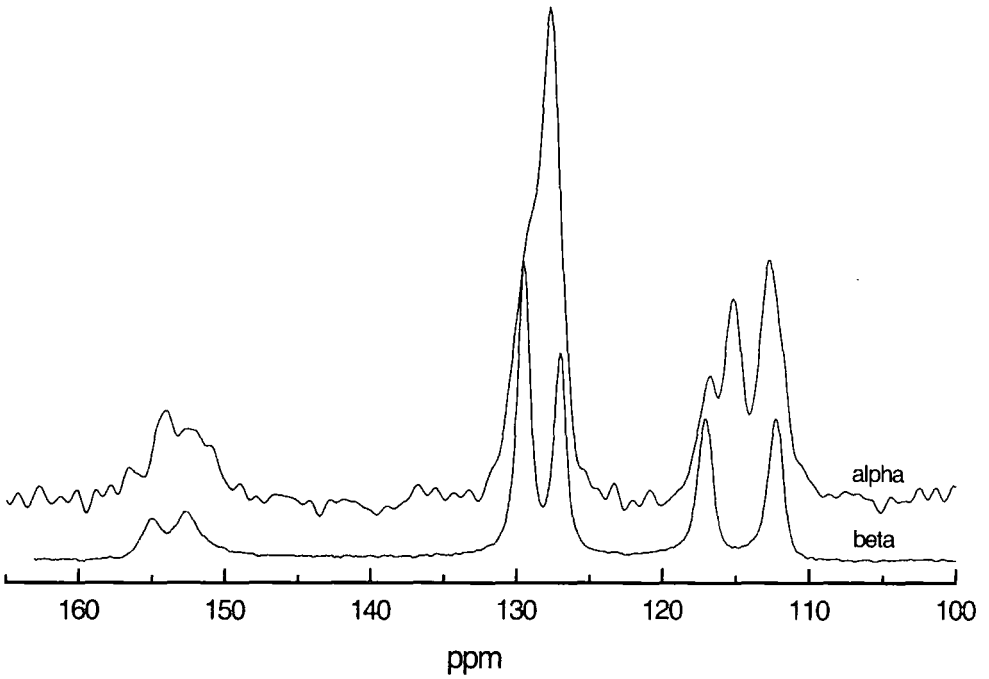

Figure. 4 Comparison of the spectrum of the α impure sample with a low value of the pulse delay (90 seconds) and the spectrum of the β form (ct = 1 ms spinning speed 4500 Hz).

I think this is an important example of how NMR can detect small impurities of one polymorph in another, since it can use, not only isotropic chemical shifts (for which differences might be difficult to detect if the impurities are small) but also dynamic properties, such as relaxation times, which, as in this case, can be very different.

Sometimes a careful analysis such as this one is necessary even to make sure of the number of polymorphs found. There has been, in fact, a study work in which ^{13}C solid-state NMR of sulfanilamide was presented[9]. In their case, although they present the ^{13}C spectrum of the δ form, the spectrum of the α and β forms that they show are basically the same whereas, for the α form, the central line is broader, not showing the shoulder due to the impurity of β, but the separation for the two peaks of C(2)/C(6), which is the greatest characteristic difference between the forms, is for both 5 ppm, as seen only for the β form. So, most likely they have two samples in which there is a mixture of α and β although in different quantities, which would explain the different XRD powder patterns. In their work, they justify the

similarities between α and β as an interconversion in the rotor as happens from spinning (3-5 kHz), but as we have seen from DSC and also as we will show from works done at high temperature, α form does not interconvert to the β, only at 401 K it will interconvert into γ.

It is necessary, therefore, especially if one would like to deduce information from conformational differences of the polymorphs from the solid-state spectrum, to have very crystalline and pure samples, giving narrow lines, since differences in the peaks can be small and not possible to be detected under poorly crystalline conditions.

4.2.2. Residual dipolar coupling

We have seen how the peaks of the carbon directly bonded to ^{14}N (quadrupolar) display broadening and splitting of the signal. This phenomenon is due to the effect (as mentioned before) of residual dipolar coupling (RDC), so called since second-order quadrupolar effects are transferred to the spin-1/2 spectrum by dipolar interactions[10]. This effect can be a complication in the spectrum, but it can give information on molecular properties such as the quadrupolar coupling constant χ, and it can also provide molecular information[11].

In figure 1 we can clearly see a 1:2 doublet. Calculation of the residual dipolar coupling can be carried out using the first-order equation (1), where s is the doublet splitting, D is the dipolar (^{13}C-^{14}N) coupling constant, χ is the ^{14}N quadrupole coupling constant, ν_N is the ^{14}N resonance frequency at the applied magnetic field, and η is the asymmetry parameter of the ^{14}N electric field gradient (EFG). α^D and β^D are the polar angles defining the orientation of the internuclear vector $\mathbf{r}_{C\text{-}N}$ in the principal axis system of the EFG.

$$s = (9/20)\, D(\chi/\nu_N)\, (\, 3\cos^2 \beta^D - 1 + \eta \sin^2 \beta^D \cos 2\, \alpha^D) \qquad (4\text{-}1)$$

where $D = \hbar (\mu_0/8\pi^2)\gamma_c\gamma_N/ (r_{C\text{-}N})^3$

We can obtain the true ^{13}C chemical shift, which is at the centre of gravity of the band, i.e. 1/3 from the more intense peak and 2/3 from the smaller one. Having done this, I have found the chemical shifts to be, for α 153.7 ppm, for the β 153.4 ppm and for γ 151.0 ppm.

It is very interesting to notice how the intensities of the peaks are inverted for the α form, the peak at higher frequency being more intense than the one at lower frequency, whereas for the other two forms it is the opposite way round. This is most likely reflecting the fact that, as seen from the crystal structure data, the amino group has its protons oriented differently from the other two forms, as indicated in table 6 of chapter 3. This means that the splitting will have a different sign for this form as opposed to the other two, since positive splittings correspond to doublets where the smaller component lies at higher frequency and negative ones to the opposite situation. When wanting to calculate the splitting, a number of factors are needed, both geometric (α_D, β_D, r_{CN}) and energetic (χ, η, Z_N).

When these factors are not known, it is usually assumed that the z axis of the quadrupole tensor has the same direction as the lone pair orbital, which is considered to be perpendicular to the NH_2 group (which, in turn, can be considered planar with the benzene ring). But in our case, approximation of the NH_2 group being planar with the ring is not possible, since, from X-ray data we have seen the differences, and from the ^{13}C spectra we see the effect of the different orientations. In this case, calculation would be complicated. If one were to use the approximation, the angle β^D would become 90°. The asymmetry parameter might be assumed to be zero, so that the angle α^D does not need to be considered, and equation (4-1) would then become:

$$s = - (9/20)\, D\, (\chi/\nu_N)$$

Thus the only other value needed would be the internuclear distance $r_{C\text{-}N}$, which could be taken from X-ray data given in table 3. Also listed are the relative dipolar coupling constants for the three polymorphs.

Polymorph	$r_{C\text{-}N}$(Å)	D(s^{-1})
α	1.374	795
β	1.368	800
γ	1.377	785

Table 3. Values for the distances of C(1)-N(1) and of the relative dipolar coupling constants .

In the particular case of sulfanilamide, the value of the quadrupolar coupling can be found in the literature[6], together with the asymmetry value. The method used for calculating the quadrupolar coupling has been through NQR (Nuclear Quadrupolar Resonance) and the data were extracted using the Townes and Daily semiempirical method[12, 13]. Values of 3.825 MHz for the coupling constant and of 0.27 for the asymmetry are evaluated. Considering these values, and considering values of 90° for both α and β, assumption probably wrong, but we can consider it now, in order to evaluate the differences from experimental, the splitting should be of 2.2 ppm for the all forms, since the difference from only the internuclear distances does not change sufficiently the values, so that probably, geometric factors are most relevant in order to evaluate the differences in the splittings, that are experimentally, 2.6 ppm, 2.3 ppm, and 2.0 ppm for respectively the α, β, and γ forms.

4.2.3. Variable Tempetature experiments

Experiments done that can give information on the dynamic properties of my systems consisted of varying the temperature. This set of experiments will give information on the mobility of the molecule as well as on relevant phase transitions between the polymorphs.

For the α and β forms, high temperature experiments did not give any changes until the respective transition temperatures (380 K for the α form and 401 K for β), when both forms turn into the γ form, as seen in the DSC. In particular, I have run a carbon spectrum up to 393 K for the β polymorph, for which not many significant changes could be seen. The comparison between the two spectra (at room temperature and at 373 K) is shown in figure 5. The separation between the peaks of the signals from C(2)/C(6) gets slightly smaller (from 4.8 ppm to 4.5 ppm) as well as it seems as if the distance between the C(3)/C(5) peak and the C(4) peak becomes smaller.

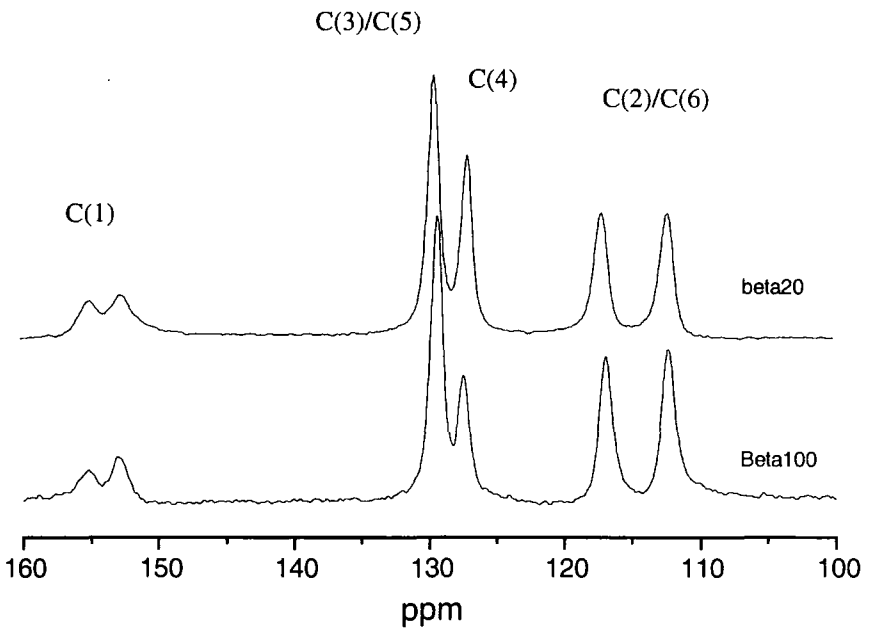

Figure 5. Comparison between spectra of the β polymorph at room temperature and at 373 K (MAS spectra acquired with a recycle delay of 50 seconds, ct=1 ms, spinning speed 4500 Hz).

The spectrum that mostly changed in varying the temperature has been the one from the γ form. When reaching the temperature of 321 K, we can clearly see that there is an internal rotation of the phenylene ring (Figure 6). The spectrum that we are seeing at the higher temperature (353 K) should correspond to the same phase, the γ

form, since from DSC analysis we saw no transitions within this range of temperatures. We can observe some broadening of the signals due to some interference from the molecular motion with the proton decoupling, which will make the proton decoupling less effective. This should also explain the changes in the central part of the spectrum, which are probably due to the fact that peaks C(3)/C(5) will also change their shape. The actual motion is not clear, although we can assume probable 180° jumps of the phenylene ring. This assumption was done by Frydman et al. [9] who found an activation energy for the ring flipping of 62.76 ± 4.2 kJ/mol.

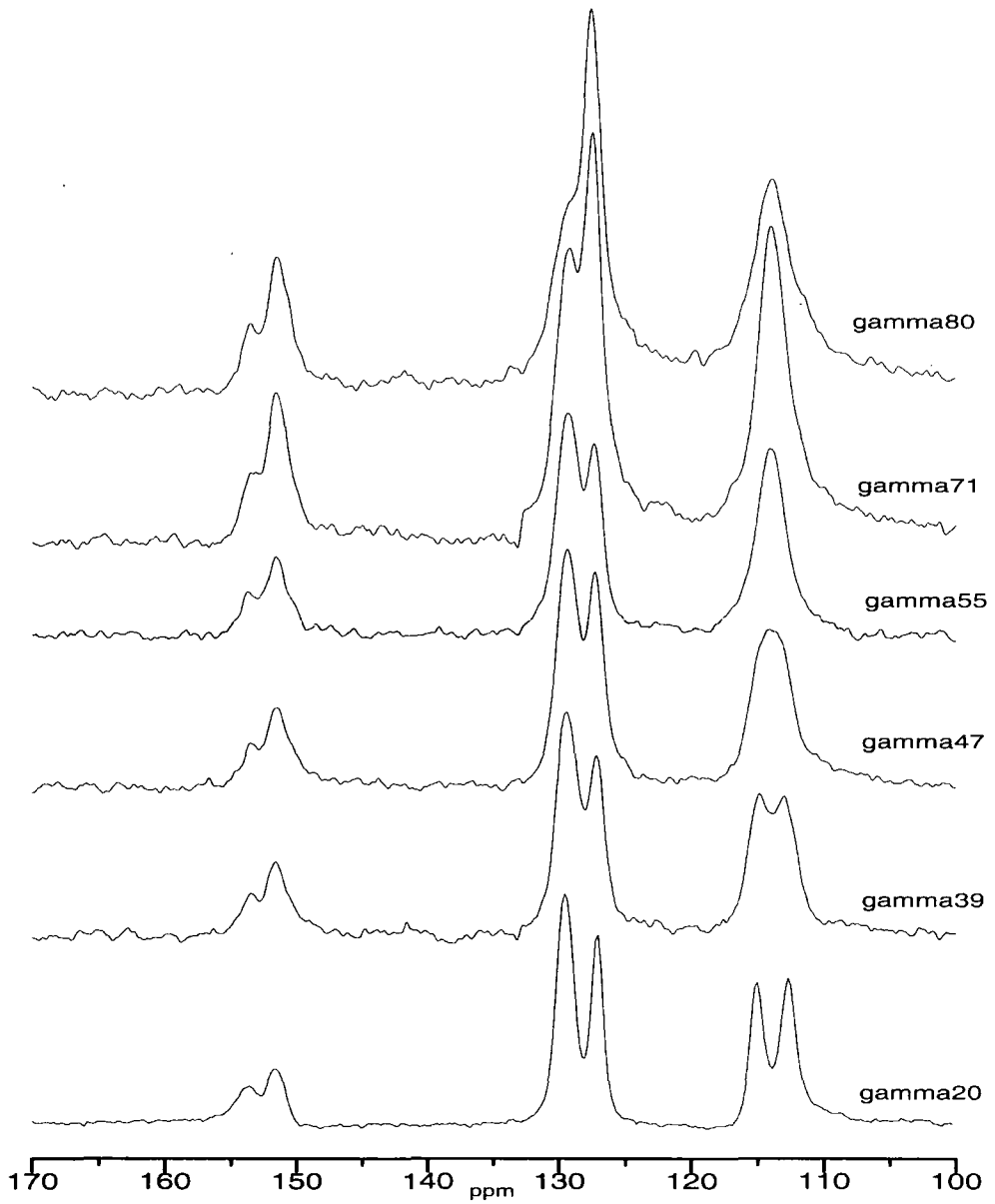

Figure 6 MAS variable temperature experiments, (room temperature, 312 K, 320 K, 328 K, 344 K, 361 K) for the γ polymorph, spinning speed 4000 Hz, ct = 1 ms, pd = 200 seconds.

4.3. ^{15}N Solid state NMR

Nitrogen-15 NMR can provide very valuable information, being very sensitive to the local environment, as well as being concerned with hydrogen bonds. The

problem with dealing with nitrogen is that it exists in a very low percentage natural abundance (0.37), one third of the ^{13}C natural abundance, and it has a very low NMR sensitivity, one fifteenth of ^{13}C. All these problems can be overcome by isotope enrichment which will also provide a means of studying each nitrogen site selectively. In this particular work, enrichment of the sample has been particularly useful.

4.3.1. Natural abundance spectra

The ^{15}N spectra were first run in natural abundance in order to understand if particular features seemed to be worth the eventual work of enrichment, but as we can see from figures 7, 8, and 9 the signal-to-noise ratio were particularly bad, especially thinking that these spectra were run at the 300 MHz spectrometer (for which signal-to-noise should be better than at lower fields). The conditions for the spectrum of the α form were: recycle delay, 120 seconds, number of transients (ns), 760, and contact time (ct), 3 ms. The spin rate was 4300 Hz. The conditions for the β spectrum were: recycle delay of 60 seconds, 800 transients, and a contact time of 1 ms, spin rate 4000. For the γ form, 120 seconds recycle delay, ns = 760, ct = 2 ms, spin rate 4150 Hz. Spectra were referenced to the nitrate peak of ammonium nitrate (NH_4NO_3) at –5.1 ppm relative to CH_3NO_2.

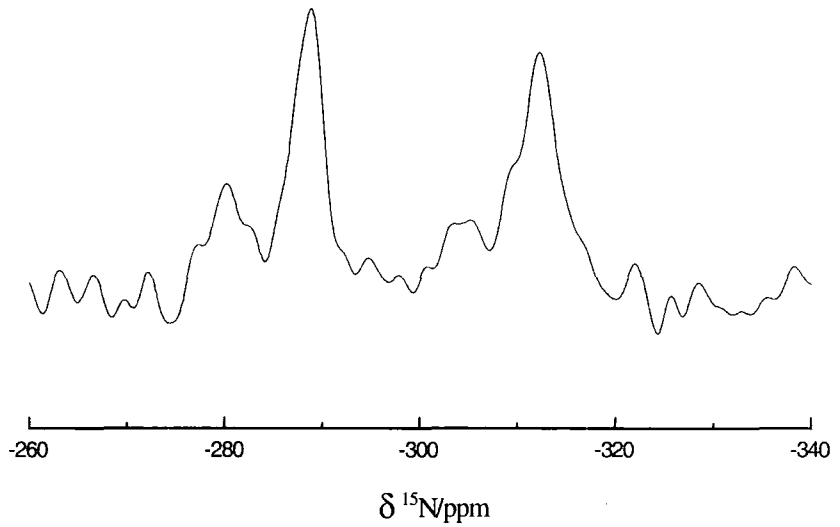

Figure 7. MAS natural abundance spectrum of ^{15}N sulfanilamide, α form. Recycle delay= 120 seconds, nt = 760, ct= 3ms, spinning speed 4300 hz.

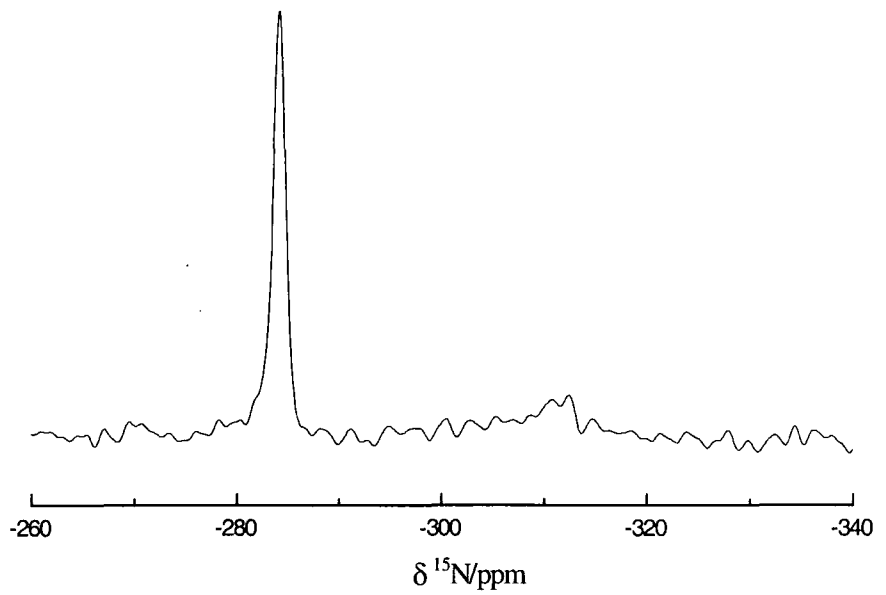

Figure 8. MAS natural abundance spectrum of ^{15}N sulfanilamide, β form. Recycle delay= 60 seconds, nt= 800, ct= 1ms, spinning speed= 4000 Hz.

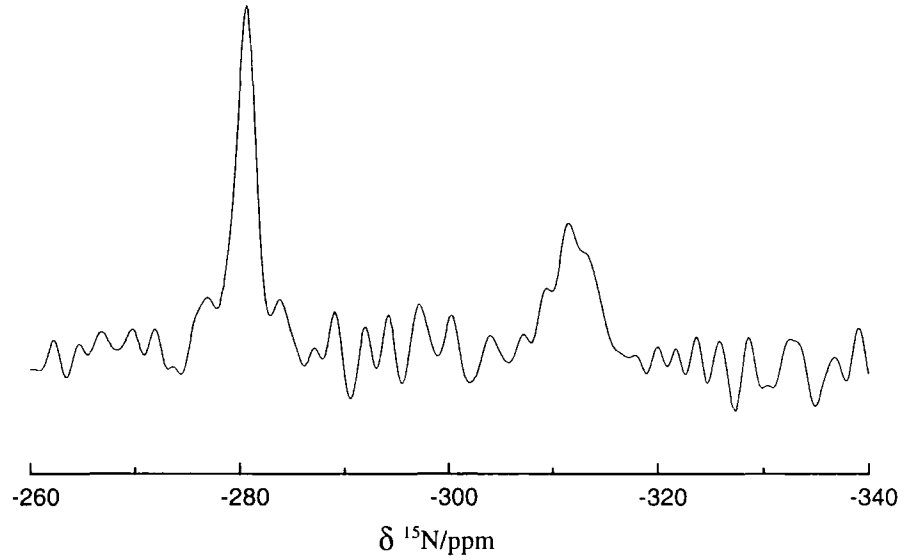

Figure 9. MAS natural abundance spectrum of ^{15}N sulfanilamide, γ form, recycle delay 120 seconds, ns= 760, ct= 2 ms, spinning speed 4150 Hz..

As we can see, although the spectra took a very long time to acquire, the signal-to-noise is bad, so that, in order to obtain other information apart from the isotropic chemical shifts (reported in table 3), enrichment was needed. Despite the poor quality of the spectra, the peak intensities seemed to have peculiar behaviour. We can clearly see that the peak corresponding to N(1) shows a lower intensity in all forms, although for the β form this effect is the most pronounced.

polymorph	^{15}N chemical shift(ppm)
α	
N(1)	-312.2
N(2)	-288.8
β	
N(1)	-312.1
N(2)	-284.1
γ	
N(1)	-312.1
N(2)	-280.6
Solution(DMSO)	
N(1)	-312.4
N(2)[7]	-284.0

Table 3. Chemical shifts values for the three forms, as obtained from the ^{15}N natural abundance spectra.

The shifts for N(1) does not change significantly between polymorphs, nor for the value in solution. The similarities between the solid value and the solution might account for the fact that hydrogen bonds have little influence for this nitrogen.

Although isotropic chemical shifts cannot bring a lot of information, it is worth pointing out that the chemical shift of N(2), depend on the values of the dihedral angle of the sulfonamide group as seen in chapter 3. The correlation is shown in graph 1, where we can see an approximately linear behaviour of the chemical shift with the dihedral angle.

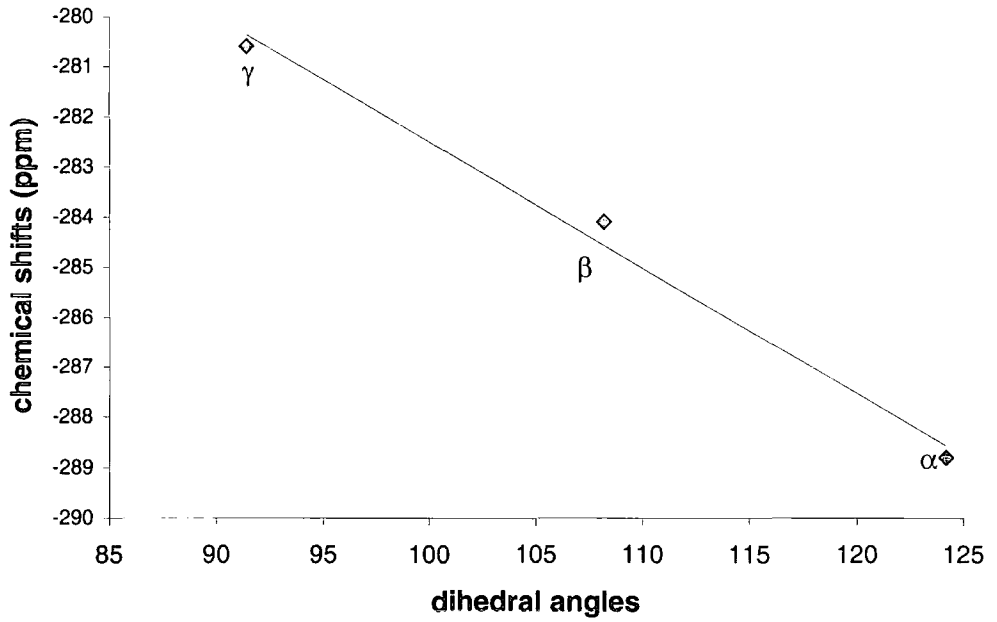

Graph 1. Correlation between the dihedral angles and chemical shift values.

It seemed worth while to enrich the sample and see how the ^{15}N spectra looked when the experiments would take less time.

4.3.2. ^{15}N enriched spectra

4.3.2.1 Isotopic enrichment

The enrichment was carried out for each nitrogen selectively, in order to be able to study each nitrogen under separate and optimal conditions.

For the enrichment of N(2) the procedure followed was similar to that given in the literature[7, 14]. Thus,12.5 ml of chlorosulfonic acid was added to acetanilide (5 g) and left refluxing for about 1 hour until no solid acetanilide was left. Ice was added to the solution, which was then filtered. A mixture of ammonium sulphate (Aldrich, 82.6% ^{15}N; 9 mmol), the sulfonyl chloride acetanilide previously prepared (18 mmol), and K_2CO_3 (72 mmol) in acetonitrile (100 ml) was cooled in an ice bath.

Water (72 ml) was then added, the flask was stoppered and the mixture was stirred magnetically overnight.

The organic layer was separated, the solvent was removed under vacuum, and the residue was recrystallized from water. Then, following reflux with acid hydrolysis (2.5 ml of concentrated HCl and 7.5 ml of H_2O), the final product was obtained with a yield of 73 %. The product was crystallised into the different forms (from water to obtain the β form, ethanol to obtain the γ form and n-butanol to obtain the α form).

The reaction path for N(2) is shown below:

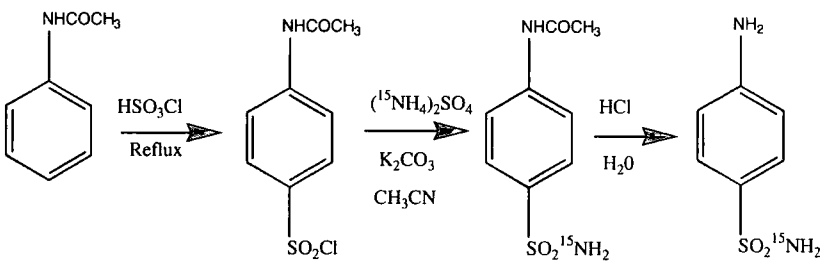

For the enrichment of N(1), 2 gr 99% enriched acetanilide (Aldrich) were added to 1 gr of non-enriched acetanilide. ^{15}N-enriched sulfonyl acetanilide was obtained as above. To it, ammonia was added and the solution was heated for about 1 hour. The hydrolysis and crystallisation were carried out as above. The yield in this case has been of 85 %.

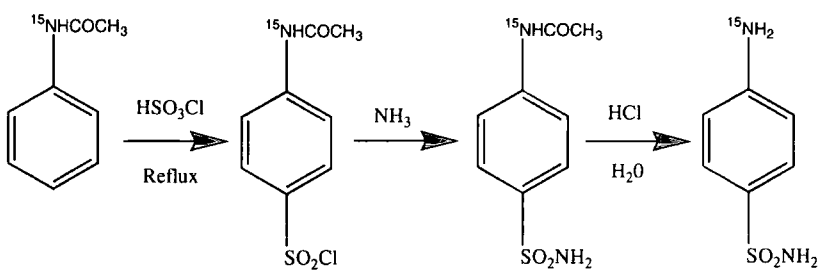

An example of the β spectrum enriched in the N(1) position is shown in figure 10 and of the sample enriched in the N(2) position, in figure 11. Both spectra were acquired through cross polarisation from protons.

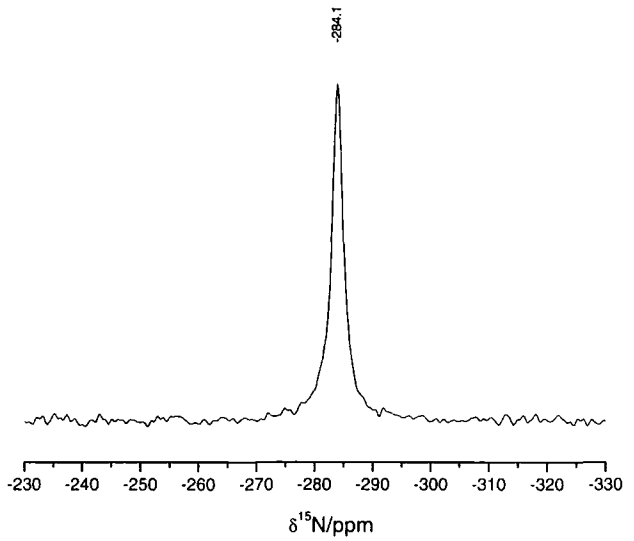

Figure 10. Spectrum of the β polymorph after enrichment in the N(2) position. Number of transients =4, ct=1, pd=30 seconds.

This particular nitrogen position showed a narrow linewidth at half height (30 Hz). For the other peak (N(1)) we can see, from figure 11, how the linewidth is broader, up to 130 Hz, so that it is again possible to detect different behaviour between the nitrogen sites.

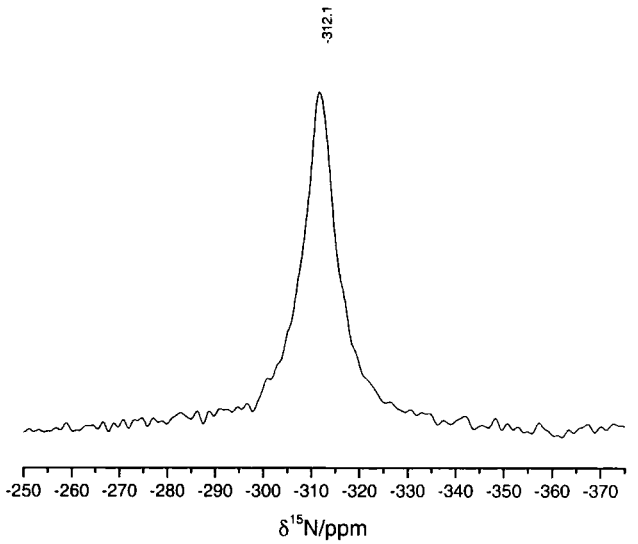

Figure 11. Spectrum of the β polymorph after enrichment in the N(1) position. Number of transients =36, ct=1, pd=30 seconds.

Having enriched the sample, a number of NMR properties could be studied that would not be possible to take into consideration otherwise, such as anisotropies and asymmetries of all the polymorphs, as well as relaxation times.

4.3.3. Anisotropic interactions

Solid-state NMR represents a unique tool for the observation of anisotropic interactions. The anisotropic interactions in organic compounds observable by solid state NMR are mainly the CSA, the magnetic dipolar coupling and the quadrupolar interaction. All of them contain information about the local magnetic environment of the observed nuclei. This information depends on molecular parameters and on the orientation of the molecule with respect to the external magnetic field. The distribution of molecular orientations in the unoriented powder sample leads to inhomogenously broadened lineshapes in static NMR spectra. Such a powder pattern reveals the eigenvalues of the interaction tensors, i.e. the CSA or dipolar coupling, which are correlated to the molecular structure.

I will only be analysing here the chemical shift anisotropy (CSA) for the different polymorphic forms, trying to understand if it is a sensitive enough probe to detect differences between the forms for the nitrogen sites, since the chemical shift anisotropy is directly related to the chemical structure.

4.3.3.1. Shielding anisotropy and asymmetry measurements

Understanding if different polymorphic forms have different anisotropies or asymmetries for ^{15}N is a task not always feasible, and there are not many studies reported in literature testifying to this fact, so that for this reason it is important to understand if polymorphism affects, not only the isotropic shift, but the anisotropic one as well. I have been able to measure these parameters for all three forms, as well as for both nitrogens. The spectra were all acquired cross polarising through protons.

The convention used for shielding parameters is that of Haeberlen[15]:

Anisotropy $\zeta = \sigma_{33} - \sigma_{iso}$

Asymmetry $\eta = \dfrac{\sigma_{22} - \sigma_{11}}{\zeta}$

Isotropic shielding $\sigma_{iso} = \dfrac{(\sigma_{11} + \sigma_{22} + \sigma_{33})}{3}$

The sign convention is that for which the chemical shift, δ, is $-\sigma_{iso}$.

The three tensor components are designated as follows:

$|\sigma_{33}-\sigma_{iso}| \geq |\sigma_{11}-\sigma_{iso}| \geq |\sigma_{22}-\sigma_{iso}|$

The programs used for fitting the spectra were two. Spinning side bands could be fitted using both programs; the first one, which is an in-house program, assumes coaxial tensors, based on the theory described by Maricq and Waugh[16]. This

program includes statistical error analysis. The program is called ssb97. The other program, which is referred to as STARS, was in-built into the 300 MHz spectrometer, and is also able to fit the lineshapes. In order to have coherent values between the programs I have used the values of the ssbfit97 program for simulation with STARS. An example of the fitting is shown in figure 12 for the α form, which was one of the most problematic cases, since the lines were quite broad.

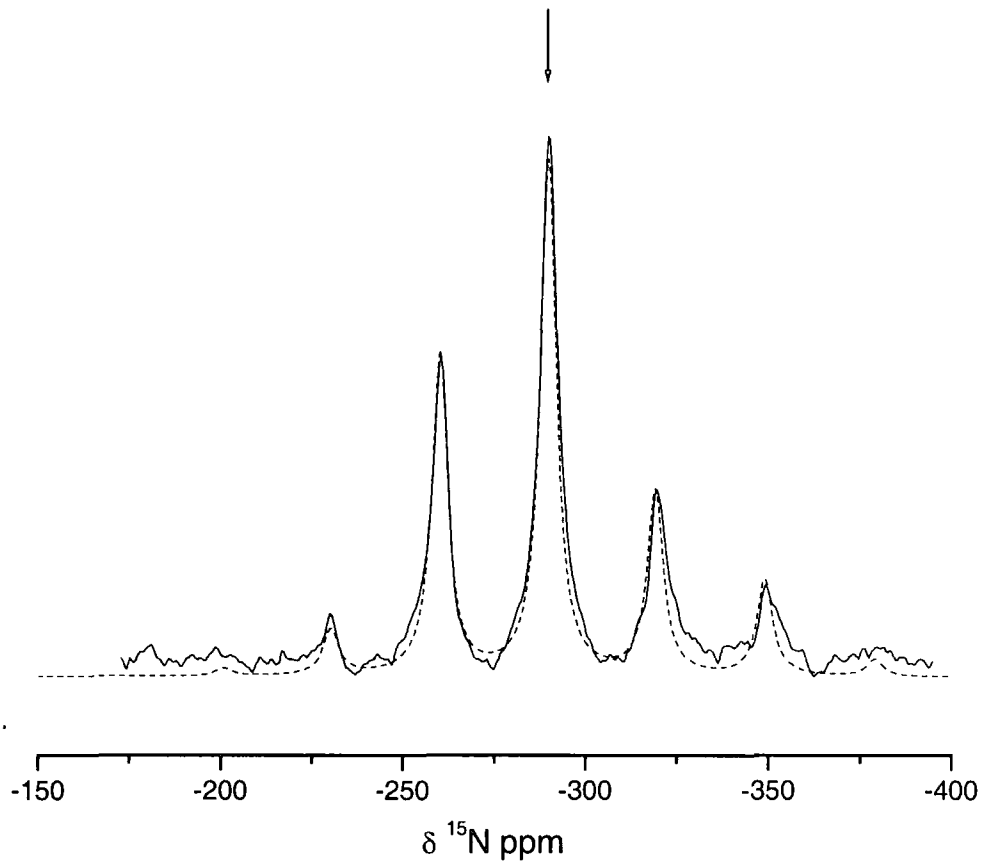

Figure 12. Spinning side bands for N(2) of the α polymorph of sulfanilamide, obtained from under MAS conditions spinning at 600 Hz, showing the fitting by the dotted line. The arrow shows the isotropic shift. The pulse delay was of 120 seconds, nt = 300, ct = 1 ms.

In figure 13 we can see the spinning side bands from the β form, when spinning at 580 Hz.

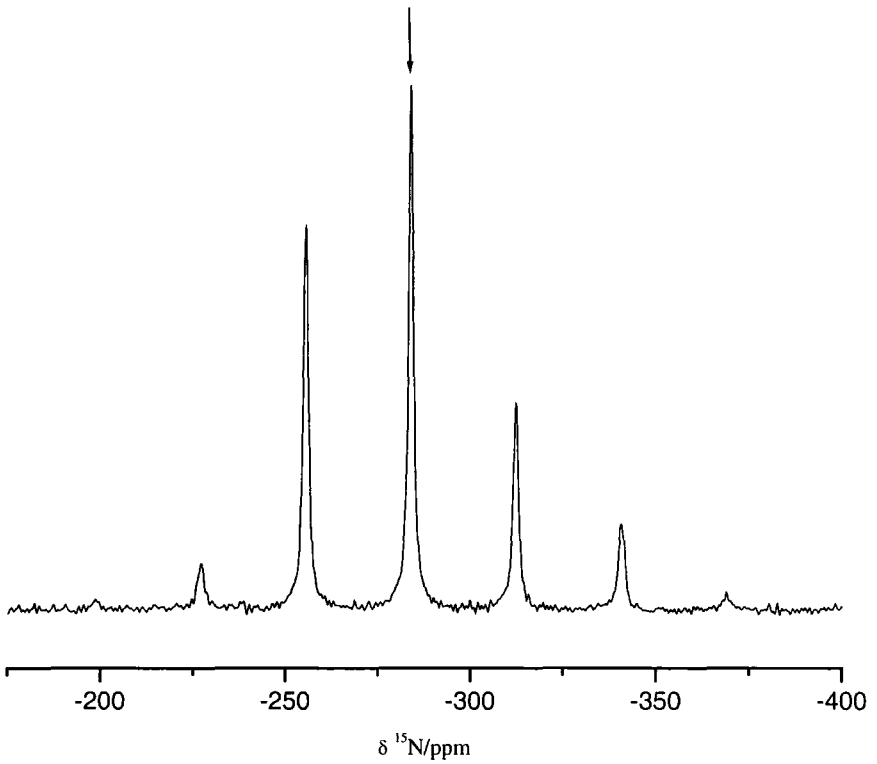

Figure 13. Spinning side bands for the β form, N(2), MAS spectrum spinning at 580 Hz, the arrow showing the isotropic peak. The pulse delay was of 50 seconds, nt= 200, ct = 1 ms.

The spinning side bands were recorded at two different frequencies in order to have a better evaluation of the measurements. In figure 14 we can see the N(2) β spectrum with the spinning side bands corresponding to a spinning speed of 370 Hz. Some small irregularities in the spectrum are visible accounting for some irregularities in the spinning speed.

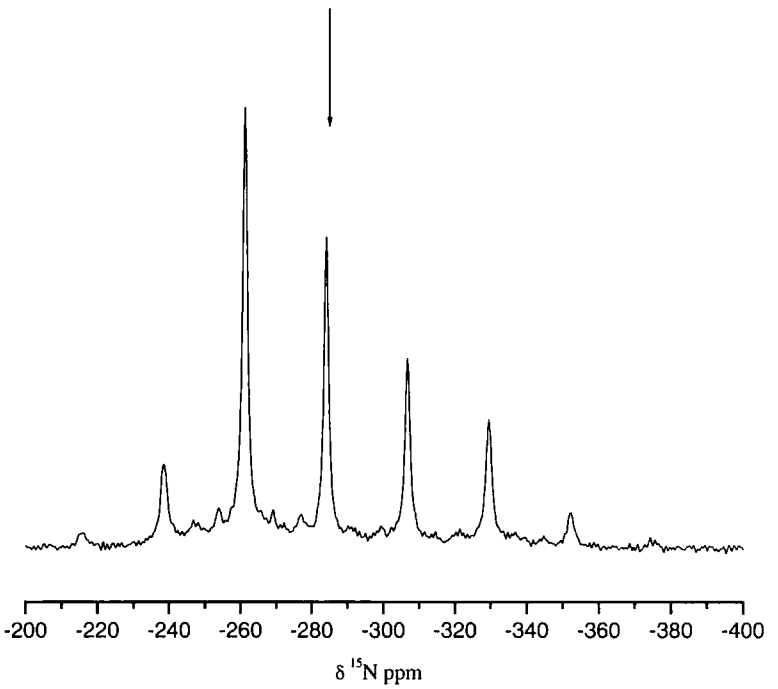

Figure 14. Spinning side bands for N(2) of the β form. MAS spectrum spinning at 370 Hz, the arrow showing the isotropic chemical shift. The pulse delay was of 50 seconds, nt= 180, ct = 1 ms.

An example of the γ form acquired when spinning at 370 Hz is shown in figure 15

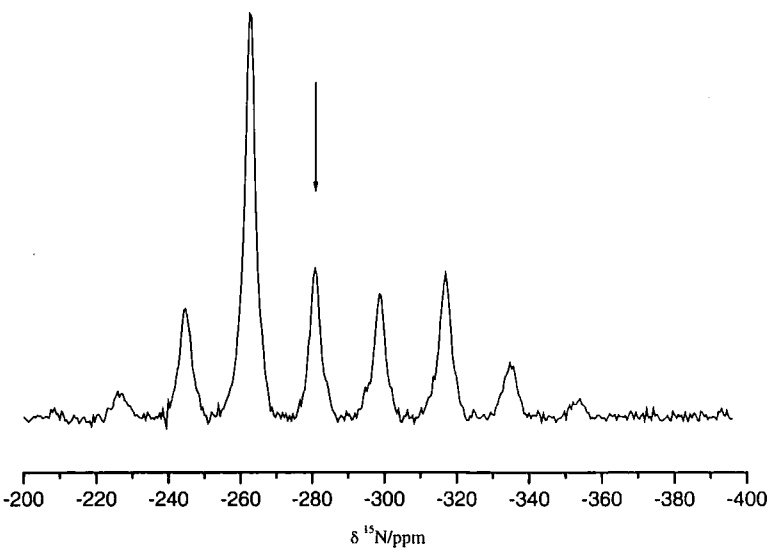

Figure 15. Spinning side bands for N(2) of the γ form from a MAS spectrum spinning at 370 Hz. The pulse delay was of 120 seconds, ct= 1 ms, nt= 200.

Measurements of asymmetries and anisotropies for N(1) were possible only by acquiring static spectra due to the fact that the anisotropy for this site was considerably smaller, and considering that the linewidths for N(1) were larger, so that overlapping of the single lines was found. Even under static conditions, however, the fitting was quite difficult, since the asymmetries were near to one, and the signal-to-noise ratio was not too good.

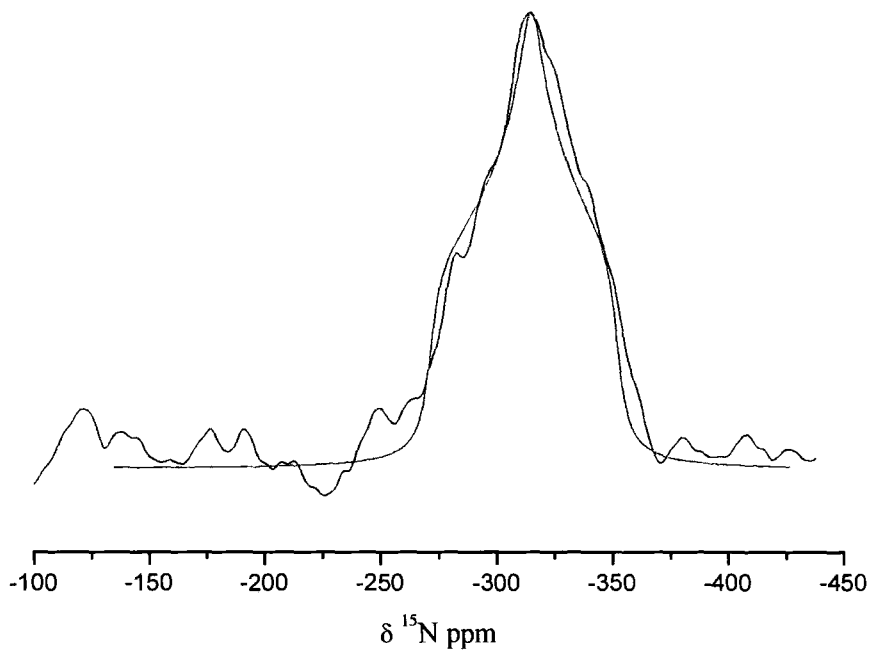

Figure 15. Static spectrum of N(1) for the α form, showing the fitting curve in red.

The results from fitting the spinning side bands for N(2) and from fitting the static curve for N(1) are shown in table 4.

Polymorph	ζ for N(2)/ppm	η for N(2)	ζ for N(1)/ppm	η for N(1)
α	70.0	0.4	±46	1
β	71.2	0.4	43	0.8
γ	67.3	0.3	±45	1

Table 4. Asymmetries and anisotropies for the two nitrogen sites of sulfanilamide.

From this study we can see how the anisotropies and asymmetries show a greater difference between the two different sites than between the three polymorphs. Values for the same nitrogen for the different polymorphs are in fact quite similar.

4.4. Relaxation time measurements

Relaxation time measurements are a very valuable tool in order to understand more about the mobility of the system under study[17]. I have measured relaxation times, longitudinal (T_1) and in the rotating frame ($T_{1\rho}$) both for proton and nitrogen. Interesting dynamic properties could be deduced form these measurements, especially when considering variable temperature experiments, that can give more precise information on mobility.

4.4.1. Longitudinal relaxation time for protons

I have measured the relaxation times of the protons via the carbon signal for all the three polymorphs. The indirect method results in different measurements of T_1 from observation of different carbon signals, though in general (when the proton spin diffusion is efficient) the values of T_1 should be identical. So, even though the decay of the signals is slightly different from one peak to the other, I will just discuss a mean value for T_1 and consider the range of observed values from the individual peaks as the probable error.

In table 5 is written the mean values of the relaxation times for the three polymorphs and the relative range of values that they assume for the different

peaks. The temperature was set to 298 K, which should correspond to 303 K, as seen from the calibration measurements.

Polymorph	T_1/s
α	94 ± 4
β	8 ± 1
γ	82 ± 5

Table 5. Relaxation times for the three polymorphs.

The experiments were done using different conditions for each polymorph. For the α form I have used a recycle delay of 240 seconds and I have arrayed the tau values as 0.1, 5, 10, 20, 50, 80, 100, 120, 150s. The long relaxation time and, consequently, the long recycle delay needed, did not allow me to have a very good signal-to-noise ratio and I had to run the experiment for only 32 acquisitions. For the γ form I have used the same conditions as for the α measurements.

When measuring the proton relaxation time for the β form, I was able to acquire the spectrum for a larger number of transients and this is probably the reason why the error is significantly smaller in this case than in the other two, together with the fact that here the recycle delay was substantially over the value of $5T_1$ whereas in the other two cases I had to cut it down to somewhat below this requirement. The other condition that was better for the measurement of T_1 for the β form was that I could consider a larger number of points (12 tau values instead of 9). I have arrayed the tau value for the β relaxation time measurement using 0.1, 1, 2, 3, 5, 8, 10, 12, 15, 20, 30, 40 seconds.

4.4.2. Spin-lock relaxation times for protons

The other measured parameter that can give information on dynamic properties of the samples was $T_{1\rho}(^1H)$, which monitors motions of the order of kHz, where T_1 monitors motions of the order of MHz.

From table 6 we can see how the behaviour of the three polymorphs is quite different when considering motions of this order of magnitude; α and β have similar values, whereas for T_1 α and γ were similar.

Polymorph	$T_{1\rho}$/ms
α	7.2±0.3
β	7.1±0.1
γ	3.0±0.1

Table 5. Values of $T_{1\rho}(H)$.

Measurements were done in two different ways, by arraying the contact time, and with a variable spin-lock measurement. The results were basically the same, with differences within the experimental error. The experiments, when considering the variable contact time, were done by arraying seventeen values: 0.1, 0.2, 0.4, 0.6, 0.8, 1, 1.2, 1.5, 2, 3, 4, 5, 6, 7, 8, 10, 12, 15 milliseconds. For the recycle delays, I have used 50 seconds for the β form, and a recycle delay of 200 s for both the α and γ forms. The number of transients for the α and γ form were of 32 where for the β form they were 64.

An example of the results from varying the contact time is shown in figure 16, where we can also see the values of T_{IS}, the rate of cross polarisation. The values of T_{IS} for the three polymorphs and for the different carbon magnetisations are shown in table 6.

Carbon site	α $T_{IS}/10^{-4}$ s	β $T_{IS}/10^{-4}$ s	γ $T_{IS}/10^{-4}$ s
C(1)	3.2 ± 0.3	4.0 ± 0.4	4.2 ± 0.5
C(2)/C(6)	1.7 ± 0.2	2.0 ± 0.1	1.6 ± 0.2
C(3)/C(5)	3.6 ± 0.1	2.0 ± 0.2	1.6 ± 0.3
C(4)	6.0 ± 0.4	5.6 ± 0.1	

Table 6. T_{IS} values for the different polymorphs.

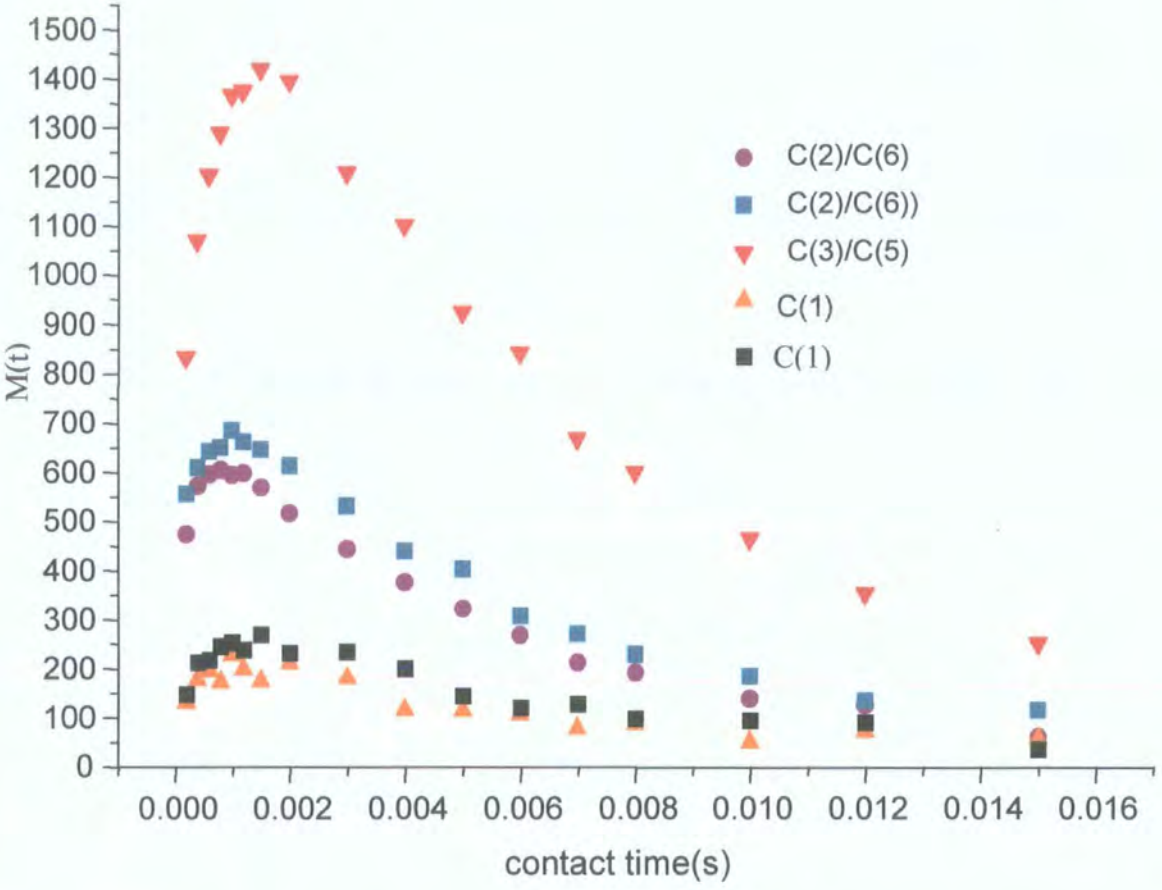

Figure 16. Behaviour of the magnetisation when varying the contact time, example of the α form.

4.4.3. Longitudinal relaxation times for nitrogens

For comparison it has proved very valuable to measure relaxation times for the nitrogen sites. The results are quite interesting, since the relaxation times measured for the different nitrogens show very different values, as well as having different values between the different polymorphic forms.

The errors here were considered from the fitting using the program Origin and the curve of an exponential decay. The values for both nitrogens are in table 7.

Polymorph	$T_1(^{15}N)$/(s) for N(1)	$T_1(^{15}N)$/(s) for N(2)
α	>200	2.58 ± 0.06
β	100 ± 2	0.212 ± 0.004
γ	>200	1.71 ± 0.04

Table 7. Values of the relaxation times for both nitrogens of the three forms of sulfanilamide.

The relaxation times of N(1) are significantly longer than the ones for N(2) showing a great lack of mobility of this particular site. It has been in fact impossible to measure the relaxation times for N(1) for the α and γ forms in a proper way, since they were too long. All I could do was to have an idea of the relaxation time. This phenomenon has enabled us not only to explain the ^{15}N spectrum for which N(1) is less intense, but it might also help us in the explanation of the ^{13}C spectrum, for which we saw that only the carbon signals due to the two carbons C(2) and C(6) next to the amino group show a splitting in the signals. Such a lack of mobility in the amino group is most likely to be the cause for this splitting.

This result is very interesting if we consider, as analysed before, that this particular nitrogen might be responsible for the enzymatic interaction, at least in some cases. This difference in the behaviour of the different polymorphs could give some more insight into the mechanism with which these molecules are active, especially if we

could extend this to other sulfa-drugs (although it would require synthesis of the other more complicated molecules). Sulfapyridine ^{15}N spectra were run for a previous study in this laboratory, and, from the spectra, it seems as if, at least for four of the five polymorphic forms analysed, the peak from the amino nitrogen is less intense than the other nitrogen peaks, so that it might be possible to consider the same kind of behaviour for sulfapyridine.

4.4.4. Spin-lock relaxation times for nitrogens

The results are shown in the table below, where these experiments were all run during the same session in order to assure that the spinlock time is of the same magnitude, since $T_{1\rho}$ depends on the particular field used to spin-lock, that in these cases were of 50 kHz.

Polymorph	$T_{1\rho}(^{15}N)$/(ms) for $\mathbb{N}(1)$	$T_{1\rho}(^{15}N)$/(ms) for $\mathbb{N}(2)$
α	0.64 ± 0.04	6.5 ± 0.3
β	0.64 ± 0.03	10.0 ± 0.1
γ	1.5 ± 0.04	4.2 ± 0.4

Table 8. Values of the relaxation spin-lock times for both the nitrogens of the three forms of sulfanilamide.

As we can see, these measurements led to smaller differences between the forms although there are significantly different values between the two nitrogen sites.

4.4.3. Variable temperature relaxation time experiments for protons

As mentioned previously, in order to get more information upon molecular motion the most valuable tool in NMR is the determination of relaxation times at different temperatures. These measurements were, again, carried out using cross polarisation through carbons, so that relaxation times were measured when acquiring the carbon

spectrum. All these measurements were carried out solely on the β form, being the one form with a relatively short proton relaxation time, so that total times for experiments would not be impossible. The results are shown in figure 17, in which the relaxation time values (in seconds) are in function of 1000/T where the temperature is expressed in Kelvin. The fitting (dashed line) is based on equation 2-7.

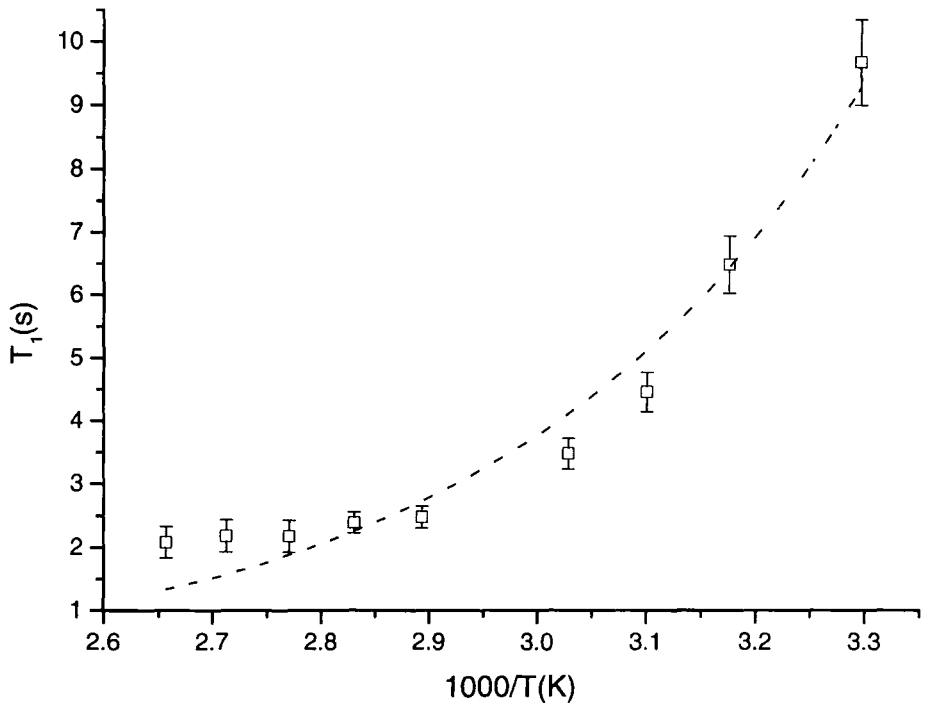

Figure 17. Relaxation time as function of temperature for protons of the β form. The fitting is shown in the dashed line.

As we can see from figure 17 we cannot reach the minimum since at about 403 Kelvin we will find a phase transformation. I have stopped below this point. The fact that no minimum was seen makes the fitting of the curve using the proper equation (2-7) quite difficult with a great order of uncertainty especially in the value obtained for the correlation time (τ_0). The value for the activation energy obtained with this fitting was of 25 ± 2 kJ/mol where the value for τ_0 presented problems being the error of the same order of magnitude of the value itself, so that

it will not be a reliable data. In order to confirm the activation energy value obtained from the fitting it is possible to consider a linear fit plotting $\ln(T_1)$ versus 1000/T. The linear fit is shown in figure 18. The value for the activation energy obtained form this fit is of 23 ± 2 kJ/mol confirming that the value for the activation energy obtained previously is quite good.

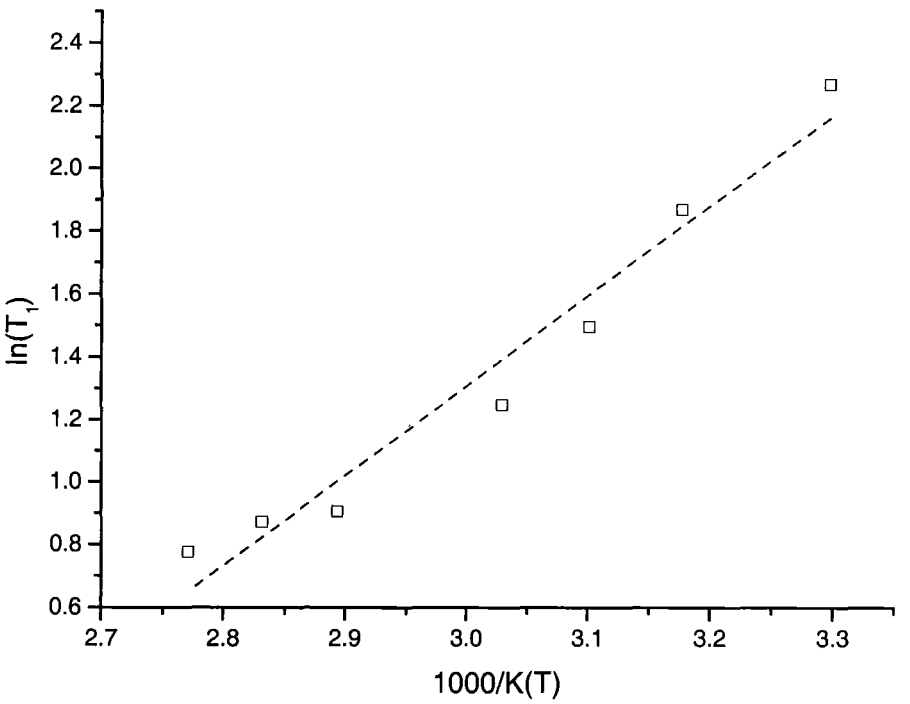

Figure 18. Linear fitting of the of the logarithm of the relaxation time of proton versus 1000/T.

I have measured proton relaxation times at the 300 MHz, even though with a different pulse sequence, detecting protons directly. Relaxation times calculated at the 300 Mhz were analogous, although the values were higher, and I was not able to detect a minimum when arriving to 393 K. The curve is shown in figure 19.

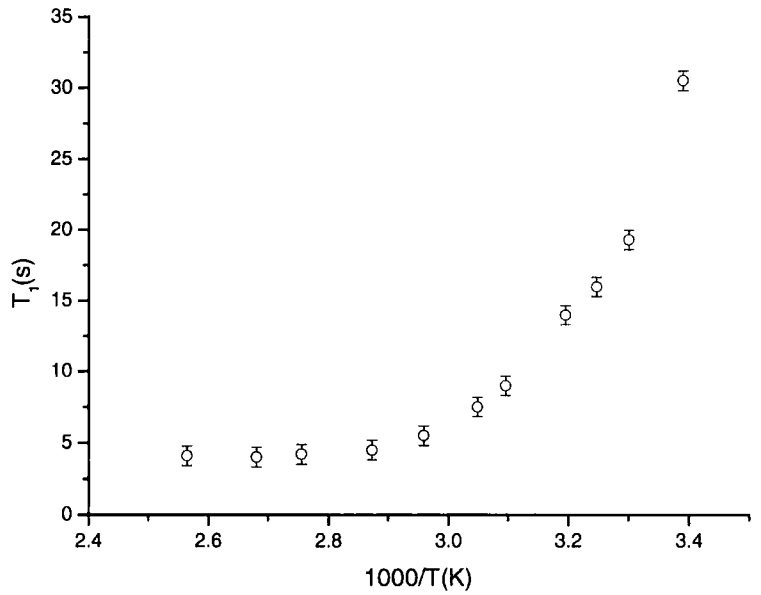

Figure 19. Relaxation time measurements at different temperature at the 300 MHz spectrometer.

The linear fit of the data obtained from the 300 MHz gave values for the activation energy that were slightly different from the one found from the 200 MHz measurements: 29 ± 1 kJ/mol. This difference might be due to the fact that for the 300 MHz measurements proton was detected directly as opposed to the 200 MHz measurements, where interference with protons from the probes were complicating the direct detection of protons at the 200 MHz.

The other parameter to try and fit would be $T_{1\rho}{}^{H}$, which is important since it gives information of movements of the order of the ms. Measurements were done on the β form and a minimum was found around 373 K, showing mobility in the order of the ms was present at this temperature. For this curve the fitting was not a problem using equation 2-10, and I was able to obtain the activation energy as well as the value for τ_0. The curve showing the fitting as well, is in figure 20.

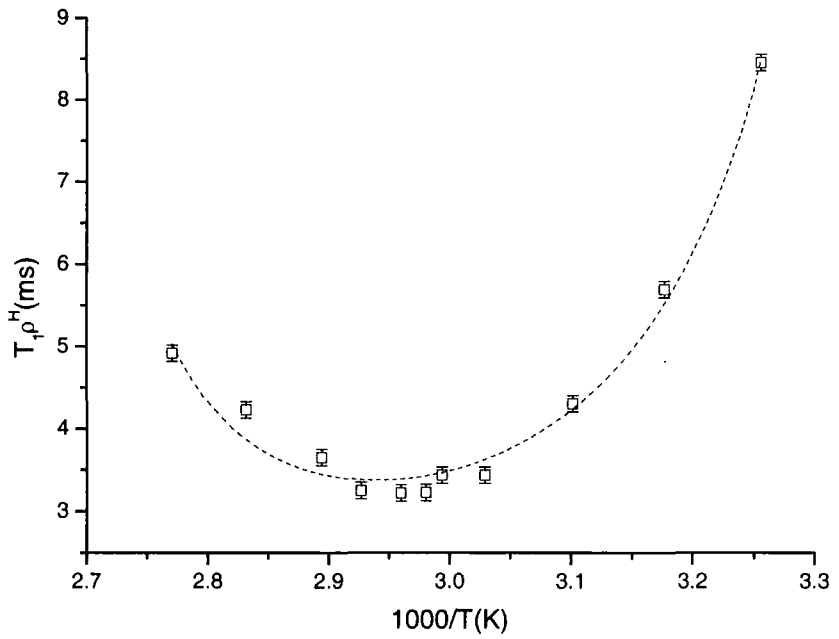

Figure 20. $T_{1\rho}{}^H$ measured at different temperatures,for the β form.

The values obtained from the fitting of the curve in figure 20 have been, for the activation energy (E_a), of 14 ± 2 kJ/mol, for τ_0, a value of $(5.4 \pm 0.5)\times10^{-8}$ s. It is interesting to notice that the motion detected by measuring $T_{1\rho}{}^H$ requires lower energy than the motion detected measuring T_1(H), although it is difficult to imagine the kind of motions that both these relaxation times detect. Some different information can be taken when considering the nitrogen relaxation times.

4.4.4 Variable temperature relaxation times experiments for nitrogens.

An analogous study was done for the nitrogens, in order to complete the picture of mobility for the molecule. Again, all experiments were performed only on the β form. The curve in figure 21 shows longitudinal relaxation times, with cross polarisation from protons, for the amido nitrogen, N(2). The curve in figure 22 shows the same relaxation time (measured with the pulse sequence T1xcp), for the amino nitrogen, N(1). The behaviours are quite different, showing greater mobility

at room temperature for N(2). A minimum is seen 295 K for N(2), where still at 393 K no minimum can be detected for N(1), so that, the behaviour seen when varying the temperature for proton relaxation times measurements, is similarly seen when measuring T_1 for N(1). The fitting curves are shown in dashed lines in figures 21 and 22. The fitting equation used was taken considering that the relaxation of the nitrogen would be more influenced by protons, so that the heteronuclear relaxation time equation was used (equation 2-9).

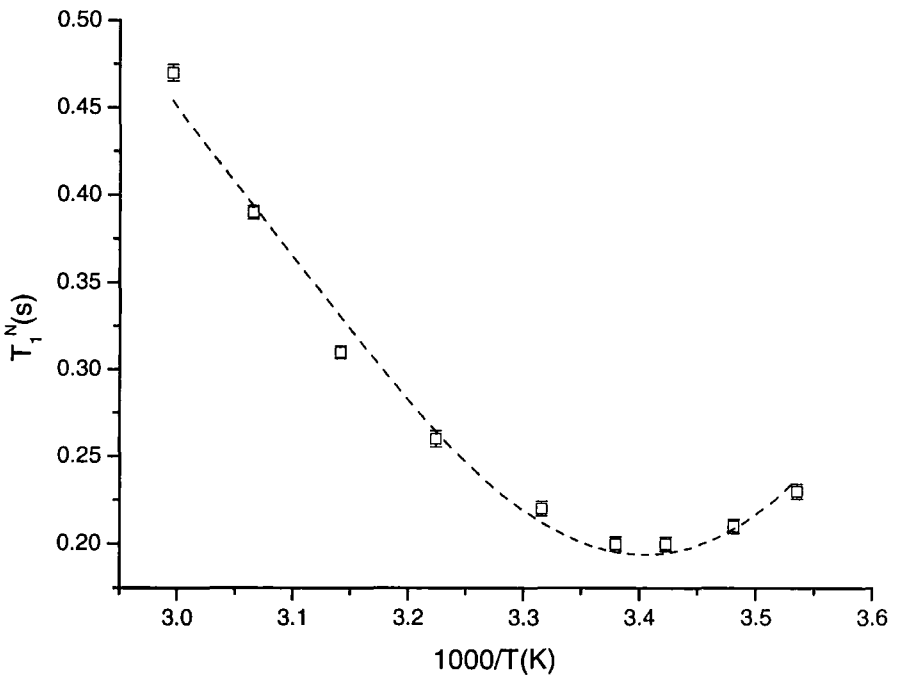

Picture 21. Variable temperature curve of the relaxation times for N(2), in the β form.

The value found from the fitting shown in figure 21 for the activation energy has been of 42 ± 4 kJ/mol.

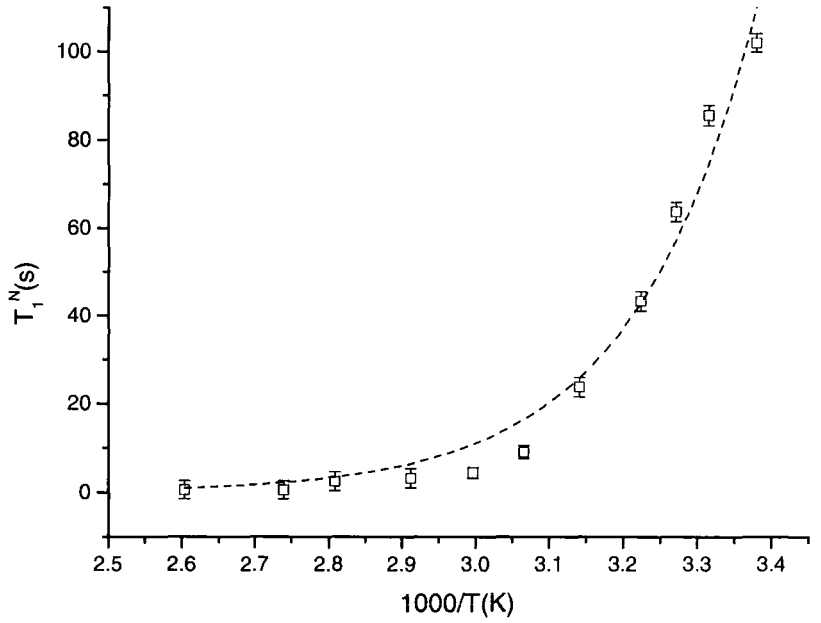

Figure 22. Variable temperature curve of the relaxation times for N(1), in the β form.

For N(1) the fitting gave a value of 49 ± 4 kJ/mol.

As we have seen all the values of the activation energy found for nitrogen are quite higher in value than the ones concerning protons, probably showing that fluctuations in the system are more far from the frequency of nitrogen than the ones for protons.

The other parameter that is important to measure is $T_{1\rho}$, as seen for the protons. Again the values for the two nitrogens are quite different showing different behaviour. The curves for $T_{1\rho}$ for protons, did not seem to add coherent information with the mobility characteristics seen until now, since for mobilities of the order of ms, there seemed to be a more complicated behaviour for the nitrogens. N(2) has generally greater values but it does not show a minimum, probably due to the fact that there more than one motion involved. Figure 23 is showing the results. In figure 24 we can see that the mobility of N(1) is, even for this range of frequencies, different from N(2).

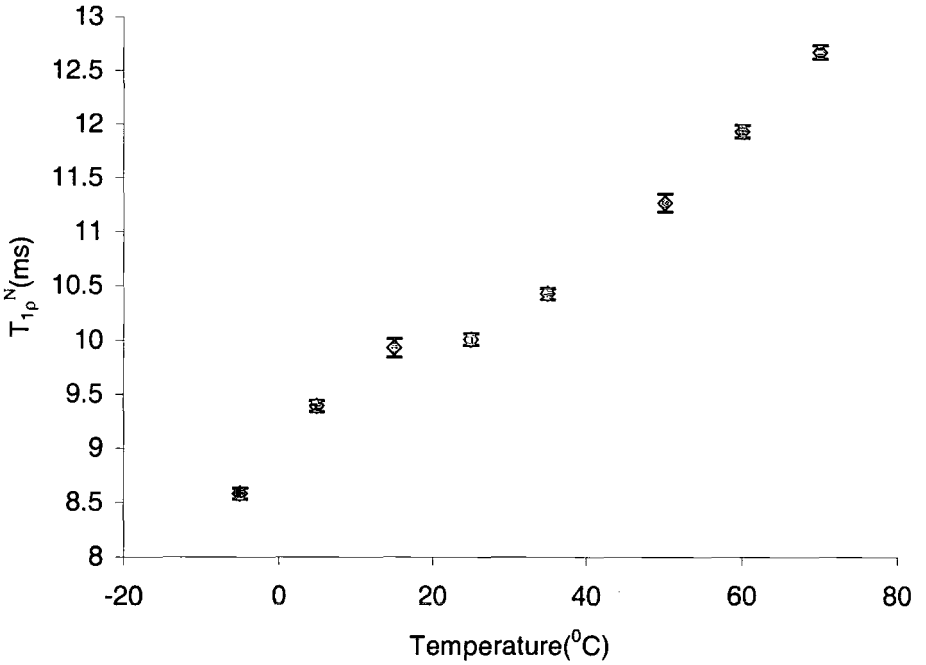

Picture 23. Results from spin-lock relaxation time measurements for N(2), for the β form.

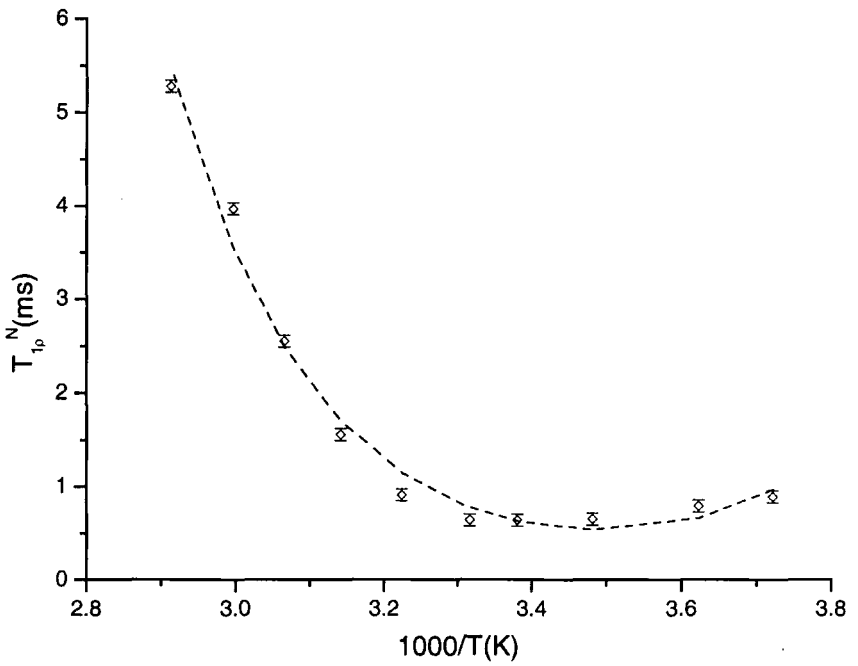

Picture 24. Results from spin-lock relaxation time measurements for N(1), for the β form.

The fitting from the curve shown in figure 24, fitted using equation 2-11. found an activation energy of 43 ± 3 kJ/mol

.

From the data of these variable temperature experiments, it has been possible to see that, the lowest value for E_a is found for the proton longitudinal relaxation times, where higher values are seen for the spin-lock relaxation time of protons as well as all the values seen for relaxation times of the nitrogens. The system that seems to be influenced more decidedly by more than one motion is N(1) when considering motions of the order of the kHz. It seems as if this system has, in any case not a simple motion, where every part of the molecule and every nucleus is influenced differently from varying the temperature and measuring the relaxation times.

4.5. The WISE experiment

Since there seemed to be a more mobile part in the proton spectrum as well, I tried to run a WISE experiment for which we would be able to a see if there is any correlation between this more mobile part of the protons and the amino nitrogen N(2). The results of this experiment, that was ran using the 300 MHz spectrometer are shown figure 25. The experiment was done spinning at a spin rate of 4 kHz, with a pulse width of 7 μs, a contact time of 1 ms, and a number of transients of 8.

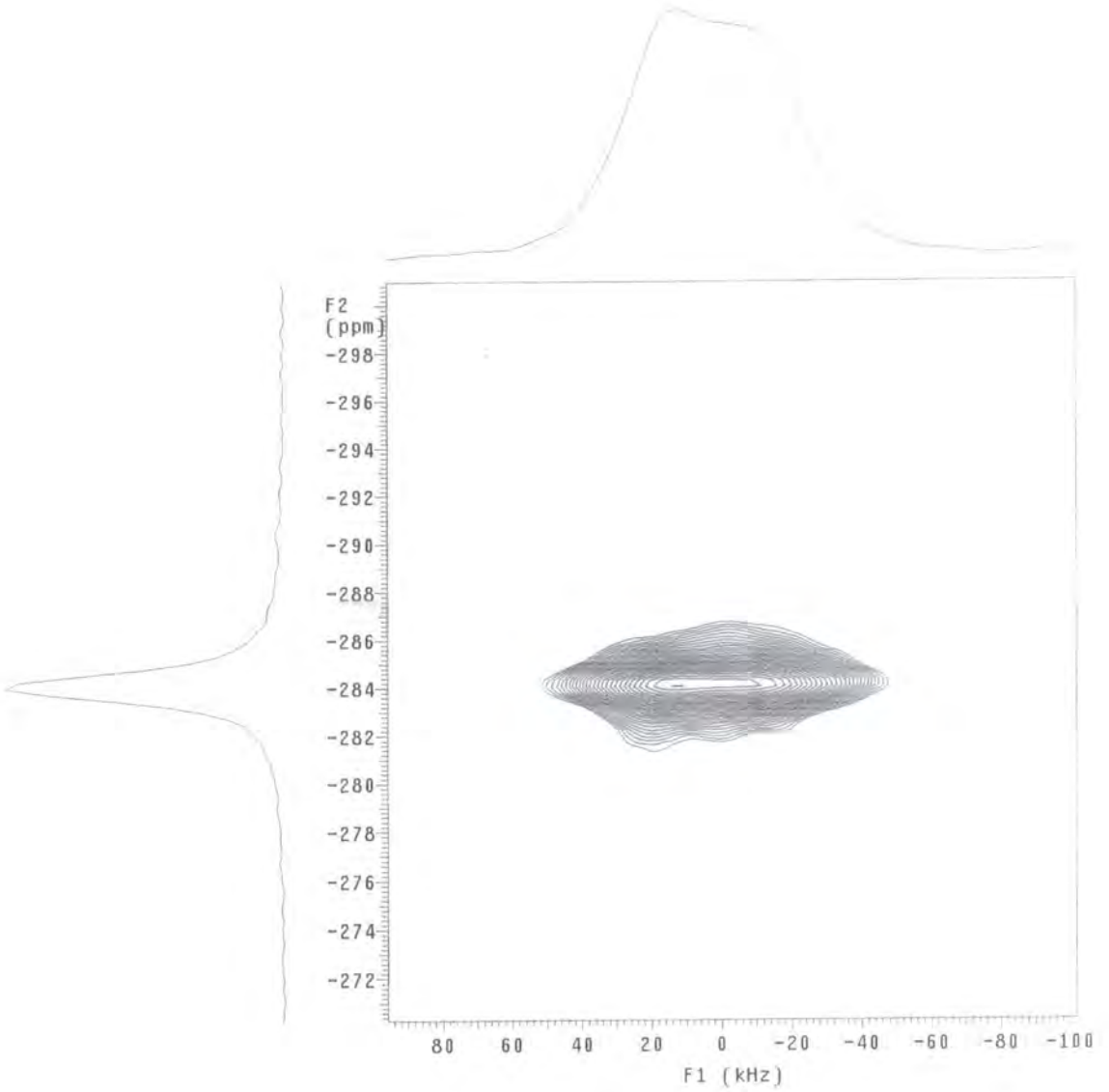

Figure 25. Wise experiment showing some correlation with the most mobile part of the proton peaks and the nitrogen peaks. Spinning speed 4 kHz, ct = 1 ms, nt = 8.

From this experiment the more mobile part of the proton is not very well defined, and there seems to be correlation with all the protons with the nitrogen peak. This is probably due to proton spin diffusion, so that there is no added information from this particular experiment.

4.6. Conclusions

Different NMR parameters have been studied for the molecule of sulfanilamide for both ^{13}C and ^{15}N. Only the complete analysis of all these parameters together has given interesting information on the characteristics of this molecule.

From the analysis of the different relaxation times of the nitrogen sites it has been possible to interpret part of the reasons for which we see the splitting in the carbon spectrum for C(2)/C(6) as due to the lack of mobility of N(1) nitrogen, which the above carbons are in an ortho position to. This has been interesting as well when considering that this nitrogen is likely to have a decisive role in the enzymatic inhibition.

Relaxation data have been taken further in analysing as well. Variable temperature relaxation times that have made possible a qualitative analysis of the concerted mobility of N(1) with the benzene ring, when considering rates in the order of the MHz , where N(2) seems to have a more independent mobility. Mobility analysis in the order of kHz has shown that the spin-lock relaxation time for N(2) is likely to be influenced by more than one movement.

Anisotropy and asymmetry analysis for the nitrogens has also shown, how even for this property the two sites have very different characteristics. This is an interesting matter when considering that previous studies on different molecular properties of sulfanilamide[1], such as the π-electron charge distribution for the two nitrogens has shown very different characteristic between the two sites. In particular Moriguchi's work[1] shows that the net charge on the amino group has a very similar value to the net charge of the analogous amino group of PABA (para-aminobenzoic acid), which as we have seen, is the molecule with which sulfanilamide competes in order to inhibit the enzyme, evidence of the essential role of this particular amino group.

Finally, the role that solid-state NMR can have in detecting impurities and analysing polymorphic mixtures, where other techniques might fail has been

demonstrated, the role in aiding better understanding in phase transformations and in relating solid state-effects seen in a simple monodimensional spectrum with conformational differences in the molecules.

4.7. REFERENCES

1) I. Moriguchi and S. Wada, *Chem. Pharm. Bull.* **1968**, *16*, 734.

2) T. W. G. Solomon,*Organic Chemistry*, 1992.

3) I. M. Klotz, *J. Am. Chem. Soc.* **1944**, *66*, 459.

4) P. H. Bell and R. O. Roblin, *J. Am. Chem. Soc.* **1942**, *64*, 2905.

5) W. D. Kumler and T. C. Daniels, *J. Am. Chem. Soc.* **1943**, *65*, 2190.

6) P. J. Bray and S. G. Greenbaum, *J. Mol. Struct.* **1982**, *83*, 35.

7) M. Pomerantz, W.Chou, M.K.Witczak and C. G. Smith, *J. Org. Chem.* **1987**, *52*, 159.

8) R. M. Silverstein and F. X. Webster,*Spectrometric identification of organic compounds*; Wiley:, 1996.

9) L. Frydman, A. C. Olivieri, L. E. Diaz, B. Frydman, A. Schmidt and S. Vega, *Mol. Phys.* **1990**, *70*, 563.

10) R. K. Harris and A. C. Olivieri, *Progress in nuclear magnetic resonance* **1992**, *24*, 435.

11) R. K. Harris, P. Jonsen, K. J. Packer and C. D. Campbell, *Magn. Res. Chem.* **1986**, *24*, 977.

12) C. H. Townes and B. P. Daily, *J. Chem. Phys.* **1949**, *17*, 784.

13) E. Schempp and P. J. Bray, *Phys. Chem.* **1970**, *4*, 522.

14) D. G. Ott,*Synthesis with stable isotopes of Carbon, Nitrogen, and Oxigen* New York, 1981.

15) U. Haeberlen,*High resolution NMR in solids: selective averaging.* New York, 1976.

16) M. M. Maricq and J. S. Waugh, *J. Chem. Phys.* **1979**, *70*, 3300.

17) J. L. Sudmeier, S. E. Anderson and J. S. Frye, *Concepts of magnetic resonance* **1990**, *2*, 197.

Chapter 5

THEORETICAL CALCULATIONS

5.1. Theoretical models

In recent years theoretical calculations have constituted a very powerful means to obtain molecular properties. I will briefly go through the developments of these calculations, although my main interest has been only in trying to find whether they are sufficiently developed enough to predict NMR properties of polymorphs.

From quantum mechanics we know that the energy and many other properties of a stationary state of a molecule may be obtained by solving the Schrödinger equation which, however, can be accurately solved in practice only for very small molecular systems. To solve the equation for systems in which more than one electron is present we must always use some kind of approximation and have an appropriate way to describe the system. A *theoretical model* is a model with which we can describe molecular systems of all sizes and simulate chemical structures and reactions using the fundamental laws of physics. Using the laws of classical physics we obtain all the molecular mechanics simulations, whereas if at the basis of our computations there are the laws of quantum mechanics we are dealing with electronic structure.

Electronic structure methods may be characterized in three major classes: semi-empirical methods, *ab initio* methods and density functional methods (DFT). If we predict single-point properties using *ab initio* methods, such as Hartree-Fock we can obtain a very high level of accuracy in the calculations even though we do not take into account electron correlation (the energy contributions arising from

electrons interacting with one another), which for molecules including double bonds is very important.

Recently, Density Functional methods have become very popular and have proved to be especially useful for the purpose of calculating NMR shielding constants[1-3]. They are based on the strategy of modelling electron correlation via general functions of the electron density and provide a way of predicting molecular properties in a computationally less demanding way than *ab initio* methods. The functionals that are now available for calculations of molecular properties include some that have been derived from pure mathematics, such as those based on the LDA[4] (Local Density approximation), although these have been proved to be insufficient for obtaining chemical shifts[5]. Among these, one that I have used for shielding calculations is SVWN, which is a widely used local-correlation functional. These are parameterless and they do not involve Hartree-Fock exchange but only the values of the electron spin densities.

Another class of functionals is one that contains parameters that have been chosen such that Khon-Shan calculations with them reproduce to a certain accuracy selected atomic or molecular data. These forms can be of the GGA (generalised gradient approximation) form i.e. they involve the density $\rho(r)$ and its gradient or of the hybrid form (they define the exchange functional as a linear combination of Hartree-Fock, local, and gradient-corrected exchange terms; this exchange functional is then combined with a local and/or gradient-corrected correlation functional). Among these there are the B1LYP[6] and B3LYP[7] functionals, where B stands for Becke (the pioneer of these hybrid functionals), the number stands for the number of parameters used to create the functional (so that B3LYP is called a three-parameter Becke functional), and LYP[8] shows that the functional is making use of the Lee-Yang-Parr correlation functional. One other hybrid functional that I have used in my calculations has been the B3PW91[9], which makes use of the Perdew-Wang gradient-corrected correlation functional. The conclusion is that there is no universal functional that works uniformly well for shielding calculations. The main problem is that for shielding constants the functional must provide an

accurate description of the density near the nucleus, whereas the functionals presently in use do not provide the correct asymptotic behaviour in the immediate vicinity of the nucleus and are consequently deficient for calculations of magnetic properties that involve $\langle r^{-3} \rangle$ operators. Another problem is that the electronic shielding of nuclei in molecules has a very small effect when compared with the total energy of the molecule, so that very accurate wavefunctions are required to calculate the effect of the shielding in a satisfactory way.

This second problem is mostly influenced by the choice of the basis-set: the mathematical representation of the molecular orbitals in the molecule. The basis set has a fundamental role in defining our theoretical models.

The simplest level of molecular orbital theory involves the use of a minimal basis set of nuclear-centred functions. These basis sets use fixed-size atomic-type orbitals. An example is the STO-3G which uses three gaussian primitives per basis function, which accounts for the 3G in its name, whilst STO stands for Slater-type orbitals. Minimal basis sets, though, are unable to expand and contract in response to different molecular situations, and they are also unable to describe the anisotropic aspects of molecular charge distribution (which are, of course, quite important for NMR calculations).

The first problem might be solved by using more than a single valence function of each symmetry type for the description of an atom. This will provide the necessary flexibility of the functions. Doubling all functions for the valence region of a minimal basis set leads to *double zeta basis sets* of which an example is 3-21G. We can also use *triple zeta basis sets* (e.g.6-311G) . In general, these sets are called **split valence basis sets**.

The problem of being able to change orbital shape can instead be solved by using **polarized basis sets** in which we include orbitals with higher angular momentum than the one required to describe the ground state. For example, polarized basis sets 6-31G* add d functions to first row atoms.

A further way to improve orbital descriptions is to use **diffuse basis sets**, which are able to describe electron density relatively far from the nucleus. Examples are 6-31+G and 6-311+G. These are very important when it is necessary to describe charged molecules. The choice of the basis set strongly depends on the molecular system that has to be studied, as well as on the resources available.

5.2. Chemical Shift Theory

When a molecular system is introduced into an external magnetic field, this field induces currents arising from the interaction of the electrons with the magnetic field. These induced currents themselves generate secondary magnetic fields that diminish or enhance the external magnetic field, which results in the phenomenon of magnetic shielding of NMR-active nuclei.

The magnetic shielding is a tensor property whose elements are given by:

$$\sigma_{\alpha\beta}=(\partial^2 E/\partial B_\alpha \partial\mu_\beta)$$

where B_α and μ_β denote the corresponding components of the external magnetic field and the magnetic moment of the considered nucleus, respectively, whilst E is the electronic energy of the system.

The calculation of NMR chemical shifts has two major problems. First, the chemical shielding tensor σ, as we have seen, is a second-order property. Such quantities are more difficult to calculate than the corresponding first-order properties. The second difficulty in the computation of NMR chemical shifts is the gauge-invariance problem which is found in all calculations of magnetic properties.

The first problem arises from the fact that $\sigma_{\alpha\beta}$ has to be determined with a perturbation treatment, and this is based on the calculation of the influence of the electrons in the presence of a magnetic field $\mathbf{B}_j$ consisting of two components, the

external magnetic field and the magnetic field due to the magnetic dipole moment μ of the considered nucleus. We can in fact write, according to classical electromagnetic theory, that the energy of a magnetic dipole μ in a field $\mathbb{B}_j$ is

$$E = - \mu \cdot \mathbb{B}_j$$

where $\mathbb{B}_j$ is defined by:

$$\mathbb{B}_j = -\sigma \mathbf{B}$$

However, this is a simplification since, as we have already mentioned, the shielding is a tensor with nine components and not a scalar quantity.

In the presence of a magnetic field described by a vector potential **A**, the hamiltonian is obtained by replacing the linear momentum **p** wherever it occurs by **p** + e**A**.
The unperturbed hamiltonian is:

$$H^{(0)} = (1/2m_e)p^2+V$$

If we replace p with (**p**+e**A**), we will in the end have:

$$H=(1/2m_e)p^2+V+(e/m_e)\mathbf{A}\cdot\mathbf{p}+(e^2/2m_e)A^2$$

This differs from the original hamiltonian by the presence of first- and second-order terms, so we can write:

$$H=H^{(0)}+ H^{(1)}+ H^{(2)}$$

The second-order contribution to the energy of the system has to be calculated using the perturbation expression:

$$E^{(2)} = \langle 0|H^{(2)}|0\rangle + \langle 0|H^{(1)}|1\rangle$$

The traditional perturbation theoretical treatment is based on the assumption that the zero-order wave function is known, including a set of the wave functions of the excited states. The first-order perturbed wave function is then written as a linear combination of these known states. This is the approach that was introduced by Ramsey to understand the shielding of non-spherically-symmetric nucleus.

If the wave function ψ^0 is known, the first term of the expression of $E^{(2)}$ (the diamagnetic part, which weakens the external magnetic field at the centre of the induced electronic motion) can be calculated easily. The problem lies in calculating ψ^1, which is present in the second term of the expression (the paramagnetic term, which enhances the external magnetic field), since it is a sum over all excited states and one must be sure to include all significant contributions.
The final expression is:

$$E^{(2)} = \langle 0|H^{(2)}|0\rangle + \sum_{n\neq 0}\{\langle 0|H^{(1)}|n\rangle \langle n|H^{(1)}|0\rangle / (E_{(0)} - E_{(n)})\}$$

The fact that one must include all the relevant excited states is the main reason why a second-order property is so difficult to calculate. The other problem with the sum-over-states treatment of Ramsey's[10] equation is that when Hartree-Fock is used the inter-electron interactions will not be calculated in the presence of the perturbing magnetic field. In order to overcome this problem Stevens[11] introduced the Coupled Hartree-Fock (CHF) perturbation theory, which allows the calculation of magnetic properties of small (mostly diatomic) molecules.

The second problem outlined above was that of a gauge origin. When applied to a molecular system, the magnetic field **B** appears in the Hamiltonian only in form of the vector potential **A** whose origin, the gauge origin, is not fixed. As long as a complete basis set is used in quantum chemical calculations, the results are independent of the choice of the gauge origin. This is not true for finite basis sets.

As we know, the molecular orbitals are written as linear combinations of atomic orbitals. The origin of the atomic orbital is located at the corresponding nucleus. This treatment does not cause any problems as long as the external magnetic field is absent.

The use of very big basis sets would overcome this problem, but obviously it would be highly demanding for computation times. An alternative way of treating the problem is to introduce gauge factors into either the atomic orbitals of the basis set or into the MO of the CHF calculation. This procedure can lead to shielding results that are independent of gauge origin, even though the calculation is an approximate one. London in 1937[12] proposed the inclusion of gauge factors in calculations by means of gauge including atomic orbitals (GIAO).

The resulting complex orbitals[13] ψ_n are used in place of the usual, real, atomic orbitals φ_n.

$$\psi_n=\varphi_n \exp[-ie/h(\mathbb{A}_n)\mathbf{r}]$$

If the complex pre-factor of the orbitals is not considered, one obtains additional contributions to the kinetic energy which depend on the distance between the orbital and the origin of the vector potential. If we were to use infinite size basis sets, this contribution would vanish over the sum of all states, but the truncation of the basis sets is actually the reason for which there is the gauge problem.

There are other techniques that achieve gauge invariance. The most important of these (IGLO[14], independent gauge for localized orbitals, LORG[15], localized orbital-local origin, and SOLO[16], second-order LORG) apply gauge factors not to atomic orbitals but to localised molecular orbitals. The most valuable advantage of the IGLO method is the possibility of analyzing the shielding effects of inner shells, bonds, and lone pairs separately, which provides a theoretical basis for a number of calculations. The IGLO calculations can give a decomposition of the magnetic shielding tensor into the contributions[17]:

$$\sigma_{\alpha\beta} = \sigma^{is}{}_{\alpha\beta} + \sigma^{bo}{}_{\alpha\beta} + \sigma^{ts}{}_{\alpha\beta}$$

where $\sigma^{is}{}_{\alpha\beta}$ stands for inner shell shielding, $\sigma^{bo}{}_{\alpha\beta}$ is caused by the bonds or lone pairs adjacent to the considered nucleus and the third term is called the through-space contribution and is caused mainly by the motion of electrons in the other localized orbitals.

Another method for calculation is IGAIM[18] (individual gauges for atoms in molecules), which uses the calculation of molecular current-density distributions. The IGAIM method amounts to constructing the induced current-density distribution of a molecule from its constituent atoms.

For my calculations I have used only the GIAO method. I will compare results obtained using the HF and density functional theory (DFT) theoretical models for the sulfanilamide molecule and its three polymorphs to calculate the shielding of both ^{13}C and ^{15}N nuclei.

5.3. ^{13}C calculations

All my calculations were undertaken with Gaussian 94[19] and Gaussian98[20], which is a program capable of performing molecule structure optimisations as well as predicting various molecular properties. The computer facilities used were mainly from Durham University, in particular the High Performance Computing service (by the name of hal), a cluster of eight Sun Ultra 80 'nodes' each with four 450 Hz Ultra Sparc Ultra Sparc II processors 2 Gbytes memory.

When calculating the theoretical shielding, in order to make a direct comparison with the experimental value, we should obtain the shielding of the reference molecule.

One way to consider the reference (which for ^{13}C would be tetramethylsilane, TMS) is to optimise the geometry of TMS to the level at which the NMR shielding is to be calculated and then to consider the shielding on this optimised molecule. However, having tried this, I have seen that not always it is possible to optimise the molecule, meaning that sometimes the geometry does not converge. The other way would be to optimise to a lower level (to which the geometry converges) and to consider the shielding on this molecule. The final way is to consider the shielding of tetramethylsilane from the experimental value. I have decided to use this last method, which is largely employed in the literature, and it is the only method in which we can have a value for the shielding that does not depend on the theoretical model used; the value for the shielding of TMS is 186.4 ppm[21].

Another approximation that we are making while performing these calculations derives from the fact that a real molecular conformation is the time average of different conformations (on the NMR time-scale), but when we calculate the shielding theoretically we assume a rigid framework which corresponds to the minimised conformation. As we will see, this might be the source of discrepancy for some carbon shielding values.

Keeping in mind these limitations of the calculations, we can compare the different and most commonly used models and basis sets for the prediction of polymorphic differences of sulfanilamide. This is shown in tables 1, 2 and 3.

	Calculated and Observed Nuclear Shielding for the alpha form (given in ppm)							
Atom	HF/6-31G**	HF/311-G**	B3LYP/6-31G**	B3LYP/6-311G**	SVWN/6-31-G**	SVWN/6-311-G**	B3PW/6-311G**	Expt
C(4)	109.0	122.9	122.4	139.3	125.0	143.6	136.1	128.0
C(3)	117.3	132.9	114.0	132.6	113.3	133.2	129.9	128.3
C(2)	86.4	100.3	94.0	111.1	95.5	114.2	108.3	113.1
C(1)	139.1	155.1	136.0	158.0	133.6	157.1	153.8	153.7
C(6)	88.5	102.9	95.0	112.5	96.3	115.4	109.7	115.3
C(5)	115.2	130.9	112.0	130.5	111.1	130.9	127.7	128.3
RMS error	19.6	7.9	16.3	5.5	16.3	6.9	4.5	

Table 1. Comparison of calculations on a single molecule of the α form of sulfanilamide.

The RMS error for the shielding values is considered as the square root of the sum of the squares of the errors divided by the number of carbons[22]. From the RMS values we can immediately see how triple zeta basis sets (6-311G**) give better results from the double-zeta ones (6-31G*).

	Calculated and Observed Nuclear Shielding for the beta form (given in ppm)							
Atom	HF/6-31G**	HF/311-G**	B3LYP/6-31G**	B3LYP/6-311G**	SVWN/6-31-G**	SVWN/6-311-G**	B3PW/6-311G**	Expt
C(4)	108.5	122.5	122.1	138.9	124.6	143.2	135.9	127.1
C(3)	116.7	132.5	115.3	133.7	111.7	134.1	131.0	129.5
C(2)	88.4	102.4	95.9	113.1	98.0	116.2	110.3	112.3
C(1)	139.1	155.1	135.6	157.4	133.0	156.3	153.2	153.4
C(6)	89.4	103.6	96.7	114.1	97.2	117.1	111.1	117.1
C(5)	118.7	133.9	112.7	131.4	114.4	131.6	128.7	129.5
RMS error	19.0	7.4	15.9	5.6	16.2	7.2	4.5	

Table 2. Comparison of calculations on a single molecule of the β form of sulfanilamide.

	Calculated and Observed Nuclear Shielding for the gamma form (given in ppm)							
Atom	HF/6-31G**	HF/311-G**	B3LYP/6-31G**	B3LYP/6-311G**	SVWN/6-31-G**	SVWN/6-311-G**	B3PW/6-311G**	Expt
C(4)	108.8	123.0	121.9	138.8	124.5	143.1	135.8	127.1
C(3)	116.7	132.1	113.8	131.8	113.1	132.2	129.6	129.6
C(2)	85.4	99.8	92.3	109.8	93.8	112.9	107.1	112.7
C(1)	134.4	150.2	132.3	153.8	130.3	153.4	149.8	151.0
C(6)	88.1	102.7	95.1	112.7	96.6	115.9	110.0	115.1
C(5)	116.8	132.2	113.5	132.2	112.6	132.7	129.2	129.6
RMS error	20.1	7.7	16.9	5.3	16.8	6.8	4.7	

Table 3. Comparison of calculations on a single molecule of the γ form of sulfanilamide.

As mentioned above considering the reference for direct comparison will always include other sources of errors, so it is also correct to correlate observed chemical shifts with the absolute shielding values. This method to assess the theoretical model used provides a visual aid for comparisons, but we should be careful in

relying on it since the values of the slope or of the correlation factor (that, when in good agreement should both be 1) are not affected by the variations of the individual shielding values but they show only an average effect.

I will give only one example of these correlations for the alpha form. Graph 1 shows correlations of the theoretical shielding versus experimental of the models using double-zeta basis sets, where graph 2 shows models with triple-zeta basis sets.

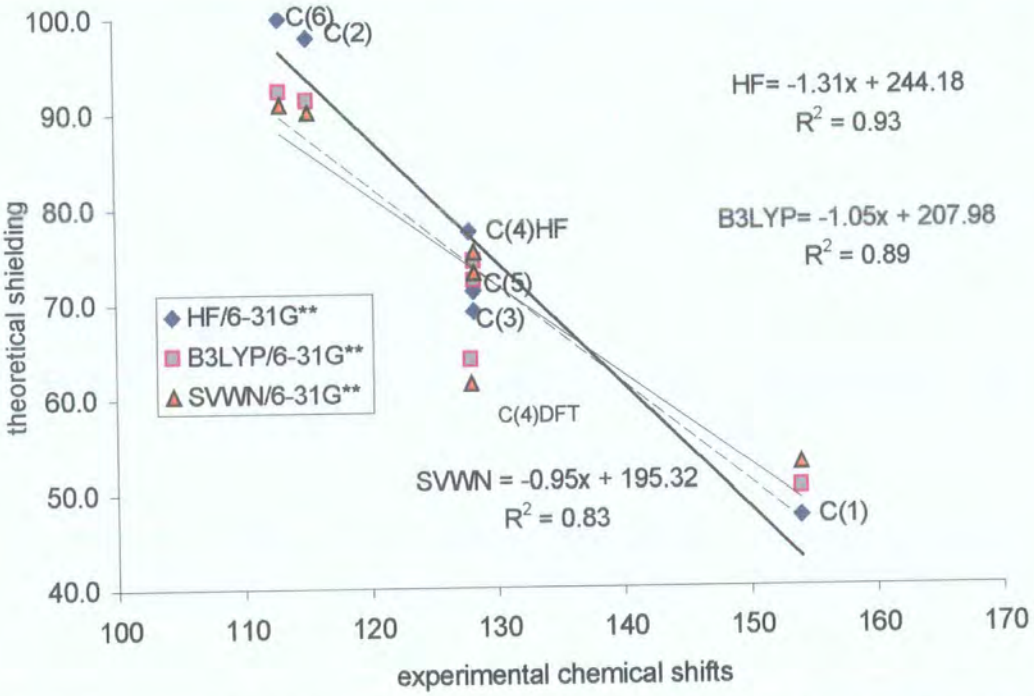

Graph 1. Theoretical shielding vs. experimental chemical shifts for the α form for HF and DFT models using the 6-31G** basis set.

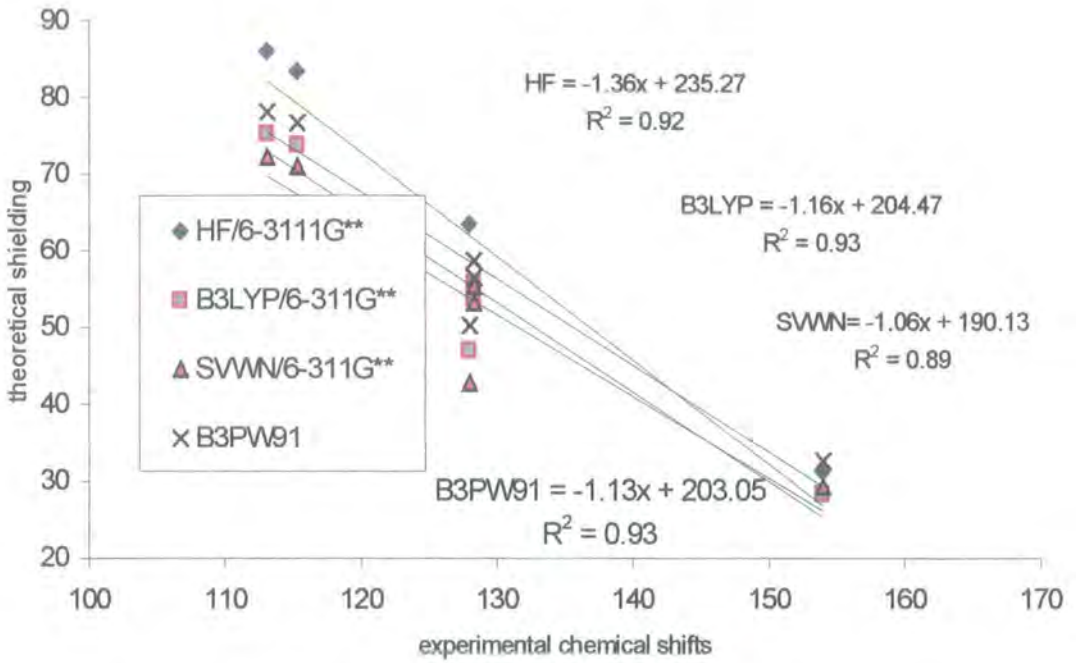

Graph 2. Theoretical shielding vs. experimental chemical shifts for the α form for both HF and DFT methods using 6-311G** basis set.

From graphs 1 and 2 it is easy to see that C(4) is the atom affected more when changing from HF to DFT methods followed by C(2) and C(6) (all showing less shielding when described with DFT methods) where C(3), C(5) and C(1) do not show great differences from one method to the other. When we use a triple zeta basis set instead of a double zeta the shielding values are generally lower, and, taking into consideration R^2 DFT methods perform better with this basis set.

The carbon that is the least well defined with all models, is C(4) , which is bonded to the sulfonamide group. This is probably because the sulfur atom is not described well enough using these basis sets.

I have tried a special basis set for the sulfur atom which makes use of a greater number of Gaussians (less contracted basis set)[23], and kept the other atoms described by 6-311G**. It seems, as shown in graph 3, that C(4) does not change its shielding but the shieldings of C(3)-C(5) are described differently, with an overall slightly better effect.

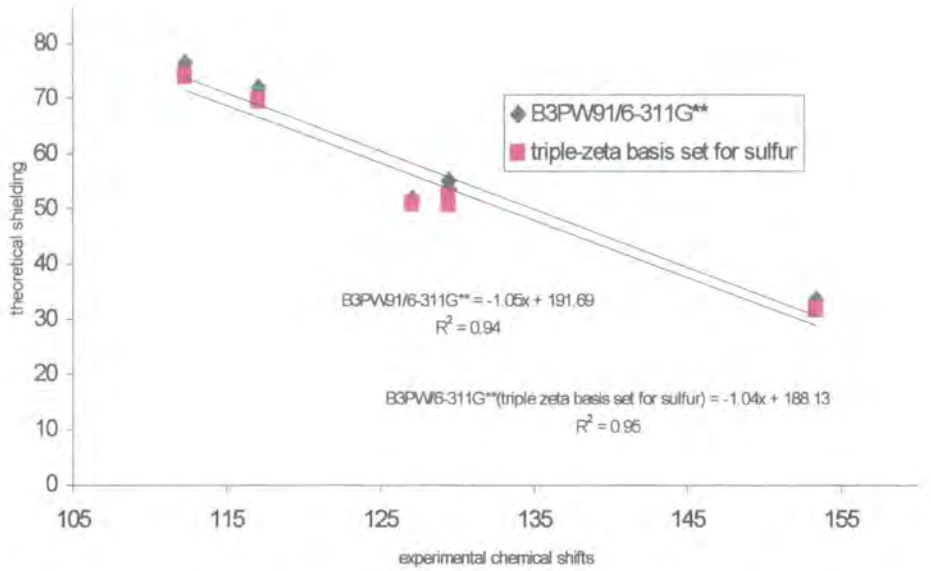

Graph 3. Shielding calculated on neutron diffraction data (for the β form) using a larger basis set to describe sulfur.

One characteristic that is important to notice in these calculations is the fact that they are sensitive enough to detect the splittings between the carbons C(2)/C(6) and C(3)/C(5). When analysing these splittings, we see that the order of magnitude for C(2)/C(6), at least for the α and γ forms, is about right. The discrepancy is mostly for C(3)/C(5), for which no splitting is seen experimentally.

Splittings alpha								
ppm	HF/6-31G**	HF/311-G**	B3LYP/6-31G**	B3LYP/6-311G**	SVWN/6-31-G**	SVWN/6-311-G**	B3PW/6-311G**	Expt
C(6)-C(2)	2.0	2.6	1.0	1.4	0.8	1.2	1.4	2.2
C(5)-C(3)	2.1	2.0	2.1	2.1	2.2	2.2	2.2	/
Splittings beta								
ppm	HF/6-31G**	HF/311-G**	B3LYP/6-31G**	B3LYP/6-311G**	SVWN/6-31-G**	SVWN/6-311-G**	B3PW/6-311G**	Expt
C(6)-C(2)	1.1	1.2	0.9	1.0	0.8	0.9	0.8	4.8
C(5)-C(3)	2.0	1.4	2.6	2.3	2.7	2.5	2.3	/
Splittings gamma								
ppm	HF/6-31G**	HF/311-G**	B3LYP/6-31G**	B3LYP/6-311G**	SVWN/6-31-G**	SVWN/6-311-G**	B3PW/6-311G**	Expt
C(6)-C(2)	2.7	2.9	2.8	3.0	2.8	3.0	2.9	2.4
C(5)-C(3)	0.0	0.0	0.3	0.4	0.5	0.5	0.4	/

Table 4. Comparison of splittings for the equivalent carbons of the phenylene ring.

The reason for this discrepancy is probably the fact that the sulfonamide group is very mobile at about room temperature (as is seen from the measurements of relaxation times for ^{15}N), whilst the amino group is quite immobile. This is a very good example of the importance of having knowledge of the mobility of the molecule before judging the correctness of results from calculations.

The fact that for the β form the C(2)/C(6) splittings are badly predicted probably arises because, for this form, intermolecular effects are more important. It is in fact the only form of the three to have three hydrogen bonds less than 3.10 Å (where the others have only two). It is also the only form for which there are neutron diffraction data[24], and this proves to be very useful since it is immediately clear how much these calculations are affected by the exact position of the protons.

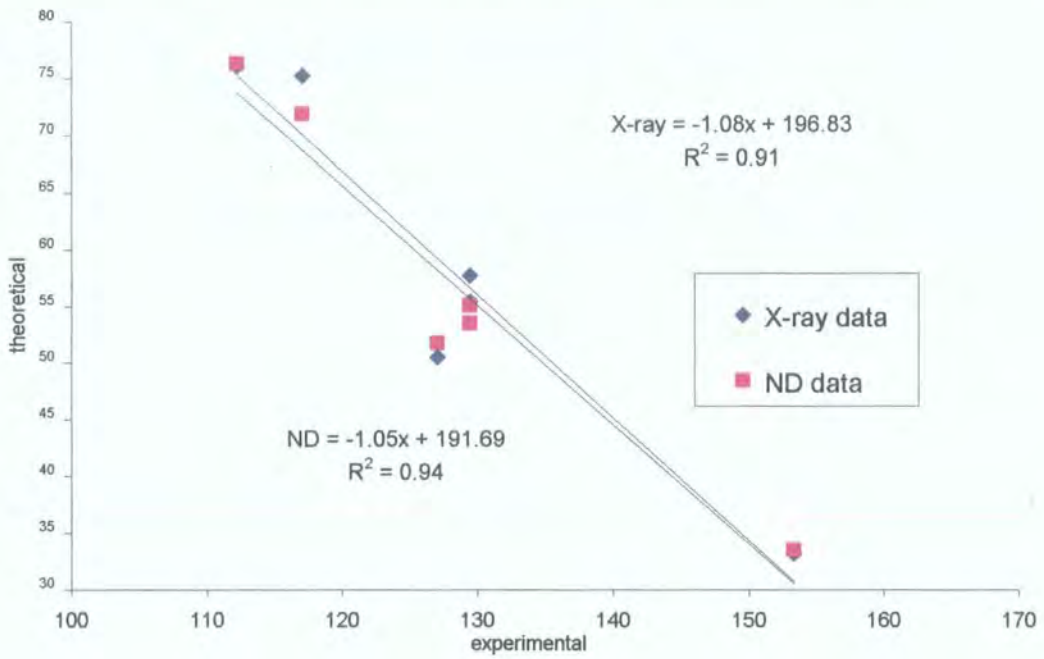

Graph 4. Shielding calculated on X-ray and ND data for the β polymorph (B3PW91/6-311G**).

This comparison shows very well how it is of considerable importance for shielding constants to be predicted starting from neutron diffraction data.

In particular it helps to explain the splitting between C(2)/C(6) since the theoretical and the experimental values are close (4.4 ppm calculated against 4.8 ppm experimental).

The first effect that one could think for influencing the shielding of these two carbons would be a distortion in the amino group. But when comparing data from X-ray analysis there are no major effects that one could attribute to this if not the length of the C(1)-N(1) bond itself being quite shorter than for the other forms. This, as we have seen before (chapter 3) is due to the resonant form (see figure 2 from chapter 3).

In table 5 we see the comparison of the different data from X-ray.

Polymorph	Bond length (Å) C(1)-N(1)	Angle C(2)-C(1)-N(1)	Angle C(6)-C(1)-N(1)	C(6)-N(1)-H(6)	C(6)-N(1)-H(6)	Dihedral C(2)-C(1)-N(1)-H(5)	Dihedral C(6)-C(1)-N(1)-H(6)
α	1.374	120.60	120.65	115.5	114.1	10.4*	21.1*
β	1.368	120.87	120.41	118.6	117.6	14.4	17.5
γ	1.377	121.75	119.48	118.7	118.1	17.7	20.9

Table 5. X-ray data for the three forms, considering part of the molecule with the amino group.

*for the α form the protons are under the ring (see crystal data chapter 3)

For the neutron diffraction data the C(1)-N(1) bond appears to be 1.385Å, and is significantly longer. The C(2)-C(1)-N(1) and the C(6)-C(1)-N(1) angles are basically the same as the X-ray (120.4 and 120.9) as well as the other angles.

When we compare the hydrogen positions, there seems to be no significant difference in the two sets of data, except that for the hydrogens attached to N(1) are a little different.

CH bonds	X-ray(Å)	ND(Å)
C(2)-H(1)	0.98	1.03
C(3)-H(2)	0.98	1.07
C(5)-H(3)	0.94	1.10
C(6)-H(4)	1.00	1.10
N(2)-H(7)	0.85	1.00
N(2)-H(8)	0.87	1.00
N(1)-H(5)	0.90	0.97
N(1)-H(6)	0.86	1.04

Table 6. Comparison between hydrogen positions from neutron diffraction data and X-ray.

Although it is difficult to interpret the exact causes for which ND data gives different shielding values from the X-ray geometry, it goes to show that small differences can significantly affect the shielding and, in principle, we should refine the positions of the protons if we could establish on one form, having ND, the best basis set to use data and then perform proton optimisations on the other forms.

This is not always possible. I have tried in different ways to optimise only the protons of the different forms, but always ended up in a relative and not absolute minimum (checked from frequency calculations on the molecule). So it is not always feasible to obtain the right optimisation of the protons.

When neutron diffraction data is not available it is as well possible to correct the shielding values considering intermolecular effects, i.e. including more than one molecule in the calculation.

5.4. ^{13}C calculations on hydrogen-bonded molecules

The first calculations of the influence of hydrogen bonding on the magnetic shielding of protons were carried out by Ditchfield[25] for protons in water dimers.

It is of interest to try such calculations for bigger systems, although it would be computationally much more demanding. In a recent review[26] Pecul et al. have calculated shielding constants for solid acetylene by considering a cluster of 13 molecules. The best way should be to take into consideration molecules that are connected through hydrogen bonds and that are the nearest ones.

The hydrogen bond networks for each polymorph of sulfanilamide were studied and dimers, trimers and tetramers, according to the case in question, were considered for the calculations using, unless otherwise specified, the X-ray data so that a direct comparison between the forms is feasible. The basis set used has been 6-31G** at a B3LYP level in order to find the entity of the improvement.

The differences for the shielding calculations were not drastic but it does seem as if some changes are present as we can see from graph 5 in which the hydrogen bonded molecule is compared with the isolated one for the α form.

To consider the hydrogen bonded molecules I have included only the hydrogen bonds less than 3.11 Å and, as previously seen, for the α form, with this cut-off, we can consider three hydrogen bonds.

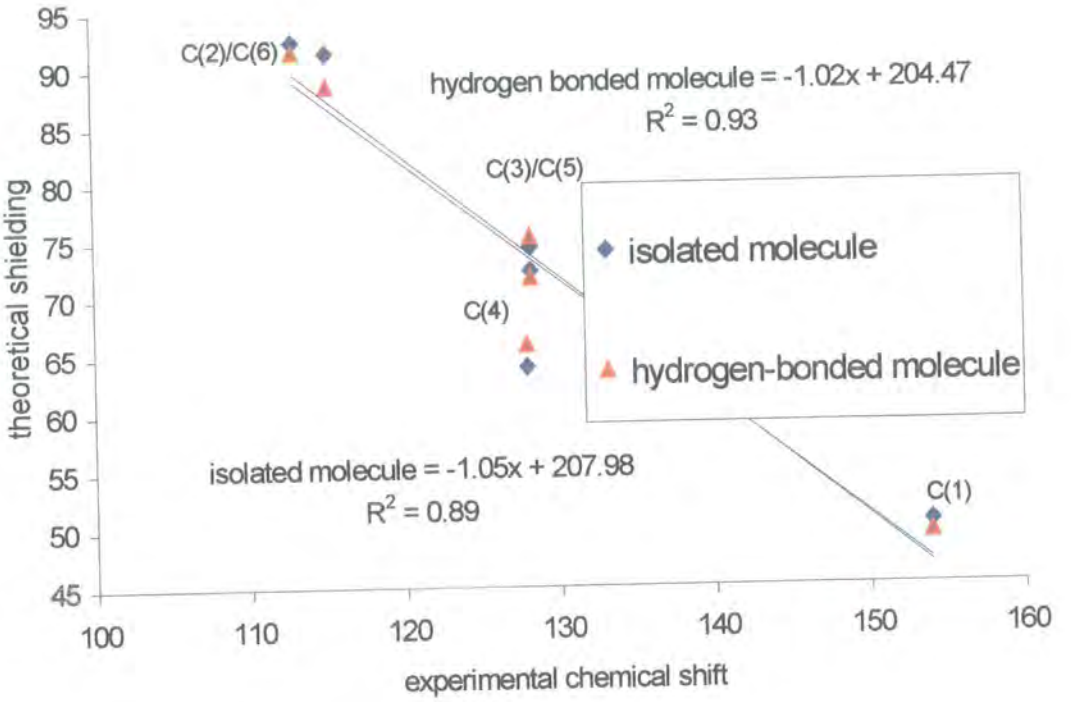

Graph 5. Shielding of the isolated molecule compared to the shielding of the tetramer in which molecule 2 (with three hydrogen bonds) is considered.

In figure 1 we see how the hydrogen bonded molecules were considered; molecule 2 is the one taken for comparison with the isolated one in the previous graph.

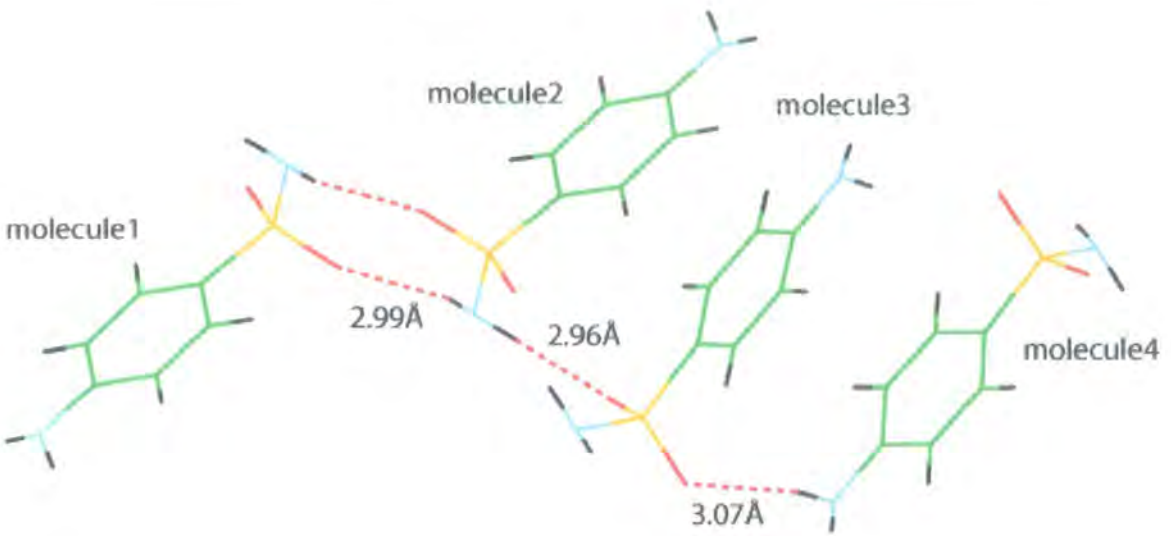

Figure 1.. Tetramer for the calculations of the α form.

The general effect when including more than one molecule in the calculation is of slight improvement in the correlation, as seen from graph 5 where we can notice a better description of the C(2)/C(6) splitting (from 1 ppm to 3 ppm) and less shielding on C(4), which brings it nearer to experimental.

The calculations were performed on the single dimers as well, from which we could see that including the molecule bonded through the 3.07Å (O(1)....N(1)) bond, there is no significant difference in the shielding, where, considering the 2.96Å hydrogen bond has an influence mostly on the molecule involving the nitrogen.
For the trimer the calculation was not too far from the tetramer.

For the β form we need to consider a tetramer when including the different hydrogen bonds, as shown in figure 2.

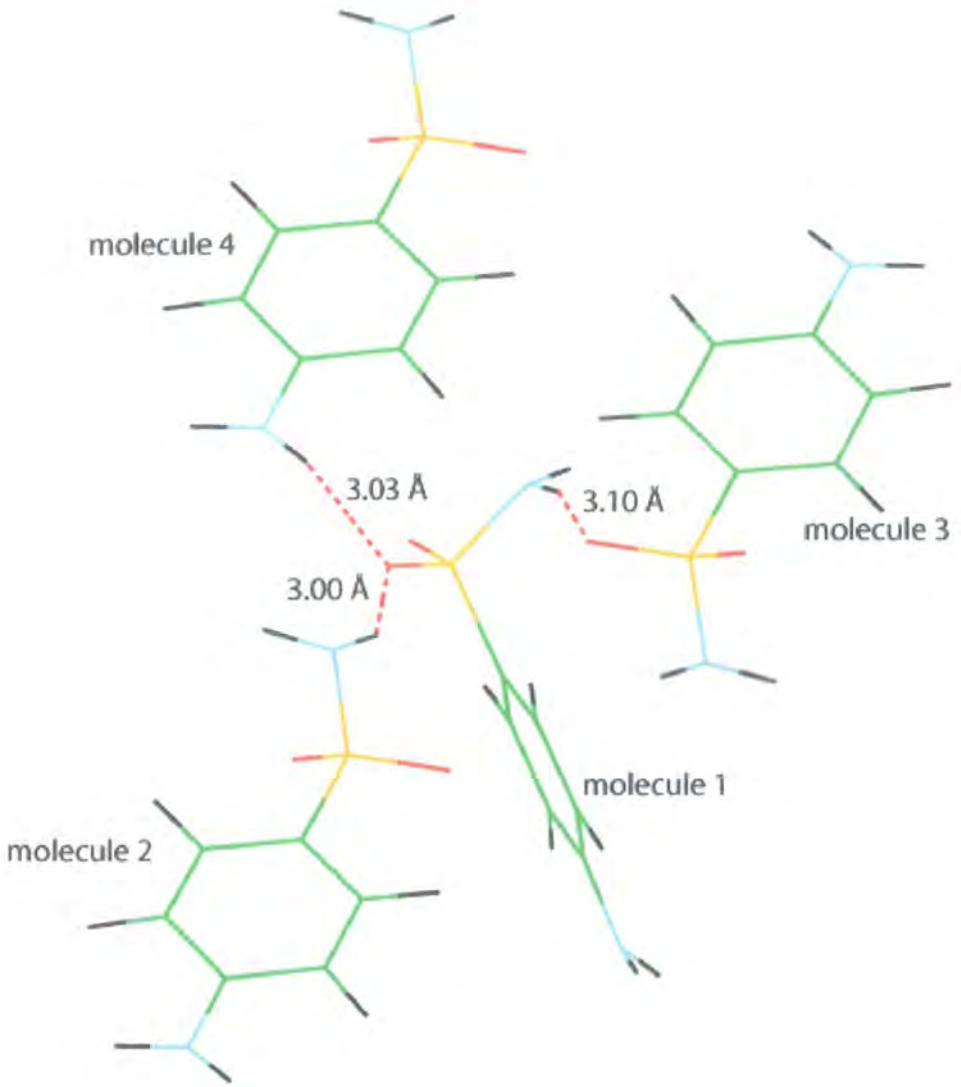

Figure. 2. Tetramer considered for the hydrogen bonding network of the β form.

Considering the changes for molecule 1 in figure 2 we can see that the overall improvement from hydrogen bonding is small, especially since the shielding of C(4) does not change a lot, but what is reassuring is that the separation between C(2)/C(6) has a greater enhancement in this case, almost reaching the experimental value of 4.9 ppm (from 0.9 ppm for the isolated molecule).

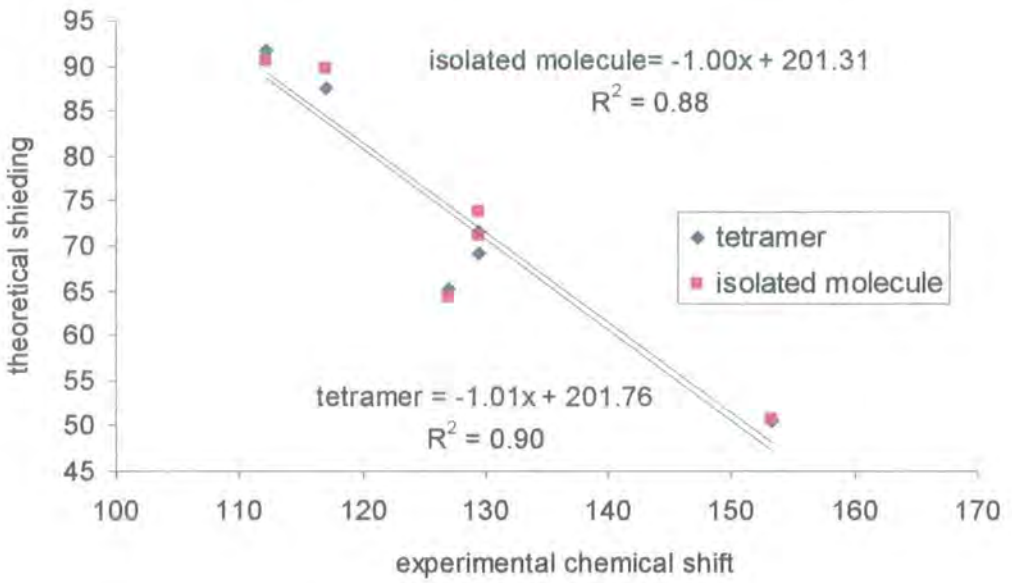

Graph 6. Intermolecular effects, calculated using the B3LYP/6-31G** basis set for the form β

When using neutron diffraction data, results for the isolated molecule are at the level reached by including more than one molecule in the calculation using X-ray data, obviously at a lower cost. We can see the comparison in graph 7.

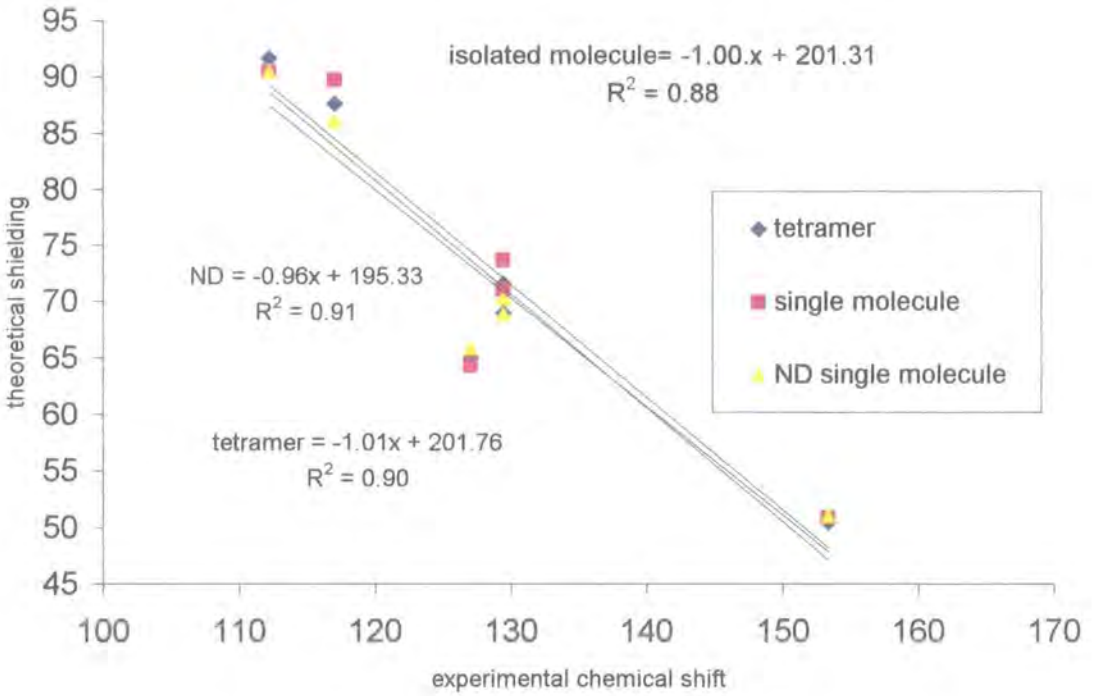

Graph 7. Comparison of the hydrogen bonded molecule from the tetramer of the β form, the isolated molecule from the X-ray and the ND data on the isolated molecule using B3LYP/6-31G**.

On the other hand, the calculation on the tetramer using neutron diffraction data does not improve the results. This is probably due to the fact that we have reached a limit of accuracy, at least at this level of basis sets.

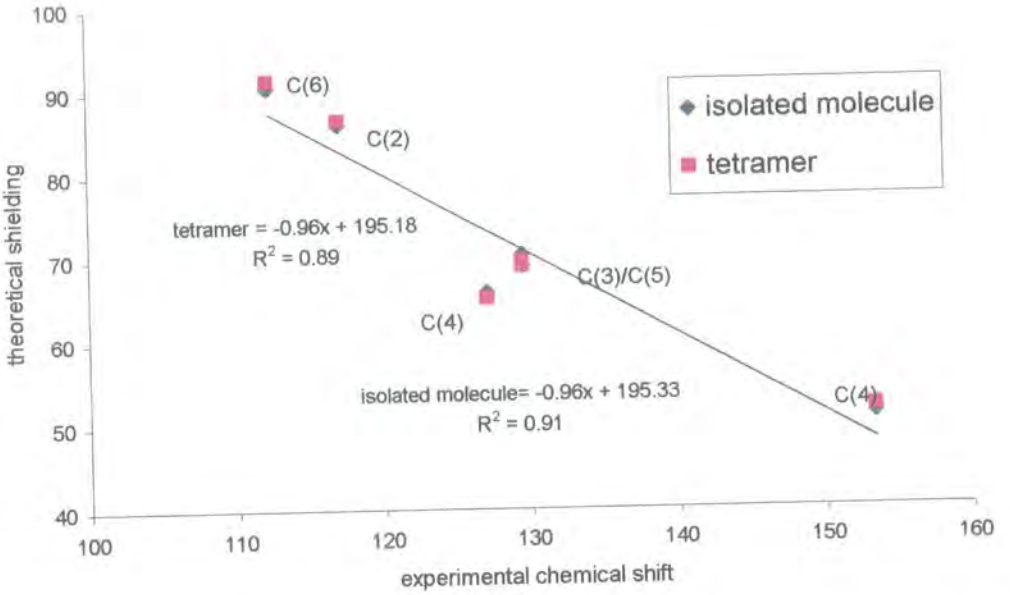

Graph 8. Comparison between the hydrogen-bonded molecule and the isolated for the β form using the neutron diffraction data using B3LYP/6-31G**.

The γ form has certainly the least changes, and it seems as if in this case hydrogen bonding patterns do not influence too much the shielding.

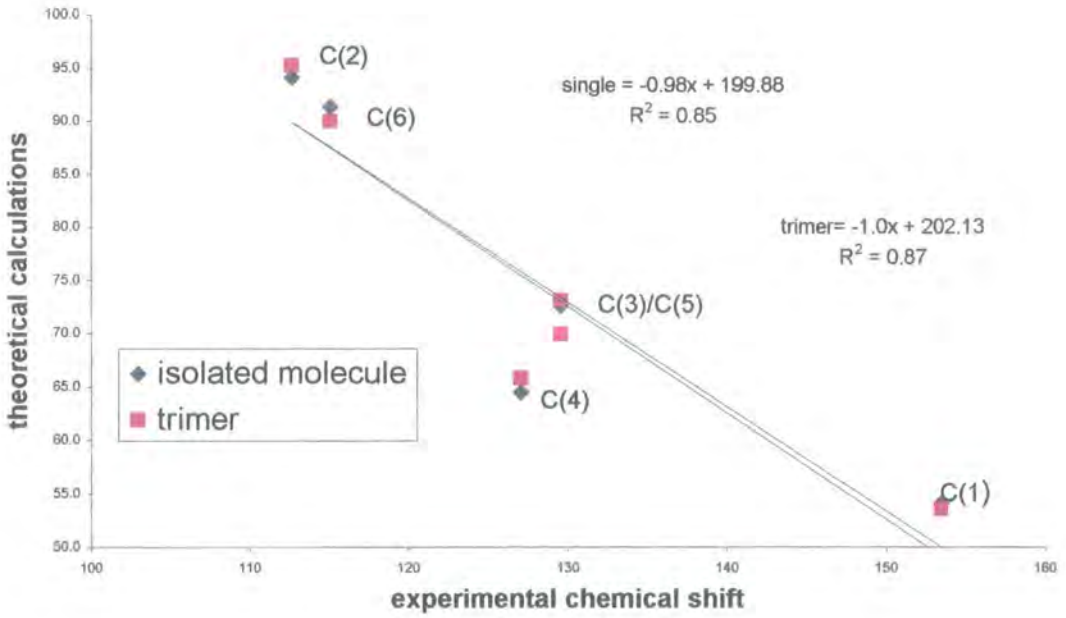

Graph 9. comparison of the isolated molecule and the hydrogen bonded for the γ form using B3LYP/6-31G**.

5.5. Calculations on the δ form

Although I have ran basically the same calculations for this form as for other not being able to compare with the experimental values makes the considerations from the results slightly different, so that I have decided to keep this part separated.

	HF/631G**	HF/6311G**	B3LYP/6-31G**	B3LYP/6-311G**	SVWN/6-31-G**	SVWN/6-311-G**	B3PW/6-311G**
C(4)	111.1	123.5	125.2	141.1	128.4	145.6	136.6
C(3)	116.5	129.9	114.2	129.7	114.3	130.7	126.7
C(2)	87.3	99.0	95.3	109.4	97.6	112.9	107.4
C(1)	137.4	153.3	137.1	157.4	135.6	157.1	152.5
C(6)	87.9	99.6	96.1	110.1	98.3	113.5	106.9
C(5)	118.3	131.7	116.2	131.8	116.2	132.7	128.7

Table 7. Chemical shifts for the δ form, in respect to TMS.

The only considerations we can make are, as done before for the other forms, on the splitting between C(3)/C(5) and C(2)/C(6), to be then compared. It seems as if for this matter there are similarities with the β form, since all differences for C(3)/C(5) are around 2 ppm, where differences between C(2)/C(6) are about 0.6 ppm. For the isolated molecule, though, we have seen that the chemical shifts are not as reliable as when considering hydrogen bonded molecules, so that this kind of calculation had to be carried out in order to have more information on the chemical shifts. In figure 3 we see the .hydrogen bonded molecules used for the calculations.

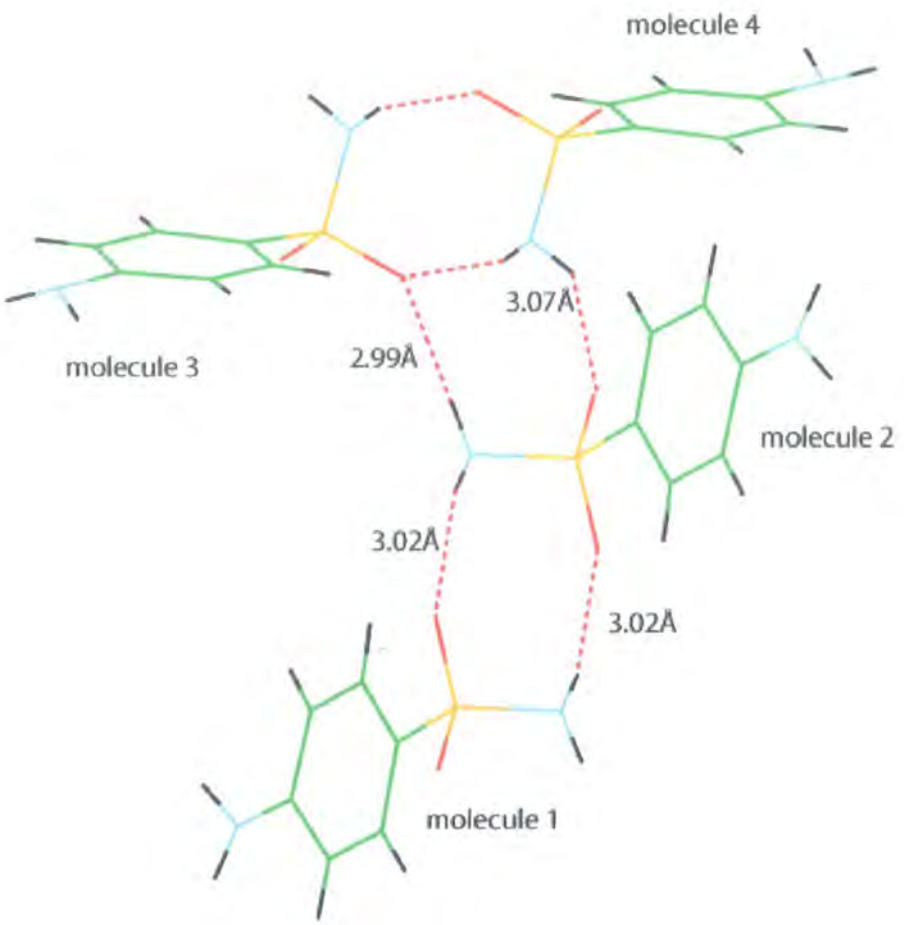

Figure. 3. Hydrogen bonding pattern for the δ form used for calculations with model B3LYP/6-31G**.

The results of the shielding values for this calculation are shown in table in correlation to the calculations at the same level (B3LYP/6-31G**) for the single

molecule so that it is easy to see which carbons are influenced more by the hydrogen bonds. (The molecule considerer for comparison is the one denoted as molecule 2 in figure 3).

	isolated	hydrogenbonded	difference
C(4)	64.3	65.2	0.8
C(3)	71.1	75.2	4.1
C(2)	90.5	94.0	3.4
C(1)	50.8	50.7	-0.2
C(6)	89.7	93.4	3.8
C(5)	73.7	74.0	0.3

Table 8. Comparison of the shielding values for the δ form for the isolated and the hydrogen bonded molecule.

As we can see, quite surprisingly, the shielding constants for the hydrogen bonded molecule are higher for all carbons except C(1), and the splittings between C(3)/C(5) and C(2)/C(6) do not change sonce the shielding for the single carbons change leaving the difference quite similar (0.5 ppm for C(2)/C(6) and 1.2 ppm for C(3)/C(5)).

This is very different from what was happening for the other forms, since in all the other forms the splittings were increasing to almost experimental values for C(2)/C(6), so that this might mean that for this form there is a smaller influence on these carbons from hydrogen bonds.

These calculations, though, as we have seen reach a maximum of credibility when neutron diffraction data are used instead of X-ray.

5.5. Shielding calculations including the effect of neighbouring charges

Another way to considering neighbouring molecules, with less expensive computations is to include charges.

There are several different ways of considering charges[27], and I will briefly illustrate some of them.

When considering atom-centred point charges, which make use of the same basis functions used to represent the wave functions, the Mulliken population analysis[28] is the oldest method. It makes use of the density matrix, assigning diagonal terms belonging to the basis set used for a given atom, to that atom and although it is frequently used, it is a method that strongly depends on the basis set. This population analysis is an arbitrary scheme for assigning charges, since atomic charges are not a quantum mechanical observable and are not unambiguously predictable from first principles. So very little can be said about the absolute magnitude of these charges, and it is particularly dangerous to compare numbers for different basis sets.

There are, however, other ways that minimise the dependence on the basis set. One of these is the NPA (natural population analysis)[29] this method does not take the basis functions as they are, but applies a series of orthogonalisations on them to obtain, at the end, basis functions that are orthogonal, unlike the original basis functions, but which still have the atom-centred characteristic of the ones it started from.

Other methods use charges derived by fitting electrostatic potentials. The point charges are so obtained by adjusting their values to fit the resulting electrostatic potential to that calculated using the electron density obtained from *ab- initio* calculations. This can be obtained by using the ChelpG option in Gaussian. One other way that I have used as well, is to use the algorithm GRID[30] which evaluates *ab-initio* electrostatic properties on a grid of discrete points surrounding the molecule. The selection of points for the fitting procedure implies the construction of an initial parallelepiped-shaped grid of spaced points. The dimensions of the grid containing the molecule involves an exclusion radius on all sides.

Points found to lie further than r_{max}, a multiplicative factor for each van der Waals radius from any nucleus, are discarded. Points inside the van der Waals envelope are rejected. The density of the points used for the fit may be modified by adjusting the grid step Δr.

This program runs in connection to Gaussian 94, so that the grid is written in a FORTRAN file that will subsequently be read by Gaussian and that will create the molecular electrostatic potential. Point charges are then derived by means of a least-squares fitting procedure.

Other methods to calculate the charges involve considering the density functional theory, without the use of molecular orbital methods. Among such methods there is the Hirschfield method, or use of the theory of Atoms in Molecules (AIM) that Bader[18] introduced.

The methods I have used have been of the first two kinds, comparing NPA point charges with potential-derived ones, both from the GRID program and from use of the ChelpG command in Gaussian, for which one considers a central molecule quantum-mechanically described by basis functions surrounded by point charges located at positions that reflect the space group symmetry of the crystal.

Thus we are looking at a central molecule with charge field perturbation (CHF). In practice I have computed the charges on a single, considered a radius of 6 Å from the centroid of the phenylene ring (arbitrary decision), placing the charges within this sphere of enclosure, and computed the NMR shielding. The results for NPA charges calculated for the three forms were all done using the B3LYP/6-31G** level of theory.

There is very little effect for the α form, whereas for the other two forms there is a common effect under which C(1) obtains a lower shielding and the difference between C(3)/C(5) is enhanced; there is an effect on C(4) only on the γ form, which has a higher shielding when surrounded by the charges.

The effect of the charges is, however more important on the ^{15}N shielding values.

5.6. ^{15}N calculations

The combination of a large shift range and the sensitivity to electronic interactions involving the lone pair makes ^{15}N shifts a very sensitive probe of both structural changes and intermolecular interactions. Despite this fact, there is very little information, in the literature, especially on the calculations, especially for the chemical shift principal axis components of nitrogen, due to the low sensitivity and long spin-lattice relaxation time of the ^{15}N nuclei.

Since, having enriched the compound, it has been possible to retrieve information about the chemical shift tensors of the three forms of sulfanilamide, I can now compare the experimental values of anisotropy and asymmetry with the calculated ones. This is important when considering solid-state effects since the principal components of the chemical shift provide more information on molecular structure than the isotropically averaged value σ_{iso}.

As previously shown in chapter 4, the convention used for shielding parameters is that of Haeberlen.

It should be especially important to see how the ^{15}N NMR chemical shifts are affected by the conformation and the hydrogen bond pattern.

For calculations of ^{15}N shielding I have used the basis set that is most common in the literature for this nucleus, namely D95**. This is a very good basis set if we consider as a criterion the accurate description of the reference molecule, which for ^{15}N calculations is nitromethane with a chemical shift of –135.8 ppm. Considering both HF and DFT methods we can see, from graph 1 and the respective table, how important it is to include electron correlation into the model used when analysing ^{15}N data.

Model used	Shielding constant for δ^{15}N/ppm of CH_3NO_2
HF/3-21G*	-224.1
HF/3-21G**	-225.5
HF/6-31G**	-215.9
HF/6-31+G*	-213.2
HF/6-31+G**	-213.3
HF/6-31++G**	-213.3
HF/6-311+G**	-250.7
HF/6-311++G**	-250.7
HF/D95**	-238.6
B3LYP/6-311G**	-149.8
B3LYP/6-31G**	-117.7
B3LYP/D95**	-134.5
B3PW91/D95**	-129.5

Table 10. Models used for the description of the ^{15}N chemical shift for the reference molecule nitromethane.

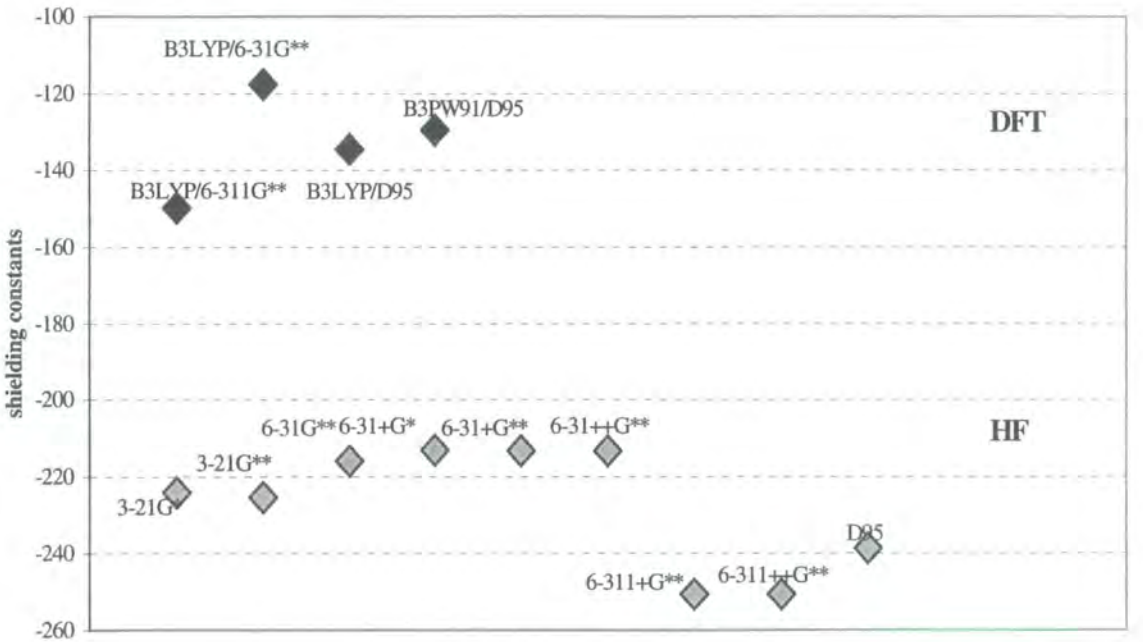

Graph 10. Graph showing the net effect when including correlation in the calculation of the shielding constants for ^{15}N in CH_3NO_2.

Since it is the model that better describes the reference compound, I have considered calculations using B3LYP/D95**(having tried to model with B3PW91/D95** as well but obtained less good results). We can immediately see, from table 10, that, when including only one molecule in the calculation the results are not too good.

		B3LYP/D95**	referenced (-135,8 ppm)	experimental	difference
α	N(1)	221.3	-357.1	-312.2	44.9
	N(2)	192.3	-328.2	-288.8	39.4
β	N(1)	221.3	-357.1	-312.1	45.0
	N(2)	194.2	-330.0	-284.1	45.9
γ	N(1)	228.1	-363.9	-312.1	51.8
	N(2)	185.0	-320.8	-280.6	40.2

Table 10. Experimental and calculated isotropic shifts (in ppm) for N(1) and N(2) of the three forms of sulfanilamide.

Especially when comparing differences found using good basis sets for ^{13}C, we can see how the shielding of ^{15}N is more difficult to correlate to experimental data, but this is quite natural since the shift is a complicated combination of diamagnetic and paramagnetic forms[31]. The errors are all of the same order of magnitude so that they could be considered as arising from a problem of referencing although if we examine the shielding values do not relate very well to the experimental shifts in terms of variations from one polymorph to the other; N(1) does not change experimentally for all three forms, whereas from the calculations a different value for the γ form is seen. For N(2) the greatest experimental shielding is for the α form whereas for the calculated shielding the greatest value is for the β form. Basically, what we can see is that the differences are still too big, and no information can be taken from calculations on an isolated molecule for which the geometry is taken from X-ray data. This is true not only for sulfanilamide but for different nitrogen-containing organic molecules; the solid effects are too important for the ^{15}N nucleus to be neglected, so that better ways of describing the molecule (such as neutron

diffraction data) or inclusion of hydrogen-bonded molecules must be used in order for the theoretical calculations to be acceptable.

This is true not only for the isotropic shielding values but for the tensor components as well. Table 11, gives the comparison between the theoretical and the experimental anisotropy and asymmetry for the isolated molecules.

		Theoretical anisotropy	**Theoretical asymmetry**	**Experimental anisotropy**	**Experimental asymmetry**
α	N(1)	56.8	0.83	±46	1
	N(2)	90.0	0.41	70	0.4
β	N(1)	51.3	0.79	43	0.8
	N(2)	86.6	0.44	71.2	0.4
γ	N(1)	50.8	0.75	±45	1
	N(2)	86.2	0.48	67.3	0.3

Table 11. Chemical shift asymmetry and anisotropy values for the three forms as considered for the isolated molecule.

The accuracy for the anisotropy and asymmetry for N(1) and N(2) are different as we have seen from experimental fitting the uncertainty is much greater when fitting N(1). From table 11 we can see that the results of the theoretical values of the anisotropies are encouraging if we consider the ratio found for the results of each nitrogen. In fact, for the α form, the ratio found for the theoretical values for the anisotropies of the two nitrogens is 0.63, where the experimental values show a ration of 0.66. Similar ratios are seen for the other two forms (0.59, theoretical and 0.62, experimental for the β form, and 0.59 theoretical and 0.64 experimental for the γ form). Considering that referencing could be a problem when considering shielding calculations, this is a result that shows some correlation between the experimental and theoretical data. What we need to do, in order to improve calculation, is, as considered for ^{13}C as well, to include hydrogen-bonded molecules and see how the calculation varies. In this case I have consider only one hydrogen-

bond per calculation so that two molecules were considered per calculation. The results are shown in table 12, where I am denoting with σ the shielding constant values obtained from the calculations and with δ the chemical shifts.

		B3LYP/D95** (σ)	referenced (-135,8 ppm) (δ)	Experimental (δ)	Difference
α(HB)	$N(1)_{3.07Å}$	212.7	-348.5	-312.2	36.3
	$N(2)_{2.99Å}$	188.3	-324.1	-288.8	35.3
	$N(2)_{2.96Å}$	189.8	-325.6	-288.8	36.8
β(HB)	$N(1)_{3.03Å}$	213.2	-349.0	-312.1	36.9
	$N(2)_{3.00Å}$	188.1	-323.9	-284.1	39.8
	$N(2)_{3.10Å}$	191.4	-327.2	-284.1	43.1
γ(HB)	$N(2)_{3.00Å}$	182.4	-318.2	-280.6	37.6
	$N(2)_{3.01Å}$	182.5	-318.3	-280.6	37.7

Table 12. Experimental and calculated isotropic chemical shifts (in ppm) for N(1) and N(2) for the three forms of sulfanilamide when hydrogen bonds are included.

		Theoretical anisotropy	Theoretical asymmetry	Experimental anisotropy	Experimental asymmetry
α(HB)	$N(1)_{3.07Å}$	-65	0.61	± 46	1
	$N(2)_{2.99Å}$	83.9	0.48	70	0.4
	$N(2)_{2.96Å}$	86.1	0.47	70	0.4
β(HB)	$N(1)_{3.03Å}$	-51	0.8	43	0.8
	$N(2)_{3.10Å}$	83.2	0.47	71.2	0.4
	$N(2)_{3.00Å}$	86.9	0.44	71.2	0.4
γ(HB)	$N(2)_{3.00Å}$	83.2	0.50	67.3	0.3
	$N(2)_{3.01Å}$	82.1	0.51	67.3	0.3

Table 13. Asymmetry and anisotropy values for the hydrogen-bonded molecules.

As is seen there is not a very great improvement, but this might be due to the fact that only one hydrogen bond was considered in the calculations, and we might need

to consider more than one, as is known to be the case for N(2) of the β form. This might prove to be very expensive computationally so I have run the calculation on a model system. In figure 5 we can see the example for the β form, in which I substituted the benzene rings of adjacent molecules with methyl groups. Before considering the shielding calculations for this model it was desirable to optimise the positions of the hydrogens of the methyl groups.

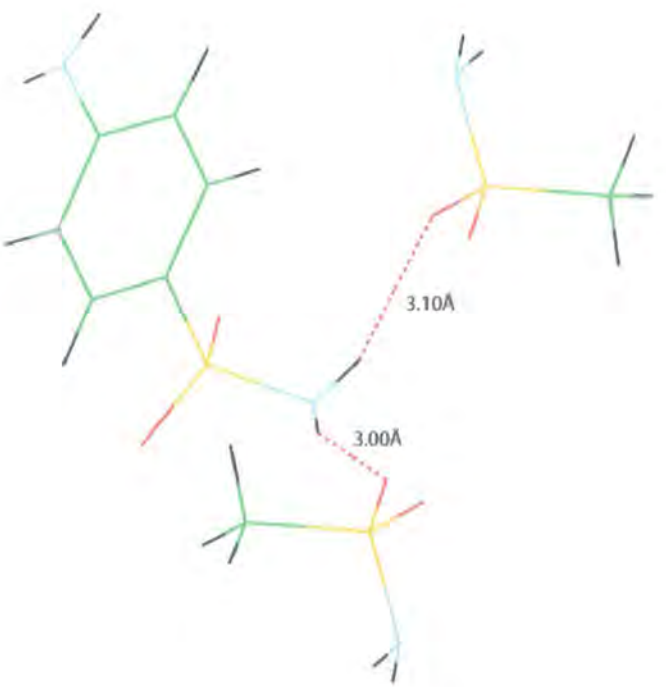

Figure 5. Computationally less expensive model for considering the hydrogen bonds of N(2) for the β form.

Including more than one hydrogen bond per atom seemed to give a slight improvement on the isotropic shift as well as in the values of asymmetry and anisotropy, in fact the chemical shift reaches a value of -322.0 ppm, meaning that the difference from experimental has lowered to a value of 37.9 ppm. The difference is not quite good enough yet but we can see how adding hydrogen-bonded molecules can lower the shielding. Considering the anisotropy, the value found has been of 84.2 ppm for the anisotropy and 0.48 for the asymmetry.

What should be most appreciated about this calculation with a model system is the actual lower computational cost, since including two full molecules (and so considering only one hydrogen bond in the calculation, as previously shown) takes around 36 hours, whereas considering the molecules in the above manner, with methyl groups substituting the benzene rings, the calculation time decreases to just little more than 6 hours.

I have also ran such calculations for the α and γ forms, which have similarly N(2) sites involved in two hydrogen bonds. Even for these there was an improvement: the difference from experimental for the isotropic chemical shift lowered to 33.7 ppm for α and to 34.6 for γ. The anisotropies and asymmetries were found to be respectively : 83.3 ppm and 0.5 for α and 80.2 ppm and 0.5 for γ, so that for these values there is basically no improvement.

The other information that one can retrieve from the shielding tensor calculations are directional data[32], that can be very useful when comparing the variations of the orientation of the shielding tensor when including hydrogen bonds in the calculations. We have seen that the -NH_2 groups in sulfanilamide are not planar but here I will approximate these groups to planarity in order to simplify the discussion, since differences in the orientations of the tensors of about 10°-15° degrees do not change the qualitative conclusions on the relative orientations of the tensors.

I have seen that, when considering N(1), when the calculations are performed on the single molecule, σ_{11} is approximately along the C-N bond, σ_{33} is perpendicular to the C-NH_2 plane and σ_{22} is in the plane C-NH_2 plane and perpendicular to the C-N bond. This is the case for all three forms. When including the hydrogen-bonds, σ_{11} will still be along the C-N bond, increasing in value, denoting, so a greater shielding, but the σ_{22} is now perpendicular to the NH_2 plane. This is not what one would expect since there should be a decrease in the shielding in the direction of the C-N bond when including hydrogen-bonds. This discrepancy with expected behaviour might be due to the fact that the calculations need to be more accurate in order to obtain reliable information on orientation of the tensor.

Considering N(2), the situation is slightly different. For the isolated molecules, the behaviour for all three forms is to have σ_{22} along the S-N bond, where σ_{11} is perpendicular to the plane of S-NH_2. For the hydrogen-bonded molecules, σ_{11} becomes perpendicular to the NH2 plane where σ_{22} is in the S-NH_2 plane and it is σ33 that lies along the σ_{33} bond. Even in this case there seems to be an increase in shielding in the direction of the S-N bond when including hydrogen-bonds.

The shielding of nitrogen will be even more influenced by the position of the attached protons, so that for ^{15}N shielding calculations ND data are even more important to compare with than in the case of ^{13}C ; in the literature it is also strongly advised to consider only ND data when trying to predict ^{15}N shielding. Some results are given in table 14:

	B3LYP/D95** (σ)	referenced(-135,8) (δ)	experimental (δ)	difference
N(1)	192.6	-328.4	-312.1	16.3
N(2)	165.1	-300.9	-284.4	16.5

Table14. Experimental and calculated isotropic shielding (σ) and chemical shifts (δ) for N(1) and N(2) of the β form of sulfanilamide with the structure taken from neutron diffraction data, considering the isolated molecule.

As is perhaps predictable the improvement is substantial and it is as well greater than the improvements when considering hydrogen-bonded molecules. As for the anisotropy and asymmetry, I have obtained for N(1) an anisotropy of –48.4 ppm which is good, but an asymmetry of 0.34 which, strangely it is not good at all. For N(2) the situation is better since an anisotropy of 83 ppm is calculated and an asymmetry of 0.35.

Considering the model in which we substitute the benzene ring with methyl groups, for the neutron diffraction data we obtain differences of 10 ppm from the experimental isotropic shift, which is quite good, but for the anisotropy and asymmetry, are very good: 77.7 ppm and 0.41. These results show very clearly how

using neutron diffraction data and including the right hydrogen bonds can give excellent results.

5.6.1. ^{15}N calculations including charges

The other way to improve the calculations would be to include the charges, as described before for ^{13}C calculations. The two methods I have used were again NPA and ChelpG, since I seemed to get worse results with the GRID program written by Chipot, previously described.

Charges methods should realistically be compared with cluster methods that are not strictly what I have done, since this would need to include more molecules in the calculation, where I have here considered only two at a time, but this would prove to be computationally quite expensive.

For both the methods used I have included 95 charges surrounding the molecule, which corresponds to a sphere of about 6 Å around the molecule; this seemed to be a big enough number to consider.

These calculations did not lead to very good results. For the α form, using ChelpG, I have found that N(1) increases its shielding quite a lot, leading to a difference of 62 ppm from the experimental value for the isotropic shift. For the case of N(2) there is basically no difference than when considering the molecule alone (the shielding is 191.0 ppm as opposed to 192.3 for the isolated molecule). The anisotropies and asymmetries that arise from the calculations are also not very good: N(1) shows an anisotropy of 60.9 ppm and an asymmetry of 0.13 where for N(2) they are respectively 91.7 ppm and 0.23.

For the β form I found what we might need to consider as a fortuitously good value for N(2) (although as we will see also that the NPA method shows improvement) since the difference with the experimental value reaches 20 ppm, but for N(1) we have the same kind of result as for the α form: the difference is increased, to a value

of 65 ppm. Analogously, for the anisotropies and asymmetries: N(1) 57.5 ppm and 0.15, and for N(2) we have 83.1 ppm and 0.43.

For the γ form we don't have major differences: the values are not very different from the ones previously seen including full molecules. The differences for this form were of the order of 50 ppm for N(1) and 44.5 for N(2). The anisotropies and asymmetries were, for N(1) of 49.3 ppm and 0.86 asymmetry, where N(2) showed values of 89.4 ppm and 0.40.

When considering the NPA (Natural Population Analysis) method we can see that the results are surprisingly better than when using ChelpG. For the α form there is not a very big difference from the calculations of the molecule without the charges; the differences from experimental are of 44.9 for N(1) and of 41.2 for N(2). The anisotropy and asymmetry are respectively 51.3 ppm and 0.8 for N(1) and 86.7 ppm and 0.4 for N(2).

There is again a net improvement in the calculations for the β form that might, since it is present for both methods, mean that this form actually does have more influence from charges surrounding the molecule that might also relate well with the considered resonance form.

The isotropic shielding is improved to differences of 22 and 17 ppm respectively for N(1) and N(2), and the anisotropies and asymmetries are 85.0 and 0.42 for N(1) and 96.9 ppm and 0.23 for N(2). For the gamma form we have differences from experimental values of 32.2 and of 35.9, and –65.9 and 0.25 are the anisotropies and asymmetries for N(1) and 90.8 ppm and 0.51 for N(2).

As we can see not all methods are at the level of considering the full molecules, but in the case of NPA the level is similar. These methods, again, are to be considered, once proved that they can give satisfying results, since they are computationally less expensive than using "cluster" methods.

Including charges, and running a shielding calculation of the sort described above (of about 100 charges surrounding the molecule), can take less than 2 hours, as opposed to the 36 h when just considering two molecules in the calculation.

5.7. Conclusions

I have tried to obtain as much information as possible from theoretical calculations of shielding values. As has been shown, using different basis sets for ^{13}C shielding can lead to different results, but no model can give fully satisfactory results, when comparing to solid-state NMR chemical shifts, when considering the isolated molecule.

When we include hydrogen-bonded molecules the calculations improve, although it is still difficult to draw definite conclusions about the chemical shift values if we cannot compare with experimental, as is the case of the δ form.

Using neutron diffraction data is the best option and very good results can be obtained. Some information can anyway be drawn from these calculations, such as the fact that the splittings between C(2)/C(6), can be mostly attributed to intermolecular interactions and is therefore mostly due to hydrogen bonds, since this splitting reaches experimental values when considering neutron diffraction data and hydrogen-bonded molecules. Most of the discrepancies found for the shielding values were for C(3)/C(5), which shows a splitting not present experimentally but we have attributed that to a mobility problem since the calculations are done considering absolutely no averaging of shielding values from motion, where, as we have previously explained there is some greater motion on the side of the molecule containing the sulfonamide group than on the one containing the amino group.
When considering ^{15}N calculations it is of basic importance to have neutron diffraction data, as the shielding values of ^{15}N will be much more influenced by the positions of the hydrogens, which will also be the ones involved in hydrogen bonds.

We have also seen how small "tricks" can improve the calculation without increasing the time for each run, such as including molecules with smaller groups, or point charges. Considering point charges still did not prove to be a good enough method to calculate shielding constants.

Including more than one hydrogen bond per atom has proved to be "vital" in order to obtain excellent results when considering neutron diffraction data; this was true for the isotropic shifts as well as the values of the anisotropies and asymmetries.

5.8. REFERENCES

1) M. Buhl, M. Kaupp, O. L. Malkina and V. G. Malkin, *J. Comp. Chem.* **1999**, *20*, 91-105.

2) K. B. Wiberg, *J. Comp. Chem.* **1999**, *20*, 1299.

3) Wilson and Amos, *Mol. Phys.* **1999**, *96*, 757.

4) G. Schreckenbach and T. Ziegler, *J. Phys. Chem.* **1995**, *103*, 1788.

5) V. G. Malkin, O. L. Malkina, L. Eriksson and D. R. Salahub,*Modern Density Functional theory: a tool for Chemistry.*; Elsevier: Amsterdam, 1995; Vol. 2.

6) A. D. Becke, *J. Chem. Phys.* **1996**, *104*, 1040.

7) A. D. Becke, *J. Chem. Phys.* **1993**, *98*, 5648.

8) C. Lee, W. Yang and R. G. Parr, *Chem. Phys. Rev.* **1988**, *B37*, 785.

9) J. P. Perdew, K. Burke and Y. Wang, *Phys. Rev.* **1996**, *B54*, 16533.

10) N. F. Ramsey, *Phys. Rev.* **1950**, *78*, 699.

11) R. M. Stevens, *J. Chem. Phys.* **1937**, *38*, 550.

12) F. London, *J.Phys. Radium* **1937**, *8*, 397.

13) J. D. Memory,*Quantum Theory of magnetic resonance parameters*, 1968; Vol. 5.

14) M. Schindler and W. Kutzelnigg, *J. Chem. Phys.* **1982**, *76*, 1919.

15) A. E. Hansen and T. D. Bouman, *J. Chem. Phys.* **1985**, *82*, 5035.

16) T. D. Bouman and A. E. Hansen, *Chem. Phys. Lett.* **1990**, *175*, 292.

17) E. Brunner and U. Sternberg, *Prog. NMR Spectr.* **1998**, *32*, 21.

18) R. F. W. Bader,*Atoms in molecules. A quantum theory*; Clarendon Press: Oxford U.K., 1990.

19) M. J. Frish, G. W. Trucks, H. B. Schelegel, G. E. Scuseria, M. A. Robb, J. R. Cheeseman, V.G.Zakrzewsi, J. A. montgomery, R. E. Stratman, J. C. Burant, S. Dapprich, J. M. Millan, A. D. Daniels, K. N. Kudin, M. C. Strain, O. Farkas, J.Tomasi, V. Barone, M.Cossi, R. Cammi, B. Mennucci, C. Pomelli, C. Adamo, S. Clifford, J. Ochtersky, G. A. Petersson, P. Y. Ayala, Q. Cui, K. Morokuma, D. K. Malick, A. D. Radbuck, K. Raghavachari, J. B. Foresman, J. Cioslowsi, J. V.Ortiz, B. B. Stefanov, G.liu, A.Liashenko, P. Piskorz, I. Komaromi, R. Gomperts, R. L. Martin, D. J. Fox, T.A. Fox, T. A. Keith, M. A. Al-Laham, C. Y. Peng, A. Nanayakkara, C.Gonzalez, M.Challcombe, P. M. W. GIll, B. G. Johnson, W.Chen, M. W. Wong, J. L. Andres, M. Head-Gordon, E. S. Replogle and J.A.Pople.,*GAUSSIAN 94*; Revision C.2 ed. Pittsburgh PA, 1995.

20) M. J. Frish, G. W. Trucks, H. B. Schelegel, G. E. Scuseria, M. A. Robb, J. R. Cheeseman, V.G.Zakrzewsi, J. A. montgomery, R. E. Stratman, J. C. Burant, S. Dapprich, J. M. Millan, A. D. Daniels, K. N. Kudin, M. C. Strain, O. Farkas, J.Tomasi, V. Barone, M. Cossi, R. Cammi, B. Mennucci, C. Pomelli, C. Adamo, S. Clifford, J. Ochtersky, G. A. Petersson, P. Y. Ayala, Q. Cui, K. Morokuma, D. K. Malick, A. D. Radbuck, K. Raghavachari, J. B. Foresman, J. Cioslowsi, J. V.Ortiz, B. B. Stefanov, G. liu, A. Liashenko, P. Piskorz, I. Komaromi, R. Gomperts, R. L. Martin, D. J. Fox, T.A. Fox, T. A. Keith, M. A. Al-Laham, C. Y. Peng, A.

Nanayakkara, C. Gonzalez, M. Challcombe, P. M. W. Gill, B. G. Johnson, W. Chen, M. W. Wong, J. L. Andres, M. Head-Gordon, E. S. Replogle and J. A. Pople. *GAUSSIAN98*; I. Gaussian, Ed.: Pittsburgh PA, 1998.

21) A. K. Jameson and C. J. Jameson, *J. Chem. Phys. Lett.* **1987**, *134*, 461.

22) J. R. Cheeseman, G. W. Trucks, T. A. Keith and M. J. Frish, *J. Chem.Phys.* **1996**, *104*, 5497-5509.

23) R. Ahlrichs and K. May, *Phys. Chem. Chem. Phys.* **2000**, *2*, 943.

24) A. M. O'Connel and E. N. Maslen, *Acta Cryst.* **1967**, *22*, 134.

25) R. Ditchfield, *J. Chem. Phys.* **1976**, *65*, 3123.

26) M. Pecul and K. Jackowsky, *Solid State NMR* **1997**, *8*, 139.

27) K. B. Wiberg and P. R. Rablen, *J. Comp. Chem.* **1993**, *14*, 1504.

28) R. S. Mulliken, *J. Chem. Phys.* **1962**, *36*, 3428.

29) A. E. Reed, R. B. Weinstock and F. A. Weinhold, *J. Chem. Phys.* **1985**, *83*, 735.

30) C. Chipot and J. G. Angyan *GRID: point multipoles derived from molecular electrostatic properties.*; Version 3.0 ed., 1994.

31) G. C. Levy and R. L. Lichter,*Nitrogen-15 Nuclear Magnetic resonance Spectroscopy*; Wiley-interscience: New York, 1979.

32) J. C. Facelli,*Shielding tensor calculations*; John Wiley: London, 1996.

Chapter 6

SOLVATE SYSTEMS

6.1. Sulfathiazole solvates

In this section I will introduce a series of systems that were obtained, at least at the beginning, in order to establish reliable crystallisation conditions for sulfathiazole polymorphs. This attempt was unsuccessful in its initial purpose but it provided us with a great number of solvates.

The solvates described in this chapter were prepared by Terry Threlfall, in general, by boiling the compound (typically 0.2 g. of sulfathiazole, but depending on solubility) in the solvent. If it would not dissolve at a reasonable temperature (under 200 °C, since sulfathiazole melts at 204 °C), more solvent was added. It seems as if the only skill needed is in the choice of quantities and cooling regime.

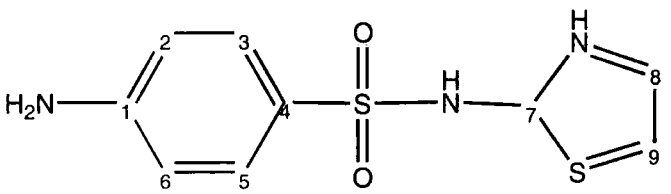

Sulfathiazole structure.

6.2. Pseudopolymorphism

Solvates are often called pseudopolymorphs, meaning the phenomenon whereby a compound is obtained in crystalline forms that differ in the nature of the included solvent. This definition also covers those cases of solvation where different crystal structures are obtained in forms which have the same solvent and solute[1]. The difference with the simple term polymorph is that the latter describes single-component systems. According to these definitions and conventions, the legal implications of the terms polymorph and pseudo polymorph are the same, so that the same characterisation studies must be done[2, 3].

Usually molecules of solvent are not included in crystals when organic compounds are recrystallised. A recent survey of the Cambridge Structural Database (CSD), shows that fully 85% of all organic crystals do not contain solvent of crystallisation[4]. The rationalisation given to this aspect has been that the crystallisation begins with solute-solvent aggregates that contain solute-solute, solute-solvent and solvent-solvent interactions. The entropic gain in eliminating solvent molecules from these aggregates into the bulk solution, and the simultaneous enthalpic gain in forming stable solute species that contain supramolecular synthons, provide an adequate driving force for nucleation and crystallisation, leading to solvent-free crystals. Although it is a rare case, it is quite interesting phenomenon that needs quite a lot of rationalisation, still not having ever been treated in a very systematic way.

The case of the solvates of sulfathiazole that I will be describing here is a very unusual one since, at least when considering the literature (which is very poor on this subject), it is an exceptionally prolific example, in the sense that almost all of the solvents that were used to crystallise sulfathiazole, not normally used for crystallisation of different polymorphs, produce solvates. It seems as if sulfathiazole also represents a unique case in its propensity for solvate formation when this system is compared with the only attempt of rationalisation of solvate formation found in literature. Through the CSD, the work mentioned before[4], it has

been seen that some solvents tend to form solvates more easily than others. It seems as if 1,4 dioxane tends to form solvates more often than other cases and when it forms solvates it is able to form them in different ways, different ratios and different conformations. This is likely to be due to the fact that this molecule is able to act as a double acceptor of strong and/or weak hydrogen bonds. It is seen that whenever this molecule is included in an organic crystal, it is almost always hydrogen bonded and, more importantly, to more than one donor.

It is interesting to compare this conclusion with the fact that for the great number of sulfathiazole solvates there is no evidence of any bonding between solvent and lattice. This probably signifies that the role of sulfathiazole is particularly important in itself to the formation of the solvates, something that can be sustained by the fact that sulfathiazole has also a high number of polymorphs, being able to crystallise in 5 different modifications[5], which is a higher number than usually seen other molecules. The reasons for which sulfathiazole prefers to crystallise with solvent molecules might lie in the fact that it is quite a flexible molecule. In all of the solvates, in fact, the flexibility of the sulfathiazole molecule is detected in the various different orientations that the two rings of the molecule can take in respect to one another, forming a twisted L shape that can be seen to offer several packing possibilities. Another factor that could influence the unique behaviour in solvate formation could be the range of different regions in the molecule of sulfathiazole, such as the aromatic ring, the heteroaromatic ring, and the heteroatom grouping, that must be favourable to different packings, allowing different interactions such as π–π interactions, n-π interactions[6].

6.3. NMR and X-ray data for sulfathiazole solvates

The interest in solvates lies especially in the insight they can give into the nature of and occurrence of solvation and crystallisation, since most of them have no pharmaceutical value, so that it has been of particular interest to analyse some of these from the NMR point of view, and to compare them to the known crystal structure data , in order to gain understanding of the factors influencing different crystallisation behaviours. The exceptionally large number of polymorphs as well as solvates of sulfathiazole makes it unique for the exploration of spectra-structure relationships, H-bonding relationships, and for factors underlying solvate formation.

The solvates synthesised were in great number (over 80!). However, only for a fraction of these was it possible to run NMR experiments because of the limited amount of product. I will not list here all the solvates of sulfathiazole obtained since a full rationalisation has not yet been done. I will here list only the ones of which we have also obtained the NMR spectra. The solvates and the assignment of their from ^{13}C solid-state NMR spectra are listed in table 1. Apart from the solvates listed, for which we were able to obtain high quality spectra, other spectra were acquired but for some reason not yet understood they were not very clear. These were of the following solvates: cyclohexanitrile, cyclooctanone, dimethylpropylenurea, diethylmalonate, 2-acetylfuran. All of these spectra were acquired using the 300 MHz spectrometer with cross-polarization experiments and flip-back, under conditions of recycle delays of 30 seconds, contact times of 3 ms, and spinning rates between 4 and 5 kHz. All the assignments of C(4) were checked with NQS experiments, so that there were only some doubts, in some cases for assignment of the peaks corresponding to C(2)/C(6) and C(9). The relative solvate resonances are shown on the molecules drawn below.

Solvate	Chemical shift values for the sulfathiazole molecule(ppm)						
	C(7)	C(1)	C(4)	C(3)/C(5)	C(8)	C(6)/C(2)	C(9)
acetone	170.3	154.0	129.1	128.1	125.9	114.2	107.1
γ-butyrolactone	170.6	153.0	123.6	130.3	123.7	114.0/111.8	111.1
cyanopyrrolidine	168.6	155.5	126.5	129.1/130.0	125.6	113.3	108.5
piperidine	171.2	152.0	131.3	137.3/132.1	129.6	115.9/113.6	107.9
dioxane	170.3	152.3	126.0	128.1	124.0	113.9/113.2	110.8
γ-valerolactone	169.7	155.0	123.6	130.8	127.1	115.3/110.7	109.0
δ-valerolactone	170.0	154.4	124.1	129.8	127.1	114.7/111.9	110.1
cyclopentanone	169.7	154.5	124.8	129.6	126.0	115.1/111.8	110.4
cyclohexanone	171.0	153.0	126.3	130.1	126.3	112.2/111.3	109.5
cycloheptanone	171.0	153.0	126.4	130.0	126.4	114.6/111.5	110.2
cyclopentanol	169.9	153.3	121.5	133.4/130.8	127.1	114.7/111.6	110.3
δ-valerolactam	169.1	155.0	125.8	130.0/128.6	124.2	115.7/112.9	111.8

Table1. Chemical shift for the solvates of sulfathiazole.

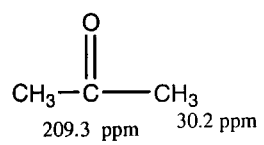

acetone

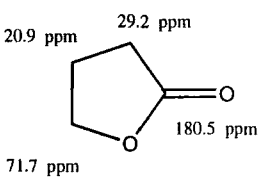

γ-butyrolactone

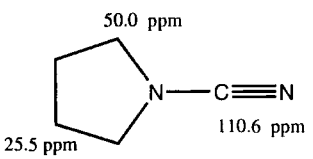

cyanopyrrolidone

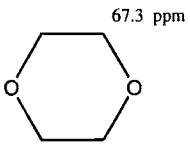

dioxane

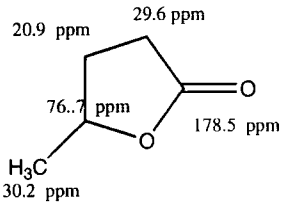

γ-valerolactone

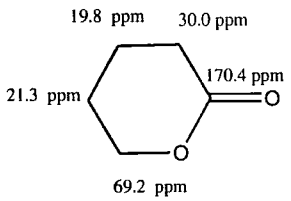

δ-valerolactone

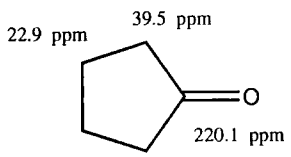

cyclopentanone

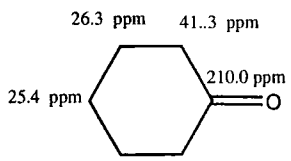

cyclohexanone

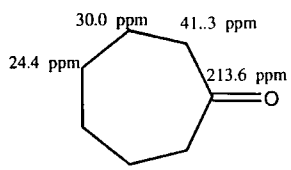

cycloheptanone

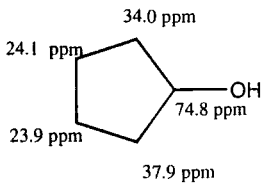

cyclopentanol

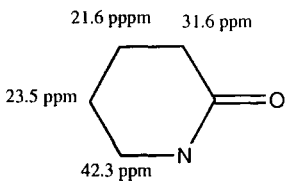

δ-valerolactam

As we can see the piperidine solvate is not listed, and the reason for this has been that the peaks seem to be very weak, and not possible to be seen from the carbon spectrum, although, crystal structure analysis confirmed the presence of the solvate molecule. The other particularities to be noted are the ones concerning cyclopentanol, that seemed to have a lack of mobility and showed all the peaks of the molecule with no symmetry, and that for δ-valerolactam for which the carbonyl peak is very low in intensity probably due to the proximity to the nitrogen.

If we analyse the differences among the chemical shifts for the listed solvates, in table 1, we can clearly see that some peaks are very similar between the different solvates. In particular, the δ-valerolactone, γ-valerolactone, cyclopentanone and γ-butyrolactone solvates, do not differ a lot from one spectrum to the other. Also, we can see that cyclohexanone and cycloheptanone solvate spectra are almost the same. The spectra for these six solvates are shown in figures 1 to 12.

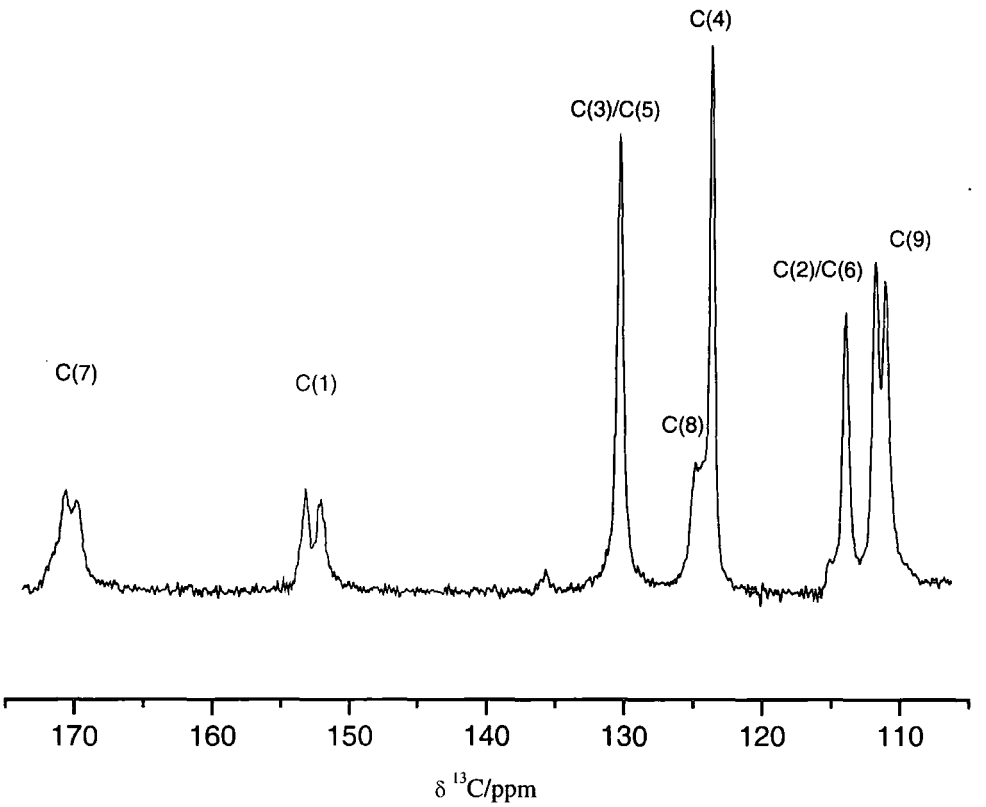

Figure 1. ^{13}C spectrum of the γ-butyrolactone solvate: enlarged view of the peaks of sulfathiazole.

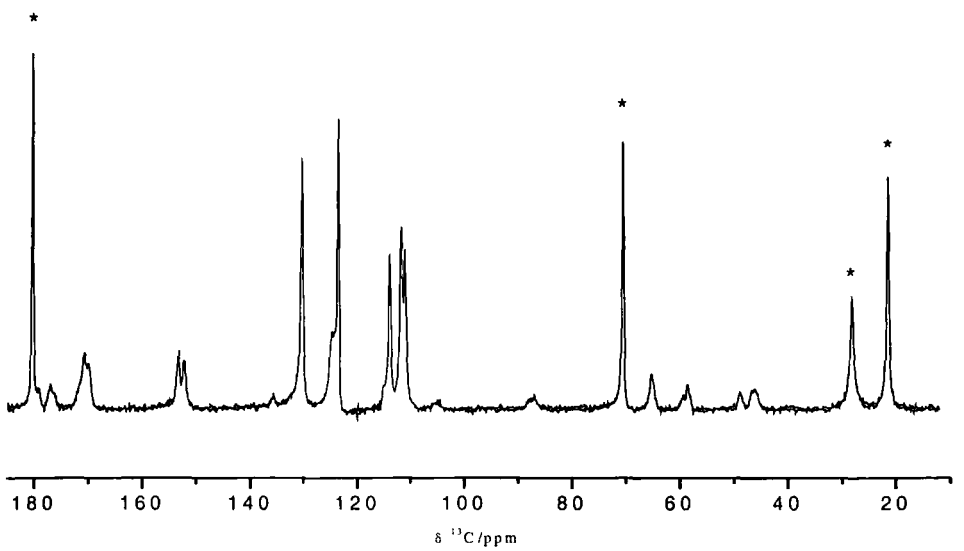

Figure 2. ^{13}C spectrum of the γ-butyrolactone solvate: full spectrum, showing the peaks of γ-butyrolactone (*).

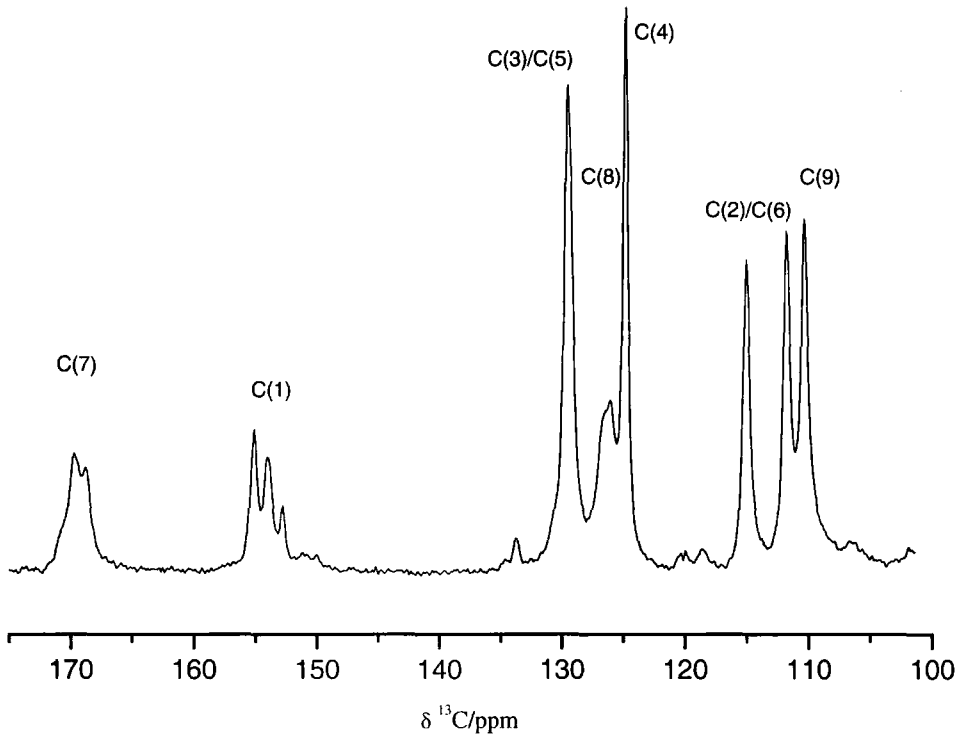

Figure 3. ^{13}C spectrum of the cyclopentanone solvate: enlarged view of the peaks of sulfathiazole.

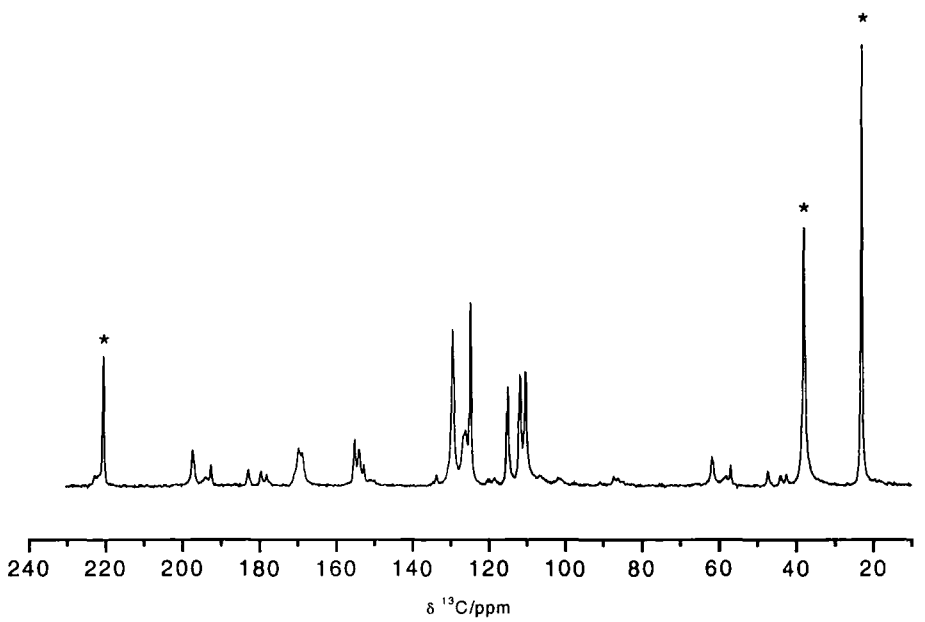

Figure 4. ^{13}C spectrum of the cyclopentanone solvate: full spectrum, showing the peaks of cyclopentanone (*).

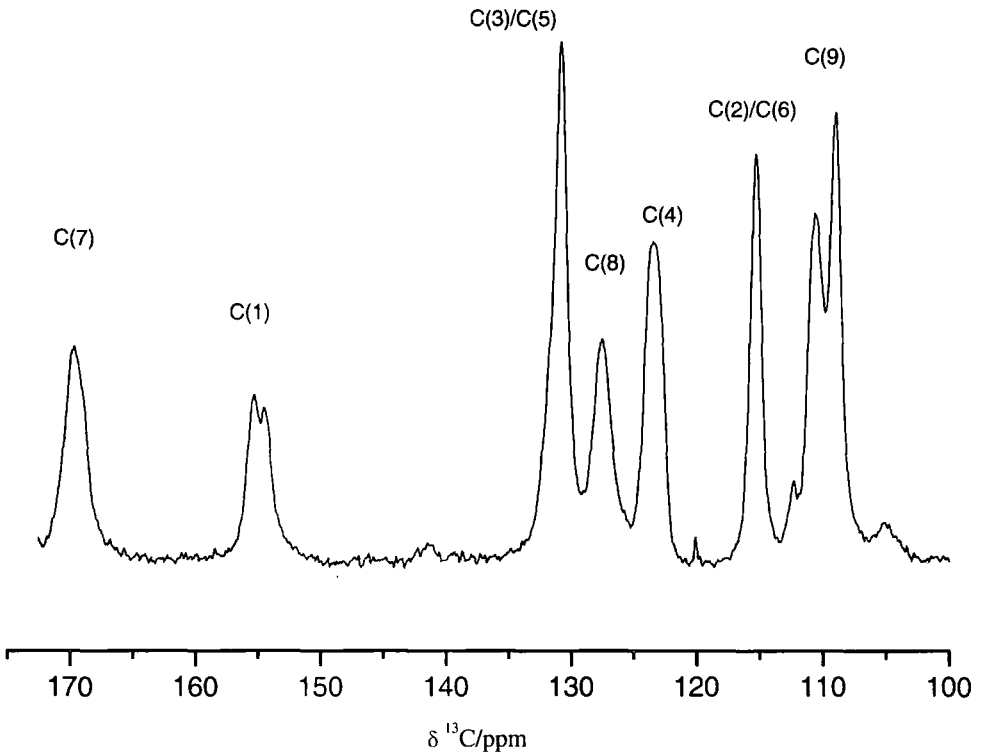

Figure 5. ^{13}C spectrum of the γ-valerolactone solvate: enlarged view of the peaks of sulfathiazole.

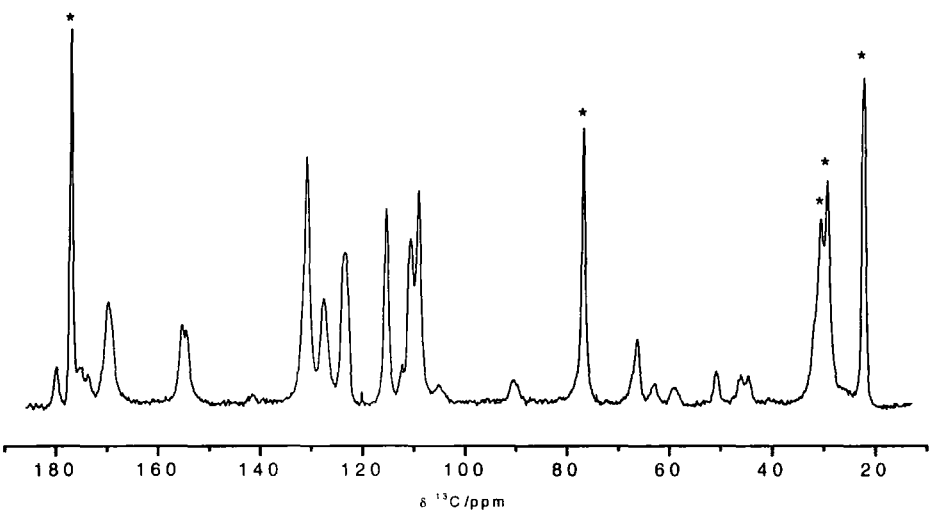

Figure 6. ^{13}C spectrum of γ-valerolactone: full spectrum, showing the peaks of γ-valerolactone (*).

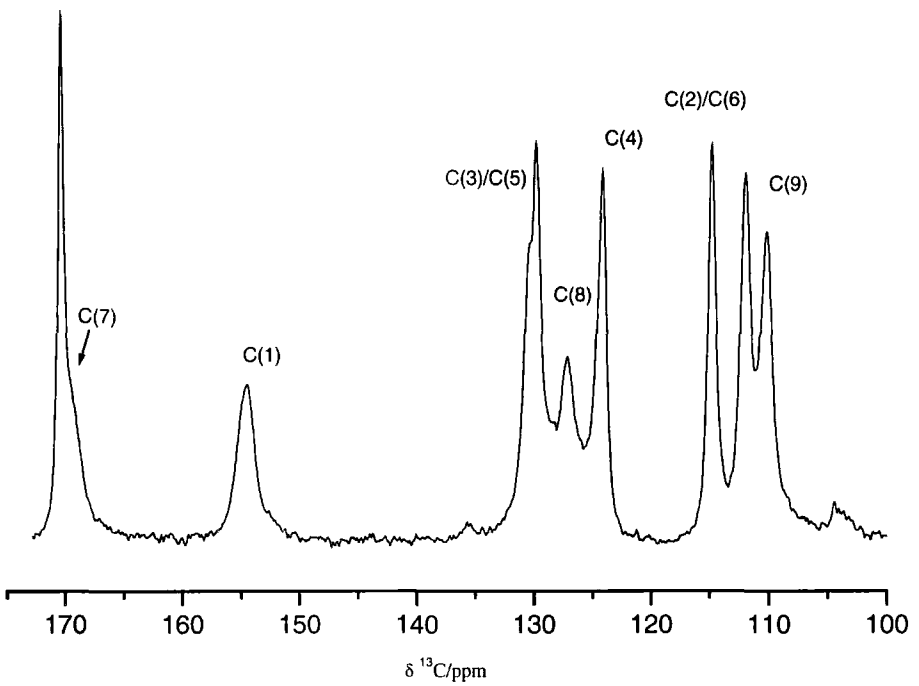

Figure 7. ^{13}C spectrum of the δ-valerolactone solvate: enlarged view of the peaks of sulfathiazole.

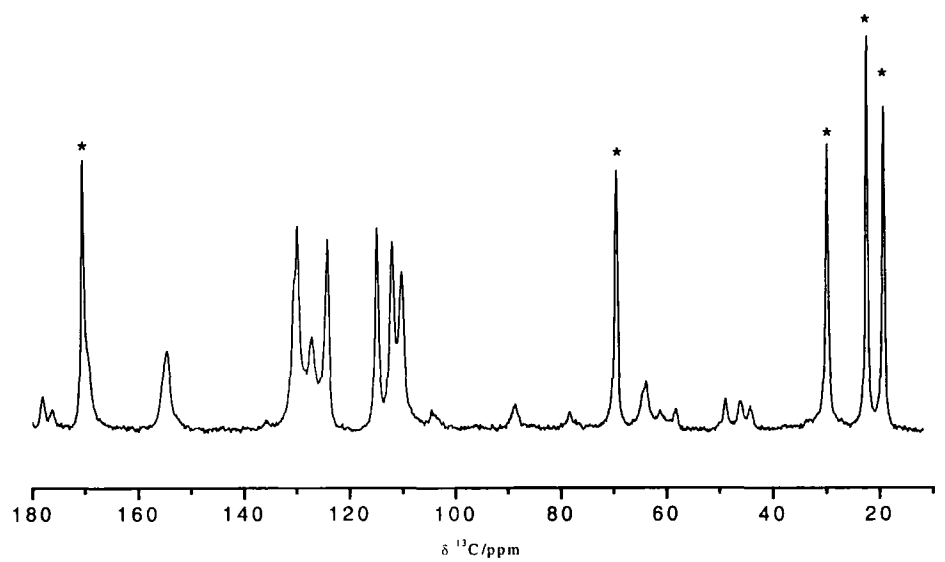

Figure 8. ^{13}C spectrum of δ-valerolactone: full spectrum, showing the peaks of δ-valerolactone (*).

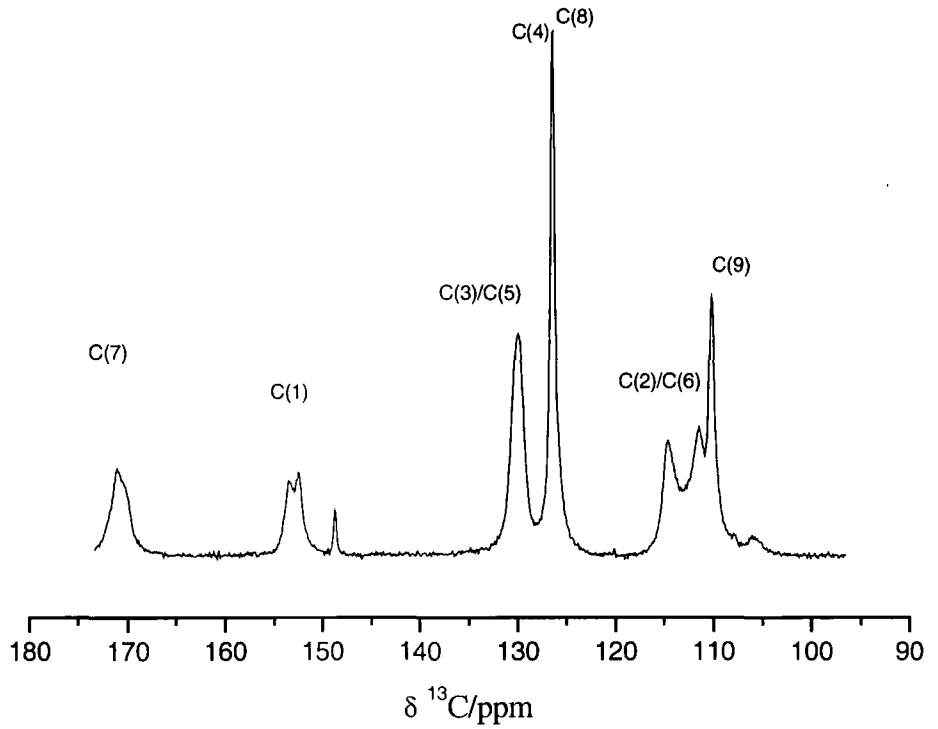

Figure 9. ^{13}C spectrum of the cycloheptanone solvate: enlarged view of the peaks of sulfathiazole.

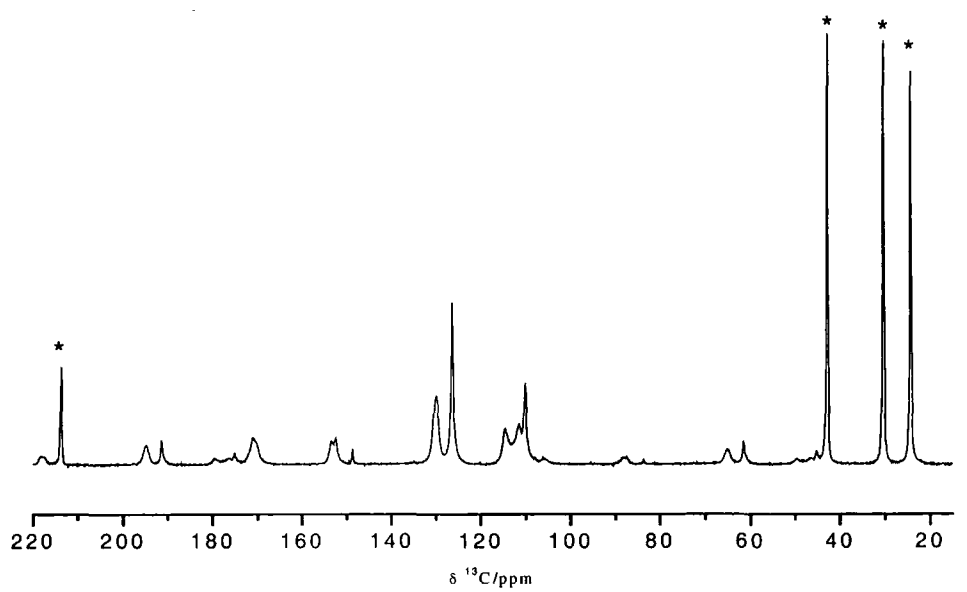

Figure 10. ^{13}C spectrum of cycloheptanone: full spectrum, showing the peaks of cycloheptanone (*).

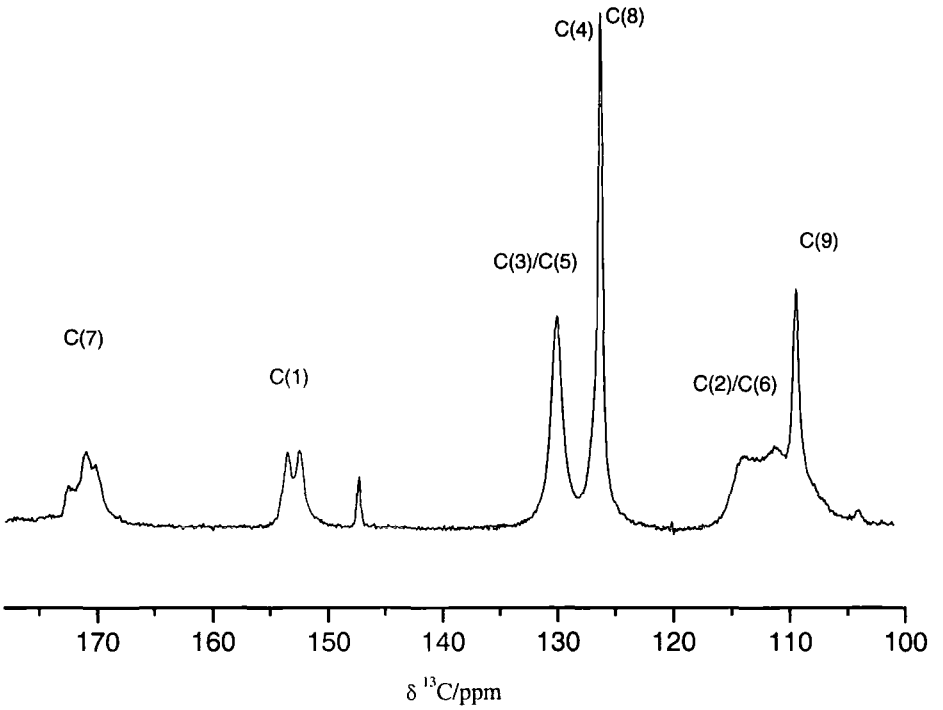

Figure 11. ^{13}C spectrum of the cyclohexanone solvate: enlarged view of the peaks of sulfathiazole.

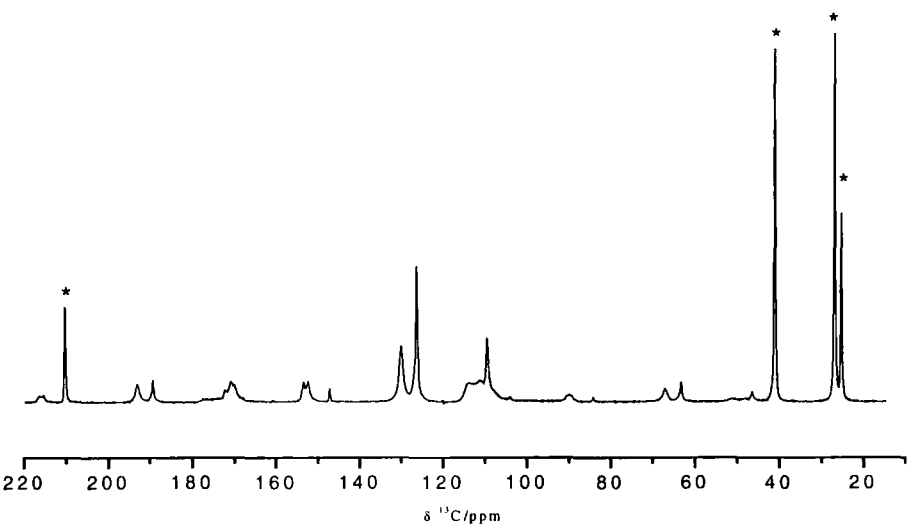

Figure 12. ^{13}C spectrum of cyclohexanone: full spectrum, showing the peaks of cyclohexanone (*).

From these spectra we can see that, as has been seen for sulfanilamide, it is only the C(2)/C(6) signals that are split, and, by analysing table 1 it can be seen that most of the solvates show this same characteristic. In fact, apart from the solvates from piperidine, cyclopyrrolidine, cyclopentanol and δ-valerolactam, they all show one peak for the two carbons C(3)/C(5). In order to understand why, we can probably relate to the situation studied for sulfanilamide. It is most likely that, even for these systems, there is some motion in the molecule on the end containing the heteroaromatic ring, and this will average out the two peaks from the signal of C(3)/C(5). It is interesting to notice that the ^{13}C spectra of sulfathiazole show splitting due to C(2)/C(6), in all the polymorphic forms, and this seems to mean that more mobility is present for the solvate than for the sulfathiazole itself.

In particular we can note that in the spectrum of cycloheptanone the peaks corresponding to C(2)/C(6) show an incipient chemical exchange, this effect is even more enhanced in the spectrum of cyclohexanone. In order to see the effect of temperature on these peaks I have run the experiment at 323 K and at 263 K (the solvate peaks were exactly the same from the room temperature experiment). The results from these experiments is shown in figures 13 and 14, but, although at 263 K it is very easy to see that the mobility of the whole molecule diminishes, as seen not only from the C(2)/C(6) peaks but from the C(3)/C(5) peaks that no longer overlap (the resonances of these peaks are, at this temperature, respectively 130.4 ppm , 129.4 ppm for the C(2)/C(6), and 114.3 ppm and 110.4 ppm for C(3)/C(5). At higher temperature, though, these peaks are difficult to see, and the signal to noise of the whole spectrum becomes significantly worse considering that at this temperature the number of repetitions has been of 1788 as opposed to the spectrum at 263 K for which only 220 repetitions were needed for the spectrum in figure 13.

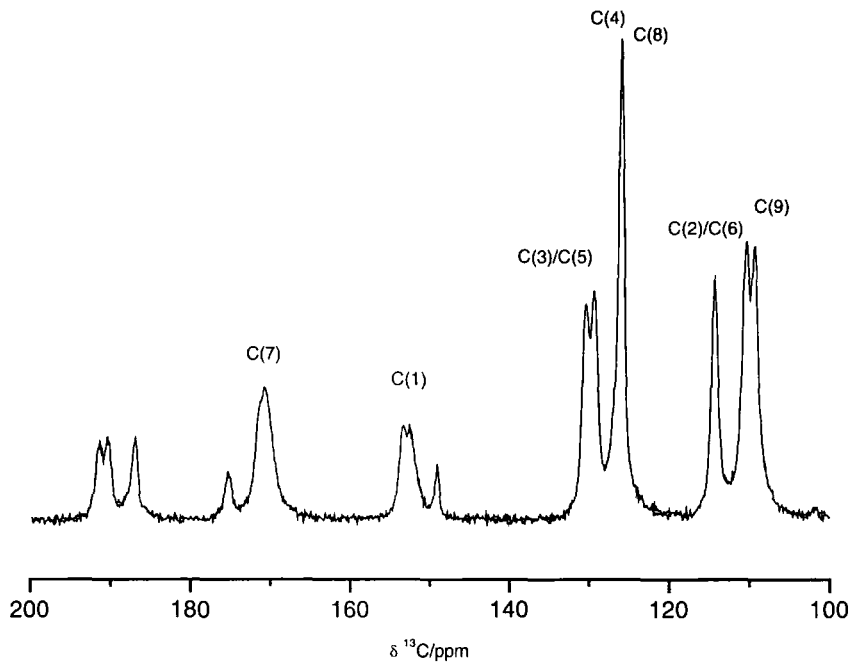

Figure 13. ^{13}C spectrum of cyclohexanone solvate at 263 K, showing all the peaks the same except for C(3)/C(5) and C(2)/C(6).

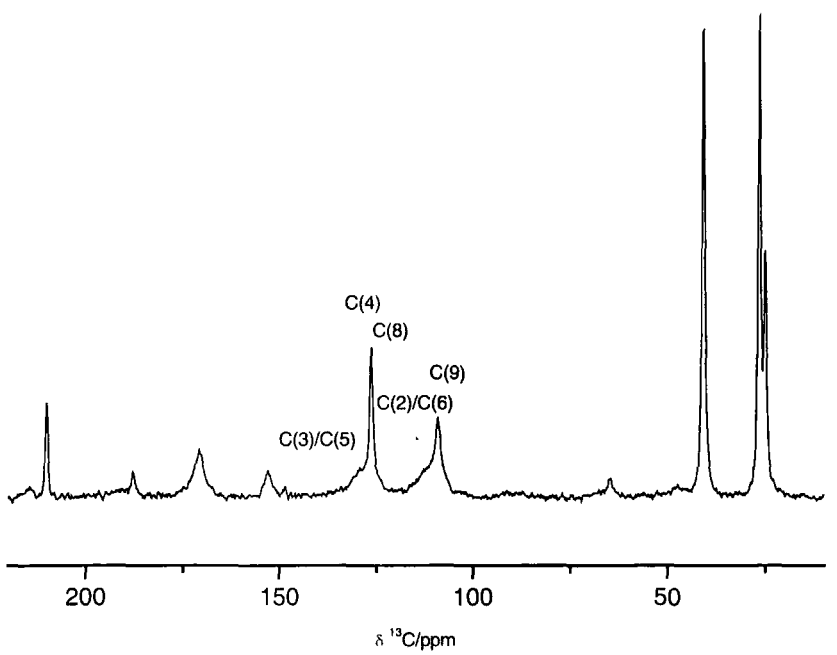

Figure 14. ^{13}C spectrum of cyclohexanone solvate at 323 K.

By looking at the crystal data, it has been very interesting to notice that the space groups and crystal cell dimensions of these of solvates were are very similar. The crystal data as well as the NMR spectra give evidence of the solvent molecule and the sulfathiazole all being in the relation of 1 to 1, with 1 molecule per asymmetric unit.

Solvate	Space group	Cell dimensions			
		a	b	c	β
δ-valerolactone	$P2_1/c$	8.583	20.625	9.520	93.66
cyclopentanone	$P2_1/c$	8.454	20.699	9.487	93.83
γ-valerolactone	$P2_1/c$	8.417	20.975	9.472	92.37
γ-butyrolactone	$P2_1/c$	8.636	19.187	9.354	91.03
cyclohexanone	$P2_1/n$	6.487	12.332	22.259	94.186
cycloheptanone	$P2_1/n$	6.613	12.074	22.085	93.44

Table 2. Crystal data, showing groups with very similar unit cell parameters.

I have compared also the bonds and angles from the crystal data, and it has been very surprising to find that there were no particular similarities for these groups, neither in the intermolecular nor in the intramolecular interactions of these two groups. The only similarity found between cyclohexanone solvate and the cycloheptanone case was the dihedral angle C(3)-C(4)-S-N, which is the greatest conformational difference among all of these compounds, and for these two compounds they were 59.6° for cyclohexanone and 62.9° for cycloheptanone which are very close considering that this angle can range, for all the solvates from 108.9° (acetone) to 59.7° (cyclohexanone). When comparing all the dihedral angles of the solvates studied, it can be seen that there are other groups for which these angles were close, although their spectra did not show similarities, so that no clear relation could be found with any of the intermolecular or intramolecular data obtained from the X-ray work and the NMR spectra.

6.4. Conclusions

A great number of solvates from sulfathiazole have been obtained and analysed both with X-ray diffraction and with ^{13}C solid-state NMR. From the NMR it has been possible to detect the same property in these systems that has been found in sulfanilamide, for which only the two carbons of the phenylene ring next to the amino group showed a splitting in the signals, a property that was not seen in the sulfathiazole molecule in the anhydrous form. Having rationalised this splitting in a greater mobility of the sulfonamide group for sulfanilamide, it is possible to extrapolate this behaviour to these systems, although no further evidence has been gathered.

Some similarities have been found that seem to reflect both the X-ray data and the chemical shifts, but these concern crystal cell dimensions. No relation could be found between bond variations among the solvates and the ^{13}C spectra. In fact when analysing the intra-molecular and inter-molecular characteristics from the crystal data, no greater similarities were found that even other solvates did not display.

6.5. REFERENCES

1) V. S. Kumar, S. S. Kuduva and G. R. Desiraju, *J. Chem. Soc. Perkin Trans. 2* **1999**, 1069.

2) D. Giron, *Thermochim. Acta* **1995**, *248*, 1.

3) R. K. Khankari and D. J. W. Grant, *Thermochim. acta* **1995**, *248*, 61.

4) A. Nangia and G. R. Desiraju, *Chem. Commun.* **1999**, 605.

5) D. C. Apperley, R. A. Fletton, R. K. Harris, R. W. Lancaster, S. Tavener and T. L. Threlfall, *J. Pharm. Sci.* **1999**, *88*, 1275.

6) G. R. Desiraju,*The crystal as a supramolecular entity*; Wiley:, 1995.

Chapter 7

INTERNUCLEAR DISTANCE MEASURING IN SOLIDS

7.1. Dipolar NMR spectroscopy

Solid-state NMR spectroscopy represents a valuable tool for determination of interatomic distances; the main advantage for NMR is its selectivity for specific isotopes, i.e. by selective isotope labels such as ^{15}N, ^{13}C, only single interactions are observable corresponding to spin pairs.

The dipolar coupling between coupled nuclei, carries direct structural information about internuclear distances; this information is encoded in the magnitude of the corresponding dipolar coupling constants ($D \sim 1/r^3$).

This is not a new discovery for solids, since, in liquid-state NMR also, dipolar interactions have a very important role in structure determination; the difference between solids and liquids being that, for liquids, distances are not directly measured, but only indirectly, via relaxation or via the Nuclear Overhauser Effect (NOE). In the solid state D is directly measurable.

In the solid state, though, as we have seen, in order to have high spectral resolution we need to work under conditions of Magic Angle Spinning (MAS), and this will attenuate, if not eliminate, dipolar coupling and related effects. Under these conditions, regaining the information about distances becomes a very important task.

The method applied in this thesis for the measurement of intramolecular dipolar couplings between ^{13}C and ^{15}N is the rotational echo double resonance[1, 2] (REDOR) experiment. This experiment is of particular importance since it allows the recoupling of dipolar interactions between different X-nuclei (for example ^{13}C and ^{15}N) by periodically inverting the sign of the dipolar interaction in the course of the experiment; hence distance information can be extracted. It is a rotor-synchronised spin-echo experiment carried out on the observed spin $\mathbb{S}$, while π-pulses, applied to the $\mathbb{I}$ nuclei during the rotor period, reintroduce the heteronuclear dipolar coupling selectively.

This decay can be adjusted to a known universal curve to determine the strength of the interaction. So far, most REDOR studies have been performed on either doubly labeled samples or systems of abundant spins, and it has been particularly used for peptides[3], of which the synthesis of enriched samples is easier. It has also been used to study the conformation of carbohydrates containing amide groups[4],to determine the conformation of membrane proteins[5], to obtain the secondary structure of proteins in general[6], and to study polymers[7]. In general we can say that its applications are mostly on poorly crystalline large molecules and proteins (since, for smaller molecules the isotopic enriching is more of a problem) and for longer distances (inter-molecular), since more information just in the first part of the curve can be extracted, making deductions easier.

7.2. Theory

When considering the REDOR experiment it is also important to revise the experiment that is the analogue in static conditions: the SEDOR (spin echo double resonance) experiment, that was first introduced in the late 1950s, and was used for distance measurment[8, 9].

7.2.1. The SEDOR experiment

In this experiments (as well as with REDOR) what we are considering is the fact that two spins in proximity to one another will experience each other's magnetic dipole fields, generally very weak compared to the applied external magnetic field, and proportional to $1/r^3$, where r is the distance between the two spins. It is worthy of notice that the dephasing that we will be measuring arises from the ^{13}C- ^{15}N local field and it involves no polarisation transfer.

At the basis of the SEDOR experiment (and this will be important for REDOR as well) there is the fact that the z-component of the local field generated by one spin ($\mathbb{S}$, the observed nucleus) can be inverted in sign simply by applying a π pulse to the other spin ($\mathbb{I}$ spin), since the z-component of the local field depends on the orientation of the $\mathbb{I}$ spin.

The pulse sequence for the SEDOR experiment is shown in figure 1.

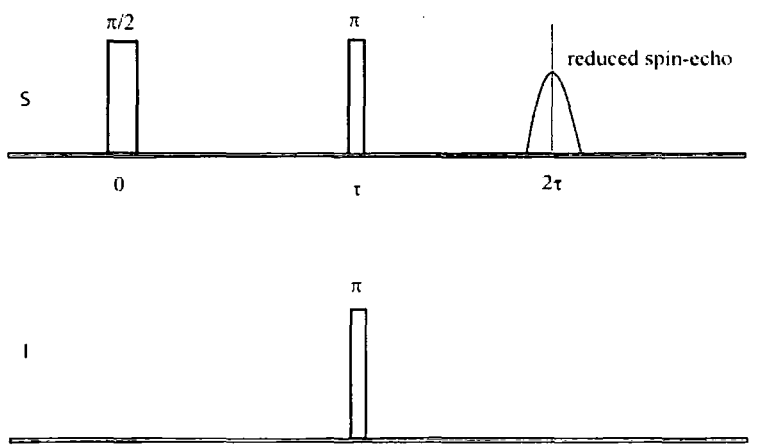

Figure 1. The SEDOR pulse sequence.

The experiment is actually to be carried on together with a comparison experiment in which no π pulses are applied to the I channel. During the time τ between the $\pi/2$ and the π pulses, the S-spin magnetisation dephases because of the interaction with

the dipolar magnetic field generated by the I spin. The actual rate of precession can be written as follows, in equation 1.

$$\frac{d\bar{S}_+}{dt} = \bar{S}_+ \times \gamma_s \bar{B}_L \tag{7-1}$$

where γ_s is the magnetogyric ratio of the **S** nucleus, $\bar{S}_+$ is the transverse component of the **S**-spin magnetisation and $\mathbf{B}_L$ is the local field generated by the I spin. This equation of motion is to be considered in the rotating frame. Applying the π pulse on the S channel will leave $\mathbf{B}_L$ unchanged so that the S-spin will start to refocus and will form, after a time τ, a spin echo. Relaxation processes will be present and will cause some loss of signal, so the signal will have amplitude:

$$S_0(2\tau) = S_i e^{-\frac{2\tau}{T_2}} \tag{7-2}$$

where T_2 is the spin-spin relaxation time and S_i is the S-spin signal intensity following the $\pi/2$ pulse.

When we perform the experiment actually shown figure 1, π pulses are applied on the I channel that will prevent refocusing of the spins, and the dephasing proportional to the local field will take place. The reduced spin-echo signal will be the cosine projection of the transverse magnetisation, as shown in equation 7-3:

$$S_r(2\tau) = S_i e^{-\frac{2\tau}{T_2}} \cos(2\varphi) \tag{7-3}$$

where φ is the dephasing angle and is equal to $\omega_d\tau$, ω_d being the angular rate due to the dipolar interaction:

$$\omega_d = \pm\frac{D}{2}(3\cos^2\vartheta - 1) \tag{7-4}$$

where ϑ is the angle between the z direction (taken as the axis of the Zeeman magnetic field) and the internuclear vector connecting the **I** and **S** spins, and D is the dipolar coupling constant which is $\frac{\mu_0 \gamma_I \gamma_S h}{8\pi^2 r^3}$ in angular frequency units.

Since the dephasing will arise from both chemical shift and heteronuclear dipolar interactions, we need, then, to evaluate the effect of dephasing due to the former, and this is done by the contemporaneous series of simple echo experiments that will take into account only the dephasing due to chemical shift (as seen from equation 7-2) and the SEDOR experiment. By doing both the experiments, T_2 effects can be eliminated by taking the ratio of the difference of the two signals.

$$\frac{S_r(2\tau)}{S_0(2\tau)} = \cos(2\varphi) \tag{7-5}$$

where 2φ can be written as $2\omega_d \tau$ since $\varphi = \int_0^\tau \omega_d dt$ that, ω_d being time independent, is equal to $\omega_d \tau$.

This equation is for a single **S-I** spin orientation, defined by the angle ϑ. For powders we need to sum over all the sample orientations, so that equation 7-5 will become:

$$\frac{S_r(2\tau)}{S_0(2\tau)} = \sum_{\vartheta} \cos(2\varphi)\sin\vartheta \tag{7-6}$$

This leads to the final result for which, just by measuring signal amplitudes, we can obtain information on the dipolar interaction for the **I-S** spin system, thus evaluating the internuclear distance.

7.2.2. The REDOR experiment

When we consider the same experiment under MAS conditions, the angle ϑ between the internuclear vector and the external magnetic field becomes time dependent, since under magic-angle spinning all second-rank interactions are then time dependent. The heteronuclear dipolar Hamiltonian, H_{IS}, which is composed of a spatial and a spin part, can be written as $H_{IS}^{int}(t) = \omega_d(\alpha,\beta,t) I_z S_z$, where the dipolar frequencies, in this case, are:

$$\omega_d(\alpha,\beta,t) = \pm\frac{1}{2} D\left\{\sin^2\beta\cos 2(\alpha+\omega_r t) - \sqrt{2}\sin 2\beta\cos(\alpha+\omega_r t)\right\} \qquad (7\text{-}7)$$

and α and β are the azimuthal and the polar angles defined by the internuclear vector in the coordinate system where the z axis is parallel to the rotor axis, as shown in figure 2.

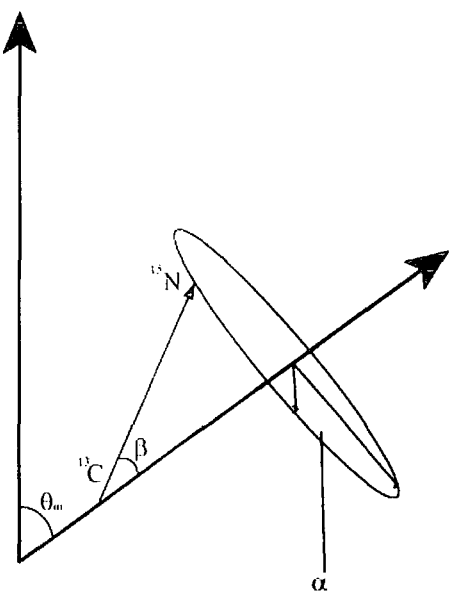

Figure 2. Coordinate system for a C-N internuclear vector under rotation about an axis at the magic angle ϑ_m.

The REDOR experiment is shown in figure 3, where, as we will see, we need, also in this case, to compare this experiment with an experiment without dephasing pulses. The difference from SEDOR is that the dipolar interaction over each rotor cycle is zero so that rotational echoes are detected at the end of each rotor cycle when no dephasing pulses are applied. The 180° pulses on the S channel are here only used in order to take account of the T_2 decay, since the dipolar field will have no effect on the amplitude, which is different from the static case.

The REDOR experiment is a three channel experiment, as shown in figure 3, where the three channels are needed although, on the protons we are only decoupling.

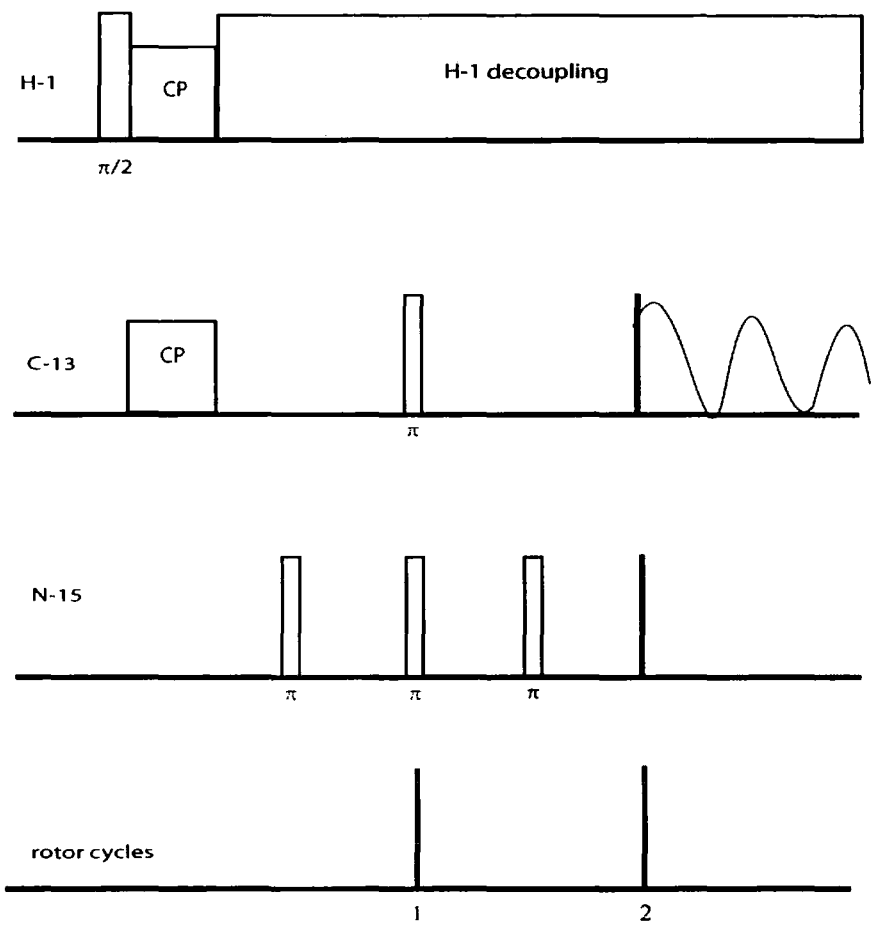

Figure 3. The REDOR pulse sequence for two rotor cycles.

To explain the outcome of the experiment, Average Hamiltonian Theory[10] can be used, which describes the $^{13}C(S)$ spin system at the completion of each rotor cycle[11, 12]. The density matrix describing the S spins stroboscopically is

$$\rho(Nt_r) = U_{\text{int}}(Nt_r)\rho(0)U_{\text{int}}^{-1}(Nt_r) \tag{7-8}$$

where N=1, 2, 3...., and t_r is the rotor period; $U_{int}(Nt_r)$ is the unitary transformation which describes the time evolution of the density matrix from t=0 (which is the end of the Cross Polarisation (CP) contact time). The time evolution is expressed in terms of the average Hamiltonian H, so that

$$U_{\text{int}}(Nt_r) = \exp(-i\overline{H}Nt_r) \tag{7-9}$$

where

$$\overline{H} = \frac{1}{T_r}\int_0^{t_r} H_{IS}^{\text{int}}(t')dt'. \tag{7-10}$$

Performing the integral in equation 7-10, for which t_r is the rotor period, can bring to an evaluation of the average dipolar frequencies, ϖ_D, which, when no dephasing pulses are applied, is:

$$\varpi_d = \pm\frac{1}{2}\frac{D}{T_r}\left[\left\{\frac{\sin^2\beta\sin 2(\alpha+\omega_r t')}{2\omega_r} - \frac{\sqrt{2}\sin 2\beta\sin(\alpha+\omega_r t')}{\omega_r}\right\}\right]_0^{t_r} \tag{7-11}$$

So that the average value of the dipolar interaction over each rotor cycle is zero, and this shows how there will be no dephasing over each rotor cycle due to the dipolar interaction, since ω_d is zero and the medium Hamiltonian is zero for N=1,2,3...

When we apply the dephasing pulse on the I spin at a time t_1, this will change the average dipolar frequency for that cycle because:

$$\varpi_D = \frac{1}{T_r}\left\{\int_0^{t_1} d(\alpha,\beta,t')dt' - \int_{t_1}^{t_r} d(\alpha,\beta,t')dt'\right\} \qquad (7\text{-}12)$$

where the sign shows the reversal of the I-S dipolar coupling at t_1.

This will be different from zero for each rotor cycle and it represents the accumulation of the phase $\Delta\phi$ due to dipolar coupling; this accumulation is equal to $\Delta\phi=d(\alpha,\beta,t)T_r$. So, for a greater number of rotor cycles we will have more dephasing due to the dipolar interaction and the diminution is proportional to the to the rotor period. The signal is then $S_f(\alpha,\beta,t) = Tr\{\rho S_x\}= \cos(\Delta\phi)$.

In terms of considering just the density matrix, we can resume as follows; at the end of one rotor period, following the 90° (S) pulse, the spin density matrix has evolved to

$$\rho(Tr) = S_x \cos(\omega Tr) + 2S_y I_z \sin(\omega Tr) \qquad (7\text{-}13)$$

where x, y, z are the rotating frame coordinates.

Due to the cyclic nature of the REDOR pulse sequence, the result after N rotor cycles is given by:

$$\rho(NTr) = S_x \cos(\omega NTr) + 2S_y I_z \sin(\omega NTr) \qquad (7\text{-}14)$$

where observation in the x-direction leads to:

$$S(\alpha,\beta,\gamma) \sim \cos(\omega NTr) \tag{7-15}$$

If we average over the powder pattern, this becomes:

$$S_f = \frac{1}{2\pi}\int_0^{\frac{\pi}{2}} d\beta \int_0^{2\pi} \sin\beta \cos[\Delta\Phi\left(a,\beta,\frac{t}{2}\right)d\alpha] \tag{7-16}$$

7.3. Experimental results

REDOR attempts were first carried out on a sample of 20% doubly enriched [2-^{13}C-^{15}N] glycine, where the dilution is necessary in order to minimise the intermolecular ^{15}N-^{13}C dipolar interactions.

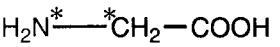

The first thing to establish is what sort of distance we are looking for. There have been a number of X-ray and neutron diffraction studies done on glycine[13-15] and from these the bond lengths were found to be between 1.474 Å and 1.479 Å and in relation to these values we can obtain dipolar couplings between 958 Hz and 945 Hz. As will be seen, the values we obtain are within this range.

We must also recall that the distance we should be measuring using NMR will be somewhat different from the X-ray value since the time-scales are very different, so that in NMR we have a measure that corresponds to $\langle r^3 \rangle$. Thus NMR typically reports longer distances due to motional averaging.

An example of REDOR results, with an array reaching 40 rotor cycles, is shown in figure 4. This experiment was recorded on the CMX 200 spectrometer using the triple-resonance probe with 5 mm rotors. The spinning rate was at 4500 ± 2 Hz

The durations of the π pulses for the ^{13}C and ^{15}N nuclei were 10 μs and 14 μs respectively.

The decoupling field was equivalent to 50 kHz. The sample was placed in the central portion of the rotor in order to supply better homogeneity of the radiofield in the REDOR experiment. The number of transients recorded was 16, the contact time was of 1.5 ms, and the pulse delay was 2 seconds. This particular experiment was carried out observing ^{13}C. Other experiments were carried out while observing ^{15}N but this is more complicated due to longer relaxation times and lower sensitivity of this nucleus, so that it is in general preferable to run REDOR experiments by observing ^{13}C.

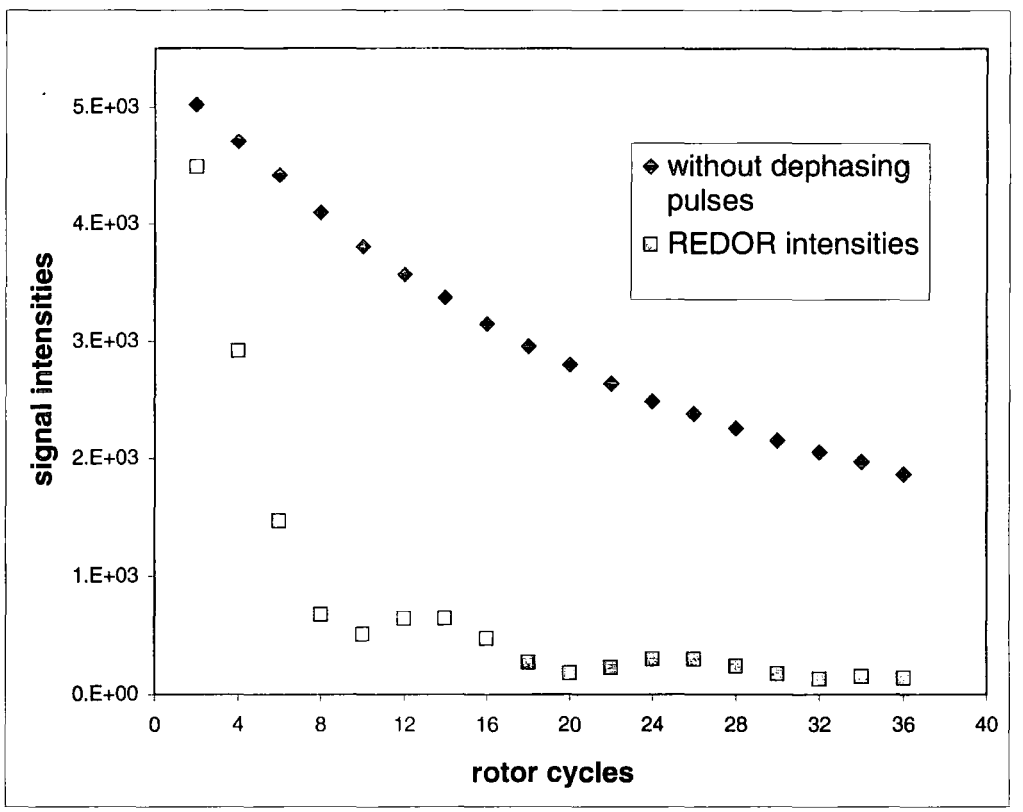

Figure 4. REDOR signal (♦) and spin-echo experiment (⊡) measured on the CMX 200 spectrometer for 20% doubly enriched [2-^{13}C-^{15}N]Glycine.

As will be seen the fitting of the data is not straightforward since a lot of factors influence the REDOR curve that are not taken into consideration when making use of equation (7-16), and this will complicate a lot the interpretation of the data. Before, analysis of the fitting, I would like to discuss briefly the various factors that

can influence the REDOR experiment and the factors that are crucial in order to consider the experimental data to be reliable.

7.3. Parameters influencing the REDOR experiment

In order to obtain a good curve there are a number of parameters that need to be well calibrated, and we need to have some knowledge of the influence that they can have on the final results.

The first important parameter that needs to be well established is the spinning speed; oscillations of about 2 Hz from the desired spinning speed are acceptable but greater oscillations can cause alteration of the REDOR signal[16]. This is, in general, not a problem since the speed controller can adjust the speed even to ± 1Hz.

Greater problems are found for pulse imperfections, decoupling power, and improper phase cycles that can all influence the outcome of the experiment. The difficulty of this experiment is, in fact, in the proper setting of all these factors.

All of the imperfections that can occur during an experiment, though, will have an effect mostly on the last part of the measurements, i.e. for long rotor cycles, as we can see from the two examples below, which show the experiment run on two different occasions. We can see that for the first part of the signal the intensities are almost the same.

Figure 5 shows the comparison between the intensities, considered as $\Delta S/S_0$, which is the normalised REDOR difference or REDOR factor and is equal to (full echo-REDOR)/(full echo) to remove the reduction of the signal due to transverse relaxation.

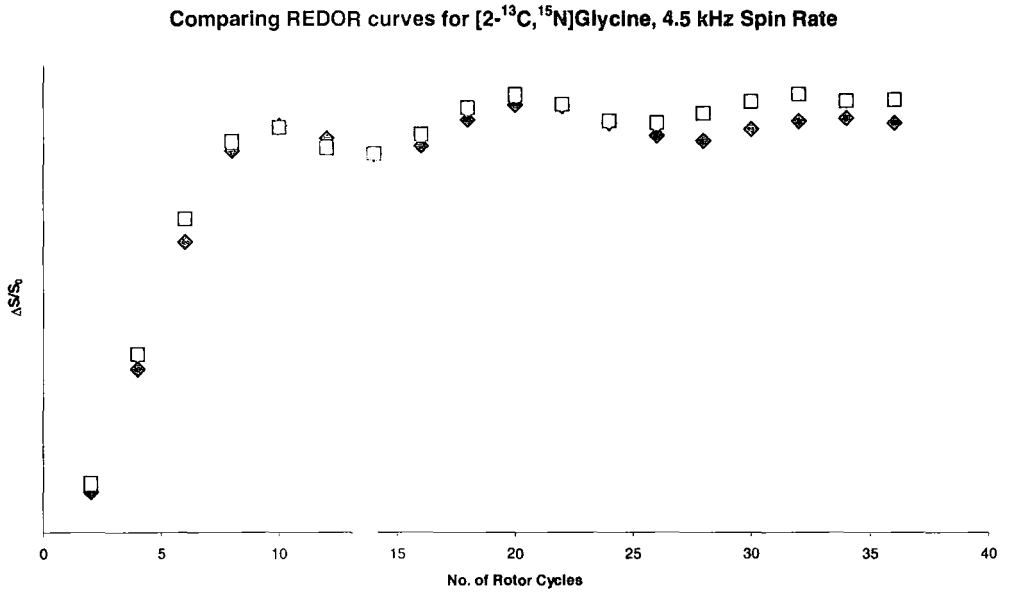

Figure 5. Comparison of REDOR experiments implemented in this laboratory on two different occasions, showing how imperfections and systematic errors are found mostly in the oscillatory region at long evolution times, whereas the short-time decay behaviour is affected very little.

The decoupling is one of the factors that can influence the outcome of the experiment, so that we have tried to see how much the curves are affected by this. Increasing the power of the decoupling field from 50 kHz to 70 kHz , in continuous wave mode (CW), in the case of glycine with the experimental conditions used above, improved the curve, although very slightly (see figure 6). The problem with high-power decoupling, though, is that there is a great risk of damaging the probe, especially for long rotor cycles, since the decoupling is on during the whole REDOR experiment. Decoupling using TPPM needs to be used, and this is what has been done using at the 600 MHz spectrometer, where, since the frequency offsets are greater, the decoupling encounters more problems.

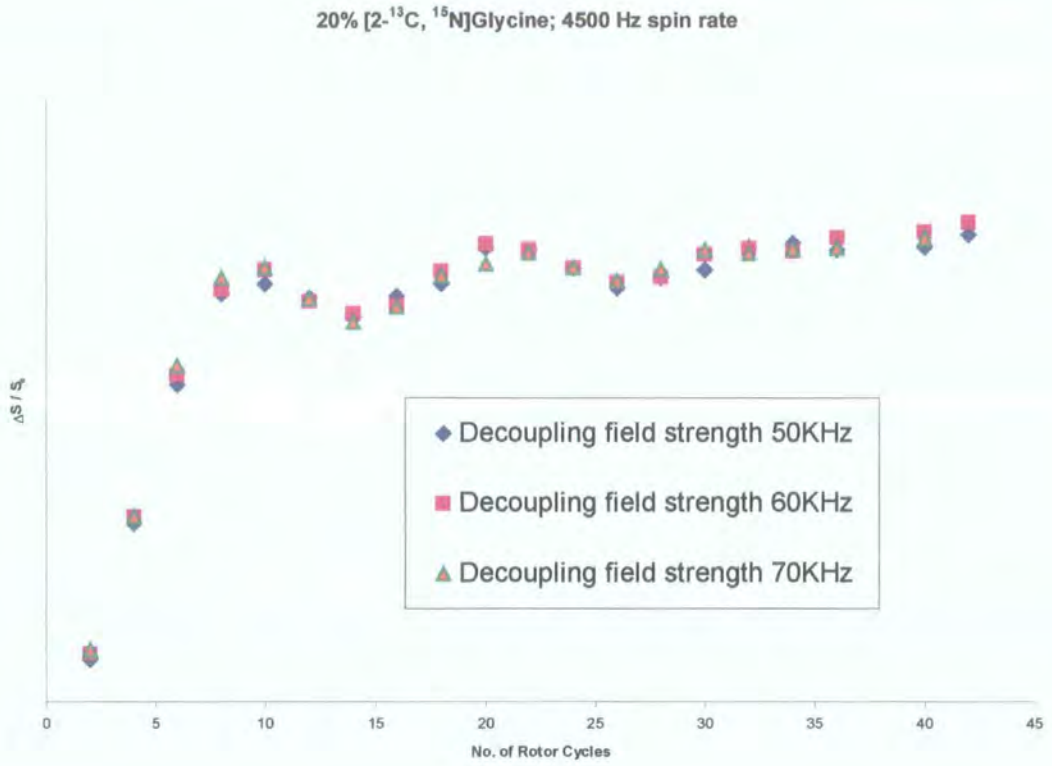

Figure 6. Showing the different $\Delta S/S_0$ REDOR experiments using different decoupling field strengths, in CW mode.

The other parameters that can influence the REDOR experiments are pulse imperfections. In order to check what kind of influence this has on the results we have considered experiments in which we were systematically changed the pulse durations. The conditions of this experiment were, for the 20% glycine, decoupling power of 50 kHz, 180° for ^{13}C 15 μs, 180° for ^{15}N, ct=1 ms, pd=3 s.

The effect on changing the pulse duration for ^{13}C when this is the observed nucleus, by about ± 1μs leads to a difference in the signal of about 1%, so that differences within this range are accepted. On the dephasing channel differences are even smaller. This is the case when the peaks are not on resonance. If pulse imperfections are present when the peaks are not on resonance, the effects are greater, so that it is important to keep the peaks on resonance.

Varying the frequency of the observed frequency and that of the dephasing nucleus showed how the effect is not observable for the dephasing channel but that the off-set of the observed frequency can give great oscillations on the non-REDOR curve, making the final analysis of the curve impossible.

The fact that there are no major differences when the peaks are off resonance is due to the fact that if the right phase scheme is applied to the π pulses of the dephasing channel, as xy-4 or xy-8, the magnetisation toggles between plus and minus very effectively.

Having established all the best experimental conditions under which the REDOR experiment has to take place we can now go on to see what the problems are when we need to analyse the data.

7.4. Fitting the data

Among the major problems of obtaining quantitative results from a REDOR experiment there is the question of evaluating the results, fitting the data and choosing the best models to consider in order to take into account all the factors that influence the oscillations.

7.4.1. Analytical methods

For fitting the data of a REDOR curve there have been numerous studies that include trying to find analytical solutions, using different models taking into account motion, or examining situations in which the condition of isolated spin pairs is relaxed.

As will be seen, the analytical solutions consist of sums of Bessel functions of the first kind. Generation of a universal dipolar-dephasing curve was done using MATLAB that has built-in procedures for generating numerical values for the Bessel functions.

The REDOR signal, normalised to the full echo signal, is given by the powder average, as previously explained:

$$\frac{S}{S_0} = \frac{1}{4\pi}\int_0^{2\pi} d\alpha \int_0^{\pi} d\beta \sin\beta \cos[2\sqrt{2} t\nu_d \cos\alpha \sin 2\beta] \qquad (7\text{-}17)$$

where $t\nu_d$ corresponds to $nD\tau_r$ where n is the number of rotor cycles, D is the dipolar coupling constant and τ_r is the rotor period. This is what is called the universal REDOR curve. In order to obtain information from this curve we need to solve it numerically, and, although it is not extremely complicated, there has been a great deal of effort in recent years, in order to find analytical solutions that would provide a more elegant and simple way of solving the problem.
Integration over α of the integral (7-17) leads to the equation:

$$\frac{S}{S_0} = \frac{1}{2}\int_0^{\pi} d\beta \sin\beta J_0[2\sqrt{2} t\nu_d \sin 2\beta] \qquad (7\text{-}18)$$

where J_0 represents a Bessel function of the first kind of zero order.

Analytical solutions of the previous integral were found first by Mueller[17]. In this paper he presented a preliminary result of the analytical solution for the REDOR experiment, as well as for TEDOR and SEDOR, as an infinite sum of Bessel functions which, he shows, quickly converges to a compact solution, that is:

$$\frac{\Delta S}{S_0} = 1 - [J_0(\sqrt{2} t\nu_d)]^2 + 2\sum_{k=1}^{\infty} \frac{1}{16k^2 - 1}\left[j_k(\sqrt{2} t\nu_d)\right]^2 \qquad (7\text{-}19)$$

The form of this function reproduces the universal REDOR curve.

In a later paper[18] it is shown how it is possible to simplify this expression even further, leading to :

$$\frac{\Delta S}{S_0} = 1 - \frac{\sqrt{2}\pi}{4} J_{\frac{1}{4}}(\sqrt{2}t\nu_d) J_{-\frac{1}{4}}(\sqrt{2}t\nu_d) \qquad (7\text{-}20)$$

Integrating (7-18) over β leads to equation (7-19) as well as showing how, although very useful, analytical solutions are not necessary to evaluate the dipolar coupling from REDOR curves.

In his paper[18] Mueller also shows how it is important to find a REDOR transform as opposed to a simple Fourier transform, since the decay of the REDOR signal is not periodic, and consequently we will obtain something more like a powder pattern, as evidenced from figure 7, in which I show the Fourier transform of the REDOR decay obtained from the glycine 20% experiment.

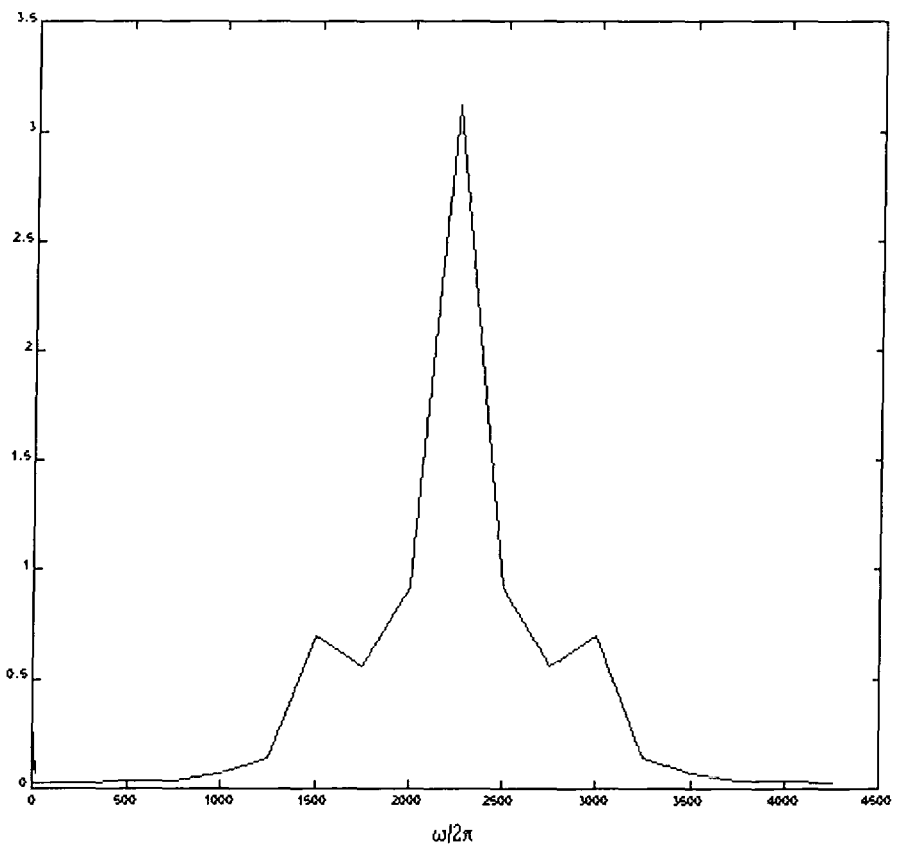

Figure 7. Fourier Transform of the REDOR signal.

Furthermore, information about the dipolar coupling from the Fourier Transform is difficult to extract, since it will be the width of the signal that is proportional to the strength of the dipolar coupling.

7.4.2. The REDOR TRANSFORM

Analytical methods, as opposed to numerical evaluation of the REDOR curve, have also been of great importance, because they can be a very powerful means to consider distribution of the coupling without any a priori assumption, since having an analytical solution can give the basis to find a way to transform it into the frequency domain in order to find single peaks corresponding to the coupling frequency.

As seen from the Fourier Transform it is difficult to extract information directly, especially when considering that additional broadening mechanisms tend to make determination of the exact edges of a powder pattern a difficult task.

What Mueller suggests[18] is to find a REDOR transform, that should be necessary to simplify data analysis, also to gain additional information from more complex systems. In fact, possessing a linear transform, would enable us to extract the dipolar coupling frequencies directly from the decay curve.

To find a linear transform one needs to find the kernel k(Dt) that transforms each signal $S(D_i t)$ from a dipolar spin pair, so that:

$$\int_0^x A_i S(D_i t) k(Dt) dt = A_i \delta(D - D_i)$$

This has been implemented as a macro in the processing program SPINSIGHT, written by Eric Brouwer.

The macro makes use of an apodization function (Blackmann-Harris) that was applied in the time domain to aid the frequency domain smoothing of the data, since the REDOR signal might not decay completely to zero in the time domain. Without this apodisation, pronounced 'sinc wiggles' appear in the spectra.

The greatest problem represented when using the REDOR transform is of signal intensities, since the REDOR transform requires highly accurate S/S_0 time-domain data.

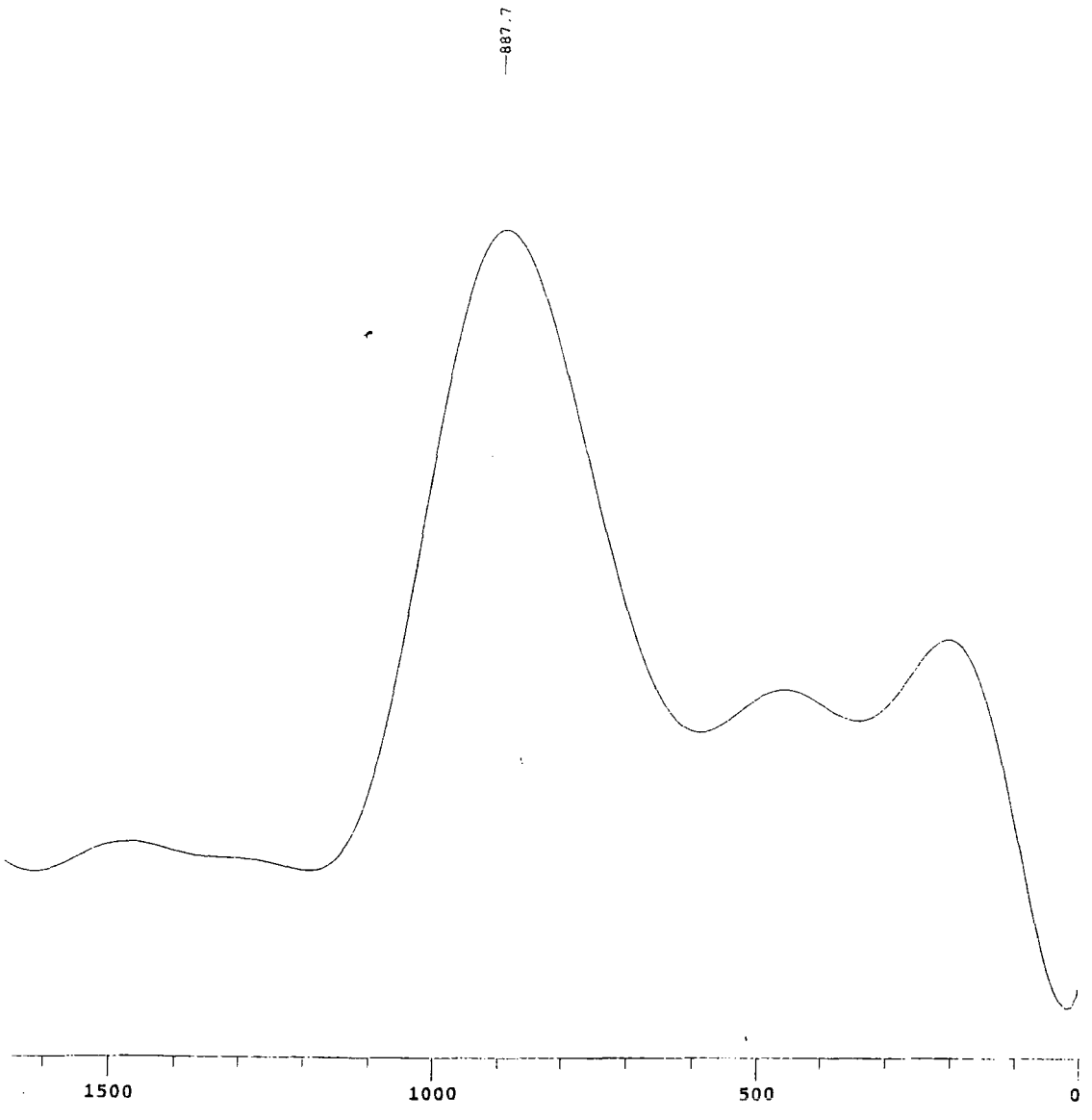

Figure 8. REDOR transform from the signal of Glycine.

Obviously this method will cause even further complications when applied to amorphous or to disordered materials, where a continuous distribution of internuclear distances may contribute to dipolar-dephasing.

The broad line seen in the REDOR transform is somewhat a task still to be solved, and analysis of the REDOR transform. There have been attempts to improve and understand better the REDOR transform proposed by Mueller[19].

Already in his paper Mueller starts to outline some problems with the functional form of the kernel, that, for one thing grows asymptotically as a function linear in time. This would mean that signals further along the decay will be weighed more heavily in the summation.

Problems encountered with the REDOR transform have made it an important task to find other methods of extracting dipolar frequencies from a REDOR signal. Three different methods are compared in a different paper by Mueller[20] et al., from which it is clear that a great number of improvements still need to be done on this kind of approach to extract the dipolar frequencies from the REDOR signal, since there are severe problems of noise; even with a 1% standard deviation severly contaminates the signal. The authors also tested the REDOR transform on glycine diluted to 10%, and the REDOR transform they obtain is completely analogous to ours, with a value of 890±20 Hz that leads to a ^{13}C-^{15}N distance of 1.50±0.01Å.

7.4.3. Fitting from analytical functions

We have tried to find the curve that best resembles our experimental data for glycine, comparing different methods (both numerical and analytical). All the ones listed above were used, but figure 9 shows the result of the fit using equation (18). All the analytical methods seemed to reproduce reasonable curve, although the fit is not very good. A value of 864 Hz is found for the dipolar coupling constant, and curves of about ±10 Hz from this one give the same order of error.

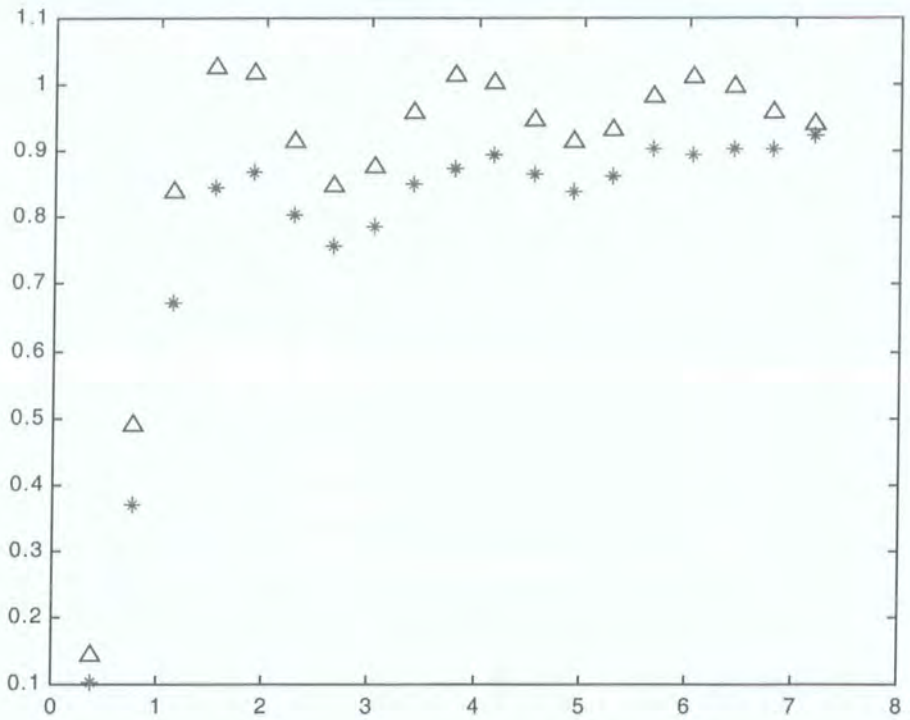

Figure 9. Fitting the REDOR curve for glycine. Δ theoretical data, * experimental. $nD\nu_r$ is the value on the x axis (where ν_r is the rotating frequency).

Although a difference of ±10 Hz is completely within literature experimental errors, we are able to do better since, when using analytical methods, as seen before, we can consider some corrections due to physical considerations.

A recent paper [21] suggests use of a multiplying factor that accounts for the isotopic dilution. In that work on [2-^{13}C, ^{15}N] glycine, dilution to 1:10 needs a factor of 0.865 in order to get a good fit. Including this factor into equation (7-20) , we can obtain the curve shown in figure 10.

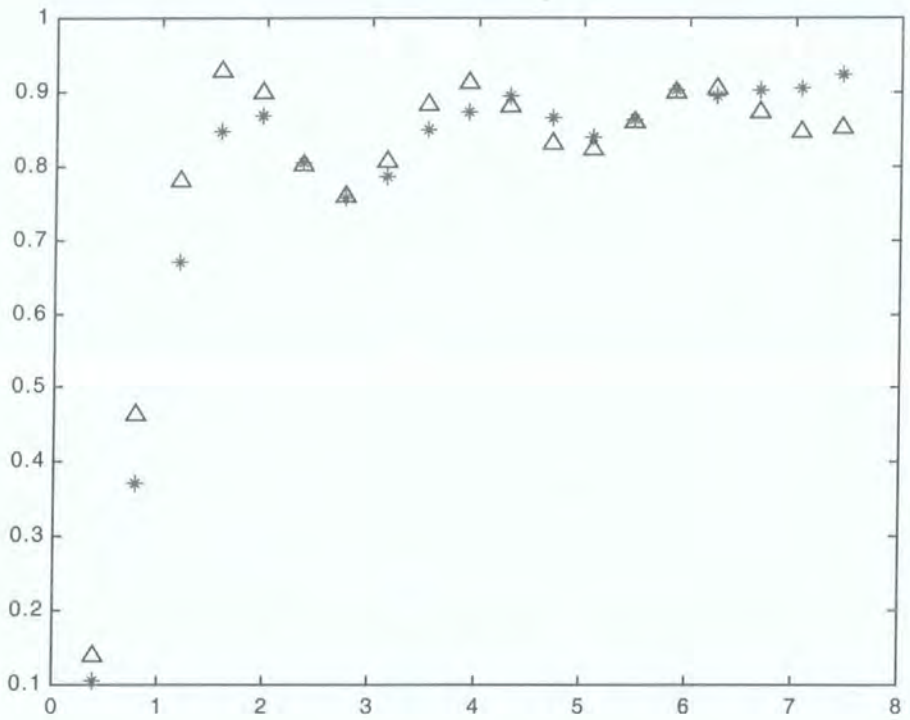

Figure 10. Fitting the REDOR curve for Glycine using a multiplying factor.
Δ theoretical data, * experimental, $nD\nu_r$ is the value on the x axis (where ν_r is the rotating frequency). including a factor of 0.897 in the fitting.

The value found for D is 882 Hz which yields a bond distance of 1.51 Å. This is still different from the experimental values taken from X-ray data but is justifiable with considerations of motion, as analysed before; from literature data we can consider distance differences of about 0.05, with NMR registering a longer value[22]. The correction factor for dilution is also considered from a more rigorous point of view, in this paper, as well as in others[3, 23], where they use the idea of considering the correction due to the percentage of enrichment. However this correction works particularly well for longer bond distances (of about 3 to 4 Å), since it corrects the first part of the REDOR curve particularly well .

It is useful, nevertheless, to consider the undiluted glycine, (99% enrichment) and to compare the values obtained, the results are shown in figure 11.

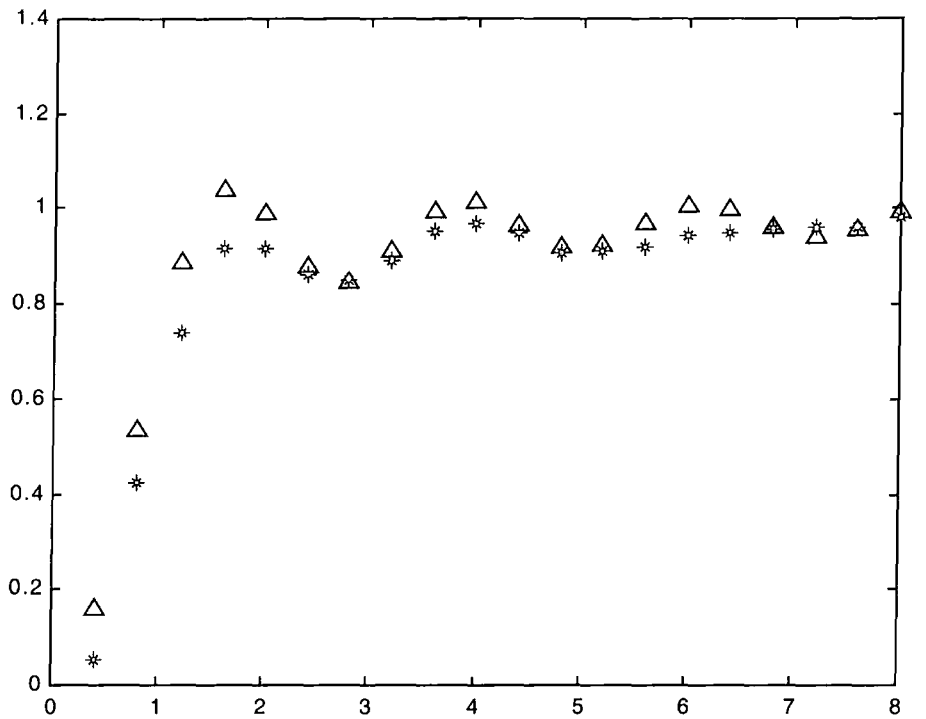

Figure 11. Fitting the REDOR curve for glycine 99% enriched Δ theoretical data, * experimental. Showing glycine at 99% enrichment with no correction. A 900Hz dipolar coupling is obtained corresponding to a bond distance of 1.50 Å.

It is to notice that the particular experiment shown in figure 11 was carried out with 256 transients where previously running the same experiment under analogous conditions, did not lead at all to such a good fit. This shows that, even with 99% enrichment and a S/N already good after 32 transients it is of considerable importance to acquire a large number of transients. The difference between the two curves, the one on the 20% diluted Glycine and the one on the 99% enriched, seems to fully justify the correction factor for taking into consideration the dilution.

There is still a question of considering why we do not get a very good correspondence between the 20% and the 99% samples as well as why there is a discrepancy between the two points that should be at the maximum dephasing of the curve. Among the various considerations to take into account, we need to consider the effect of a finite pulse on the scaling of the dipolar coupling[21]. In

particular we need to consider this scaling factor when radiofrequency irradiation occupies a significant fraction of the rotor period.

This effect is considered for different π-pulse phasing schemes, with calculations of the first-order average Hamiltonian. The conclusion from the paper by Jaroniec[21] is that we need to correct our coupling constant by a factor which is:

$$k = \frac{D_{IS}^{eff}}{D_{IS}} = \frac{\cos((\frac{\pi}{2})\varphi)}{1-\varphi^2}$$

where φ is the fraction of the rotor period occupied by the RF pulses defined in the range of $0 \le \varphi \le 1$ It is equal to $\frac{2\tau_p}{\tau_r}$ where τ_p is the 90° pulse deviation and τ_r is the time for a rotor cycle. As we can see from the formula, for small values of φ we do not need to consider the correction.

In the experiments carried out during my work I have used dephasing 180° pulses shorter than 16 μs and spinning speeds lower than 5500 Hz for which we obtain a φ of 0.09, so that no corrections are needed.

Having considered all different effects that can influence the REDOR experiment on the trial sample, it is important now to apply all these considerations to the actual sample, for which I studied REDOR in detail.

7.5. θ –REDOR experiment

Theta REDOR[24] experiments were performed. This experiment is important when we cannot consider that one S spin (in our case ^{13}C, the nucleus we observe) is coupled to only one I spin (^{15}N). The signal intensity, in this case, will not only depend on the distance between the two nuclei, but on their mutual orientation as well.

This will mean that there is no unique universal REDOR dipolar dephasing curve when the observe nucleus is coupled to several I spins.

The theta–REDOR experiment consists of a modification of the REDOR experiment in the sense that during the evolution period, where all the pulses are 180° on the I channel for the normal REDOR, the middle pulse of the evolution period is of an angle θ for the θ-REDOR experiment. The effect of the θ pulse is that it does not change the spin state of all of the I spins, as would occur for a π pulse. This is particularly important for small values of θ, since it is less probable that more than one of the n I spins coupled to the S spin will change their spin state, so that we will see only dephasing due to one coupling. The attempts we have made were for theta values corresponding to of 3 μs, 5 μs, 7 μs, 10 μs. The experiment for 10 μs should correspond to the normal REDOR experiment.

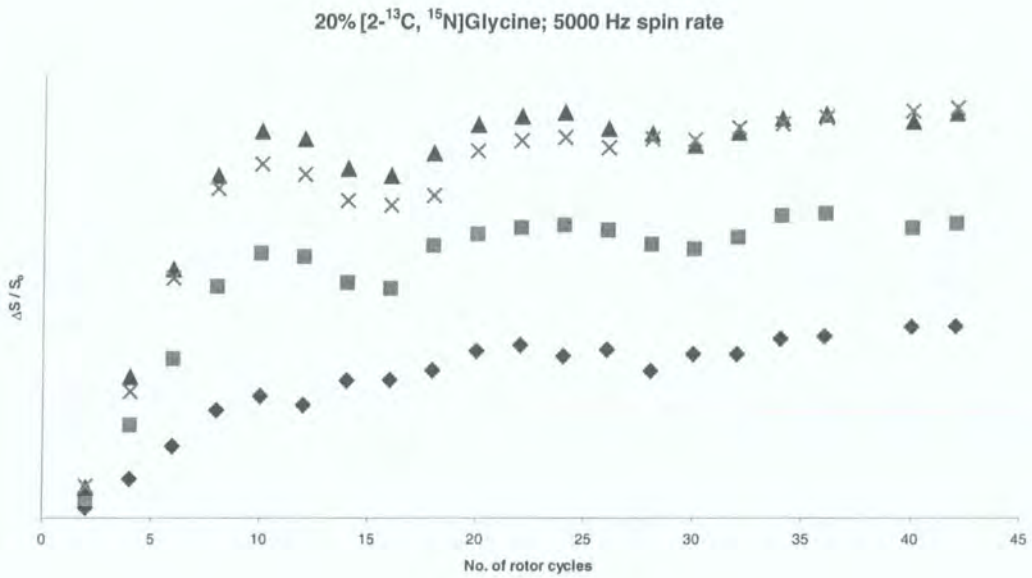

Figure 13.. θ-REDOR experiment for different angles on Glycine, 20% enriched. The different curves correspond to the different angles used; ♦ theta=3μs, ■ theta = 5 μs, ▲ theta = 7μs, X theta = 10μs.

As we can see, the effect of the dephasing is decreased as we decrease the θ pulse, but in fact there should not be too much effect due to other couplings in this sample, since intermolecular distances from the ^{13}C to the nearest ^{15}N are of 5.69 Å and 5.15 Å, leading to couplings only of the order of 20 Hz.

7.6. Average hamiltonian theory for fitting

The other way I have used to try to fit the data has been a program written for MATLAB by Sack[25] using average Hamiltonian theory. The program takes into consideration integration over a different number of angles.

We can see that the fitting of the data has the same kind of problem as using the other analytical forms (Fig. 5,6,7). From his thesis we can see that he is able to fit the REDOR curve for Glycine perfectly but we must consider that he is using a 98% ^{15}N , 99% ^{13}C enriched sample. I have tried the fitting with the 99% Glycine and considered how the integration over a different number of angles influences the curves.

I have considered the dipolar coupling of 945 Hz that should correspond to the distance obtained from X-ray, 860 Hz, that we have found to fit better using analytical curves. I show here three examples of fitting with this program.

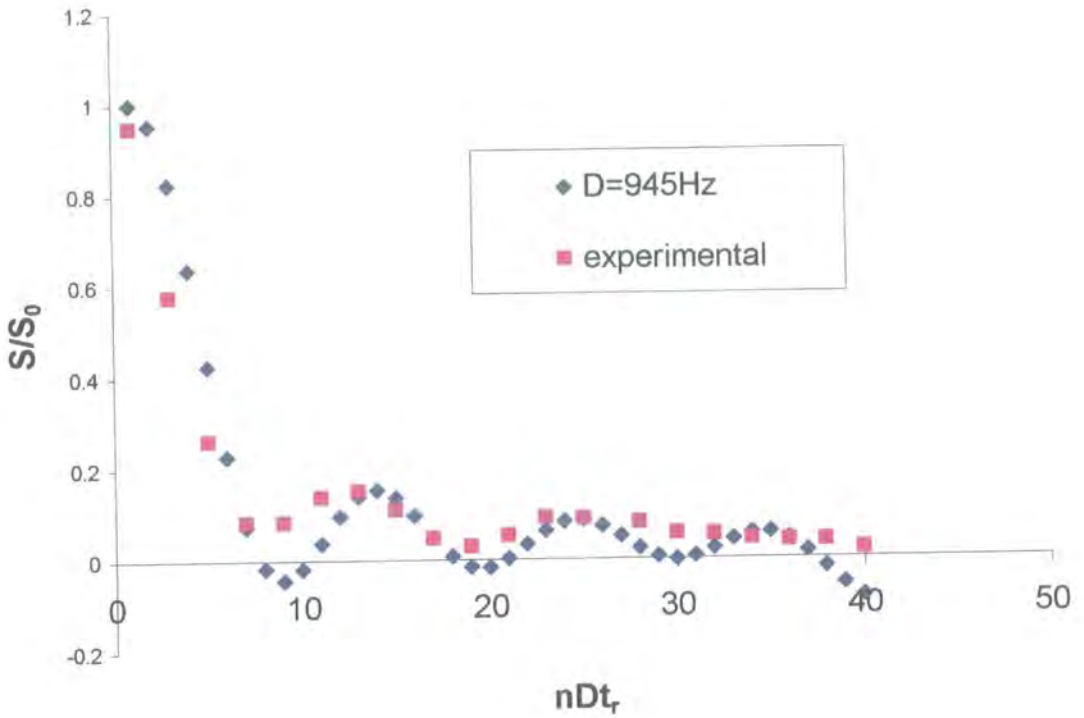

Figure 14. Glycine 99% doubly enriched fitted using average Hamiltonian Theory, integrated over 300 angles.

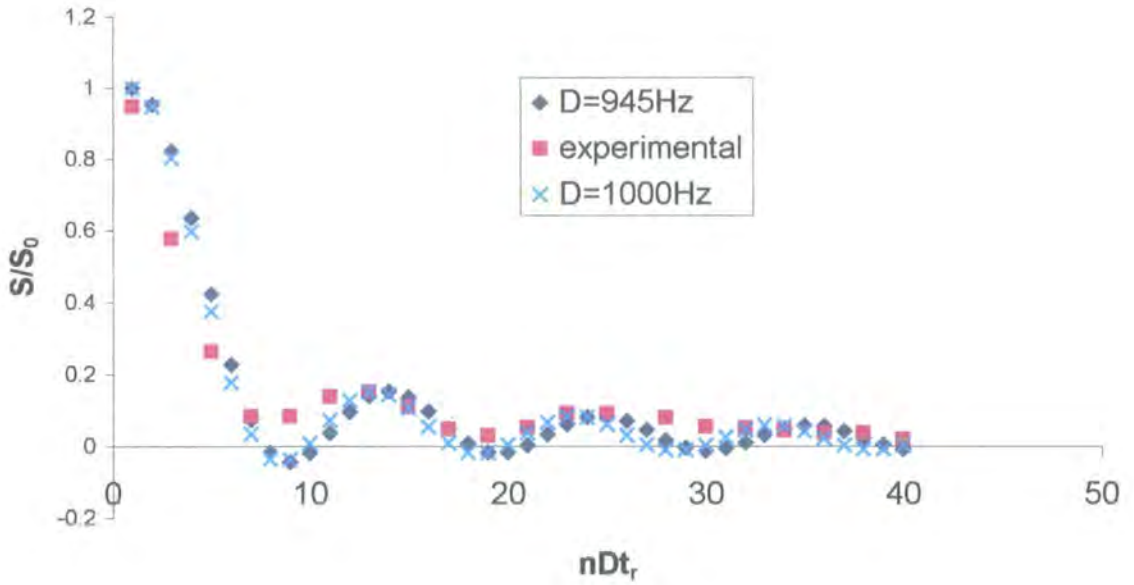

Figure 15.. Glycine 99% doubly enriched fitted using average Hamiltonian Theory, integrated over 537 angles.

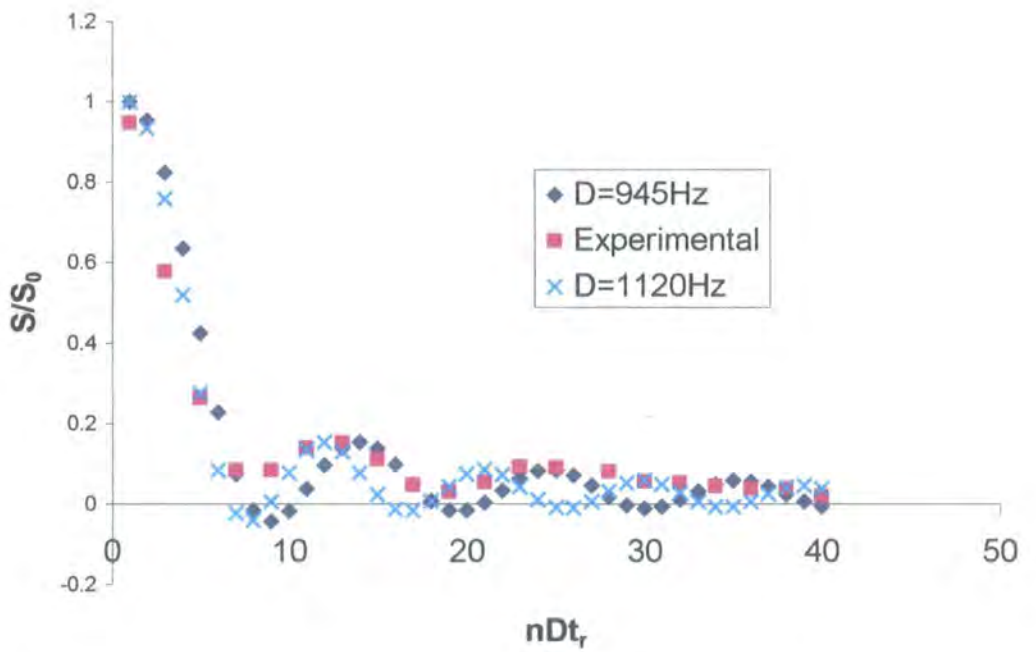

Figure 16. Glycine 99% doubly enriched fitted using average Hamiltonian Theory, integrated over 1154 angles.

As we can see, the best fitting using this program leads to different values when the dipolar coupling is significantly larger than the value it should have, leading to distances of about 1.42 Å.

7.6. Correction of the REDOR curve using models

All the equations shown above, numerical or analytical, showed only the case for two isolated spins, the system not influenced from any motion effects, but this is not usually the case, so that all or at least some of these factors should be considered in the models used for fitting. Since one of the samples was diluted to 20% the intermolecular interactions influenced the signal less. When we move from a simple system like glycine to one which has more particular problems, we need different considerations.

7.6.1. A particular example: the BRL55834 sample

The REDOR study was done in order to carry out a distance measurement on this sample, which was previously studied in this laboratory by Susan Campbell[26], although, the doubly enriched sample had not yet been synthesised.

The chemical name of this sample is (3S-trans)-1-[3,4-dihydro-3-hydroxy-2,2-dimethyl-6-(pentafluoroethyl)-2H-1-benzopyran-4-yl]-2-piperidone.

The molecular formula is $C_{18}H_{20}NO_3F_5$ and the molecular weight is 393.96 g mol^{-1}.

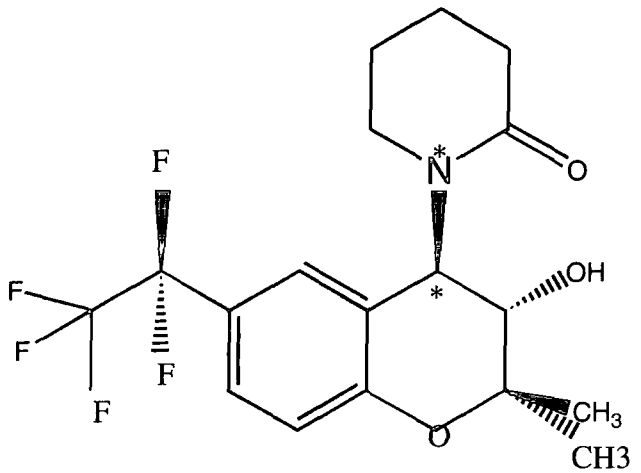

Figure 17. Structure of the sample BRL55834 showing the enriched positions (*).

The drug formulated from this compound is a calcium channel activator for smooth muscle and was being developed to treat asthma. The dubious efficiency has made progress in development of this compound stop. This sample has two possible polymorphs. The doubly-enriched polymorph which was provided corresponds to polymorph II. Unfortunately, this has the more complicated spectra, for both carbon and nitrogen, as shown below in figures 18 and 19.

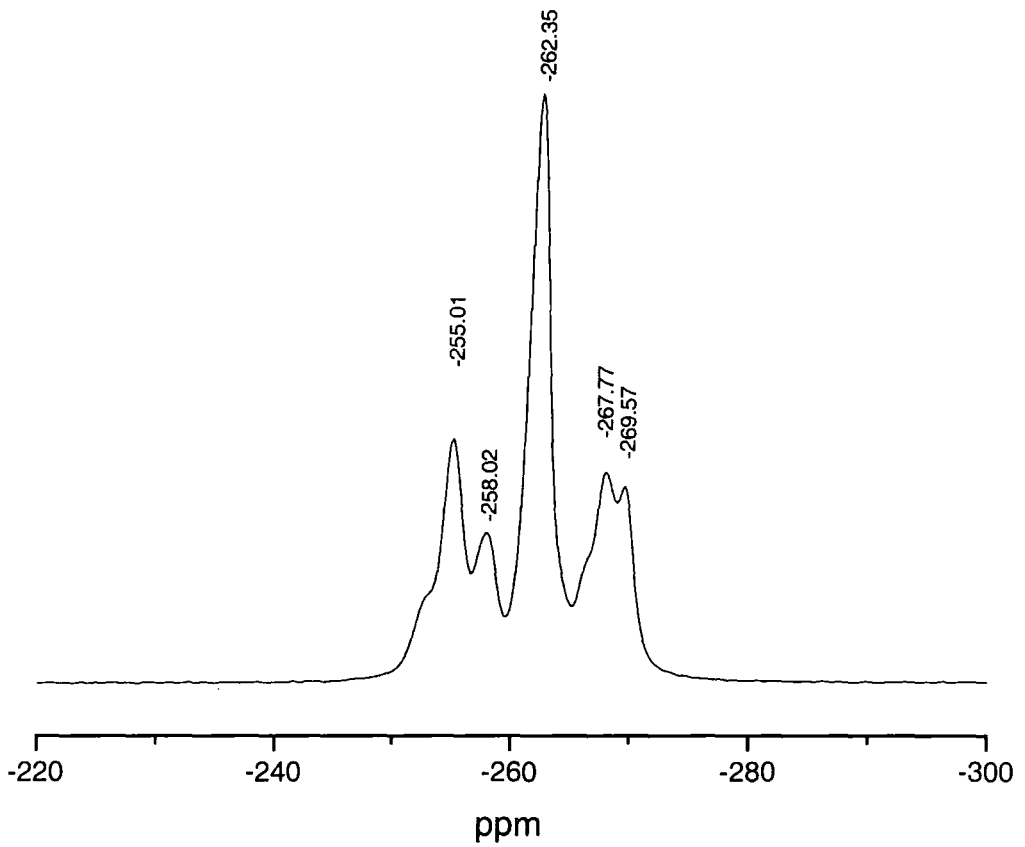

Figure 18. ^{15}N spectrum of isotopically enriched BRL55834, corresponding to polymorph II. The CMX200 spectrometer was used.

For this system, it is probably necessary to consider some effects due to what might be a disorder, for which we would not be able to define spin geometries precisely. The values of the couplings will also be subject to local distribution effects. This assumption was based on the observation of different chemical shifts for the single sites of both carbon and nitrogen, that were enhanced when running the spectra at a higher field. The ^{13}C spectra at 200 MHz and 600 MHz are shown below (figures 19 and 20), where we can see that there are at least three different peaks for ^{13}C, that were not very distinguishable at the lower field.

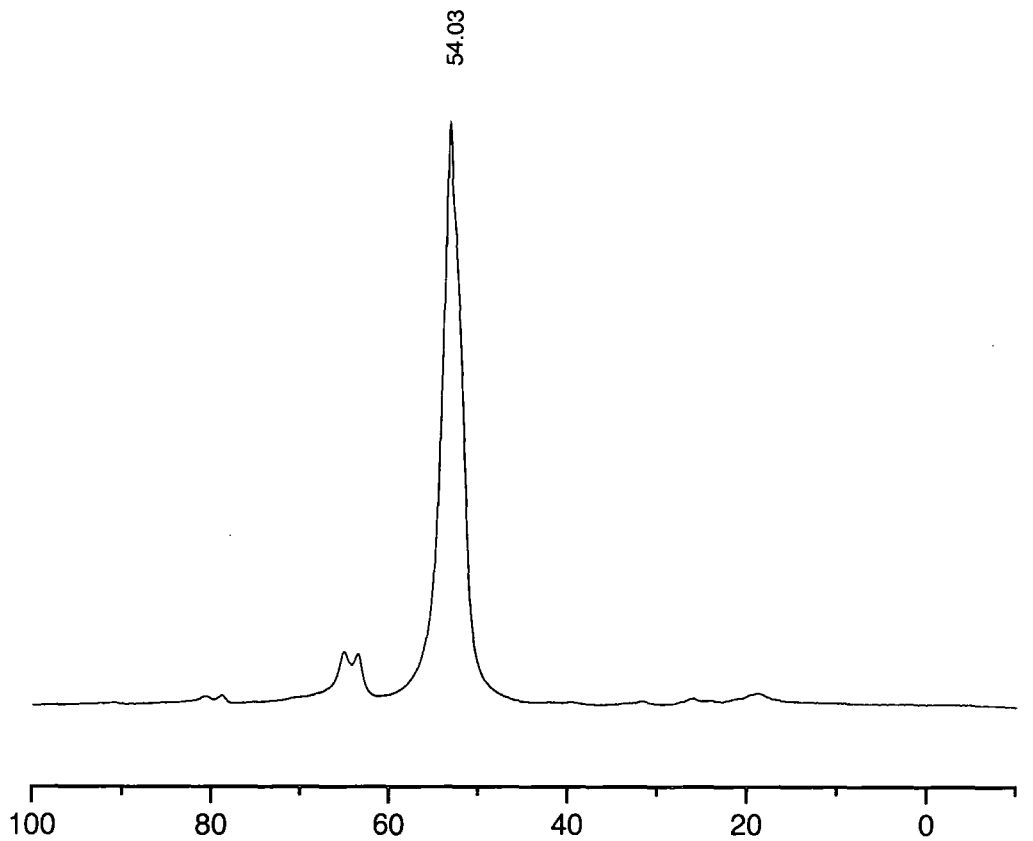

Figure 19. ^{13}C spectrum of the enriched sample BRL55834 using the 200 CMX spectrometer.

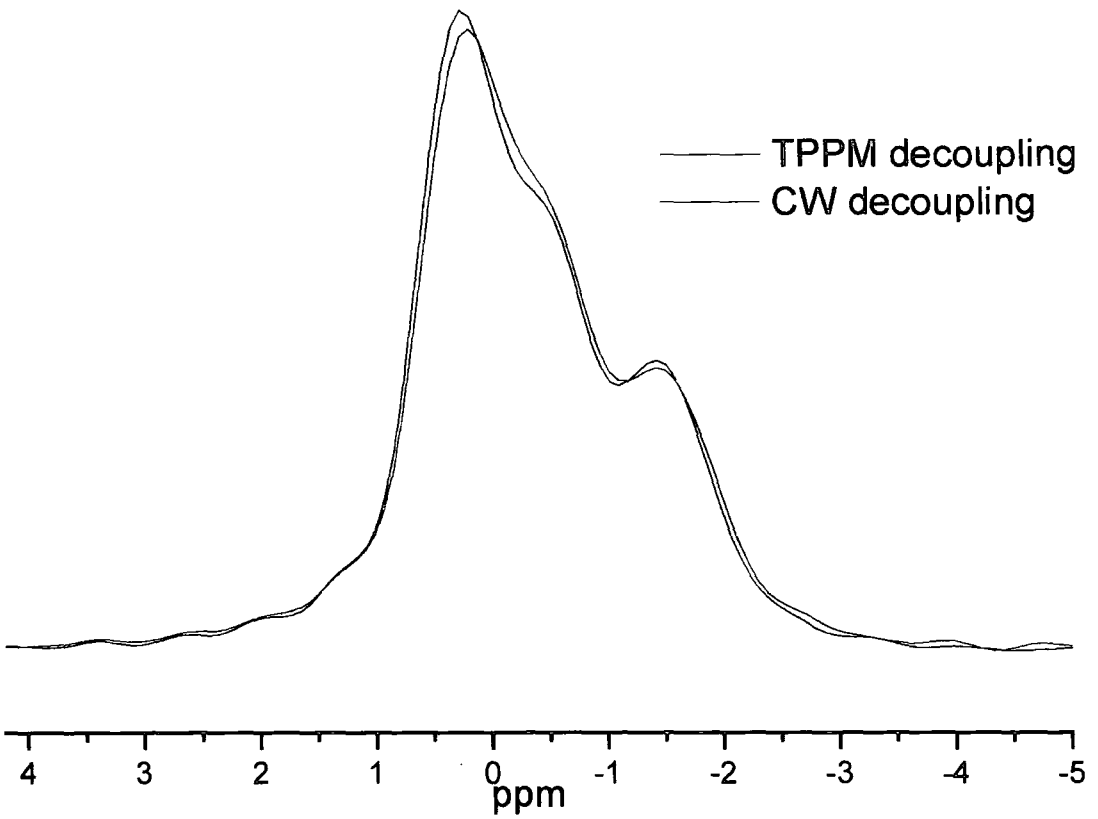

Figure 20. Comparison of different decoupling regimes on the ^{13}C spectrum obtained from the 600 Infinity spectrometer.

The decoupling was performed with both CW decoupling and TPPM, but no major difference was seen. However the REDOR experiment on the 600 Infinity was performed using TPPM decoupling, since, for smaller intensities this difference might have a greater effect. The suggestion of using TPPM decoupling in REDOR experiments is analysed in a paper by Mitchell [27, 28] and the effects are also analysed in later papers[29].

No crystal structure is known of this sample since single crystals were not obtained. This might be a problem of the sample being particularly mobile. This is supported by the fact that the proton spectrum shows particularly narrow bands, as shown (figure 21).

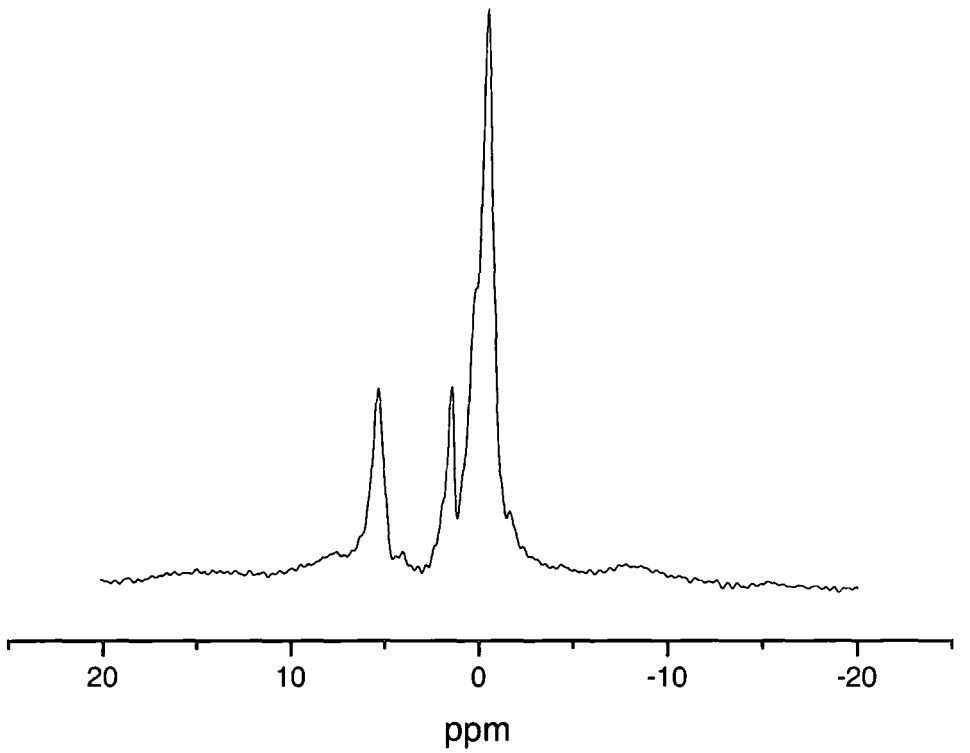

Figure 21. Proton spectrum of the sample BRL55834.

The fact that there is more than one peak for the ^{13}C as well complicates the REDOR experiment even more. We can see that, especially for the carbon, three different sites become very well defined at higher field.

In order to get some idea of the bond length I have both checked distances for related compounds in the Cambridge Structural Database Service (CSDS) as well as having optimised the molecular geometry at different levels using Gaussian 98. The Cambridge database, suggested that the distance between the ^{13}C and the ^{15}N should be very near to 1.484Å.

From the total optimisation at different levels we found the distances shown in table 1.

LEVEL of OPTIMISATION	Ditance(Å)
HF/STO3G	1.475
HF/3-21G**	1.492
B3LYP/3-21G**	1.491
B3LYP/6-31G**	1.491

Table 1. Bond distances obtained using different models.

From figure 22 we can see the conformation obtained from total optimisation of this molecule using the level HF/3-21G**

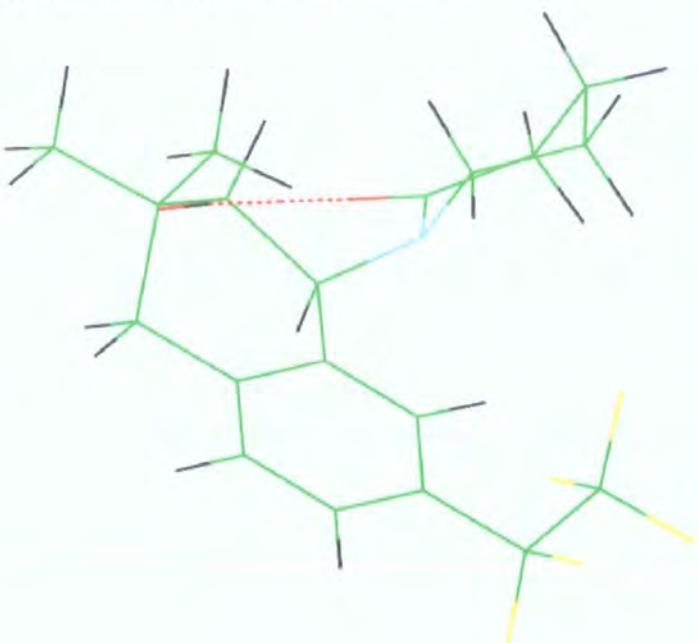

Figure 22. Optimised structure of the BRL55834, from which it seems as if there is close contact between the two oxygens, since the distance between them is of 2.80 Å.

The problems of this sample seem to be various, from mobility, to considering the possibility of more than one molecule in the asymmetric unit. Having considered previously all the analytical solutions, we need now to consider different models in

order to be able to correct the universal curve, which considers only two isolated spins, in an immobile conditions. In particular three different models can be considered if we relax the conditions of equidistant, isolated, static hetoronuclear pairs of spins[30].

Different algorithms are presented for calculating the REDOR dephasing when (i) the isolated pairs have a distribution of internuclear distances; (ii) the observed spin is coupled to more than one other spin; and (iii) the observed spins are in relative motion. All of these models can deviate the curve from a good fit.

For conditions (ii) and (iii), knowledge of the relative orientations of the spins is required, for which the algorithms become quite complicated so that these models were not taken into consideration in this study.

The one option that was possible to take into consideration was the first algorithm presented in this paper for which it can be demonstrated that the observed dephasing can be considered as the sum of different REDOR curves; I have considered three different couplings since we se at least three ^{13}C sites.

Since the fitting of this compound seemed very difficult I tried to apply this model to the curves obtained on both the 200 CMX and the 600 Infinity spectrometers. The results are shown below:

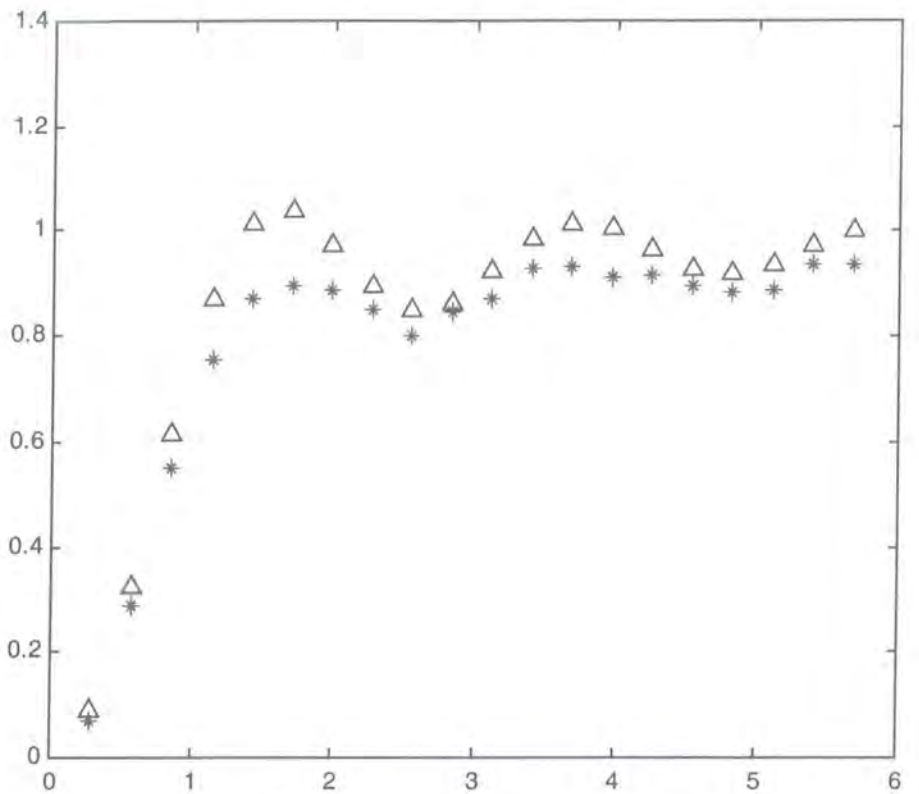

Figure 23. REDOR curve fitted using equal contributions from three frequencies, of 792 Hz, 842 Hz and 891 Hz. The data are from the CMX 200 spectrometer.

These three frequencies with which I have fitted the curve in figure 23 correspond to the distances respectively of 1.57Å, 1.54Å and 1.50Å.

When trying to fit using only one frequency the results are definitely worse but this does not necessary mean that this model represents the best one to use. The values at the 600 MHz were not as well fitted. This might be due to the fact the chemical shifts here are more spread out over the frequency range.

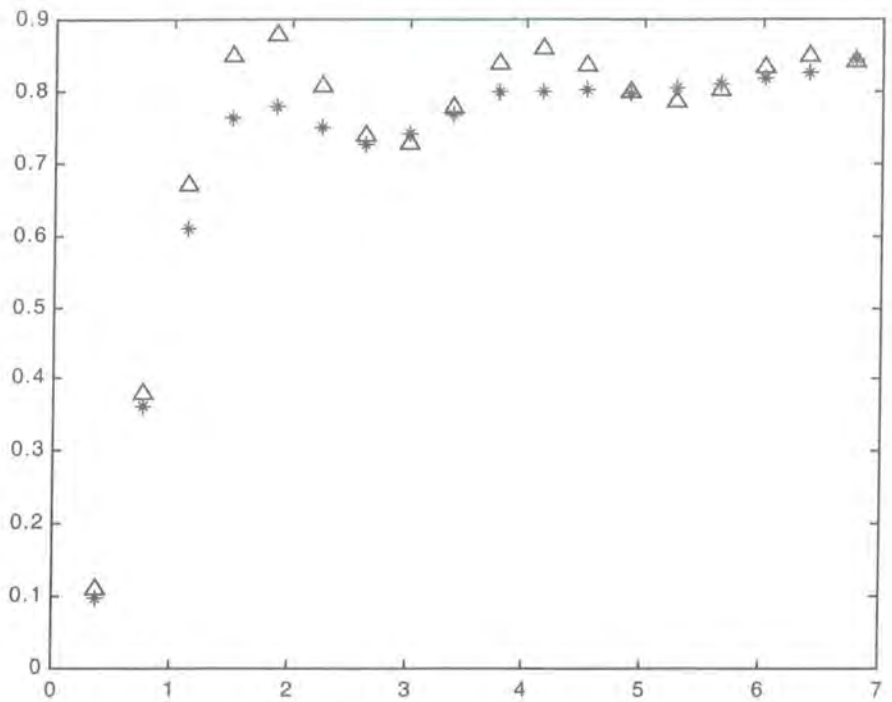

Figure 24. REDOR curve fitted using equal contributions from three frequencies, of 820 Hz, 890 Hz and 940 Hz.

The data is from the Infinity 600. The corresponding distances are: 1.55, 1.51 and 1.48 Å, using a correcting factor of 0.85.

As we can see, the distances do not agree completely from one spectrometer to the other and a problem found with the higher field was that the intensities were all smaller, so that a correcting factor of 0.85 was needed as used for the 20% enriched glycine but this was not justified in this case so that probably this dataset should not be considered at all.

7.7. Analytical approximations

There is one last consideration that needs to be done, and it concerns the evaluation of only the first part of the REDOR curve when there are problems with the fitting. All previous treatments were considering analytical simulations, making considerations on the particular model, or not. Since sample BRL55834 has been quite difficult to study, I would like here to point the attention only to the first part

of the REDOR curve that will anyway, contain most of the information needed for the dephasing and that will be independent from geometry calculations[31].

Different calculations have shown that the initial part of the REDOR curve can be approximated analytically, thereby avoiding the full numerical calculation procedure. The analytical approximation is based on the usual expansion:

$$\cos x = 1 - \frac{x^2}{2} + \frac{x^4}{24} - .....$$

Truncation after the second term, in the limit for which $x = \Delta\phi = \omega N T_r \ll 1$, results in a first order approximation, for which we can write:

$$\frac{\Delta S}{S_0} = k(NcDTr)^2$$

where k is a dimensionless constant equal to 1.066. This approximation was first found Pan and Gullion[2] in their original paper on REDOR.

This equation is particularly important if we consider that D^2 is proportional to the heteronuclear dipolar second moment, M_2, where quantitatively we find that:

$$\frac{\Delta S}{S_0} = \frac{4}{3\pi}(NcTr)^2 M_2$$

Thus, for short intervals ($0<\Delta S/S<0.3$), the strength of the internuclear dipole coupling can be expressed easily in terms of a second moment. Below I show the curve with the first- and second-order approximations. Unfortunately, within this range there are never enough points for short internuclear distances, but it is a particularly useful analysis for systems where there is no ad hoc information on spin geometry.

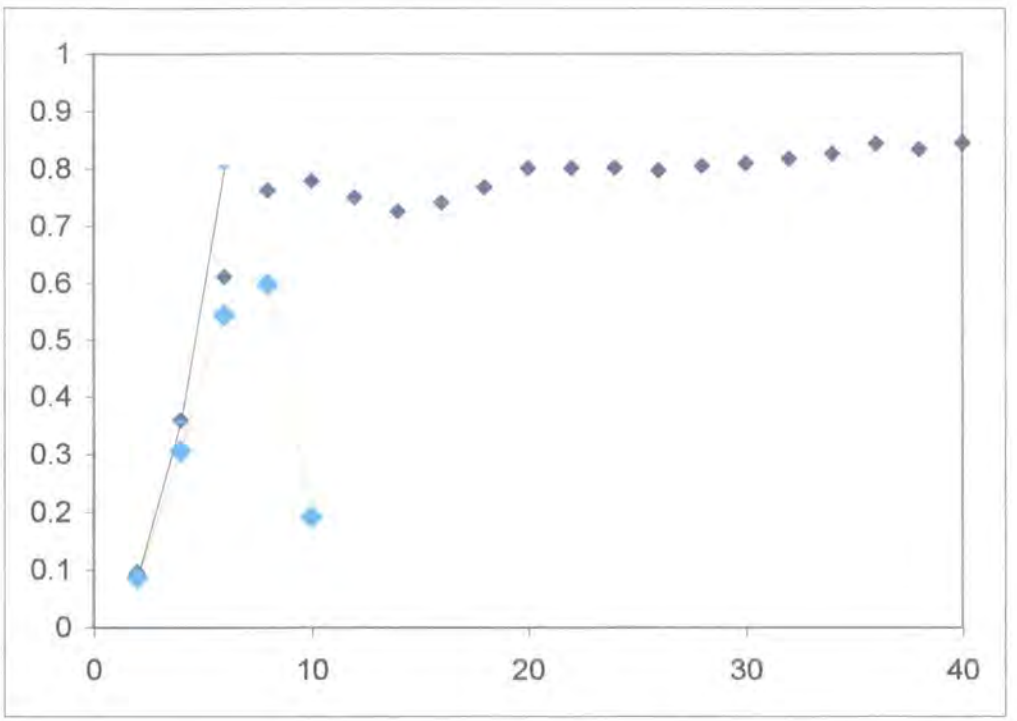

Figure 24. The REDOR curve (♦) can be approximated analytically using the first-order(-) and the second-order approximations (♦).

No quantitative conclusion can be drawn, from these analytical approximations, at least not for systems that dephase fast, since we need to consider only 30% of the total signal and for fast dephasing there is too little information in this small part of the curve.

7.8. Conclusions

I have analysed many different ways of considering the REDOR experiment. From evaluation of the literature, it seems as if this experiment is mostly used for longer distances (3-4 Å) since there is probably an intrinsic error of about 0.5Å in the distance measurements. Also, since every dipolar coupling has to be converted into the cube of a distance, which will make differences enhanced.

We have also seen, complications in interpretation, for which the best way to fit the data is still an open issue. When complicated systems are to be evaluated, obviously, the matter will become even more problematic, making the analysis of

the curve almost impossible, and extraction of the distances becomes a difficult issue.

7.9. REFERENCES

1) T. Gullion and J. Schaefer, *J. Magn. Reson.* **1989**, *81*, 196.

2) Y. Pan, T. Guillon and J. Schaefer, *J. Magn. Res.* **1990**, *90*, 330.

3) A. Naito, K. Nishimura, S. Tuzi and H. Saito, *Chem. Phys. Lett.* **1994**, *229*, 506.

4) I. Sack, S. Macholl, J. H. Fuhrhop and G. Buntkowsky, *Phys. Chem. Chem. Phys.* **2000**, *2*, 1781.

5) H. Saito, S. Tuzi, S. Yamaguchi, S. Kimura, M. Tanio, M. Kamihira, K. Nishimura and A. Naito, *J. Mol. Struct.* **1998**, *441*, 137.

6) T. Asakura, J. Ashida, T. Yamane, T. Kameda, Y. Nakazawa, K. Ohgo and K. Komatsu, *J. Mol. Biol.* **2001**, *306*, 291.

7) J. R. Garbow, D. M. Snyderman, E. E. Remsen, D. L. Kurdikar and A. J. Solodar, *Macomolecules* **1998**, *31*, 3931.

8) D. E. Kaplan and E. L. Hahn, *J. Phys. Radium* **1958**, *19*, 821.

9) C. P. Slichter,*Principles of Magnetic Resonance*; Springer- Verlag: New York, 1990.

10) U. Haeberlen and J. S. Waugh, *Phys. Rev.* **1968**, *174*, 453.

11) A. E. Bennett, R. G. Griffin and S. Vega, *NMR Basic Principles and Progress* **1994**, *33*, 1.

12) S. Dusold and A. Sebald, *Annual Reports of NMR Spectroscopy* **2000**, *41*, 185.

13) P. G. Jonsson and A. Kvick, *Acta Cryst.* **1927**, *28*, 1827.

14) R. E. Marsh, *Acta Cryst.* **1958**, *11*, 654.

15) L. F. Power, K. E. Turner and F. H. Moore, *Acta Cryst. Sect. B* **1976**, *36*, 11.

16) T. Gullion, *Concepts in Magnetic Resonance* **1998**, *10*, 277.

17) K. T. Mueller, *J. Magn. Reson.* **1995**, *113 A*, 81.

18) K. T. Mueller, T. P. Jarvie, D. J. Aurentz and B. W. Roberts, *Chem. Phys. Lett.* **1995**, *242*, 535.

19) J. B. d. E. Caillere, *J. Magn. Reson.* **1998**, *133*, 273.

20) F. G. Vogt, D. J. Aurentz and K. T. Mueller, *Mol. Phys.* **1998**, *95*, 907.

21) C. P. Jaroniec, B. A. Tounge, C. M. Rienstra, J. Herzfeld and R. G. Griffin, *J. Magn. Reson.* **2000**, *146*, 132.

22) K. Nishimura, A. Naito and H. Saito, *J. Phys. Chem. B* **1999**, *103*, 8398.

23) K. Nishimura, A. Naito, S. Tuzi and H. Saito, *J. Phys. Chem. B* **1998**, *102*, 7476.

24) T. Gullion and C. H. Pennington, *Chem. Phys. Lett.* **1998**, *290*, 88.

25) I. Sack *Structure elucidation of organic solids using heteronuclear dipolar solid state NMR spectroscopy.*, 1998.

26) S. Campbell *Pharmaceutical Polymorphism: An investigation using SSNMR*; Durham, 1998.

27) D. J. Mitchell and J.N.S.Evans, *Chem. Phys. Lett.* **1998**, *292*, 656.

28) G. McGeorge, D. W. Aldermann and D. M. Grant, *J. Magn. Reson.* **1999**, *137*, 138.

29) A. K. Mehta, D. J. Hirsh, N. Oyler, G. P. Drobny and J. Schaefer, *J. Magn. Res.* **2000**, *145*, 156.

30) J. M. Goetz and J. Schaefer, *J. Magn. Res.* **1997**, *127*, 147.

31) M. Bertmer and H. Eckert, *Solid State NMR* **1999**, *15*, 139.

Chapter 8

FUTURE WORK

This work has been important in order to relate different techniques such as solid-state NMR and X-ray analysis and gain information on systems that show polymorphic behaviour. It has been mainly a study of sulfanilamide, which, despite its simplicity, showed quite interesting features in both ^{13}C and ^{15}N solid-state NMR spectra, testifying to the very different parameters that can be detected and related to polymorphism. ^{15}N enrichment of other, more complicated sulfa-drugs such as sulfathiazole or sulfapyridine, could lead to a good understanding of the behaviour of the whole family of sulfa-drugs, then being able to relate better, the effects seen in the solid-state spectra to single crystal X-ray data.

In general, for other systems also, the REDOR experiment should be a field into which a great amount of work should be concentrated since it can lead to information on internuclear distances on systems for which it would be impossible to run single-crystal experiments, e.g. compounds as not able to crystallise properly. Unfortunately, as seen for the case of BRL55834, the REDOR experiment itself can prove to be difficult to obtain. For this sample, in particular, the most important thing would be to obtain the polymorph displaying the simplest ^{13}C and ^{15}N spectrum that should, most likely, contain only one molecule per asymmetric unit, so that the REDOR experiment will simplify greatly on this sample.

APPENDIX

Conferences attended

"New Techniques in Magnetic Resonance" British Radiofrequency Spectroscopy Group.

1st December 1999, Institute of Physics, 76 Portland place, London.

"15th European Experimental NMR Conference" 12-17 June 2000, University of Leipzig, Germany.

"15th international meeting on NMR Spectroscipy" Royal Society of Chemistry, University of Durham, 8-12 July 2001.

Publications

"Effects of polymorphic differences in sulfanilamide as seen through 13C and 15N solid –state NMR spectra" A. Portieri, R.K. Harris, T. Threlfall, R. Lancaster, R. Fletton. In final stage of preparation.

Posters presented and talks given

Solid-State NMR of Sulfa-Drugs.
"15th European Experimental NMR Conference" 12-17 June 2000, University of Leipzig, Germany.

NMR discussion group-Polymorphic behaviour of sulfa drugs, Talk given. 21st of September, University of Oxford.

Solid-State NMR of Sulfa –Drugs.

Prize winner of the I.C.I. Poster Competition. University of Durham 22nd of Decmber 2000.

Solid-state NMR of Sulfa-Drugs.

"15th international meeting on NMR Spectroscipy" Royal Society of Chemistry, University of Durham, 8-12 July 2001.